Spring 5-10-2019

MAINTENANCE OF GENETIC AND EPIGENETIC STABILITY DURING DNA DOUBLE-STRAND BREAK REPAIR AND DNA REPLICATION

Nathaniel E. Wiest
University of New Mexico

Nathaniel Edward Wiest

Candidate

Biomedical Sciences

Department

This dissertation is approved, and it is acceptable in quality and form for publication:

Approved by the Dissertation Committee:

Alan E Tomkinson, PhD, Chairperson

Mary Ann Osley, PhD

Diane S Lidke, PhD

David Y Lee, MD/PhD

MAINTENANCE OF GENETIC AND EPIGENETIC STABILITY DURING DNA DOUBLE-STRAND BREAK REPAIR AND DNA REPLICATION

by

Nathaniel E. Wiest

B.S., Biology, University of New Mexico, 2010

DISSERTATION

Submitted in Partial Fulfillment of the
Requirements for the Degree of

DOCTOR OF PHILOSOPHY
BIOMEDICAL SCIENCES

The University of New Mexico
Albuquerque, New Mexico

MAY, 2019

DEDICATION

This dissertation is dedicated to…

The Author of the awe-inspiring mysteries we seek,

the search to understand nature for the betterment of the human condition,

the love of family, friends, and mentors that gives life its deeper meaning,

and to Elani

ACKNOWLEDGEMENTS

I would like to begin by acknowledging the members of my committee on studies for their support and guidance through my PhD studies. Furthermore, I gratefully acknowledge the review of this manuscript by John Petrini of the Memorial Sloan Kettering Cancer Center in New York.

I next acknowledge my PhD co-mentors, Mary Ann Osley and Alan Tomkinson, for their countless contributions to my development as a scientist and as a human being.

I started my PhD in the lab of Mary Ann Osley, where I learned the art of thorough science. The countless hours spent analyzing data from multiple perspectives, planning experiments, reviewing presentations, discussing papers, and considering both positive and negative experimental results with you helped to establish the solid foundation upon which any career in science I am fortunate enough to lead will be built. Furthermore, your amiability, industry, compassion, thoughtfulness, and humility are characteristics that I will strive to emulate in any leadership position entrusted to me in the future.

I performed my Aim 2 research in the lab of Alan Tomkinson. Under Alan's tutelage, I learned to think and operate as an independent scientist. I cannot thank you enough for the trust you placed in me that helped my confidence as a researcher to grow exponentially.

Next, I acknowledge the past and present members of the Osley lab, all of whom have been friends and mentors to me throughout my training. I offer my sincerest gratitude to Cory Hillyer for her constant friendship and support, and for being a pillar of stability and organization in the impeccable Osley lab. To Scott Houghtaling and Kelly Trujillo, the lab postdocs when I started in 2011, I cannot thank you enough for showing me the ropes of the awesome yeast model system, and for brightening the lab with your humor and confidence. Finally, to the current postdocs Lindsey Long and Po-Hseun Lee, I thank you for your friendship and assistance.

I next acknowledge the past and present members of the Tomkinson Lab who have played many significant roles throughout my training. First, to the incredible senior research scientist Annahita Sallmyr I say thank you for the countless times you have

assisted me in any number of experiments, and I say thank you again for the numerous times you have lifted my spirits with your caring and compassion. To fellow Tomkinson lab graduate students Timothy Howes and Ishtiaque Rashid, I thank you for your companionship. To Rhys Brooks, a research track medical student, I say thank you for your encouragement and help as I transition back to the trials of medical school. To Zhimin Peng, a former postdoc, I say thank you for showing me the ropes when I joined the Tomkinson lab and for your constant willingness to help with any question.

I next would like to thank the Biomedical Sciences Graduate Program and the combined UNM MD-PhD program for providing me with this training opportunity and for keeping me on track. I offer a special thanks to former MD-PhD program director Fernando Valenzuela, whose enthusiasm and outreach to prospective applicants was contagious. To the many incredible fellow students in the BSGP and MD-PhD programs, I cannot thank you enough for the community and friendship over these last years.

To the members of the coffee club, including Daniel Purcell and Mohammad Abbas, thanks for the caffeine and for your true friendship.

Next, I would be remiss if I failed to mention the UNM combined BA/MD program that brought me to UNM for my premedical training, and the UNM Biology Honors program, including my former mentors David Hanson and Nora Perrone-Bizzozero, who oversaw my first benchtop research efforts that sparked my love of basic science. To the fellow students who became friends and then family in the BA/MD program, including Joshua Sheak who is in the MD-PhD program with me, I will be eternally grateful for the friendship we share.

Finally, I would like to thank my family, including my parents Anne and Phil, my brothers Jonathan and Stephen, my grandparents John, Clarice, and Nana, and all of my Cousins, Aunts, and Uncles, including the Milpitas Wiests for your incredible love and support. I would also like to thank the Albuquerque South African community for adopting me- *baie dankie!* To my in-laws in Kentucky, your constant love and support have meant the world to me. And finally, I thank my beautiful wife Elani for helping me to grow into the man I've always wanted to be, and for going through the inconvenience of carrying our son. There is a bright future ahead, and I am glad to have your hand in mine as we go towards it together.

Maintenance of Genetic and Epigenetic Stability during DNA Double-Strand Break Repair and DNA Replication

by

Nathaniel Edward Wiest

B.S., Biology, University of New Mexico, 2010
Ph.D., Biomedical Sciences, University of New Mexico, 2019

ABSTRACT

Eukaryotic genomes are assembled into a complex of DNA and proteins known as chromatin. The packaging of DNA into chromatin is the foundational strategy that cells use to both compress genomic DNA into nuclei and regulate access to its contents. The basic repeating subunit of chromatin is the nucleosome, composed of an octamer of two copies of each of the core histone proteins H2A, H2B, H3, and H4 around which 146 bp of DNA are tightly wrapped. While the compaction of genomes into chromatin offers cells significant advantages, it also presents serious challenges to fundamental processes that maintain genome integrity, including DNA repair and replication. Nucleosomes must be disrupted to allow access to damaged DNA by repair factors. Additionally, the millions of nucleosomes that package genomic DNA are displaced during DNA replication. After their displacement, nucleosomes must be faithfully restored to preserve proper chromatin compaction and regulation of access to DNA that underlie transcriptional programs and cellular identity. Thus, the processes that maintain genome and epigenome stability are intricately linked.

In the first aim of this dissertation, I examined the role of the conserved SWI/SNF ATP-dependent nucleosome remodeler in the repair of DNA double-strand breaks (DSBs) in yeast. I demonstrated that SWI/SNF facilitates the actions of the MRX

complex at the DSB, including the eviction of KU, initiation of DNA end resection, recruitment of long-range resection factors, and activation of the DNA damage response. Furthermore, I showed that this activity of SWI/SNF is related to its role in the efficient eviction of nucleosomes near a DSB. This study contributes to an understanding of the roles of the clinically relevant SWI/SNF complex in mediating accurate repair of DSBs in the context of chromatin.

In the second aim, I examined the role of DNA Ligase I (Lig1) in coordinating chromatin assembly and maturation on newly replicated DNA in mammalian cells. I accumulated preliminary data demonstrating that Lig1 may influence the deposition of the linker histone H1 on DNA during replication, and that that Lig1 may also contribute to the recruitment of DNA methylation machinery. These combined studies provide novel information on two critical processes that maintain genetic and epigenetic stability in eukaryotes.

TABLE OF CONTENTS

CHAPTER 5

LIST OF FIGURES

CHAPTER 1

CHAPTER 2

CHAPTER 4

LIST OF TABLES

CHAPTER 2

Chapter 1

Introduction

1.1 Overview of Genome and Epigenome Maintenance

The *Homo sapiens* somatic nucleus contains two copies of the human genome that, at around three billion base pairs of DNA per copy, would measure nearly 2.5 meters in length if extended from end to end (Venter et al., 2001; Weier et al., 1995). The vast blueprint for the human organism is packaged *in vivo* into nuclei that average only around 8 μm in diameter (Greeley et al., 1978). This remarkable feat of compaction is achieved by assembling genomic DNA into a complex of DNA, RNA, and proteins known as chromatin. The packaging of eukaryotic DNA into chromatin allows for much more than compaction, however. Chromatin is protective—DNA that is packaged into chromatin is less susceptible to damage from reactive oxygen species, a common byproduct of oxidative metabolism (Enright et al., 1992). In addition, the packing of DNA into chromatin also endows upon cells the remarkable ability to regulate access to specific regions of the genome. The regulated access to DNA is the cornerstone strategy that cells use to control transcriptional programs for all cellular functions, including differentiation from pluripotent stem cells into specific cell types and responses to environmental and endogenous stimuli (Arney, 2004; Jaenisch and Bird, 2003; Rossetto et al., 2010). In short, the packaging of DNA into chromatin is fundamental for cellular identity and function, and is therefore essential to life in eukaryotes.

While the packaging of DNA into chromatin offers many advantages, it also raises formidable challenges. If DNA is packaged incorrectly, for example due to a mutation in a chromatin remodeling enzyme, the ensuing alterations in gene transcription

can contribute to the development of cancer even in the absence of a hypermutagenic state (Lee et al., 2012; McKenna et al., 2008). Furthermore, if chromatin is not correctly remodeled around damaged DNA in order to facilitate the recruitment and activity of repair enzymes, the repair process can fail, leading to cell death (Price and D'Andrea, 2013). On a global level, the entire structure of chromatin packaging the genome, known as the epigenome, must be disrupted in order for the replication machinery to access and duplicate the DNA sequence (MacAlpine and Almouzni, 2013). Following disruption, correct chromatin packaging then needs to be faithfully reestablished in order to maintain the transcriptional programs that characterize cell identity and function. Genome and epigenome stability are therefore intricately linked processes that require multiple mechanisms, many of which are poorly understood, to ensure their fidelity. In this dissertation, I have explored the mechanisms that contribute to genome and epigenome stability during two essential cellular processes—DNA double-strand break repair and DNA replication. In addition, I present optimizations to two recently developed techniques— isolation of proteins on nascent DNA (iPOND) and its native derivative protocol accelerated native iPOND (aniPOND) – that promise to help unlock novel mechanisms that link genome and epigenome stability.

1.2 Critical Mechanisms of Genome Stability

1.2.1 *DNA Double-Strand Break Repair*

Of the many lesions that can afflict genomic DNA, none are more toxic than DNA double-strand breaks (DSBs). While the frequency of DSBs is low, with an estimated ~10 DSBs generated daily in a dividing human cell compared to over 10,000

DNA lesions resulting from other types of damage (Lieber, 2010a; Lindahl, 1993), it is critical that these rare but highly genotoxic lesions be accurately repaired to prevent cellular outcomes that include senescence (Noda et al., 2013), apoptosis (Roos and Kaina, 2013), and potentially oncogenic genome instability (McKinnon and Caldecott, 2007). Notably, DSB misrepair has been demonstrated to lead to insertions, deletions, chromosomal translocations, and a loss of heterozygosity (LOH) of tumor suppressor genes (Ceccaldi et al., 2016; Kramer et al., 1994; Moynahan and Jasin, 1997).

Cells are equipped with two major pathways to effect the repair of DSBs. The first, non-homologous end joining (NHEJ), is a template and cell-cycle independent process that involves the direct re-ligation of broken ends (Lieber, 2010a). While usually an accurate process if the DNA ends are ligatable, end joining can lead to insertions or deletions when the bases are damaged to the extent that they require additional end processing in order to make the ends suitable for ligation (Bétermier et al., 2014). The second major pathway of DSB repair is homologous recombination (HR). Unlike NHEJ, HR is a cell-cycle dependent process that requires a homologous donor sequence, generally a sister chromatid, in order to replace the damaged segment of DNA (Sung and Klein, 2006). It is important for cells to use the correct DSB repair pathway based on cell cycle phase and lesion context. For example, cells tightly regulate the expression and function of components of the HR machinery to ensure that recombination occurs predominantly in late S-G2 phases when a sister chromatid is present, as inappropriate recombination in G1 between homologous chromosomes can lead to LOH (Panier and Durocher, 2013). In contrast, cells regulate the NHEJ and HR machinery to ensure the use of of HR to repair DSBs on replicating chromosomes (Lee et al., 2015; Sonoda et al.,

1998). Thus, cells tightly regulate the control of DSB repair pathway choice to ensure the correct pathway is utilized for optimal repair outcomes (Chapman et al., 2012).

A schematic of the general mechanisms of DNA DSB repair in the context of pathway choice is presented in **Fig 1.1**. As shown in **Fig 1.1** (right), in the case of NHEJ, the DSB is recognized by NHEJ-promoting KU complex, which binds to DSB ends with very high affinity (Blier et al., 1993). In yeast, KU forms a higher order complex with Nej1, Dnl4-Lif1, and the Mre11/Rad50/Xrs2 complex (MRX) that serves to bridge the DNA ends in order to maintain their intermolecular proximity and seal the break

(Chen and Tomkinson, 2011; Davis and Chen, 2013; Zhang et al., 2007). In mammals, the canonical end joining (c-NHEJ) complex consists of KU, XLF, Lig4-XRCC4, DNA-PKcs, and Artemis (Lieber, 2010a). Interestingly, Lig4-independent end joining events by a backup mechanism known as alternative-NHEJ (alt-NHEJ) have been identified (Bennardo et al., 2008). DSB repair by alt-NHEJ, including by the microhomology-mediated end joining (MMEJ) pathway, is implicated in mutagenesis due to increased limited end resection that reaveals microhomologies. There is, however, an alternate view emerging in which alt-NHEJ pathways may play a physiological role in promoting cell survival as a backup pathway when HR fails (Sfeir and Symington, 2015).

In contrast to NHEJ, the HR pathway is initiated by the formation of a key repair intermediate— 3′ single-strand DNA (ssDNA). As illustrated in **Fig 1.1** (left), in the case of HR, when MRX (Mre11/Rad50/Nbs1, MRN in mammals) association predominates at the break, it will form a complex with Sae2 (CtIP in mammals) to digest the 5′ strands for a distance of 100-300 bp, leaving 3′ ssDNA overhangs that are a poor substrate for KU

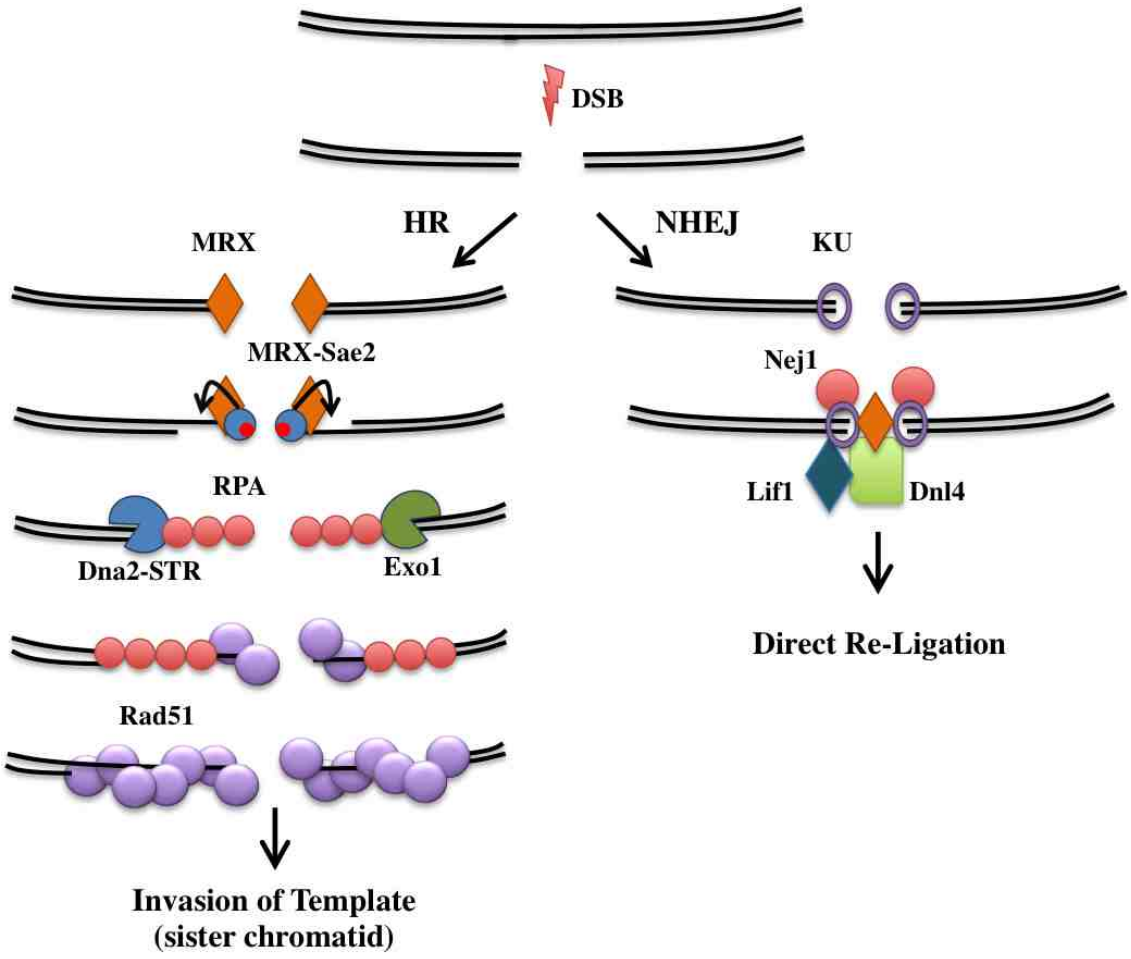

Figure 1.1. DNA double-strand break repair and pathway choice between HR and NHEJ in budding yeast. During NHEJ (right), the KU complex recognizes the DSB ends and recruits the associated end joining factors Nej1, Lif1, Dnl4, and MRX to stabilize and ligate the ends. During HR (left), the MRX complex stabilizes on DSB ends and interacts with Sae2 to initiate the processing of the 5′ break ends, producing 3′ ssDNA overhangs that are extended by the long-range exonucleases Exo1 and Sgs1-Dna2. The ssDNA is coated first by RPA followed by active replacement with the Rad51 nucleofilament that proceeds to strand invasion of the homologous template.

binding (Foster et al., 2011; Garcia et al., 2012; Zhu et al., 2008). The initial short overhangs are then extended for many kilobases in both directions from the break to generate long stretches of recombinogenic ssDNA in a process termed long-range resection (Daley et al., 2015; Garcia et al., 2012). The long-range resection machinery consists of two separate factors, Exonuclease 1 (Exo1) and the nuclease/helicase complex Dna2-Sgs1/Top3/Rmi1 (Dna2-STR; BLM-Topo IIIα/RMI1/RMI2, BTR in mammals), that operate independently and redundantly to process breaks (Daley et al., 2014; Ferretti et al., 2013; Zhu et al., 2008). The ssDNA is first coated by Replication Protein A (RPA), which serves both to repel KU association with breaks and to stimulate the activity of long-range resection enzymes (Chen et al., 2013a; Krasner et al., 2015). RPA is then actively replaced by the Rad51 recombinase, which forms a nucleoprotein filament that mediates a search for homology in the donor template and subsequent strand invasion of the donor template (Krejci et al., 2012; Zhou and Wang, 2004). Following invasion of the template, repair synthesis occurs, followed by second end capture and formation of a double Holliday junction, which is finally resolved by the actions of a class of structure specific endonucleases termed resolvases (Jasin and Rothstein, 2013; Wyatt and West, 2014). After ligation by a DNA ligase enzyme (see **Chapter 1.2.3.**), the repair process is complete.

As the generation of ssDNA effectively selects HR versus NHEJ, cells regulate DNA end resection on multiple levels. First, the expression of components of the resection machinery is regulated during the cell cycle with their activities stimulated by CDK-dependent phosphorylation events to ensure that resection pathways are only fully active in S-G2 phases (Huertas et al., 2008; Symington, 2016; Tomimatsu et al., 2013).

Second, proteins that block end resection associate to a greater extent with DSBs in G1 phase. These include KU and yeast Rad9 (53BP1 in mammals) (Bunting et al., 2010; Ferrari et al., 2015; Lee et al., 2015; Mimitou and Symington, 2010). In S-G2 phases, KU is phosphorylated in a manner that decreases its affinity for DSBs to assist in its removal from break ends. In addition, yeast Fun30 removes Rad9, and mammalian Brca1 removes 53BP1 (Chen et al., 2013b; Eapen et al., 2012; Lee et al., 2015; Roy et al., 2012).

The essential roles of DSB repair in maintaining genome stability are evident from the observed genome instability and cancer predisposition syndromes that occur upon inactivation or deregulation of DSB repair proteins (Hanahan and Weinberg, 2011; Hoeijmakers, 2001). Conversely, the targeting of DSB repair defects in cancer cells is a promising avenue for therapeutic intervention (Helleday et al., 2008; Kelley et al., 2014). For example, targeting the HR defect observed in BRCA1$^{-/-}$ and BRCA2$^{-/-}$ breast and ovarian cancer cells with PARP inhibitors was the first major successes in targeting a DNA repair defect in cancer therapy (Bryant et al., 2005). The synthetic lethality of PARP inhibitors in *BRCA1* and *BRCA2* mutant cancers is thought to be mediated by multiple mechanisms, including an increased dosage of cellular DSBs due to impaired PARP-mediated SSB repair, abnormal stabilization of PARP-1 on DNA leading to obstruction of replication forks, and a loss of PARP1-mediated replication fork restart that is essential in the absence of HR (Helleday, 2011).The growing utility of targeting repair pathways in cancer is perhaps second only to the targeting of the most important pathway for genome stability—DNA replication.

1.2.2 *DNA Replication*

Due to the antiparallel nature of duplex DNA strands and the defined 5′ to 3′ polarity of DNA synthesis, one strand is synthesized in a continuous manner while the opposite strand is synthesized discontinuously in short segments known as Okazaki fragments (Ogawa and Okazaki, 1980; Watson and Crick, 1953; Watson and Baker, 2008). The basic reactions that characterize these two mechanisms, known as leading- and lagging-strand synthesis, respectively, are illustrated in **Fig 1.2** and are further expanded upon below.

Pre-replication complexes are assembled in the G1 phase and their firing during S phase is tightly controlled (Bell and Labib, 2016). After replication forks have fired in S phase, the strands in front of the advancing replication fork are separated by the actions of the eukaryotic replicative helicase, the CMG (Cdc45/MCM/GINS) complex (Kang et al., 2012). The engine of the CMG complex is the MCM helicase, a heterohexameric complex belonging to the AAA+ superfamily of ATPase enzymes (Bochman and Schwacha, 2009). By itself, MCM will only unwind ~200bp of DNA before dissociating (Bochman and Schwacha, 2009). However, during *in vivo* replication, both Cdc45 and the Sld5/Psf1/Psf2/Psf3 (GINS) complex associate with MCM to increase its processivity and activity (Bell and Labib, 2016). After CMG unwinds the duplex DNA strands, the ssDNA is coated by Replication Protein A (RPA), a heterotrimeric protein complex that is the eukaryotic homolog of the bacterial single-strand DNA-binding protein (SSB), which contributes important roles in replication initiation, elongation, and DNA damage signaling (Iftode et al., 1999; Zou et al., 2006). During DNA replication, RPA stimulates the activity of DNA polymerases and contributes to the recruitment and regulation of other replication factors (Oakley and Patrick, 2010).

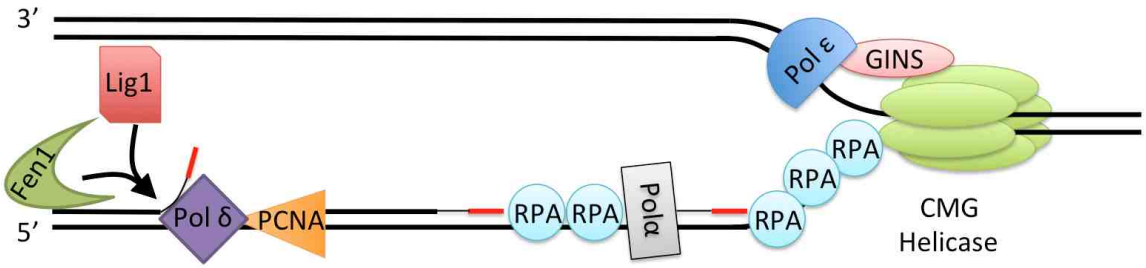

Figure 1.2. Model of semiconservative DNA replication in eukaryotes. The CMG helicase complex separates duplex DNA in front of the advancing replication fork. The leading-strand (top) is synthesized in a continuous manner by the processive polymerase Pol ε, which is targeted to the leading-strand by an interaction with the GINS complex. The lagging-strand (bottom) is synthesized discontinuously in short segments known as Okazaki fragments. Pol α/Primase initiates Okazaki fragment synthesis by depositing a short RNA/DNA hybrid primer. Single-stranded DNA is coated by RPA until the processive polymerase Pol δ, which is directed to the lagging-strand by an interaction with PCNA, fills the gap between Okazaki fragments. Pol δ/PCNA displaces the previous primer, after which it is cleaved by Fen1 and the nick is sealed by Lig1, creating a continuous strand of DNA.

Three DNA polymerases catalyze the canonical reactions of DNA replication. DNA polymerase α (Pol α)/Primase is a four subunit complex that primes the synthesis of the new DNA strands by depositing a short hybrid RNA/DNA primer (Muzi-Falconi et al., 2003; Perera et al., 2013). On the leading-strand, this primer is extended by the highly processive DNA polymerase ε (Pol ε), whereas on the lagging-strand the primers for each Okazaki fragment are extended by the processive DNA polymerase δ (Pol δ) (Kunkel and Burgers, 2014). Strand specificity for each of the replicative DNA polymerases is mediated in part by protein interactions: Pol ε is targeted to the leading-strand by an interaction with the GINS complex whereas Pol δ is targeted to the lagging-strand by an interaction with the replicative sliding clamp Proliferating Cell Nuclear Antigen (PCNA)

(Bermudez et al., 2011; Langston and O'Donnell, 2008; Lu et al., 2002). Studies with *in vitro* reconstituted replication factors and DNA templates have demonstrated that Pol ε is processive on the leading-strand due to its preferential interaction with CMG. In contrast, Pol δ strongly outcompetes Pol ε in competitive binding study with PCNA, supporting the model that specific interactions between CMG and PCNA asymmetrically target Pol ε to the leading-strand and Pol δ to the lagging-strand, respectively (Georgescu et al., 2014). While Pol δ can partially compensate for the loss of Pol ε in reconstituted leading-strand replication reactions, this enzyme is distributive and not processive in leading-strand replication, leading to a reduced rate of replication (Georgescu et al., 2014). The partial activity of Pol δ on the leading-strand supports genetic studies from yeast demonstrating that the polymerase activity Pol ε is not essential for cell viability. Pol ε polymerase mutants do, however, proceed slowly through S-phase, thereby supporting the observation that Pol δ inefficiently replicates the leading-strand (Dua et

al., 1999; Kesti et al., 1999). It is of note that the polymerase strand specificity model has faced some challenges (Johnson et al., 2015). Indeed, recent *in vitro* reconstituted replication reactions have shown that leading-strand synthesis is most efficient when Pol δ initiates synthesis, followed by polymerase switching to Pol ε (Yeeles et al., 2017). Moreover, while Pol ε can polymerize *in vitro* lagging-strand synthesis, the resulting Okazaki fragments are non-ligatable (Devbhandari et al., 2017). Therefore, recent data supports an amendment of the classical strand specificity model to include Pol δ as a factor that facilitates and can serve as backup for leading-strand synthesis, while Pol ε appears restricted to the leading strand (Devbhandari et al., 2017; Yeeles et al., 2017).

Multiple challenges to genome stability can occur during DNA replication. First, mutations can arise when bases are misincorporated by polymerases (Kunkel, 2004). While the proofreading exonuclease activity of the processive DNA polymerases reduces the error rate from 10^{-4} – 10^{-6} to 10^{-7} to 10^{-8} (Kunkel, 2004), a number of errors are still retained in the daughter strands. Under normal circumstances, the misincorporated bases are precisely excised and replaced by correctly matched bases by the mismatch repair (MMR) pathway (Modrich, 2006). Both polymerase proofreading activity and MMR are frequently inactivated in tumors (Modrich, 2006; Rayner et al., 2016). An alternative form of misincorporation is the accidental incorporation of ribonucleotides instead of deoxyribonucleotides during replication, a process that is reversed by the enzymes RNAse H1 and RNAse H2 or topoisomerase I (Lazzaro et al., 2012; Reijns et al., 2012; Williams et al., 2016). Ribonucleotides need to be removed from DNA due to their ~100,000x greater propensity for spontaneous base hydrolysis compared with deoxyribonucleotides, and because of their topological effects on DNA structure that

impact chromatin compaction and cell function (Dalgaard, 2012). That removal of ribonucleotides from DNA is important for human health is illustrated by Aicardi-Goutières syndrome, which is caused by hypomorphic mutations of RNase H2 that lead to severe inflammation in childhood (Crow et al., 2006).

Another source of replication errors occurs when replication forks encounter obstacles such DNA lesions or transcription complexes (Yeeles et al., 2013). On the lagging-strand, lesions are not always problematic because the frequent priming of new Okazaki fragments by Pol α/Primase allows lagging-strand synthesis to continue by skipping over blockages (Yeeles et al., 2013). Following replication, remaining lagging-strand ssDNA gaps are repaired by postreplication repair (Broomfield et al., 2001). On the leading strand, however, blocking lesions are considered more problematic due to the fact that CMG translocates upon the leading-strand and because the leading-strand is much less frequently re-primed compared with lagging-strand synthesis (Fu et al., 2011). In order to allow synthesis to continue past a blocking lesion, a conserved class of DNA polymerases known as trans-lesion synthesis (TLS) polymerases are recruited to the fork by an interaction with ubiquitylated PCNA (Ulrich and Takahashi, 2013). TLS polymerases have specialized structures that allow them to place a base opposite a lesion (Waters et al., 2009). Due to their being more error prone than the processive DNA polymerases Pol δ and Pol ε, TLS polymerases can introduce errors that contribute to carcinogenesis (Makridakis, 2012). Additionally, some cancers rely upon TLS polymerases to bypass chemotherapy-introduced lesions, leading to the active investigation of small molecular TLS inhibitors as novel targeted chemotherapy agents (Korzhnev and Hadden, 2016). In addition to TLS bypass synthesis during replication,

some studies have also supported a model in which the leading-strand is able to be re-primed and the lesions repaired by TLS polymerases in a post-replicative manner (Daigaku et al., 2010; Karras and Jentsch, 2010). Therefore, it is likely that both TLS and fork restart are utilized to ensure that replication continues to completion.

If the replication fork is unable to bypass a lesion, or if the fork encounters a SSB, replication forks can collapse into one-end DSBs that require HR to allow the fork to restart (Hashimoto et al., 2011). The mechanism of HR-mediated fork restart resembles a subpathway of HR known as break-induced replication (BIR), in which recombination establishes a unidirectional replication fork that can be copied until the end of the chromosome (Anand et al., 2013; Lydeard et al., 2010). Alternatively, forks may reverse and then restart in a Rad51-mediated mechanism (Zellweger et al., 2015). The mechanisms that guard genome stability during replication are further discussed below in the context of the enzymes that perform the final step in all repair processes— DNA ligases.

1.3 Role of DNA Ligase Enzymes in Genome Stability

Excerpted from: Tomkinson, A.E., Howes, Timothy R.L, and Wiest, N.E. (2013). DNA ligases as therapeutic targets. *Translational Cancer Research* 2(3): 203-214.

1.3.1 *Overview of DNA Ligases and Genome Stability*

The identification of DNA repair defects in inherited human diseases that are characterized by predisposition to cancer, including inherited forms of colon and breast cancer, provides compelling evidence that the cellular mechanisms that maintain genome

stability play a critical role in suppressing cancer formation (Friedberg et al., 2005). Since genomic instability is a hallmark feature of sporadic as well as hereditary cancers, it is likely that alterations in one or more of the mechanisms that maintain genome stability occur at some stage during the development of most cancers. Although it has been assumed that these alterations in the DNA damage response contribute, at least in part, to the therapeutic activity of cytotoxic DNA damaging agents such as cis-platinum and doxorubicin, they remain poorly characterized, particularly in sporadic cancers. The recent development of poly (ADP-ribose) polymerase inhibitors as therapeutics that selectively target the DNA repair defect in hereditary breast cancers has stimulated interest in defining abnormalities in the DNA damage response in sporadic cancers and the development of inhibitors of other DNA repair proteins that may have utility as anti-cancer agents (Lord and Ashworth, 2008). Since DNA joining is required to complete almost all DNA repair events and there are three human genes encoding DNA ligases with different but overlapping functions in DNA replication and repair (Ellenberger and Tomkinson, 2008), DNA ligase inhibitors with defined specificity can potentially be combined with different DNA damaging agents to target a wide variety of DNA repair pathways. In this review, we summarize our current understanding of the cellular functions of human DNA ligases (**Fig 1.3**) and recent studies that identify DNA ligases as potential biomarkers for abnormal DNA repair and demonstrate the potential clinical utility of DNA ligase inhibitors in cancer treatment (Newman et al., 2015; Rassool and Tomkinson, 2010; Tomkinson et al., 2013)

Involvement of Human DNA Ligases in DNA Replication and Repair Pathways	
Nuclear DNA Metabolism	
DNA Replication	DNA ligase I DNA ligase III (backup)
Mismatch Repair	Unknown
Base Excision Repair	DNA ligase III (short-patch) DNA ligase I (long-patch)
Nucleotide Excision Repair	DNA ligase III (constitutive) DNA ligase I (S-phase)
Single-Strand Break Repair	DNA ligase III (short-patch) DNA ligase I (long-patch)
Homology-Mediated Double-Strand Break Repair	Unknown
Non-Homologous End Joining Double-Strand Break Repair	DNA ligase IV DNA ligase III (alternative) DNA ligase I (alternative)
Mitochondrial DNA Metabolism	
DNA Replication	DNA ligase III
DNA Repair	DNA ligase III

Figure 1.3. Roles of the three eukaryotic DNA ligases in DNA replication and repair pathways.

1.3.2 *Structure and Function of Human DNA Ligases*

DNA ligases maintain the integrity of the phosphodiester backbone of duplex DNA by catalyzing phosphodiester bond formation (Ellenberger and Tomkinson, 2008). All DNA ligases utilize the same three-step reaction mechanism (**Fig 1.4**). In humans, the DNA ligases encoded by the three *LIG* genes are ATP-dependent (Ellenberger and Tomkinson, 2008). In step 1, ATP is hydrolyzed, resulting in the covalent linkage of an AMP moiety to a specific lysine residue within the DNA ligase active site and the release of pyrophosphate. Next, the AMP moiety is transferred from the adenylated ligase to the 5' terminus of a DNA nick with 5' phosphate and 3' hydroxyl termini, generating a DNA-adenylate intermediate. Finally, the non-adenylated DNA ligase interacts with the DNA adenylate and, using the 3' hydroxyl as a nucleophile, links the termini via a phosphodiester bond, releasing AMP.

Human DNA ligases and other ATP-dependent DNA ligases contain a common catalytic core consisting of an oligonucleotide/oligosaccharide binding- fold (OB-fold) domain and an adenylation domain (AdD) that are found in all DNA ligases and other nucleotidyl transferases including RNA ligases and mRNA capping enzymes (Ellenberger and Tomkinson, 2008). While these two domains comprise the minimum unit that can perform the DNA ligation reaction, the activity of the catalytic core of human DNA ligases is greatly enhanced by an additional conserved N-terminal DNA-binding domain (DBD) (Ellenberger and Tomkinson, 2008; Pascal et al., 2004). In the absence of DNA, the catalytic region of human DNA ligases encompassing the OB-fold, AdD and DBD adopts an extended, asymmetric conformation (Ellenberger and

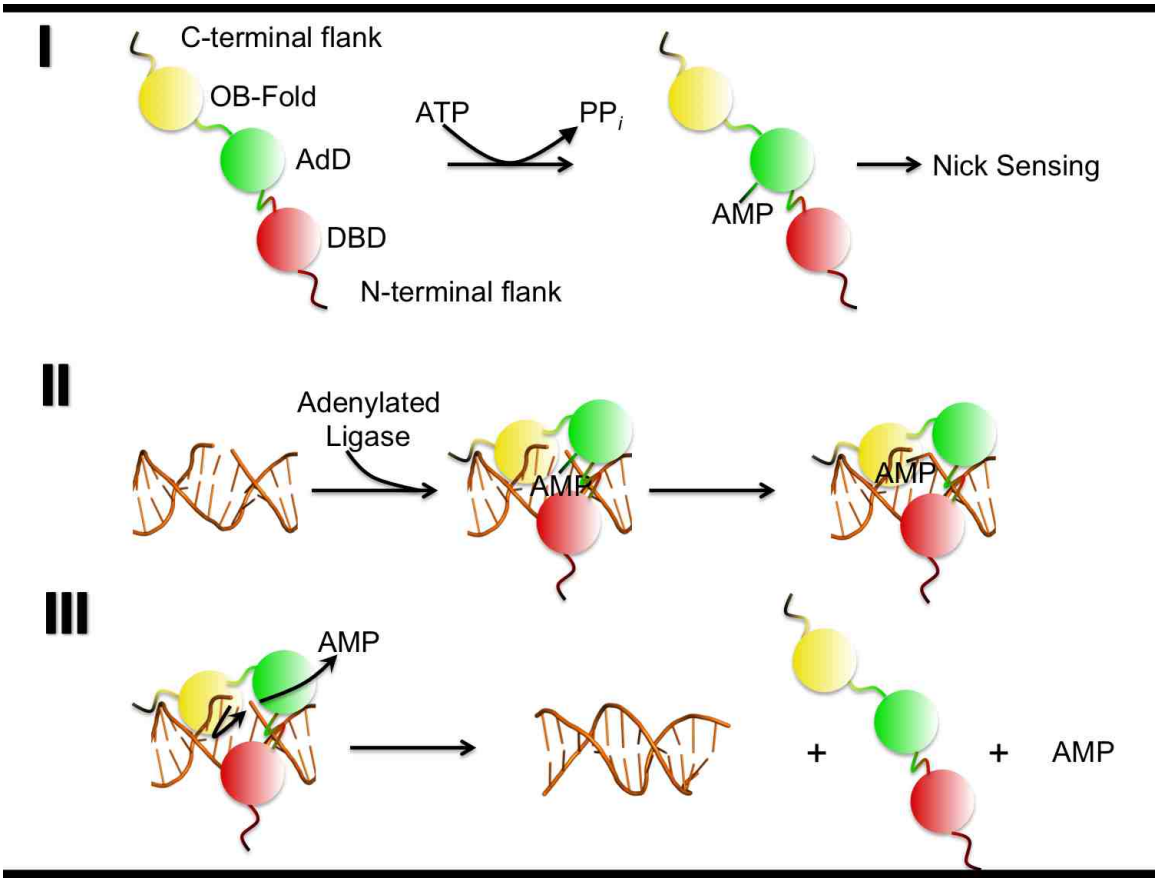

Figure 1.4. Steps in the DNA ligation reaction. (I) The catalytic region of the DNA ligase consisting of the DNA binding domain (DBD, red), adenylation domain (AdD, green) and oligonucleotide/oligosaccharide binding-fold (OB-Fold, yellow), interacts with ATP to adenylate an active site lysine within the adenylation domain (AdD, green), releasing pyrophosphate; (II) When the adenylated ligase recognizes and binds to a DNA nick, it undergoes a conformational change such that the DBD, AdD and OB-fold encircle the nick. Within this compact structure, the AMP moiety is transferred from the ligase polypeptide to the 5' phosphate of the nick; (III) The non-adenylated ligase polypeptide utilizes the 3' hydroxyl terminus of the nick as a nucleophile to attack the 5' DNA-adenylate, resulting in phosphodiester bond formation and the release of the ligase polypeptide and AMP

Tomkinson, 2008; Tomkinson et al., 1990). The structures of the catalytic regions of DNA ligase I and DNA ligase III revealed that these enzymes form similar ring-shaped structures around nicked DNA. Thus, the catalytic regions of the DNA ligases are flexible and undergo large conformational changes during the ligation reaction. It is assumed that the catalytic region of DNA ligase IV will behave in a similar manner. Recently, the structure of the DBD of DNA ligase IV was determined by X-ray crystallography in the absence of DNA (De Ioannes et al., 2012). As expected, the DBD of DNA ligase IV has a similar overall structure to the DBDs of DNA ligases I and III. Notably, the availability of atomic resolution structural information has permitted the use of rational structure-based approaches to identify small molecule inhibitors of human DNA ligases.

In contrast to the DBD and catalytic core of human DNA ligases I, III and IV, the regions in these enzymes adjacent to the catalytic region are much more diverse. Furthermore, unlike the *LIG1* and *LIG4* genes, the *LIG3* gene encodes multiple DNA ligase polypeptides that have different N- and C-terminal regions (**Fig 1.5**). An alternative translation initiation mechanism generates polypeptides that either have or lack an N-terminal mitochondrial localization signal from *LIG3* mRNA (Lakshmipathy and Campbell, 1999). This signal sequence is removed during entry into mitochondria and so the nuclear and mitochondrial versions of DNA ligase IIIα encoded by this mRNA transcript are very similar in size. In addition, a germ cell-specific alternative splicing mechanism generates polypeptides with different C-terminal sequences

(Dulic et al., 2001; Mackey et al., 1997). At the C-terminus of the DNA ligase IIIα polypeptide there is a breast and ovarian cancer susceptibility protein 1 C-terminal

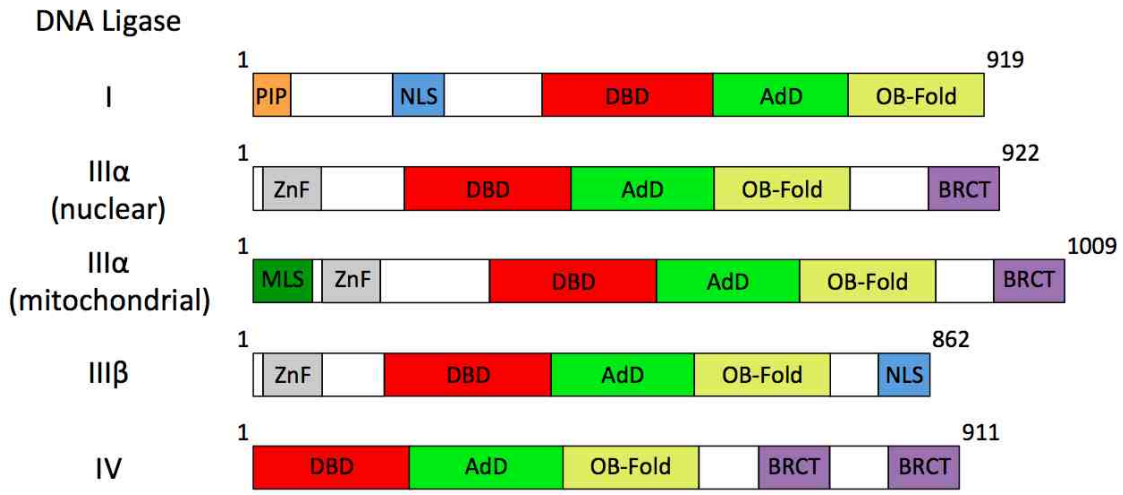

Figure 1.5. DNA ligase polypeptides encoded by the human *LIG* genes. All DNA ligases contain a conserved catalytic region consisting of a DNA-binding domain (DBD, red), an adenylation domain (AdD, green) and an oligosaccharide/oligonucleotide binding-fold (OB-Fold, yellow) domain. The *LIG1* gene encodes a single polypeptide with a nuclear localization signal (NLS, blue) and proliferating cell nuclear antigen interacting box (PIP, orange) motif within a non-catalytic N-terminal region. The *LIG3* gene encodes multiple polypeptides, each of which contain an N-terminal zinc-finger (ZnF, grey). Mitochondrial and nuclear DNA ligase IIIα are generated by alternative translation initiation with the mitochondrial version having an N-terminal mitochondrial localization signal (MLS, dark green). Both of the DNA ligase IIIα polypeptides have a C-terminal breast and ovarian cancer susceptibility protein 1 C-terminal (BRCT, purple) domain. An alternative splicing event in male germ cells generates DNA ligase IIIβ which has a C-terminal nuclear localization signal (NLS, blue) in place of the BRCT domain. The *LIG4* gene encodes a single polypeptide that contains two C-terminal BRCT domains separated by a linker region.

(BRCT) domain that mediates an interaction with the C-terminal BRCT domain of nuclear DNA repair protein X-ray cross complementing protein 1 (XRCC1)

(Caldecott et al., 1994; Mackey et al., 1997; Nash et al., 1997). Structural analysis of the BRCT-BRCT heterodimer revealed that residues adjacent to the XRCC1 domain contribute to heterodimer interface, favoring formation of the DNA ligase IIIα/XRCC1 heterodimers rather than homodimers of DNA ligase IIIα and XRCC1 (Cuneo et al., 2011). In the DNA ligase IIIβ polypeptide, the C-terminal BRCT domain is replaced by a short sequence that acts as a nuclear localization signal (Mackey et al., 1997). All the DNA ligase III polypeptides have an N-terminal zinc finger domain (ZnF) that, in concert with the DBD, plays a key role both in the initial recognition of DNA strand breaks and intermolecular ligation (Cotner-Gohara et al., 2008; Mackey et al., 1999; Taylor et al., 1998). BRCT domains also occur in DNA ligase IV. In this case, there are two tandemly arrayed BRCT domains within the C-terminal region of DNA ligase IV. As with DNA ligase IIIα, the DNA ligase IV BRCT domains are critical for an interaction with a partner protein, the DNA repair protein X-ray cross complementing protein 4 (XRCC4)

(Grawunder et al., 1997; 1998a; 1998b). Structural studies have shown that within the DNA ligase IV/XRCC4 complex, the two BRCT domains encircle the coiled-coil region of the XRCC4 homodimer and that the linker region between the BRCT domains of DNA ligase IV makes the majority of the contacts with XRCC4 (Doré et al., 2006; Sibanda et al., 2001; Wu et al., 2009). The only recognizable motifs within the N-terminal region of DNA ligase I are a nuclear localization signal and a proliferating cell nuclear antigen (PCNA) interacting protein (PIP) box which, as the name suggests, interacts with PCNA (Levin et al., 1997; Montecucco et al., 1998; 1995).

1.3.3 *Cellular Functions of Human DNA Ligases*

Nuclear DNA Replication

There is compelling evidence that DNA ligase I is the major replicative DNA ligase (Ellenberger and Tomkinson, 2008; Howes and Tomkinson, 2012). Human DNA ligase I is recruited to nuclear DNA replication foci via its PIP box-dependent interaction with PCNA (Montecucco et al., 1998). In addition, it also interacts with replication factor C (RFC), a clamp loader that loads the trimeric PCNA ring onto DNA during Okazaki fragment synthesis (Levin et al., 2000; Vijayakumar et al., 2009). Finally, cell lines (46BR and 46BR.1G1) established from an immunodeficient human patient with mutated *LIG1* alleles have reduced DNA ligase I activity and severely impaired Okazaki fragment joining (Barnes et al., 1992; Henderson et al., 1985; Levin et al., 2000). As expected, DNA ligase I activity is essential for embryogenesis in mice but, surprisingly, it was possible to establish cell lines from *Lig1* null embryos that had a defect in joining Okazaki fragments similar to the human 46BR cell lines (Bentley et al., 1996; 2002). The viability of *Lig1* null cells indicates that another DNA ligase participates in nuclear DNA replication in the absence of DNA ligase I. Recent studies in chicken DT40 and human cells have shown that DNA ligase IIIα but not DNA ligase IV, is essential for nuclear DNA replication in the absence of DNA ligase I (Arakawa et al., 2012; Le Chalony et al., 2012). XRCC1, which interacts with and stabilizes nuclear DNA ligase IIIα, and poly (ADP-ribose) polymerase 1 (PARP-1), which initiates the repair of DNA single strand breaks (SSB)s (Caldecott et al., 1994; 1995; Nash et al., 1997; Okano et al., 2003), are also required for nuclear DNA replication in DNA ligase I-deficient cells. Thus, it appears that, in the absence of DNA ligase I, Okazaki fragment joining is accomplished,

at least in part, through a SSB repair mechanism in which ADP-ribosylated PARP-1 recruits the DNA ligase IIIα/ XRCC1 complex via its interaction with XRCC1 (Le Chalony et al., 2012).

Mitochondrial DNA replication and repair

Genetic inactivation of the mouse *Lig3* gene results in embryonic lethality at an even earlier stage than *Lig1* and *Xrcc1* null embryos (Bentley et al., 1996; 2002; Puebla-Osorio et al., 2006; Tebbs et al., 1999). Furthermore, although *Lig1* and *Xrcc1* deficient mouse embryonic cell lines were established from the embryos (Bentley et al., 1996; 2002; Tebbs et al., 1999), it was not possible to establish a *Lig3* null cell line, suggesting that the *Lig3* gene is required for cell viability (Puebla-Osorio et al., 2006). This has been confirmed in recent studies showing that the *Lig3* gene is indeed essential because it encodes the only mitochondrial DNA ligase (Gao et al., 2012; Simsek et al., 2012). These observations were predicted by earlier studies showing that alternative translation initiation generates nuclear and mitochondrial versions of DNA ligase IIIα and that mitochondrial DNA ligase IIIα functions independently of XRCC1 (Lakshmipathy and Campbell, 1999; 2000). Furthermore, depletion of DNA ligase IIIα levels by siRNA resulted in reduced numbers of copies of the mitochondrial genome and increased accumulation of SSBs in mitochondrial DNA (Lakshmipathy and Campbell, 2001). Thus, mitochondrial DNA ligase IIIα plays an essential and unique role in the replication and repair of the mitochondrial genome (**Fig 1.3**).

Nuclear DNA Excision Repair

There are three pathways that excise mismatched and/or damaged bases from DNA: mismatch repair (MMR), base excision repair (BER) and nucleotide excision repair (NER). The major function of the MMR pathway is to correct mistakes in newly synthesized DNA made by the DNA replication machinery (Friedberg et al., 2005). Although significant progress has been made in elucidating the molecular mechanism of MMR, the identity of the DNA ligase (or DNA ligases) that completes this repair pathway has not been established definitively.

There is compelling evidence linking both DNA ligase I and DNA ligase IIIα with BER. This repair pathway is initiated when a DNA glycosylase recognizes and excises a damaged base (Friedberg et al., 2005). After the resultant abasic site is cleaved, there are two possible subpathways to complete the repair (Ellenberger and Tomkinson, 2008; Frosina et al., 1996; Kubota et al., 1996; Matsumoto et al., 1999). In short-patch BER, DNA polymerase β removes the remaining 5' sugar-phosphate residue and inserts a single nucleotide, generating a ligatable nick that is sealed by the DNA ligase IIIα/XRCC1 complex (Ellenberger and Tomkinson, 2008; Kubota et al., 1996). This pathway is thought to be active across the entire genome in non-dividing cells and throughout the cell cycle. In contrast, the long-patch BER pathway, in which a longer repair patch is inserted by either DNA polymerase δ or ε and repair is completed by the action of DNA ligase I in conjunction with FEN-1, appears to occur only during S phase and to be linked to the DNA replication machinery (Ellenberger and Tomkinson, 2008; Frosina et al., 1996; Matsumoto et al., 1999). Analysis of DNA ligase-deficient human and mouse cells have given paradoxical results regarding the contribution of DNA ligase I- and DNA

ligase IIIα-dependent BER to cell survival after DNA alkylation damage. For example, human DNA ligase I-deficient 46BR cells are sensitive to DNA alkylating agents (Levin et al., 2000; Teo et al., 1983a; 1983b), whereas *LIG1* null mouse embryonic fibroblasts and mouse embryonic fibroblasts that express a mutant version of DNA ligase I that is equivalent to the enzyme expressed in 46BR cells are not (Bentley et al., 1996; 2002; Harrison et al., 2002). This could be explained if DNA ligase I-dependent BER predominates in human cells whereas DNA ligase IIIα- dependent BER predominates in mouse cells. However, the characterization of mouse cells lacking nuclear DNA ligase IIIα led to the conclusion that DNA ligase I-dependent BER is the major pathway in the mouse cell-types examined (Gao et al., 2012; Simsek et al., 2012). These discrepancies may reflect differences in the relative contributions of DNA ligase I- and DNA ligase IIIα-dependent BER and the extent of the functional redundancy between these BER subpathways in different cell types.

Nucleotide excision repair (NER) removes helix-distorting lesions such as ultraviolet light (UV)-induced photoproducts (Friedberg et al., 2005). In contrast to BER, the DNA lesion is removed by the excision of an oligonucleotide 24-32 nucleotides in length, followed by repair synthesis and ligation (Friedberg et al., 2005). For many years it was assumed that human DNA ligase I completed NER ligation because of the UV light sensitivity of 46BR cells and the activity of DNA ligase I in conjunction with the replicative DNA polymerases δ and ε in reconstituted NER reactions (Aboussekhra et al., 1995; Araújo et al., 2000; Teo et al., 1983a). However, more recent studies have shown that DNA ligase I only accumulates at NER sites in proliferating cells, whereas DNA ligase IIIα and XRCC1 are recruited to NER sites regardless of cell cycle stage

(Moser et al., 2007). Thus, DNA ligase I appears to function in a S phase-specific subpathway of NER, whereas the DNA ligase IIIα/XRCC1 complex functions in an NER subpathway that is active in all phases of the cell cycle and presumably in non-dividing cells (Moser et al., 2007). As with BER, the relative contributions of DNA ligase I-and DNA ligase IIIα-dependent NER and the extent of the functional redundancy between these NER subpathways may vary between different cell types.

Nuclear SSB Repair

SSBs are generated in numerous different ways, including as repair intermediates during excision repair, by erroneous topoisomerase I activity, and by DNA damaging agents such as reactive oxygen species (ROS) (Caldecott, 2008). As mentioned above, DNA SSBs are predominantly detected by PARP-1 although PARP-2 may also contribute (Amé et al., 1999; Ménissier de Murcia et al., 2003). The binding of PARP-1 to SSBs activates its polymerase activity resulting in the synthesis of poly (ADP-ribose) chains on PARP-1 itself and other nearby proteins (Friedberg et al., 2005). The DNA ligase IIIα/XRCC1 complex is then recruited to SSBs primarily by an interaction between XRCC1 and poly (ADP-ribosylated) PARP-1 (Okano et al., 2003; 2005). Given the recruitment of XRCC1 and DNA ligase IIIα to SSBs, it was surprising that cells lacking nuclear DNA ligase IIIα did not exhibit a defect in SSB repair similar to cells with reduced levels of XRCC1 (Gao et al., 2012; Katyal and McKinnon, 2011; Simsek et al., 2012). Thus, it appears that there is an as yet poorly defined DNA ligase I-dependent SSB repair pathway (Katyal and McKinnon, 2011).

Nuclear DSB repair

As with SSBs, DSBs are produced by many different mechanisms. For example, they arise during programmed cell events including meiotic recombination and immunoglobulin gene arrangements (Friedberg et al., 2005). They are also generated during normal DNA replication and, to an even greater extent, during replicative stress. Finally, they can be generated either directly by the action of a DNA damaging agent or indirectly as a consequence of the replication fork encountering an unrepaired SSB (Friedberg et al., 2005). There are multiple repair pathways for these highly cytotoxic lesions that can be divided into two groups depending upon whether or not the repair reaction involves extensive DNA sequence homology (Lieber, 2010a; San Filippo et al., 2008). While the DNA ligases that participate in the homology-dependent DSB repair pathways have not been definitively identified, it is well-established that DNA ligase IV is a key component of the major non-homologous end-joining (NHEJ) pathway, which is functional throughout the cell cycle, repairs most DSB lesions and completes V(D)J recombination (Grawunder et al., 1998a). This pathway is initiated by the Ku70/Ku80 complex, which binds to DNA DSB ends and recruits the other components of the repair pathway, including DNA-dependent protein kinase catalytic subunit (DNA PKcs), Artemis and DNA ligase IV/ XRCC4 (Lieber, 2010a). A key step in NHEJ is the juxtaposition of DNA ends that is mediated by interactions between DNA PKcs molecules (DeFazio et al., 2002). In addition, there are multiple end processing activities that act on the juxtaposed DNA ends to generate ligatable termini (Lieber, 2010a). As a consequence of this end processing, NHEJ is characterized by small insertions and

deletions at the break site but usually the previously linked DNA ends are joined back together (Lieber, 2010a).

Several DNA ligase IV-deficient individuals have been identified with symptoms that include radiation sensitivity, immunodeficiency and developmental delay

(Girard et al., 2004; O'Driscoll et al., 2001; Riballo et al., 1999). As with the *LIG1* and *LIG3* genes, genetic inactivation of *LIG4* resulted in embryonic lethality in the mouse (Barnes et al., 1998; Frank et al., 1998). Cells that lack *LIG4* are viable

(Grawunder et al., 1998a; Lieber, 2010a), demonstrating that this repair pathway is not essential. Analysis of NHEJ-deficient cells revealed the presence of an alternative (alt) NHEJ pathway that also appears to be active in wild type cells albeit at a low level (Corneo et al., 2007; Fattah et al., 2010; Simsek and Jasin, 2010; Yan et al., 2007). Repair of DSBs by alt NHEJ is characterized by large deletions, resulting from extensive resection, and frequent chromosomal translocations (Lieber, 2010b; Nussenzweig and Nussenzweig, 2007). DNA ligase IIIα is the major enzyme acting in alt NHEJ but, surprisingly, this pathway does not appear to involve XRCC1 (Boboila et al., 2012; Simsek et al., 2011; Wang et al., 2005). There is also evidence for a minor DNA ligase I-dependent subpathway of alt NHEJ (Simsek et al., 2011).

1.4 Properties and Modification of Chromatin

1.4.1 *Organization of DNA into the Nucleosome*

The structure of chromatin is nonrandom. While preliminary models based upon interpretation of early X-ray diffraction studies suggested that the DNA may be coated with protein in a uniform superhelix (Paedon and Wilkins, 1972), evidence soon emerged

that DNA is instead packaged into repeating elements. A critical experiment supporting this hypothesis demonstrated that the digestion of chromatin with rat liver nuclease revealed a pattern of digestion in which fragments appeared at multiples of a minimum unit of length, suggesting that defined lengths of DNA were protectively packaged into a repeating structure (Hewish and Burgoyne, 1973). Efforts by many labs soon identified the elements of this basic repeating unit of chromatin, termed the nucleosome (reviewed in van Holde, 1989).

The nucleosome consists of a core of eight histone proteins consisting of two copies each of histones H2A, H2B, H3, and H4 that associate with ~146 bp of DNA, which wraps around the histone octamer core. Between adjacent nucleosomes is a stretch of DNA, termed linker DNA, that is more vulnerable to digestion by enzymes such as micrococal nuclease (Clark, 2010). The linker DNA of metazoans is normally occupied by the linker histone H1 that binds DNA at its entry and exit into the nucleosome, where it covers an additional 20 bp of DNA (Thomas, 1999). The length of DNA associated with a single nucleosome plus its associated linker DNA is known as the nucleosome repeat length (NRL). Interestingly, the NRL is shorter in simpler eukaryotes such as budding yeast (~165bp) and longer in humans (~200bp), with the most commonly found NRL in nature being 197 bp (Szerlong and Hansen, 2011; Widom, 1992). The length of the NRL has implications for chromatin compaction, as discussed below in chapter **1.3.2**.

A significant amount of information about the interaction between histones and DNA in the nucleosome was garnered by the first X-ray crystal structure of a nucleosome core particle assembled with 146 bp of DNA (Luger et al., 1997). In addition to revealing information about the interactions between core histone proteins, the structure revealed

information about the atomic interactions between the histone proteins and the DNA that account for the strong association of the nucleosome with DNA. These include nonpolar interactions with the deoxyribose groups and hydrogen bonds and ionic links that occur between the basic and hydroxyl side chain groups of the histone proteins and the phosphate oxygen atoms of the DNA (Luger et al., 1997). Another striking feature that the crystal structure highlighted is the protrusion of the N-terminal histone tails from the core structure (Luger and Richmond, 1998). Cells utilize the accessibility of these tails for post-translational modification (PTM), generating what is commonly referred to as the "histone code" (Strahl and Allis, 2000). The histone code regulates binding and activity of proteins for every nuclear process, including DNA compaction and DNA damage signaling, as discussed in section **1.4.3**.

1.4.2 *Chromatin Compaction* in vitro *and* in vivo

Many of the physiochemical properties of chromatin compaction were elucidated from early electron microscopy studies examining the effect of various ions and salt conditions on the structure of chromatin preparations (Finch and Klug, 1976; Thoma et al., 1979). It is from these early studies that the "beads on a string" model of nucleosomes first appeared. These studies identified that H1-containing chromatin forms an extended and relaxed conformation under very low salt conditions (0.2 mM EDTA, 1 mM TEACl), in which individual nucleosomes can be observed. Chromatin then condenses stepwise into higher order structures upon the addition of monovalent cations until reaching maximum in *vitro* compaction above 60 mM NaCl into a 300 Å (30 nm) fiber (van Holde, 1989). Compared with monovalent cations, divalent cations such as Mg^{2+}

powerfully compact chromatin, with maximum compaction being reached with only 0.5 mM Mg^{2+} (van Holde, 1989). H1-depleted chromatin has defects in cation-induced chromatin compaction and forms less compact and poorly defined structures, indicating that H1 plays a critical role in efficient compaction (Finch and Klug, 1976; Thoma et al., 1979; Woodcock et al., 1984). More recently, methods including real-time confocal microscopy of intact nuclei have been developed to determine the effects of osmolality on nuclear structure and chromatin compaction (Finan et al., 2008; Irianto et al., 2013). These studies demonstrated that compaction is proportional to osmolality within a physiologic range; however, exposing nuclei to osmotic extremes (either hyper or hypoosmotic) can lead to irreversible compaction, an observation that may have relevance in certain disease states (Irianto et al., 2013; Jäckle et al., 2001).

Although the compaction of chromatin into 30 nm fibers has been demonstrated *in vitro*, chromatin needs to compact multiple orders of magnitude more in order to reach the compaction levels observed in chromosomes *in vivo* (van Holde, 1989). Early microscopy studies of isolated chromosomes suggested that chromosomes are made up of multiple layers of organized loop domains (Benyajati and Worcel, 1976). This has led to a model merging *in vitro* and *in vivo* observations to suggest that 30 nm fibers fold in an orderly and sequential manner into defined higher order structures such as chromosome loops (Luger et al., 2012).

There are known structural elements of nucleosomes that contribute to their compaction, including prominent roles for histone tails. Interactions between histone tails mediate cross fiber interactions, and the clipping of N-terminal histone tails from nucleosomes leads to chromatin decompaction (Arya and Schlick, 2006; 2009; Duncan et

al., 2008). Regulated histone tail clipping may represent a process utilized by cells to modulate transcription and differentiation (Dhaenens et al., 2014). The process of chromatin compaction is also greatly facilitated by linker histones with chromatin arrays with longer NRL lengths forming more compact fibers (Routh et al., 2008). Spermatid development is a biologically relevant example of the role of NRL in chromatin compaction. During late spermatogenesis, the NRL of spermatids increases from ~195 bp to ~ 225 bp, contributing to the compaction of chromatin to such an extent that it becomes resistant both to degradation by micrococcal nuclease and even disruption by physical means including sonication (Kennedy and Davies, 1982; Marushige and Marushige, 1978). This high degree of compaction is thought to be important for genome stability and species propagation by protecting the paternal genome from physical and chemical damage (Rathke et al., 2014).

Interestingly, the classic view of orderly nucleosome array compaction has been recently challenged both by studies suggesting that 30 nm fibers are an *in vitro* artifact as well as by data suggesting that chromatin fiber compaction may be non-uniform and contain elements of randomness. This has led to a newer model in which compaction is generated by interdigitation of nucleosome arrays based on local nucleosome overcrowding (Fussner et al., 2011; Luger et al., 2012; Tremethick, 2007). While the exact mechanism leading to the formation of the nucleosome arrays that comprise tertiary chromatin structure is unclear, certain factors are known to play key roles in *in vivo* chromatin compaction. These include histone-post translational modifications (Bannister and Kouzarides, 2011) and ATP-dependent chromatin remodeling (Flaus and Owen-

Hughes, 2011), both of which are discussed below in the context of their regulation during processes that maintain genome stability.

1.4.3 *Regulation of Chromatin Structure by Histone Post-Translational Modifications*

The deposition of histone PTMs can serve to both directly and indirectly modify chromatin structure and regulate protein recruitment and activity on chromatin. On a direct level, histone PTMs can cause intrinsic structural changes in nucleosomes by modifying histone-DNA and histone-histone interactions (Bowman and Poirier, 2015). Histone lysine acetylation, among the first two histone PTMs discovered along with methylation (Allfrey et al., 1964), neutralizes the positive charge of lysine causing the loss of a charge interaction with the phosphate backbone of DNA. The acetylation of H4K16 is a potent example of the possible structural consequences of histone modification. Reconstitution of nucleosome arrays with nucleosomes containing H4K16ac *in vitro* disrupts 30 nm fiber formation and impedes the formation of cross-fiber interactions (Shogren-Knaak et al., 2006). Furthermore, H4K16 acetylation by the MOF histone acetyltransferase *in vivo* de-represses chromatin resulting in increased transcription (Akhtar and Becker, 2000; Zippo et al., 2009). Multiple other PTMs, including phosphorylation, methylation, and ubiquitylation can occur at sites of key interactions between histones and DNA, leading to destabilization of nucleosomes and chromatin fibers and promoting DNA entry site unwrapping that facilitates chromatin remodeling (Bowman and Poirier, 2015).

Indirect effects of histone PTMs are modulated by proteins that are recruited in a specific manner by domains that recognize PTMs (Bottomley, 2004). The general model of the "histone code" is that specific enzymes deposit modifications in a controlled manner ("writers"). These modifications are then recognized by other proteins ("readers") to modulate their recruitment and activity, followed by regulated enzymatic removal by "erasers" (Musselman et al., 2012; Strahl and Allis, 2000). With recent advances in quantitative mass spectrometry analysis of histone peptides, the library of histone PTMs has increased from well known modifications such as acetylation and methylation to include more recently discovered modifications such as butyrylation and formylation, the biological functions of which are still in the early stages of elucidation (Dawson and Kouzarides, 2012; Stunnenberg and Vermeulen, 2011). A ground-breaking manuscript in 2011 described 67 new histone PTMs and validated one of them, lysine crotonylation, as a conserved mark of active promoters and enhancers (Tan et al., 2011). It is important to note that histone PTMs can have both dual structural and indirect roles. For example, H4K16ac acts to increase transcription not only through disrupting chromatin compaction but also by recruiting BRD4, a member of the transcriptional elongation complex, to facilitate transcription elongation (Zippo et al., 2009). Additionally, histone PTMs are by nature reversible with the regulation of both their deposition and removal important for maintaining genome stability (Butler et al., 2012).

An important example of a histone PTM that influences genome stability is phosphorylation of the H2A variant H2A.X on serine 139 to form γH2A.X. First identified as a modification that is rapidly deposited on chromatin in response to ionizing radiation-induced DSBs (Rogakou et al., 1998), γH2A.X has been extensively studied for

its roles in DSB repair and genome stability. After DSBs are formed, the DNA damage response-signaling PI3K-like kinases Ataxia Telangiectasia Mutated (ATM) and Ataxia Telangiectasia and Rad3-Related (ATR), as well as DNA-dependent protein kinase (DNA-PK), phosphorylate H2A.X histones on serine 139 for megabases adjacent to the DSB within a matter of minutes (Bonner et al., 2008). Phosphopeptide binding studies demonstrated that mediator of DNA damage checkpoint protein 1 (MDC1) interacts with γH2A.X via its BRCT domain (Stewart et al., 2003). MDC1 was subsequently demonstrated to assist in the recruitment or retention of multiple DSB repair factors, including the Mre11/Rad50/Nbs1 (MRN) complex, 53BP1, and BRCA1

(Lou et al., 2006; Lukas et al., 2004). The observation that $H2AX^{-/-}$ mice exhibited growth retardation, immunodeficiency, and radiosensitivity further solidified the role of γH2A.X in genome stability (Celeste et al., 2002). Notably, these phenotypes were recapitulated in $MDC1^{-/-}$ mice (Lou et al., 2006), highlighting the key role of this mediator protein. In yeast, H2A S129 phosphorylation (the equivalent of γH2A.X) was found to spread for kilobases on either side a DSB and to contribute to the recruitment of multiple repair proteins, including chromatin remodelers (Foster and Downs, 2005; Unal et al., 2004), indicating that this mark has central conserved functions in DSB repair throughout eukaryotes.

The complexity of histone PTM physiology is illustrated by the discovery that H2A.X S139 phosphorylation additionally initiates a cascade of H3 acetylation, creating a cooperative activation loop that facilitates the recruitment of other DNA repair factors, including the chromatin remodeler SWI/SNF (Lee et al., 2010). Interestingly, emerging evidence suggests that γH2A.X has roles in chromatin biology outside of DSB repair

(Ismail and Hendzel, 2008). These non-canonical functions for H2A.X S139 phosphorylation include roles in meiotic sex chromosome inactivation (Turinetto and Giachino, 2015), embryonic stem cell self-renewal and pluripotency (Turinetto et al., 2012), and the maintenance of cellular senescence (Rodier et al., 2010). While γH2A.X is a classic example of a histone PTM that mediates genome stability, many other histone PTMs also participate in processes that mediate genome stability (Bannister and Kouzarides, 2011), including by facilitating the activity of an essential class of enzymes that modulate chromatin structure— ATP-dependent chromatin remodeling complexes.

1.4.4 *ATP-Dependent Chromatin Remodeling*

ATP-dependent chromatin remodeling complexes utilize the energy liberated from ATP hydrolysis to restructure nucleosomes. There are four families of ATP-dependent chromatin remodelers (the SWI/SNF, ISWI, CHD and INO80 families) that are conserved throughout eukaryotes, and which participate in processes related both to chromatin organization and disruption (Clapier and Cairns, 2014). While these various remodelers have diverse compositions—from single subunit remodelers such as yeast Fun30/mammalian SMARCD1 to the 15 subunit INO80 complex—the mechanism of ATP-dependent nucleosome remodeling by these remodelers contains commonalities (Conaway and Conaway, 2009; Costelloe et al., 2013). Studies from the SWI/SNF, ISWI, and CHD families of ATP-dependent chromatin remodelers have demonstrated that all of these remodelers contain ATPase/Translocase domains that function to translocate DNA along nucleosomes (Saha et al., 2005; Zofall et al., 2006). This translocation produces microscopically visible loops of DNA that dissociate from the nucleosome (Lia et al.,

2006), leading to a model in which DNA loops generated by ATP-dependent translocation are propagated around the octamer, causing either sliding of the nucleosome along the DNA strand, or enabling the eviction or substitution of histones in the octamer that are exposed when their encircling DNA is dissociated (Mueller-Planitz et al., 2013). Interestingly, ATP-dependent chromatin remodelers have physical interactions with core histone proteins, suggesting the possibility that the remodelers may influence histone octamer structure in a manner separate from DNA translocation (Dang and Bartholomew, 2007; Racki et al., 2009). Indeed, a recent study demonstrated that interaction of the ISWI remodeler motor protein SNF2H with nucleosomes leads to histone octamer core distortions that facilitate remodeling (Sinha et al., 2017). Therefore, ATP-dependent chromatin remodelers directly modify both the DNA and core histone proteins forming the nucleosome.

Despite enzymatic similarities between ATP-dependent chromatin remodelers, differing outcomes are observed when different remodelers interact with chromatin. One outcome is the introduction of chromatin organization in the form of spaced nucleosome arrays and higher-order chromatin structures mediated by the ISWI and CHD family remodelers after replication (Varga-Weisz and Becker, 2006; Yadav and Whitehouse, 2016). An opposite effect is the disruption of nucleosome array structure and the sliding and eviction of nucleosomes by the SWI/SNF family of remodelers (Lorch et al., 2006; Schnitzler et al., 2001; Schwabish and Struhl, 2007). A third outcome is observed with SWR1 remodelers, which replace canonical H2A-H2B dimers with variant H2A.Z-H2B dimers (Gerhold et al., 2015). The various functions of chromatin remodelers contribute significantly to to processes that mediate genome stability, as discussed below.

1.5 Chromatin Remodeling during DSB Repair and Replication

1.5.1 *Chromatin Remodeling during DNA Double-Strand Break Repair*

The activity of repair proteins at DNA DSBs is modified both by histone PTMs and by ATP-dependent chromatin remodelers. While γH2A.X is perhaps the most well studied histone PTM in DSB repair (reviewed in section **1.4.3**), multiple other histone PTMs modulate the cellular response to these deleterious lesions. These include modifications to each of the core histones, including phosphorylation, acetylation, ubiquitylation, and methylation, which affect repair factor recruitment to and retention at DNA DSBs, and chromatin compaction (Freudenreich, 2014; Hunt et al., 2013).

Many key observations about chromatin modification during DSB repair were made in budding yeast due to the genetic tractability of this model organism. Pioneering work beginning over a decade ago in this model system demonstrated a variety of important roles for ATP-dependent chromatin remodelers in the repair of DNA DSBs. Multiple groups identified that ATP-dependent chromatin remodelers previously studied for their roles in transcription, including the INO80, SWI/SNF, and RSC complexes

(Ng et al., 2002; SHEN et al., 2000; Sudarsanam and Winston, 2000; Sudarsanam et al., 2000), were also recruited to the sites of DSBs (Chai, 2005; Tsukuda et al., 2005). Over the next few years, multiple roles for these chromatin remodelers in disrupting chromatin structure and facilitating repair processes were identified and a temporal sequence of their recruitment was established (**Fig 1.6**).

The RSC remodeler is recruited within 15 minutes to a defined DSB site, where it was demonstrated to slide nucleosomes proximal to the break to create stretches of

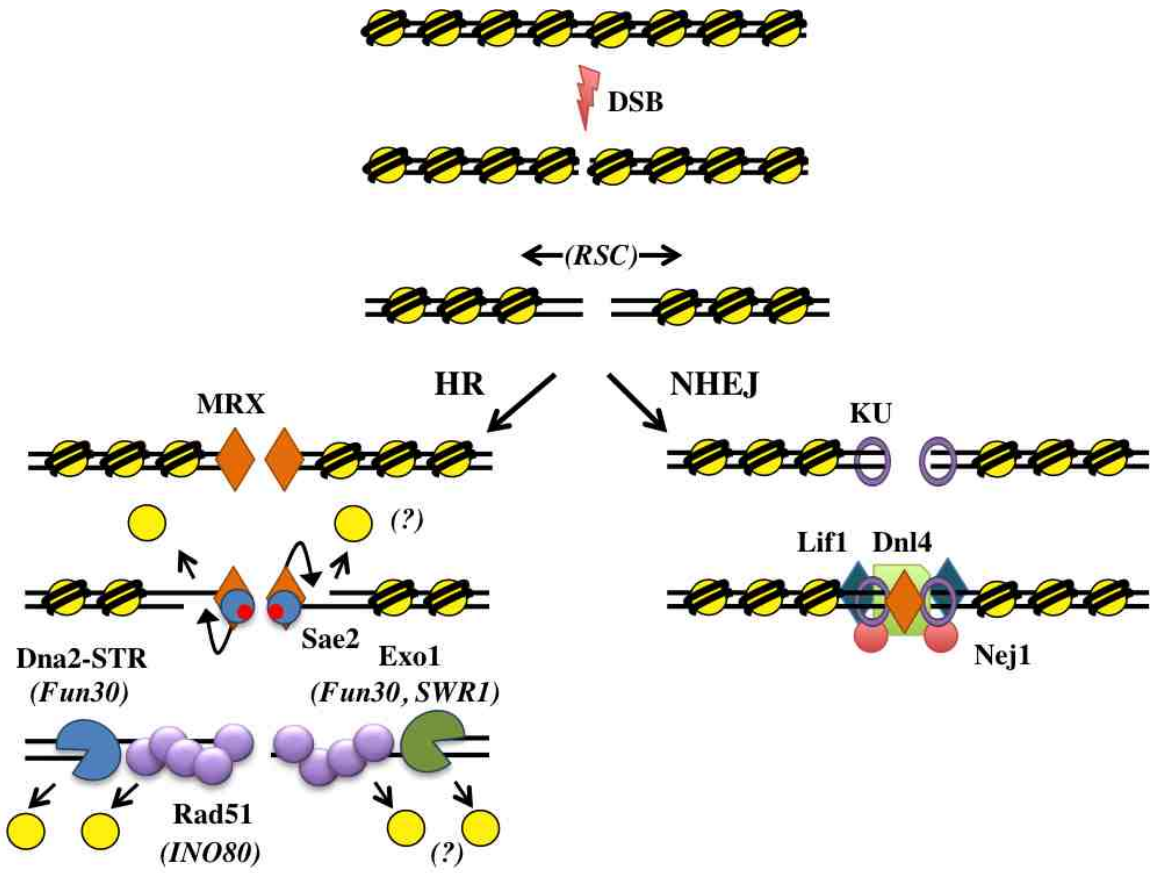

Figure 1.6. A model for chromatin remodeling during DSB repair in budding yeast. After a DSB is formed, the RSC complex acts rapidly to slide nucleosomes away from the break. The generation of nucleosome-free DNA at the break by RSC facilitates the recruitment of both KU for NHEJ (right) and MRX for HR (left). After MRX associates with ends for HR, the complex interacts with Sae2 to initiate DNA end resection. The initial, short 3′ ssDNA overhangs are extended by the Dna2-STR complex and Exo1, which are assisted by Fun30 and SWR1 recruitment to process the nucleosome barriers to resection. Finally, Rad51 nucleofilament deposition is assisted by INO80, which helps by evicting nucleosomes. Other factors that assist in evicting nucleosomes to facilitate the initial and long-range resection processes are unknown, as indicated by *(?)*, and are examined in Aim I of this dissertation.

nucleosome-free DNA (Kent et al., 2007). This sliding of nucleosomes away from the DSB by RSC was found to facilitate the recruitment of both the HR-promoting MRX complex and the NHEJ-promoting KU complex (Shim et al., 2007). The SWI/SNF complex, which is recruited later (after ~45 minutes), plays a critical pre-synaptic role as evidenced by the loss of strand invasion during HR in *Swi/Snf* mutants (Chai, 2005), though many details of the functions of SWI/SNF remain unclear. Interestingly, the INO80 complex was found to be already present on chromatin, likely due to its role in transcription. INO80 contributes to HR repair by facilitating nucleosome eviction for many kb on either side of the break (Tsukuda et al., 2005). Notably, nucleosome eviction by INO80 correlated with efficient formation of the Rad51 nucleoprotein filaments on DNA, suggesting that Rad51 filament formation preferentially occurs on nucleosome-free DNA (Tsukuda et al., 2005). These early observations strongly suggested that the coordinated disruption and modification of chromatin structure by ATP-dependent chromatin remodelers is essential for successful DSB repair. The role of these remodelers in maintaining genome stability was further demonstrated by the sensitivity to DNA damaging agents observed upon inactivation of these complexes (Chai, 2005; Tsukuda et al., 2005).

Since these early observations, more recent work has identified further chromatin modifications that facilitate DSB repair, especially in regard to the long-range resection process during HR. The Fun30 ATP-dependent nucleosome remodeler was found to physically associate and travel with the long-range resection factors Exo1 and Dna2-STR to evict the yeast 53BP1 ortholog, Rad9, from nucleosomes, thereby enhancing the rate of long-range resection (Chen et al., 2013b; Eapen et al., 2012). Furthermore, the SWR1

complex was also found to facilitate long-range resection by replacing H2A with H2AZ to generate nucleosome structures more amenable to resection by Exo1 (Adkins et al., 2013). There are, however, conflicting reports regarding the participation of chromatin remodelers in the initial phase of DNA end resection mediated by MRX and Sae2 (Tsabar and Haber, 2013). Thus, the identities and roles of the factors that assist MRX-Sae2 in resection initiation remain open questions.

After the necessary chromatin disruption has occurred to allow DSB repair to finish successfully, chromatin needs to be restored around the break site. Recent work has investigated chromatin restoration after DSB repair, demonstrating that the histone chaperones ASF1A, ASF1B, CAF-1 and HIR1 contribute to restoration of nucleosomes after completion of DSB repair in human cells (Li and Tyler, 2016). Previous work demonstrated the same phenomenon in *Xeonopus* and yeast cells, and also revealed that chromatin reassembly is linked to DNA damage checkpoint recovery (Chen and Tyler, 2008; Gaillard et al., 1996). While many questions remain about the identities and activities of factors involved in chromatin restoration following DSB repair, these results demonstrate important conserved roles for histone chaperones in linking genomic and epigenomic stability.

It is important to note that, while the roles of many ATP-dependent chromatin remodelers in DSB repair were discovered and are most well described in budding yeast, mounting data suggests that aberrancies in these conserved complexes contribute to genome instability and cancer development in humans (Mayes et al., 2014; Skulte et al., 2014). In particular, there are mounting research efforts to determine the role of SWI/SNF in genome and epigenome stability due to the observation that SWI/SNF

complexes are inactivated in one in five human malignancies (Kadoch and Crabtree, 2013; Kadoch et al., 2013). This dissertation addresses the roles of SWI/SNF in DNA DSB repair in the budding yeast model system in Aim I, as described in section **1.6**.

1.5.2 *Chromatin Disruption and Reestablishment during Replication*

During S-phase, the entire complement of nucleosomes that package the eukaryotic genome into chromatin must be disrupted so that DNA polymerases can access the DNA structure without hindrance (MacAlpine and Almouzni, 2013). Replication-associated nucleosome disruption appears to be mediated by multiple factors. Data from *in vitro* reconstituted replication reactions with chromatinized templates have demonstrated that the CMG complex by itself does not efficiently remove nucleosomes; rather, the addition of histone chaperones, chromatin remodelers, and lysine aceyltransferases is necessary for efficient replication of nucleosome-containing DNA (Kurat et al., 2017). After disruption, chromatin must be reestablished correctly on the newly synthesized DNA strands to maintain the correct epigenetic state of the daughter cells. This reestablishment occurs in multiple phases, with rapid nucleosome assembly followed by maturation of the newly deposited chromatin (Groth et al., 2007). Additionally, DNA methylation needs to be maintained on the daughter strands to maintain cellular identity and transcription states (Cedar and Bergman, 2009; Smith and Meissner, 2013). A general model of the reestablishment of both nucleosomes and DNA methyl marks on DNA daughter strands is presented in **Fig 1.7**.

Nucleosomes are reestablished on newly synthesized DNA in a 1:1 mixture of parental and new histones (MacAlpine and Almouzni, 2013). Initial evidence that histone

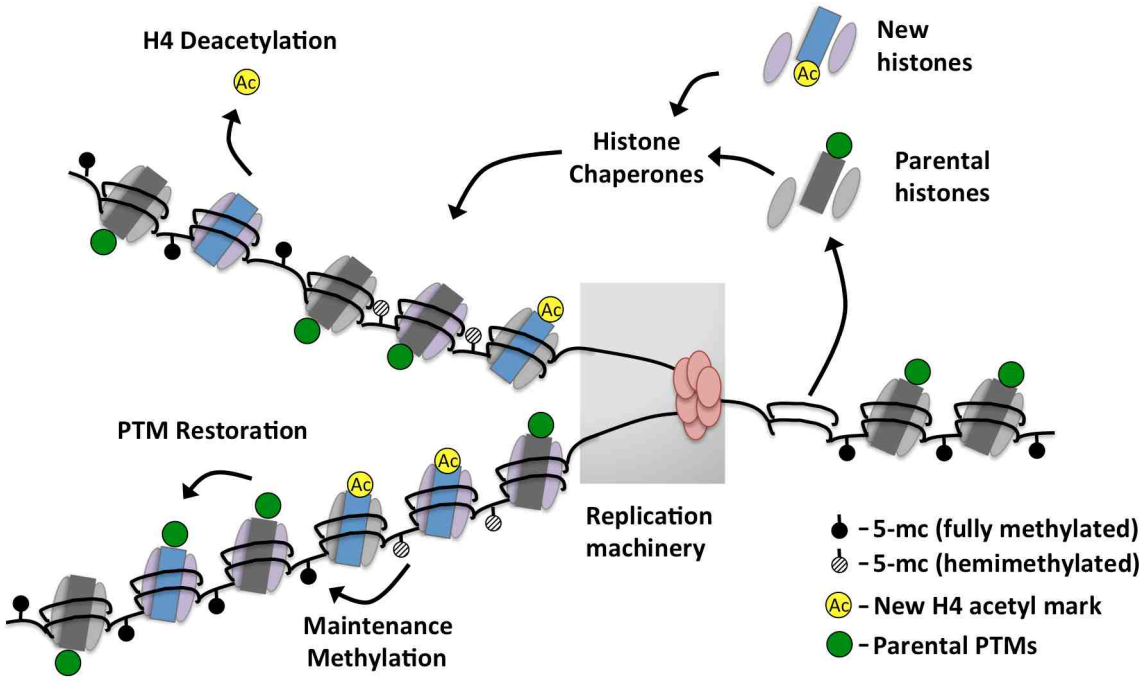

Figure 1.7. Events in the replication of chromatin and DNA methylation marks on DNA daughter strands during S-phase replication. Histone chaperones mediate the removal of histones in front of the advancing replication fork and subsequently coordinate their deposition on newly synthesized DNA in a 1:1 mix of parental and new histones. New histone H4 contain K5ac and K12ac marks that need to be removed to facilitate proper chromatin compaction. During chromatin maturation, the H4 acetyl marks on new H4 are removed and the parental histone PTMs are restored on adjacent nucleosomes. 5-methylcytosine (5-mc) is replicated in a semi-conservative manner resulting in hemimethylated CpG sites on daughter strands. After replication, maintenance methylation restores the full methylation status of CpG sites. Model is based upon a template provided by Dr. Mary Ann Osley and is used with permission.

chaperones were involved in chromatin reassembly came from the discovery of the role of Chromatin Assembly Factor I (CAF-1) in chromatin reassembly after nucleotide excision repair of UV-damaged bases (Gaillard et al., 1996). Since then, more than ten different histone chaperones with affinities for specific histones and histone variants have been characterized as contributors to nucleosome reassembly after disruption from DNA repair and replication (Burgess and Zhang, 2013). These include defined roles for CAF-1 in the deposition of $(H3\text{-}H4)_2$ tetramers (Liu et al., 2012), and Nucleosome Assembly Protein 1 (Nap1) in the deposition of H2A-H2B dimers (Aguilar Gurrieri et al., 2016). Newly synthesized histones are not immediately deposited on chromatin. The association of $(H3\text{-}H4)_2$ tetramers with CAF-1 requires handoff of H3-H4 dimers from the chaperone anti-silencing function 1 (Asf1). This handoff in yeast is mediated by H3K56ac on newly synthesized H3 molecules (Li et al., 2008; Mello et al., 2002). While the role of H3K56ac in human cells is not synonymous with yeast (Das et al., 2009), certain modifications of newly synthesized histones, including the acetylation of H4K5 and H4K12, are conserved from *Tetrahymena* to humans (Sobel et al., 1995).

Histone chaperones are targeted to replicating DNA by interactions with replication proteins. For example, CAF-1 interacts with PCNA (Shibahara and Stillman, 1999; Zhang et al., 2000), Asf1 and FACT interact with the MCM helicase (Schulz, 2006; Tan et al., 2006), and HIRA interacts with RPA (Zhang et al., 2017). In addition, RPA may also directly bind H3-H4 to retain displaced histones on replicating DNA (Liu et al., 2017). Following nucleosome deposition, histone PTMs need to be correctly re-established. Careful SILAC mass spectrometry experiments have demonstrated that histone PTMs are globally diluted 1:2 after replication and are slowly restored to pre-

replication levels over time; however, certain methylation modifications are rapidly restored (Alabert et al., 2015). The rapidly restored histone PTMs include H3K9me3 and H3K27me3, which are marks critical to cellular identity that recruit their cognate lysine methyltransferase enzymes, Suv39h1 and EZH2, respectively, for rapid self-propagation (Aagaard et al., 1999; Hansen et al., 2008; Margueron and Reinberg, 2010; Wang et al., 2012). In addition to reestablishment of parental histone PTMs, the K5 and K12 acetylation marks on newly synthesized H4 incorporated into chromatin must be removed to ensure heterochromatin compaction (Taddei et al., 1999).

Concomitant with chromatin maturation, 5-methylcytosine (5-mc) marks on DNA need to be restored on newly synthesized DNA daughter strands to maintain both cellular identity and the repression of transcriptionally inactive regions (Bird, 2002; Kass et al., 1997). DNA methylation marks are established by the *de novo* methyltransferases DNMT3A and DNMT3B during development, mostly on CpG pairs, and are maintained during DNA replication by the maintenance methyltransferase DNMT1 (Hackett and Surani, 2012; Illingworth and Bird, 2009; Meng et al., 2015). During replication, 5-mc is transmitted in a semiconservative manner, resulting in hemimethylated daughter DNA duplexes as demonstrated in **Fig 1.7** (Probst et al., 2009). DNMT1 is recruited to hemimethylated DNA in multiple ways. First, DNMT1 itself has affinity for hemimethylated DNA (Hermann et al., 2004). Second, DNMT1 physically interacts with PCNA (Iida et al., 2002). Third, DNMT1 interacts with UHRF1, a protein that strongly binds to hemimethylated DNA (Bostick et al., 2007), to form a complex that is required for fully efficient methylation of genomic DNA (Liu et al., 2013). The multiple interactions of DNMT1 with PCNA and UHRF1 ensure efficient methylation of daughter

strands to protect genome stability and suppress tumorigenesis (Pacaud et al., 2014). In addition to replication-dependent targeting of DNMT1, the H3K9 methyltransferase G9A can recruit DNMT1, DNMT3A, and DNMT3B to imprinting control regions (ICRs) in stem cells (Zhang et al., 2016).

After assembly of nucleosomes, linker histone H1 is deposited (see sections **1.4.1** and **1.4.2**). Many questions about events in chromatin deposition and maturation remain unanswered. For example, the positioning of nucleosomes in budding yeast correlate strongly with the locations of Okazaki fragment ligation (Smith and Whitehouse, 2013), suggesting that DNA ligation may influence chromatin deposition or vice versa. Additionally, little is known about the deposition of histone H1 (Harshman et al., 2013). This dissertation address the role of DNA ligase I in the assembly and maturation if chromatin in **Aim 2**, as described below.

1.6 Dissertation Overview, Specific Aims, and Hypotheses

This dissertation addresses significant gaps in the scientific knowledge pertaining to two processes that link genome and epigenome stability, namely the role of the chromatin-disrupting SWI/SNF ATP-dependent nucleosome remodeler in DNA double-strand break (DSB) repair by homologous recombination (HR) in Aim 1 (**Chapter 2**), and the role of DNA Ligase I in coordinating chromatin assembly and maturation in Aim 2 (**Chapter 4**). In addition to addressing these gaps, I present optimizations to a groundbreaking technique, accelerated native isolation of proteins on nascent DNA (aniPOND), that allows for a quantitative and spatiotemporal examination of proteins associated both with replication forks and with newly synthesized DNA at time points

after replication in mammalian cells (**Chapter 3**). The scientific advances presented in this dissertation contribute to new hypothesis-generating models of both chromatin remodeling during DSB repair and the regulation of histone H1 deposition and DNA methylation after DNA replication (**Chapter 5**). The methodological advances presented in this dissertation with the aniPOND technique will empower researchers to discover novel links between genome and epigenome stability. The specific aims and hypotheses addressed of this dissertation are as follows:

Specific Aim 1- To elucidate the role of the SWI/SNF ATP-dependent nucleosome remodeler in DNA double-strand break repair in *Saccharomyces cerevisiae*.
In this aim, I build upon published data showing that SWI/SNF is essential for mating-type switching, a HR-dependent process, in budding yeast. I address the hypothesis that SWI/SNF activity at DNA DSBs promotes HR-repair by facilitating DNA end resection and repair factor recruitment. Specific Aim 1 is explored in detail in **Chapter 2**.

Specific Aim 2- To elucidate the relationships between DNA Ligase I, nucleosome assembly, and chromatin maturation during DNA replication in mammalian cells.
In this aim, I build upon observations from the literature demonstrating that Okazaki fragment ligation and nucleosome positioning are linked processes. I address the hypothesis that ligation of Okazaki fragments by DNA Ligase I represents a key regulatory step linking lagging-strand DNA synthesis with chromatin reassembly and maturation on nascent DNA. Specific Aim 2 is explored in detail in **Chapter 4.** Optimizations to the aniPOND technique that enabled studies for Specific Aim 2 are presented in **Chapter 3**.

Chapter 2

The SWI/SNF ATP-dependent nucleosome remodeler promotes resection initiation at a DNA double-strand break in yeast

Wiest, N., Houghtaling, S., Sanchez, J., Tomkinson, A., and Osley, M.A. The SWI/SNF ATP-dependent nucleosome remodeler promotes resection initiation at a DNA double-strand break in yeast. Submitted to *Nucleic Acids Research* on January 24, 2017. Accepted for publication.

2.1 Abstract

DNA double-strand breaks (DSBs) are repaired by either the non-homologous end joining (NHEJ) or homologous recombination (HR) pathway. Pathway choice is determined by the generation of 3′ single-strand DNA overhangs at the break that are initiated by the action of the Mre11-Rad50-Xrs2 (MRX) complex to direct repair towards HR. DSB repair occurs in the context of chromatin, and multiple chromatin regulators have been shown to play important roles in the repair process. We have investigated the role of the SWI/SNF ATP-dependent nucleosome-remodelling complex in the repair of a defined DNA DSB. SWI/SNF was previously shown to regulate presynaptic events in HR, but its function in these events is unknown. We find that in the absence of functional SWI/SNF, the initiation of DNA end resection is significantly delayed. The delay in resection initiation is accompanied by impaired recruitment of MRX to the DSB, and other functions of MRX in HR including the recruitment of long-range resection factors and activation of the DNA damage response are also diminished. These phenotypes are correlated with a delay in the eviction of nucleosomes surrounding the DSB. We propose that SWI/SNF orchestrates the recruitment of a pool of MRX that is specifically dedicated to HR.

2.2 Introduction

DNA double-strand breaks (DSBs) are potent cytotoxic lesions that must be accurately repaired to prevent cellular senescence, apoptosis, or oncogenic transformation (Mladenov et al., 2016). Cells encounter a barrage of genomic insults that can lead to the formation of DSBs, including exogenous sources such as ionizing radiation, environmental toxins, and chemotherapeutic agents, as well as endogenous sources such as reactive oxygen species (ROS) and DNA replication stress (Mehta and Haber, 2014). There are two major pathways to correct DSBs: non-homologous end joining (NHEJ) and homologous recombination (HR). NHEJ is a cell-cycle independent process that involves the direct rejoining of broken ends. While it can be error-free, especially with DSB ends that are complementary and free of base damage, when the DSB ends are non-complementary or chemically altered, such as in breaks generated by ionizing radiation, end processing is required to make them ligatable, resulting in insertions and deletions (Bétermier et al., 2014). In contrast, HR is a highly accurate but cell-cycle dependent process that requires a homologous template such as a sister chromatid for copying in order to replace the damaged segment of DNA (Jasin and Rothstein, 2013). It is imperative that cells utilize the correct DSB repair pathway depending on cell cycle stage and lesion context, such as at a collapsed replication fork (Saleh-Gohari et al., 2005; Sonoda et al., 1998), in order to prevent or limit genome instability and ensure organism survival.

A key repair intermediate that drives pathway choice is 3′ single-strand DNA (ssDNA) generated at break ends (Cejka, 2015; Symington and Gautier, 2011). After a DSB is generated, both the NHEJ-promoting Ku70/Ku80 (KU) complex and the

multifunctional Mre11/Rad50/Xrs2 (MRX in yeast; Mre11/Rad50/Nbs1, MRN in mammals) complex rapidly associate with DSB ends. When KU binding predominates, generally during G1 phase, accessory NHEJ proteins are recruited to bridge, process and ligate the break ends (Davis and Chen, 2013; Lieber, 2010a). In contrast, during S-G2 phases, the MRX/MRN complex associates with Sae2/CtIP to initiate the process of DNA end resection, which generates 3′ ssDNA overhangs that antagonize KU association, channeling the DSB ends into the HR pathway (Clerici et al., 2005; Rathmell and Chu, 1994).

During HR, DNA end resection occurs in two distinct phases. The initial phase is carried out by MRX/MRN in conjunction with Sae2/CtIP, creating short 100-300 bp 3′ ssDNA overhangs (Garcia et al., 2012; Zhu et al., 2008). In the next phase, known as long-range resection, there are resection activities— Exonuclease 1 (Exo1) and the nuclease/helicase complex Dna2-Sgs1/Top3/Rmi1 (Dna2-STR; BLM-Topo IIIα/RMI1/RMI2, BTR in mammals) — that extend the ssDNA tracts for many kilobases on either side of the break (Daley et al., 2014; 2015; Garcia et al., 2012; Zhong et al., 2008). The ssDNA is first coated by Replication Protein A (RPA), which is then actively replaced by the Rad51 recombinase to form a nucleoprotein filament that mediates homology search and strand invasion (Wang and Haber, 2004).

The initiation of end resection is tightly regulated in cells to prevent inappropriate recombination, for example during G1 or early S phase when a sister chromatid is not available (Hustedt and Durocher, 2017). In G1 phase cells, KU and mammalian 53BP1, as well as the yeast 53BP1 ortholog Rad9, accumulate on DSB ends, where they antagonize the initiation of end resection (Bunting et al., 2010; Ferrari et al., 2015; Lee et

al., 2015; Mimitou and Symington, 2010). The nuclease activity of MRX/MRN is also impaired in G1 phase cells due to the low CDK-dependent phosphorylation of Sae2/CtIP (Cannavo and Cejka, 2014; Huertas et al., 2008), whereas in S and G2 phases cells, multiple resection factors, including Sae2/CtIP, Dna2, and Exo1, have increased expression and/or phosphorylation that enhance their participation in resection (Symington, 2016). Furthermore, KU is reported to be modified by phosphorylation, ubiquitylation, and neddylation, promoting its removal from DSB ends in S and G2 phase cells (Brown et al., 2015; Lee et al., 2015; Postow et al., 2008). BRCA1 replaces 53BP1 in mammals and CDK-phosphorylated Fun30 antagonizes yeast Rad9, thereby removing additional barriers to resection and enhancing the recombinogenic environment in late S and G2 phases (Chen et al., 2013a; 2016; Panier and Boulton, 2013). Thus, it is apparent that the initiation of DNA end resection is controlled by multiple mechanisms because this is a key step in determining repair pathway choice.

Since DNA end resection and other steps in DSB repair occur in the context of chromatin, chromatin regulators play influential roles in repair outcomes. While some chromatin regulators deposit covalent modifications on histone tails to facilitate DNA damage signaling and repair factor recruitment (Hunt et al., 2013), others alter the structure of chromatin either by replacing canonical histones with histone variants or by moving or evicting nucleosomes. These latter functions are carried about by a class of enzymes known as ATP-dependent nucleosome remodelers, which utilize the energy of ATP hydrolysis to modify histone-DNA interactions (Zhou et al., 2016). In yeast, multiple ATP-dependent nucleosome remodelers, all of which are conserved and diversified in higher eukaryotes, are recruited to DNA DSBs (Hargreaves and Crabtree,

2011; Osley et al., 2007; Tsabar and Haber, 2013). For example, the RSC complex is recruited almost immediately after a DSB is formed, inducing a rapid shift of nucleosomes next to a DSB (Kent et al., 2007; Shim et al., 2007). This activity is posited to facilitate both KU and MRX recruitment to break ends and to promote the formation of cohesion to tether the broken region to the donor locus (Oum et al., 2011; Shim et al., 2007). The INO80 complex is recruited to a DSB later and participates in the sequential eviction of nucleosomes on either side of a DSB, an activity that facilitates Rad51 nucleoprotein filament formation (Tsukuda et al., 2005). While there are conflicting reports about the role of RSC or INO80 in DNA end resection (Tsabar and Haber, 2013), two other remodelers have been demonstrated to facilitate long-range resection. The SWR-C complex replaces canonical H2A with the variant H2A.Z to promote long-range resection by the Exo1 pathway (Adkins et al., 2013), whereas the Fun30 nucleosome remodeler travels with the long-range resection machinery to facilitate resection through nucleosomes by removing the Rad9 checkpoint protein from chromatin (Chen et al., 2013b; Costelloe et al., 2013; Eapen et al., 2012). Finally, the prototypical ATP-dependent nucleosome-remodeling complex, SWI/SNF, is recruited to DNA DSBs, where it plays a critical but unknown role in pre-synaptic events during HR (Chai, 2005).

In this study, we have investigated the role of SWI/SNF in DSB repair in budding yeast. We provide the first evidence that SWI/SNF is required for the timely initiation of DNA end resection during HR. This role appears to be mediated through the action of SWI/SNF in the recruitment and/or stabilization of the MRX complex at DSB ends. We also observed that nucleosome eviction at a DSB is delayed in a SWI/SNF mutant, suggesting that the chromatin remodeling activity of SWI/SNF may contribute to its role

in MRX recruitment and resection initiation. Together our results reveal critical early roles for SWI/SNF in orchestrating successful DSB repair by HR.

2.3 Materials and Methods

Strains and Growth Conditions

S. cerevisiae strains are listed in **Table 2.1**. Gene knockouts and epitope tagging were performed by genomic recombination with PCR-amplified cassettes (Janke et al., 2004). Strains were pre-grown to $O.D._{600nm}$ 0.4-0.6 in YPD medium (1% yeast extract, 2% peptone, 2% dextrose). Cells were then diluted into pre-induction GLGYP medium (3% glycerol, 2% D-lactate, 0.05% dextrose, 1% yeast extract, 2% peptone, pH 5.5) and grown for 12-15 hr until mid-log phase. To induce a *MAT* DSB, galactose was added to 2% and cells were harvested at time points after addition.

Cell Cycle Analysis

Fluorescence activated cell sorting (FACS) was performed as previously described (Trujillo and Osley, 2012). Briefly, approximately 0.6 $O.D._{600nm}$ units of mid-log phase cells were fixed in 3 volumes of ethanol, followed by storage at -20°C for up to one month. Before staining, approximately 0.2 $O.D._{600nm}$ units of cells were removed and resuspended in TE (10 mM Tris, 1 mM EDTA, pH 8.0) with 100 µg/mL RNAse A and incubated at 37°C overnight, followed by incubation in pepsin solution (0.48% HCl, 5% pepsin in TE) for 30 minutes. After resuspension in Sybr Green solution (0.25% NP-40, 0.02% SYBR-Green I in TE) for 24-36 hr at 4°C, cells were briefly sonicated before sorting on a FACScalibur machine using CellQuest Pro software (BD Biosciences). A

Table 2.1. *S. cerevisiae s*trains.

Strain	Genotype	Source/Reference
JKM179	*MATα Δho hml::ADE1 hmr:ADE1 ade1 leu2-3,112 lys5 trp1::hisG ura3-52 ade3::GAL10-HO*	Lee *et al* 1998
MAO249	JKM179, *HTB1*-FLAG	Tsukuda *et al* 2005
MAO639	MAO249, *snf5::KAN*	This Study
MAO870	MAO249, *EXO1*-9myc	This Study
MAO875	MAO249, *EXO1*-9myc *snf5::KAN*	This Study
MAO886	MAO249, y*ku70::HPH snf5::KAN*	This Study
MAO888	MAO249, y*ku70::HPH*	This Study
MAO991	MAO249, *snf5::KAN* + pRS316	This Study
MAO993	MAO249, *snf5::KAN* + pRS416-*SNF5-HA*	This Study
MAO1047	MAO249, *exo1::NAT*	This Study
MAO1049	MAO249, *exo1::NAT snf5::KAN*	This Study
MAO1051	MAO249, *DNA2*-9myc	This Study
MAO1068	MAO249, *DNA2*-9myc *snf5::KAN*	This Study
MAO1063	MAO249, *sgs1::NAT*	This Study
MAO1065	MAO249, *sgs1::NAT snf5::KAN*	This Study

minimum of 30,000 events were collected for each sample. Data were exported to FlowJo software for gating, visualization, and analysis.

Chromatin Immunoprecipitation

Chromatin immunoprecipitation (ChIP) was performed as previously described, with minor modifications (Trujillo et al., 2011). Briefly, 30 to 50 $O.D._{600nm}$ units of mid-log phase cells were fixed with 1% formaldehyde for 30 minutes, quenched with 125 mM glycine for 5 minutes, washed with PBS, and stored at -80°C. Pellets were resuspended in FA Lysis Buffer (50 mM HEPES-KOH pH 7.5, 140 mM NaCl, 1 mM EDTA, 1% Triton X-100, 0.1% Sodium Deoxycholate) supplemented with 1x protease inhibitor cocktail (Sigma P2714) and 1 mM phenylmethylsulfonyl fluoride (PMSF). 0.45 g of 425-600 μm glass beads (Sigma G8772) were added and cells were disrupted by vortexing for 17 min at 4°C (Scientific Industries SI-D248). Lysates were centrifuged and the soluble fraction was discarded. Chromatin was solubilized by sonicating the pellet on ice in FA Lysis Buffer supplemented with protease inhibitors using a Branson 250 sonifier with a microtip probe for six 10-second cycles on output 3, with a minimum one minute break between pulses. Sonicated lysates were centrifuged, and the clarified, sonicated chromatin fractions were removed, quantitated by Bradford assay with BSA standards (Bradford, 1976), and stored at -80°C.

A specified amount of sonicated chromatin was diluted to 1 mL in FA Lysis Buffer containing protease inhibitors. A 5% input (INP) sample was removed, and then antibody was added before overnight incubation at 4°C (see **Table 2.2** for ChIP conditions). Protein A/G beads (40 μl) were then added and incubated for 2 hr at 4°C

Table 2.2. ChIP conditions.

Protein	Sonicated Chromatin	Antibody
Mre11	250 µg	2 µl Rabbit α-Mre11 (Patrick Sung)
Exo1-9myc	500 µg	5 µl Mouse α-Myc (Fisher Sci. 05419MI)
Dna2-9myc	500 µg	8 µl Mouse α-Myc (Fisher Sci. 05419MI)
Rfa	500 µg	0.5 µl (Wolf-Dietrich Heyer)
Rad51	250 µg	0.75 µl (Wolf-Dietrich Heyer)
Hdf1 (Ku70)	500 µg	1 µl Rabbit α Hdf1 (Alan Tomkinson)
FLAB-H2B	250 µg	50 µl M2 Agarose Slurry (Sigma A2220)

(Santa Cruz Biotechnology sc-2003), followed by sequential washes with FA Lysis Buffer, FA Lysis Buffer plus high salt (500 mM NaCl), Li-Cl Buffer (0.25 M LiCl, 0.5% NP-40, 0.5% Sodium Deoxycholate, in TE), and TE. Immunocomplexes (IP) were eluted from beads with 1% SDS in TE by incubating at 65°C for 15 min. IP and INP samples were incubated in Pronase solution (2 mg/mL pronase plus 10 mM $CaCl_2$) at 42°C for 2 hr. Samples were then incubated at 65°C overnight to reverse crosslinks, and DNAs were purified using a QIAquick PCR Purification kit (Qiagen).

Quantitative Real-Time PCR

DNAs isolated for ChIP and end resection assays were analyzed by quantitative real-time PCR using a Step One Plus instrument (Bio-Rad). For each reaction, 5 µl of DNA (diluted 1:10 for IP and 1:50 for INP) was added to a 20 µl reaction mixture consisting of 0.75X Maxima Sybr Green Master Mix (Thermo Fisher Scientific) and 0.15 µM forward and reverse primer in nuclease-free water (see **Table 2.3** for primer sequences). Samples were performed in triplicate and relative quantitations were obtained by plotting cycle numbers against a standard curve generated from six serial 1:10 dilutions of genomic DNA (gDNA) prepared in the same manner as a ChIP INP sample, with the first dilution containing 2 ng/µl of gDNA as measured by a NanoDrop spectrophotometer (Thermo Fisher Scientific).

In general, signals at *MAT* loci were first normalized to the *POL5* INP signal to adjust for DNA quantity, and then normalized for the fraction of cells containing a *MAT* DSB using primers that span the *MAT* HO cut site. For both ChIP and end resection experiments, signals at time points represent the fraction of the signal at T0 (pre-

Table 2.3. Primers used for quantitative real-time PCR.

Primer Name	Sequence (5′ to 3′)
POL5 For	TCCTTGTTCACCTTTGGTGGA
POL5 Rev	GTGTTCCCATAGTCTACCCATCG
HO *MAT* Cut For	GCAGCACGGAATATGGGACTA
HO *MAT* Cut Rev	TCCGTCACCACGTACTTCAGC
MAT-r 0.1kb For	ACGTGGTGACGGATATTGGG
MAT-r 0.1kb Rev	CTCTATAAGGCCAAATGTACAAACACA
MAT-r 1.8kb For	ACGCCGCGAGTCTTATGC
MAT-r 1.8kb Rev	TTAGAACGGCGATCGACGA
MAT-r 3.1kb For	CTAATGCTGCAAAATCCATATGCT
MAT-r 3.1kb Rev	CTCTATGGTGTTTTTACCTACCGC
MAT-r 6.1kb For	CCCAATAGGCATAATCCTCGA
MAT-r 6.1kb Rev	CGTGGGTATTGTACGACTTTT
MAT-r 12.0kb For	TTCCTGTTCCTGCACTCCGT
MAT-r 12.0kb Rev	GGCAAACGAGTGGCTCTTCA
ACT1 For	GCCCCAGAAGCTTTGTTCCATC
ACT1 Rev	ATGGAGCCAAAGCGGTGATTTC
MET28 For	GCAAGAGCGGAGAAGAAAGAACA
MET28 Rev	GTTTCTTGCGAATGCGGAACCG
PHO11 For	TGAAGCCGAGTCTGCTGGTG
PHO11 Rev	GGACACGAATGGTGGGCACT
MRE11 For	CACCAAAACCGCTTCCAGAA
MRE11 Rev	TTTGGCGTCCTTGATGCTCT
RAD50 For	TTGAATTTGGCAAGCCTCTGA
RAD50 Rev	TACCTGAACCATTCATGCCG
XRS2 For	TGTGGCGCAGAATCAAAGAC
XRS2 Rev	TGCCTCTGCAATGTTGGGA
YKU70 For	ATGCATTTGGCAATAGTGGAGA
YKU70 Rev	AACCTGTTTCATCCACTTGATCG
YKU80 For	CATACATTCCCGTGACCATCTCCA
YKU80 Rev	CTACGTAGTCTGCACCATAACG
SAE2 For	GATCAAAATCCCCCCCAGG
SAE2 Rev	CCTGAGTGGAGGGAAAATCCA
EXO1 For	CAAATCACGCAAAGGCCAT
EXO1 Rev	TGACCTGGCACCAATAAGGC
DNA2 For	TGATTTTGGACGAGGCAAGTC
DNA2 Rev	GAGGTCCCAAAGCGACAGG
SGS1 For	ACTTTACCGTTCCCCGAACA
SGS1 Rev	CACGGCCGGTTTCTTGATAA
TOP3 For	TGCGACCGGGAAGGAGAGTA
TOP3 Rev	TTGCCTCTCTTGGCCTCCTG
RMI1 For	CGAGGTCATCACTCAAGTGGACA
RMI1 Rev	GCAGTTGTTATCCGCCACATTCC
FUN30 For	AGGCCGTAGTGGAAGGTTTTG
FUN30 Rev	GCTGGTGCTGGAGTAGGTTC

induction). There were two exceptions to this general rule. First, for Exo1-Myc ChIPs, which have low signal and are highly affected by background, the signals were further normalized to the *POL5* IP signal to account for background fluctuations (Shim et al., 2010) (S.E. Lee personal communication). Second, for the FLAG-H2B ChIPs, the *POL5* IP signal was used to normalize for DNA quantity.

DNA End Resection and Long-Range Kinetics Analysis

For end resection assays, either INP DNA from corresponding ChIP experiments was utilized or 15 µg of sonicated chromatin was freshly prepared. Resection kinetics were analyzed as previously described (Eapen et al., 2012). Briefly, the time required for 25% resection to occur (0.75 fraction intact) at locations to the right of the *MAT* DSB was interpolated by assuming a linear relationship between time points from the resection graphs. The times to 25% resection were then plotted against the distances from the *MAT* DSB, with distance on the y-axis and time on the x-axis, and the slope of the line was obtained by linear regression, yielding the resection rate ($\Delta y/\Delta x = \Delta\text{distance}/\Delta\text{time}$, or kb/hr). A minimum of three loci were used for regression analysis.

Western Blot Analysis

TCA lysates were prepared as previously described (Trujillo et al., 2011). Briefly, 10 $O.D._{600nm}$ units of mid-log phase cells were collected and washed with 20% TCA, and pellets were stored at -80°C. Pellets were resuspended in 20% TCA, 0.5 g of 425-600 µm glass beads (Sigma G8772) were added, and lysates were prepared by vortexing with a Turbo Vortexer (Scientific Industries SI-D248) for 15 min at 4°C. Lysates were

incubated for 10 min on ice and precipitated proteins were collected by centrifugation. Pellets were resuspended in Laemli Buffer (5% SDS, 10% glycerol, 0.25 M unbuffered Tris, 0.01% Bromophenol Blue), boiled for 5 min, centrifuged, and the soluble fraction was removed for standard SDS-PAGE. Primary antibodies used were Rabbit α-Rad53 1:2,000 (Abcam ab104232) and Mouse α-beta Actin 1:20,000 (Abcam ab8224). Immunoblots were analyzed by probing with HRP-conjugated secondary antibodies (Bio-Rad), incubating with Clarity ECL substrate reagent per manufacturers instructions (Bio-Rad), and exposing to X-Ray film (Pheonix Research Products), which was then developed with a Konica SRC-101 developer. Films were digitized, and band densitometry was performed using Quantity One software (Bio-Rad) with one pixel local background subtraction.

RNA Expression Analysis

Total RNA was harvested from exponentially growing cells in YPD using a hot phenol method as previously described (Collar and Oliviero, 2001). For cDNA synthesis, RNA was first treated with RQ1 RNAse-free DNase to remove residual genomic DNA (Promega), and cDNA was synthesized using the SuperScript III First-Strand Synthesis System with Oligo$(dT)_{20}$ primers (Invitrogen). Quantitative real-time PCR was performed as described above with gene specific primers, and signals were normalized to *ACT1* to adjust for RNA quantity (see **Table 2.3** for primer sequences).

Statistical Analysis

Data were expressed as mean ± one standard deviation. For comparison of one variable, a two-tailed unequal variance *t*-test was performed. For comparison of two variables, a two-way unequal variance ANOVA with Holm-Sidak post-hoc was performed. All statistical analyses were performed using SigmaPlot software.

2.4 Results

SWI/SNF facilitates the initiation of DNA end resection

To investigate repair protein and end resection dynamics at DSBs, we utilized an established site-specific DSB assay (Jensen and Herskowitz, 1984). In this assay, addition of galactose to the medium leads to the rapid induction of the HO endonuclease, which introduces a single DSB within the yeast mating-type (*MAT*) locus. We used a strain in which the *MAT* homology regions *HMLα* and *HMRa* were also deleted, leading to a *MAT* DSB that can initiate but not complete HR (Lee et al., 1998). However, the initial events of recombinational repair, including repair factor recruitment and 5′ to 3′ DNA end resection, as well as DSB repair by non-homologous end joining (NHEJ), can be monitored spatiotemporally (Haber, 2012; White and Haber, 1990; Wu et al., 2008). As previously shown, end resection initiated rapidly after DSB induction at *MAT* in wild-type (WT) cells (**Fig 2.1A**) (Llorente and Symington, 2004; White and Haber, 1990; Zhu et al., 2008). To address the role of the SWI/SNF complex in HR, we deleted *SNF5*, a core subunit that is required to form an intact SWI/SNF complex (Peterson et al., 1994) and found that there was a 1-2 hr delay in the initiation of resection at *MAT* in the *snf5*Δ mutant strain, as well as a reduction in the extent of resection (**Fig 2.1A**; **Fig 2.2A-C**).

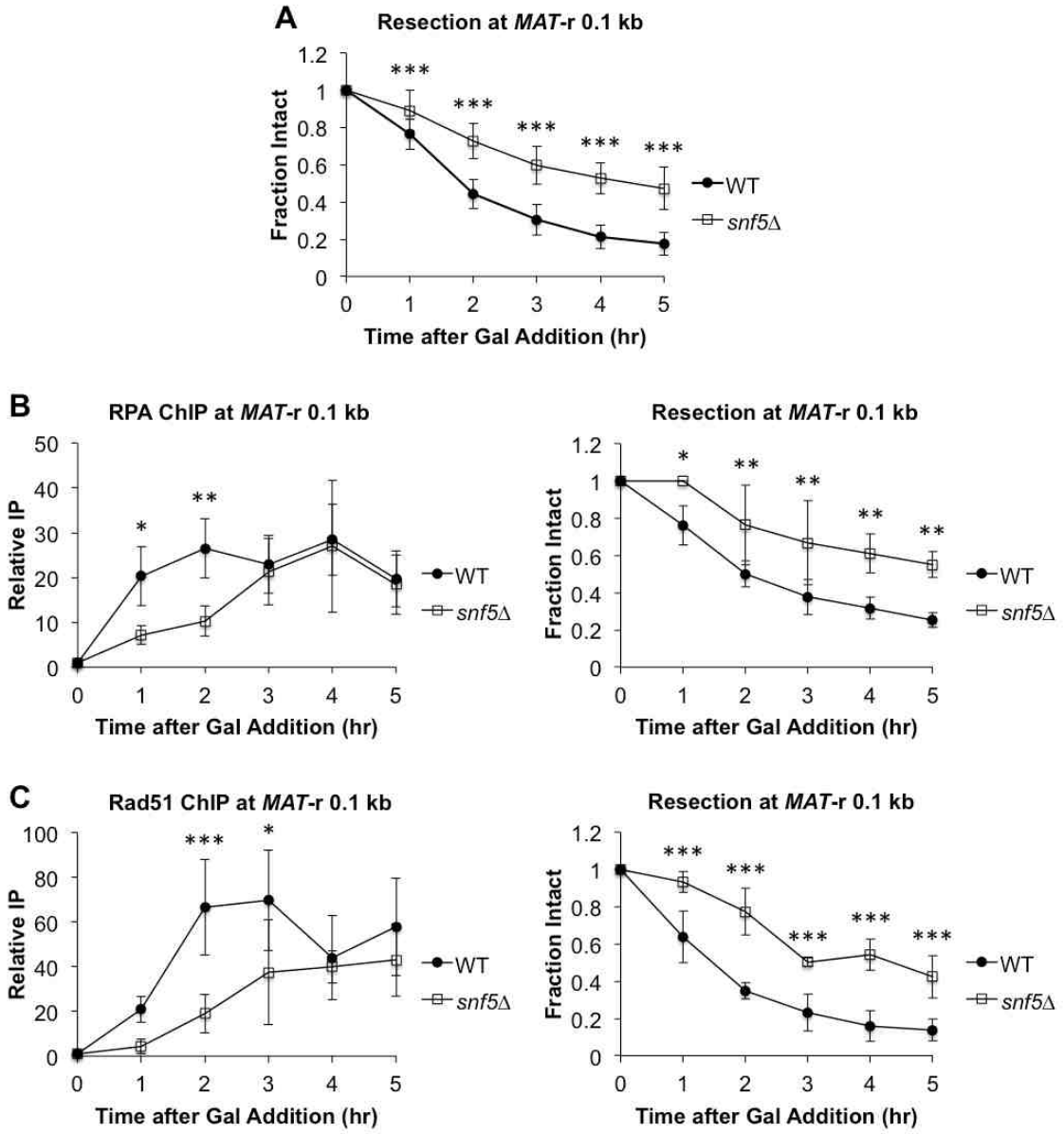

Figure 2.1. Initiation of DNA end resection at *MAT* is impaired in *snf5*Δ cells. (A) Asynchronous WT (n=9) and *snf5*Δ (n=10) cells were harvested at 1 hr intervals after addition of galactose to induce a *MAT* DSB. Resection was monitored by qPCR with primers that anneal 0.1 kb to the right of the *MAT* DSB. (B) Recruitment of RPA 0.1 kb to the right of the *MAT* DSB was monitored by ChIP (left) and DNA end resection was simultaneously monitored (right) in WT (n=3) and *snf5*Δ (n=3) asynchronous cells after addition of galactose to induce a *MAT* DSB. (C) Recruitment of Rad51 0.1 kb to the right of the *MAT* DSB was monitored by ChIP (left) and DNA end resection was simultaneously monitored (right) in WT (n=3) and *snf5*Δ (n=3) asynchronous cell populations as described in B. Error bars denote one standard deviation. Statistical differences between WT and *snf5*Δ at time points were assessed by two-way ANOVA with Holm-Sidak post-hoc analysis. * = $p<0.05$. ** = $p<0.01$. *** = $p<0.001$.

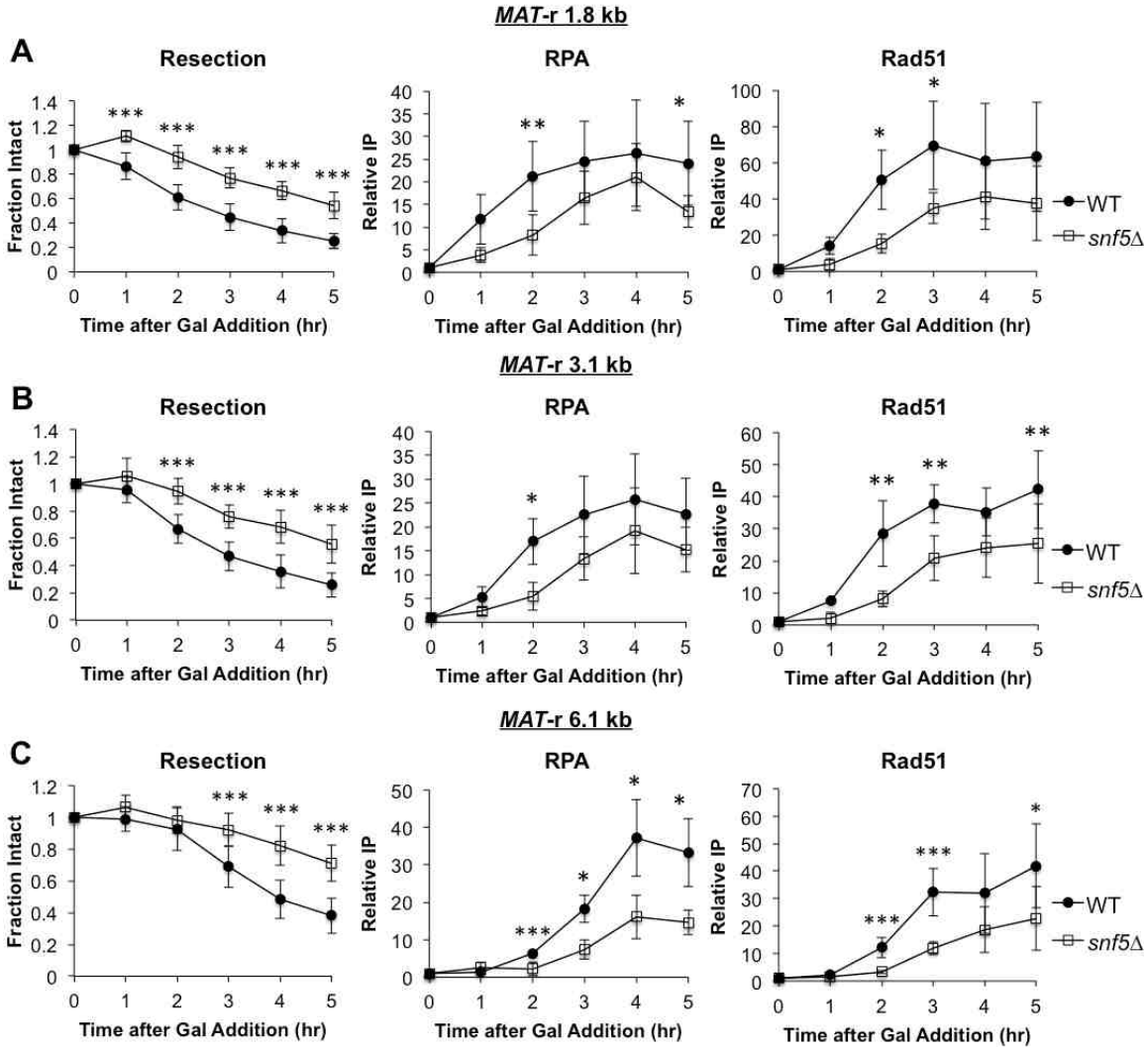

Figure 2.2. DNA end resection and ssDNA-binding protein recruitment are impaired in *snf5*Δ at distal *MAT* positions. Asynchronous WT (n=3) and *snf5*Δ (n=3) cells were harvested at 1 hr intervals after addition of galactose to induce a *MAT* DSB. DNA end resection, RPA and Rad51 recruitment were simultaneously monitored in WT (n=3) and *snf5*Δ (n=3) asynchronous cell populations as in Figure 1 with primers annealing (A) 1.8 kb, (B) 3.1 kb, and (C) 6.1 kb to the right of the break. Error bars denote one standard deviation. Statistical differences between WT and *snf5*Δ at time points were assessed by two-way ANOVA with Holm-Sidak post-hoc analysis. * = $p<0.05$. ** = $p<0.01$. *** = $p<0.001$.

Consistent with the defect in the initiation of resection the *snf5*Δ mutant strain, there was also a delay in the recruitment of both the RPA single-stranded DNA binding protein (**Fig 2.1B**) and Rad51 recombinase (**Fig 2.1C**) to the DSB in *snf5*Δ cells, and diminished recruitment of these factors distal to the break (**Fig 2.2A-C**).

While the results suggested a previously uncharacterized role for SWI/SNF in the initiation of DNA end resection, it was possible that this was an indirect effect. This prompted us to examine the impact of deleting *SNF5* on cell cycle distribution, as this influences the expression and activity of multiple components of the resection machinery (Symington, 2016) and the efficiency by which the *MAT* DSB itself is formed. We found that an asynchronous population of *snf5*Δ cells contained approximately 20% more G2/M phase cells than WT cells, and that both WT and *snf5*Δ cell populations demonstrated a shift from G1 phase to G2/M phase after addition of galactose to the pre-induction medium (**Fig 2.3A-B**). Thus, the resection impairment in *snf5*Δ is not due to an accumulation of cells in G1 phase. While there was rapid cleavage at *MAT* in WT cells after addition of galactose, *MAT* cleavage was less efficient in *snf5*Δ cells (**Fig 2.4A**). Because either reduced transcription of *GAL-HO* in *snf5*Δ cells or increased nucleosome occupancy at the *MAT* HO cut site could account for this phenotype, we explored both possibilities (Haber, 2012). In agreement with the known role of SWI/SNF in facilitating the transcription of inducible genes, including *GAL10, SUC2,* and *HO* (Peterson and Herskowitz, 1992; Stern et al., 1984), transcription of *GAL-HO* was modestly impaired in *snf5*Δ cells after addition of galactose to the medium (**Fig 2.4B**). In contrast, no difference was observed in nucleosome occupancy at the *MAT* HO cut site, consistent with previous nucleosome mapping around the *MAT* DSB in *snf5*Δ cells (Kent et al.,

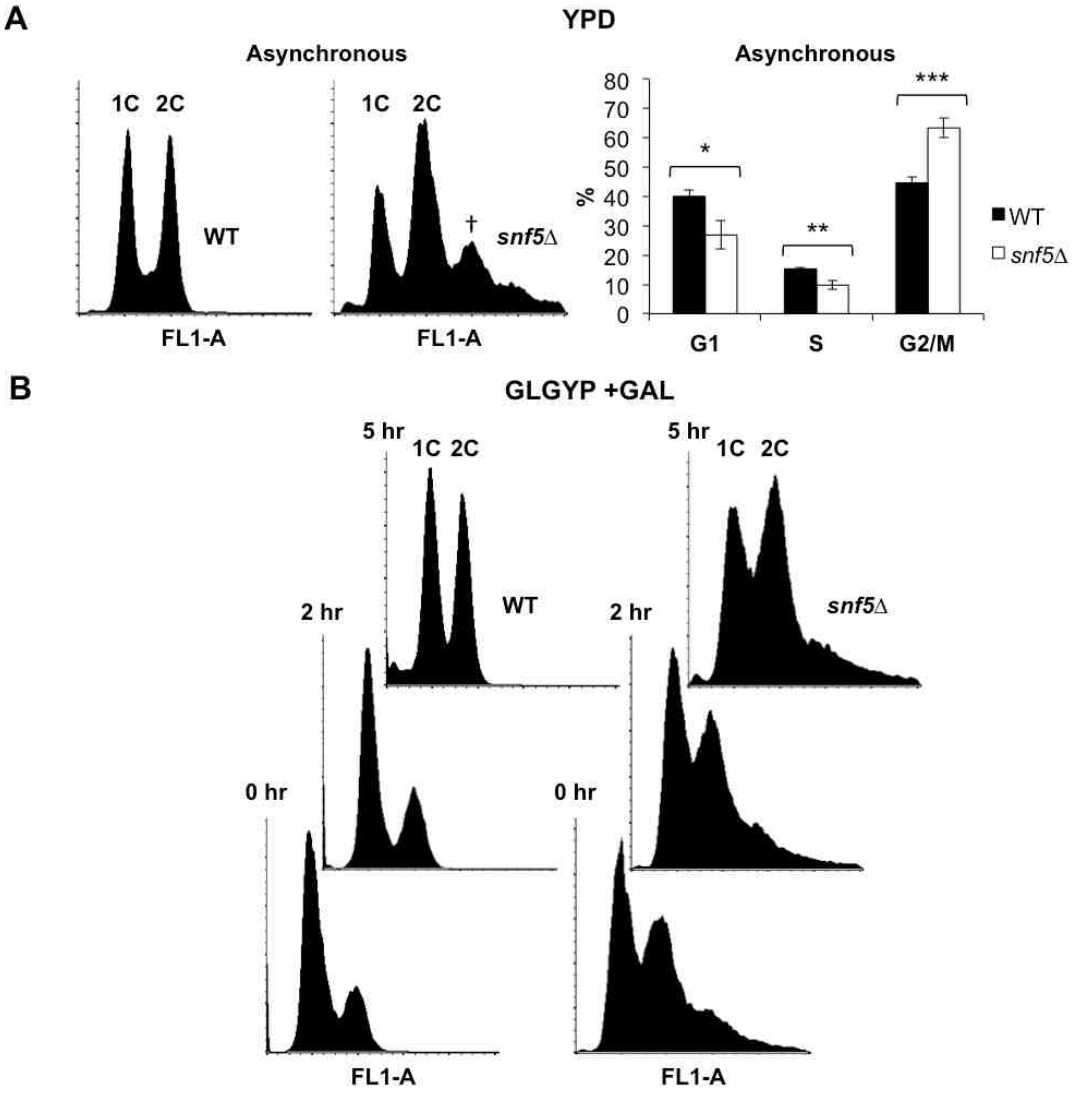

Figure 2.3. Cell cycle distribution in WT and *snf5*Δ strains. (A) Asynchronous, mid-log populations of WT and *snf5*Δ cells in glucose-containing rich media (YPD) were collected and processed for FACS. Left panels represent WT and *snf5*Δ cell cycle distributions. The >2N signal (†) in *snf5*Δ may represent flocculated cells. The right panel represents the distribution of asynchronous WT (n=3) and *snf5*Δ cells (n=3) in G1, S, and G2/M phases. Error bars denote one standard deviation. Statistical differences between WT and *snf5*Δ were assessed by Student's *t*-Test. * = $p<0.05$ ** = $p<0.01$ *** = $p<0.001$. (B) WT and *snf5*Δ cells were grown in pre-induction medium (GLGYP) to mid-log phase and then collected and processed for FACS before (0 hr) and at 2 and 5 hr after addition of galactose to induce a *MAT* DSB.

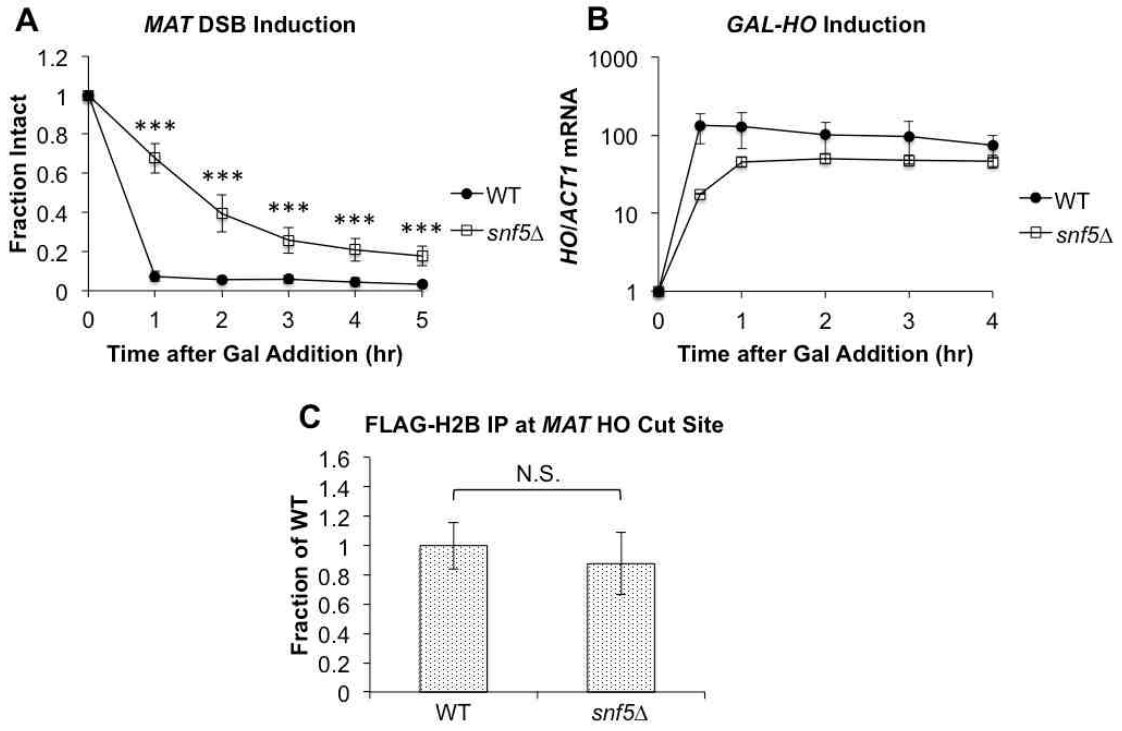

Figure 2.4. Effect of *snf5*Δ on *GAL-HO* transcription and nucleosome occupancy at the *MAT* HO cut site. (A) DSB induction at *MAT* was measured in WT (n=11) and *snf5*Δ (n=10) cells at 1 hr intervals after galactose induction using qPCR with primers spanning the *HO* cut site. Error bars denote one standard deviation. Statistical differences between WT and *snf5*Δ at time points were assessed by two-way ANOVA with Holm-Sidak post-hoc analysis. *** = $p<0.001$. (B) *GAL-HO* transcript levels were measured in WT (n=2) and *snf5*Δ (n=2) cells after galactose induction by RT-qPCR. Error bars denote one standard deviation. (C) Nucleosome occupancy at the *MAT* HO cut site in WT (n=4) and *snf5*Δ (n=4) cells in pre-induction medium (GLGYP) was measured by ChIP of FLAG-tagged histone H2B using primers spanning the HO cut site. Error bars denote one standard deviation. Statistical difference between WT and *snf5*Δ was assessed by Student's *t*-Test. N.S.= not significant.

2007) (**Fig 2.4C**). To account for the decrease in *MAT* cleavage in *snf5*Δ cells, all data presented, including end resection and repair factor recruitment, have been adjusted for the fraction of cells containing a *MAT* DSB as described in Materials and Methods.

SWI/SNF controls MRX recruitment to DSB ends

The observation that *snf5*Δ cells had a defect in the initiation of DNA end resection led us to investigate the upstream events in DSB repair that determine pathway choice between HR and NHEJ. Two complexes compete for DSB ends: Mre11/Rad50/Xrs2 (MRX; Mre11/Rad50/Nbs1, MRN in mammals) and Ku70/Ku80 (KU). When MRX binding predominates, generally in G2/M phase, Sae2 (CtIP in mammals) stimulates the endonucleolytic activity of MRX to initiate the first phase of DNA end resection (Mimitou and Symington, 2008). Furthermore, the activity of MRX contributes to KU dissociation from the DSB, facilitating further end resection (Wu et al., 2008). When KU binding predominates, generally in G1 phase, it blocks DNA end resection and recruits accessory NHEJ factors, including the MRX complex, which in this context acts as an end-bridging factor rather than as a nuclease (Chen et al., 2001; Davis and Chen, 2013; Shao et al., 2012).

We examined the recruitment of these pathway-regulating complexes to DSB ends in both WT and *snf5*Δ cells after DSB induction. While there was an ~4.5 fold decrease in Mre11 binding to the *MAT* DSB in *snf5*Δ cells (**Fig 2.5A**), Ku70 was recruited at higher levels and retained longer at the break in the mutant (**Fig 2.5B**). Complementing the *snf5*Δ strain with a plasmid bearing a wild-type *SNF5* gene completely rescued the DSB induction, MRX binding, and DNA end resection

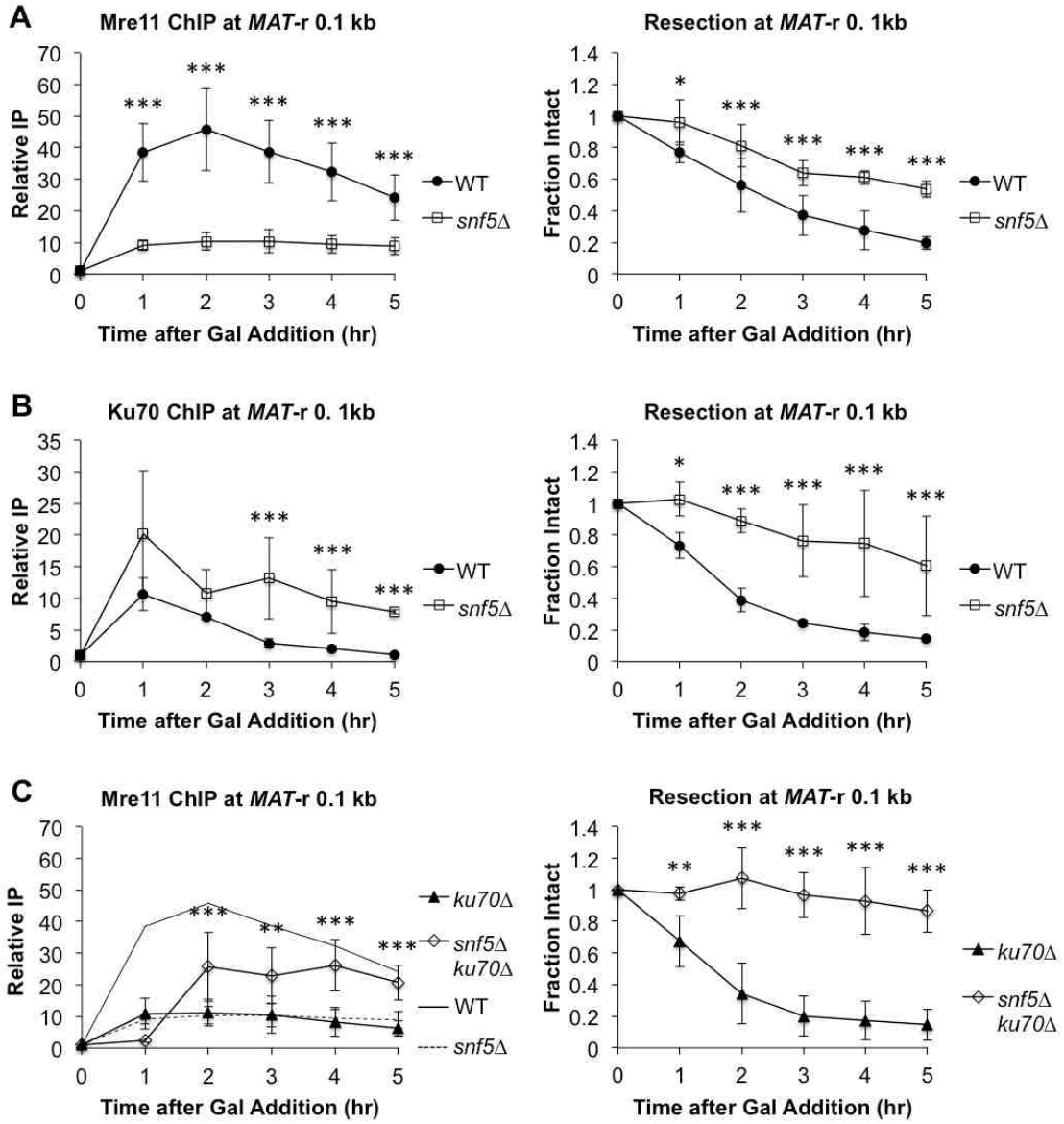

Figure 2.5. SWI/SNF regulates recruitment of MRX to a *MAT* DSB. (A) Asynchronous WT (n=7) and *snf5*Δ (n=6) cells were harvested at 1 hr intervals after addition of galactose to induce a *MAT* DSB. Recruitment of Mre11 0.1 kb to the right of the *MAT* DSB was monitored by ChIP (left) and DNA end resection was simultaneously monitored (right). (B) Asynchronous WT (n=3) and *snf5*Δ (n=3) cells were harvested after addition of galactose. Recruitment of Ku70 (left) and DNA end resection (right) were monitored as in A. (C) Asynchronous *ku70*Δ (n=5) and *snf5*Δ*ku70*Δ (n=3) cells were harvested after addition of galactose. Recruitment of Mre11 (left) and DNA end resection (right) were monitored as in A. WT (solid line) and *snf5*Δ (dashed line) Mre11 ChIP recruitment data from A are overlaid on the graph. Error bars denote one standard deviation. Statistical differences between strains at time points were assessed by two-way ANOVA with Holm-Sidak post-hoc analysis. * = $p<0.05$ ** = $p<0.01$ *** = $p<0.001$.

phenotypes of *snf5*Δ, demonstrating that the results were not due to the presence of another mutation in this strain (**Fig 2.6A-C**). Furthermore, the *snf5*Δ mutation did not alter the expression of genes encoding MRX or KU components (Sudarsanam et al., 2000) (**Fig 2.6D**). Together, these data argue that SWI/SNF has a direct role in recruiting MRX to DSB ends.

We initially considered a model in which MRX and KU directly compete for binding to DSB ends and that SWI/SNF promotes the binding of MRX over KU. In support of this model, deletion of *KU70* in *snf5*Δ cells partially rescued MRX recruitment to the *MAT* DSB (**Fig 2.5C**). However, we noted that *snf5*Δ*ku70*Δ cells exhibited reduced growth, increased accumulation in G1 phase, and a failure to enter S phase after DSB induction (**Fig 2.7A**). These phenotypes were accompanied by a lack of end resection (**Fig 2.5C**, right panel) and increased impairment in DSB induction compared to the *snf5*Δ single mutant (**Fig 2.7B**). Thus, we speculate that the partial rescue of MRX recruitment in the *snf5*Δ*ku70*Δ double mutant may represent the presence of stalled, inactive MRX that is unable to initiate end resection. Moreover, MRX recruitment was significantly decreased in *ku70*Δ cells (**Fig 2.5C**, *ku70*Δ), as others have also shown (Wu et al., 2008; Zhang et al., 2007). Thus, as discussed in more detail below, a paradigm of simple competition for ends does not account for the known roles of MRX in both HR and NHEJ. Instead, our data are consistent with an alternative model in which there are HR-active and NHEJ-active pools of MRX at DNA ends (Wu et al., 2008), with SWI/SNF promoting the association of the pool of HR-active MRX.

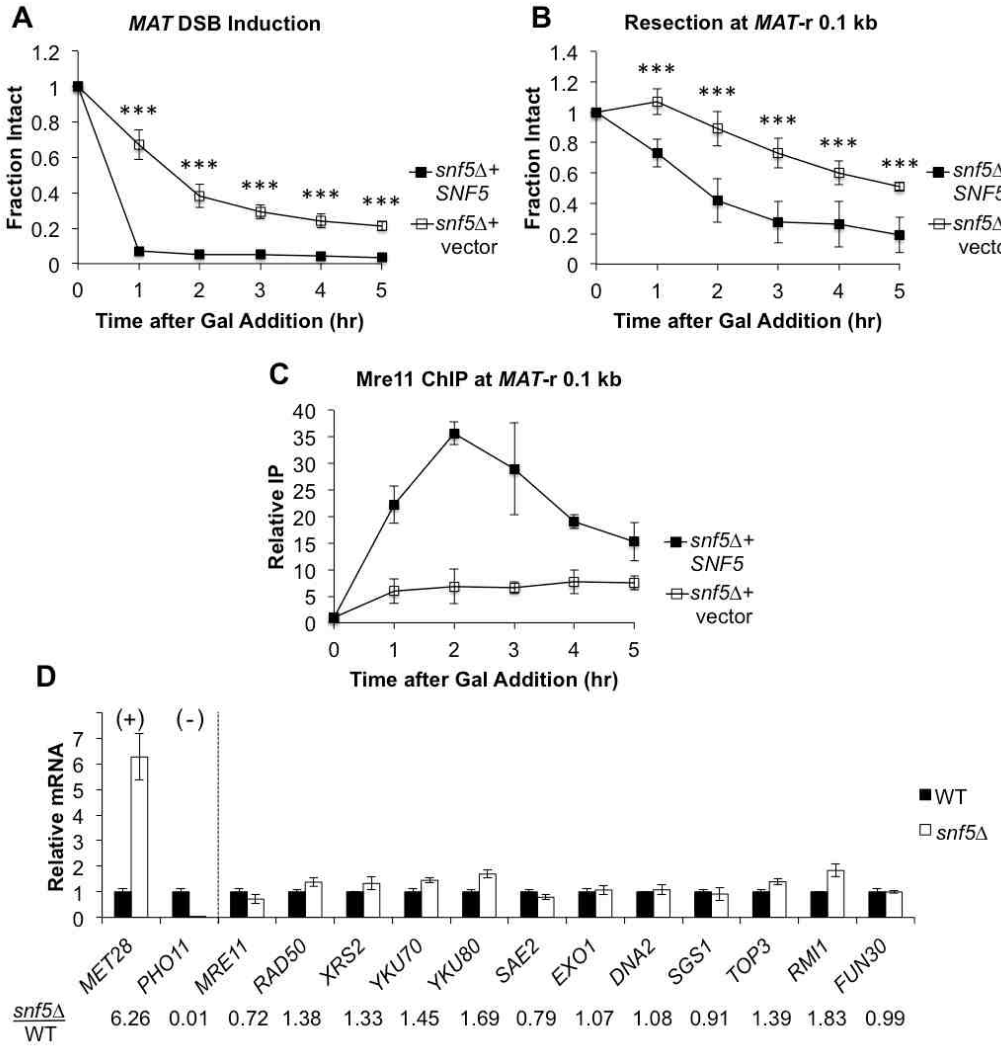

Figure 2.6. Complementation of *snf5*Δ phenotypes with a plasmid carrying *SNF5*. Asynchronous *snf5*Δ + pRS316 (vector) (n=3) and *snf5*Δ + pRS416-*SNF5-HA* (*SNF5*) (n=3) cells were harvested after addition of galactose to induce a *MAT* DSB. (A) DSB induction was monitored by qPCR with primers spanning the HO cut site. (B) DNA resection 0.1 kb to the right of the *MAT* DSB was monitored by qPCR. Error bars denote one standard deviation. Statistical differences between strains at time points were assessed by two-way ANOVA with Holm-Sidak post-hoc analysis. *** = $p<0.001$. (C) Asynchronous *snf5*Δ + vector (n=2) and *snf5*Δ + *SNF5* (n=2) cells were harvested after addition of galactose to induce a *MAT* DSB. Recruitment of Mre11 0.1 kb to the right of the *MAT* DSB was monitored by ChIP. Error bars denote one standard deviation. (D) Transcript levels from indicated genes in WT (n=2) and *snf5*Δ (n=2) asynchronous cells were measured by RT-qPCR. Signals were normalized to *ACT1* RNA levels, with WT levels set as 1.0. Errors bars denote one standard deviation. *MET28* and *PHO11* represent control genes that are either be de-repressed or repressed in the absence of SWI/SNF, respectively {Sudarsanam:2000df}.

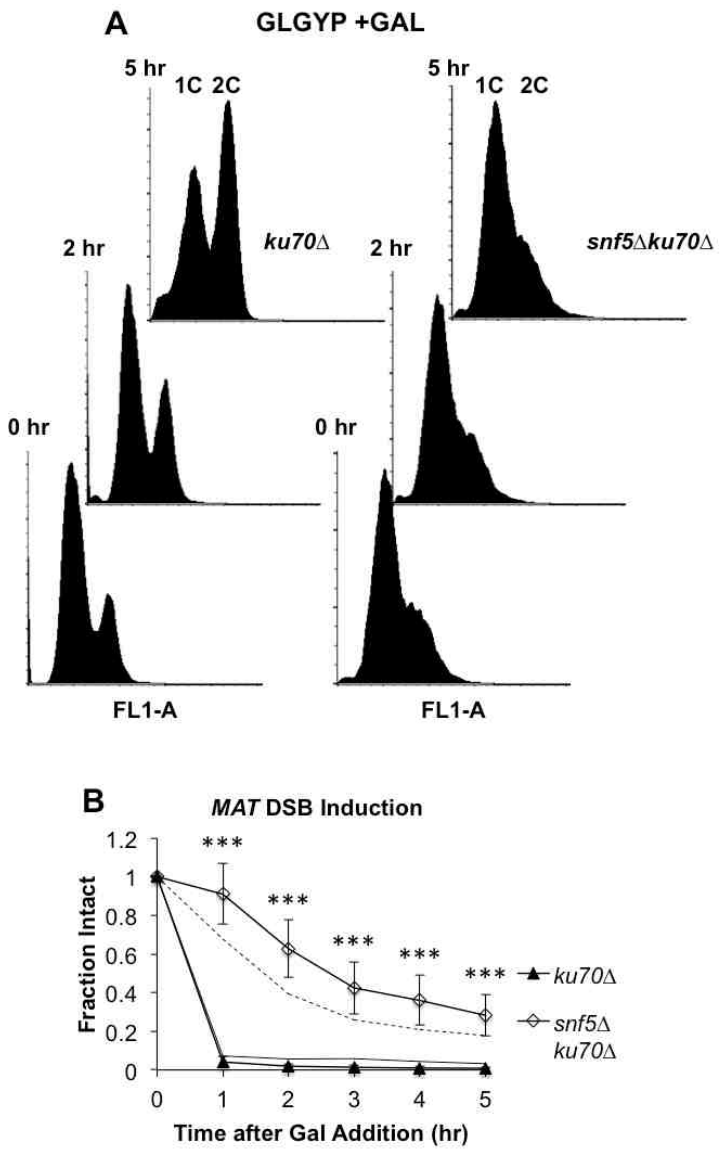

Figure 2.7. Effect of *snf5*Δ*ku70*Δ on cell cycle. (A) *ku70*Δ and *snf5*Δ*ku70* cells were grown in pre-induction medium (GLGYP) to mid-log phase and then processed for FACS both before (0 hr) and at 2 and 5 hr after addition of galactose to induce a *MAT* DSB. (B) Asynchronous *ku70*Δ (n=6) and *snf5*Δ*ku70*Δ (n=3) cells were harvested after addition of galactose, and DSB Induction was monitored by qPCR with primers spanning the cut site. Error bars denote one standard deviation. Statistical differences between strains at time points were assessed by two-way ANOVA with Holm-Sidak post-hoc analysis. *** = $p<0.001$. WT (solid line) and *snf5*Δ (dashed line) DSB induction data from supplemental Figure 2A are overlaid for comparison.

*Activation of the DNA damage response is impaired in snf5*Δ

The DNA damage response (DDR) can be initiated by both the yeast ATR homolog Mec1, which is activated by pathologic ssDNA generation, and the yeast ATM homolog Tel1, which associates with damage-recruited MRX (Gobbini et al., 2013). As we observed both impaired DNA end resection and reduced MRX recruitment to a *MAT* DSB in *snf5*Δ cells, we investigated whether the DDR response was also altered in this mutant. We found that DDR activation, as measured by phosphorylation of Rad53, was abolished in *snf5*Δ (**Fig 2.8**). Interestingly, the magnitude of the defect in Rad53 phosphorylation was greater than the magnitude of the defects in initiation of end resection and MRX recruitment (compare **Fig 2.1A** and **Fig2.5A** to **Fig 2.8**). This could be due to the recently discovered non-chromatin role for the SWI/SNF ATPase subunit, Snf2, in activating the Mec1 kinase (Kapoor et al., 2015). Thus, in *snf5*Δ cells, both the signaling events for DDR activation and Mec1-mediated signal transduction are impaired.

Long-range resection is delayed in *snf5*Δ and relies upon Exo1

DNA resection during HR is a multistep process consisting of an initial resection phase mediated by MRX-Sae2 (MRN-CtIP in mammals) that generates short, 3′ ssDNA overhangs, and a subsequent long-range resection phase mediated by either Exonuclease 1 (Exo1) or the nuclease/helicase complex Dna2-Sgs1/Top3/Rmi1 (Clerici et al., 2005; Daley et al., 2015; Garcia et al., 2012; Zhu et al., 2008) (Dna2-STR). Our observation that *snf5*Δ cells had defects in both initial DNA resection and MRX recruitment to the *MAT* DSB led to the prediction that long-range resection would also be impaired. To

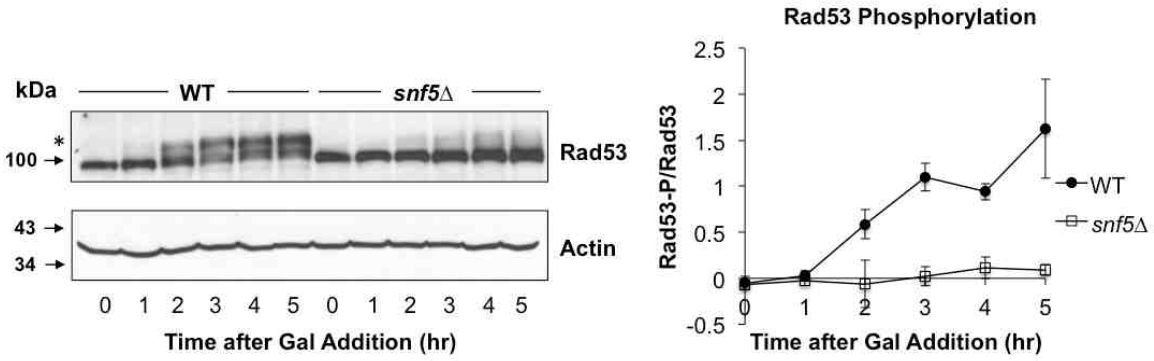

Figure 2.8. Rad53 phosphorylation is impaired in *snf5*Δ. (A) Representative immunoblot of lysates from WT and *snf5*Δ mid-log phase cells before (T0) and at 1 hr intervals after addition of galactose to induce a *MAT* DSB. Blots were probed with antibodies against Rad53 and Beta-actin, which served as a loading control. Phosphorylated Rad53 (*). Images were adjusted for increased brightness. (B) Ratio of phosphorylated to unphosphorylated Rad53 was determined by densitometry of two independent immunoblots. Error bars denote one standard deviation.

address the role of SWI/SNF in the long-range resection pathways, we measured resection at distal locations from the *MAT* DSB in WT and *snf5*Δ cells and examined the effect of *exo1*Δ and *sgs1*Δ mutations in both WT and *snf5*Δ backgrounds on long-range resection after *MAT* DSB induction. While initiation of resection was delayed in *snf5*Δ compared to WT cells (**Fig 2.9A**; **Fig 2.10A**, left panel), resection initiated at the same time in the *exo1*Δ and *sgs1*Δ single mutants as in WT cells (**Fig 2.9A**). Furthermore, when combined with *snf5*Δ, the loss of either *EXO1* or *SGS1* did not further delay the initiation of resection over that seen in *snf5*Δ cells (**Fig 2.9A**; **Fig 2.10B-C**, left panels), confirming that Exo1 and Dna2-STR do not participate in the initiation of DNA end resection (Zhu et al., 2008).

In contrast to the results proximal to the *MAT* DSB, both *exo1*Δ and *sgs1*Δ cells demonstrated impaired long-range resection to the right of the break (**Fig 2.9B**; **Fig 2.10B-C**, middle and right panels). Although long-range resection was delayed in *snf5*Δ cells because of the defect in resection initiation, the pattern of resection was otherwise similar to that seen in WT cells (**Fig 2.9B**; **Fig 2.10A**, middle and right panels). Interestingly, deletion of *SGS1* in *snf5*Δ cells only modestly decreased long-range resection, whereas resection was completely abolished 12 kb to the right of the break in a *snf5*Δ*exo1*Δ double mutant (**Fig 2.9B**; **Fig 2.10B-C**). To gain further insight into the characteristics of long-range resection in these strains, we interpolated the time to 25% resection (0.75 fraction intact by qPCR) at various distances to the right of the *MAT* DSB (Eapen et al., 2012) (**Fig 2.9C**). By using the time to 25% resection immediately next to the break as a measure of resection initiation, we found that initiation was delayed by ~1.3 hr in all *snf5*Δ strains compared to *SNF5* cells, and that timely initiation depended

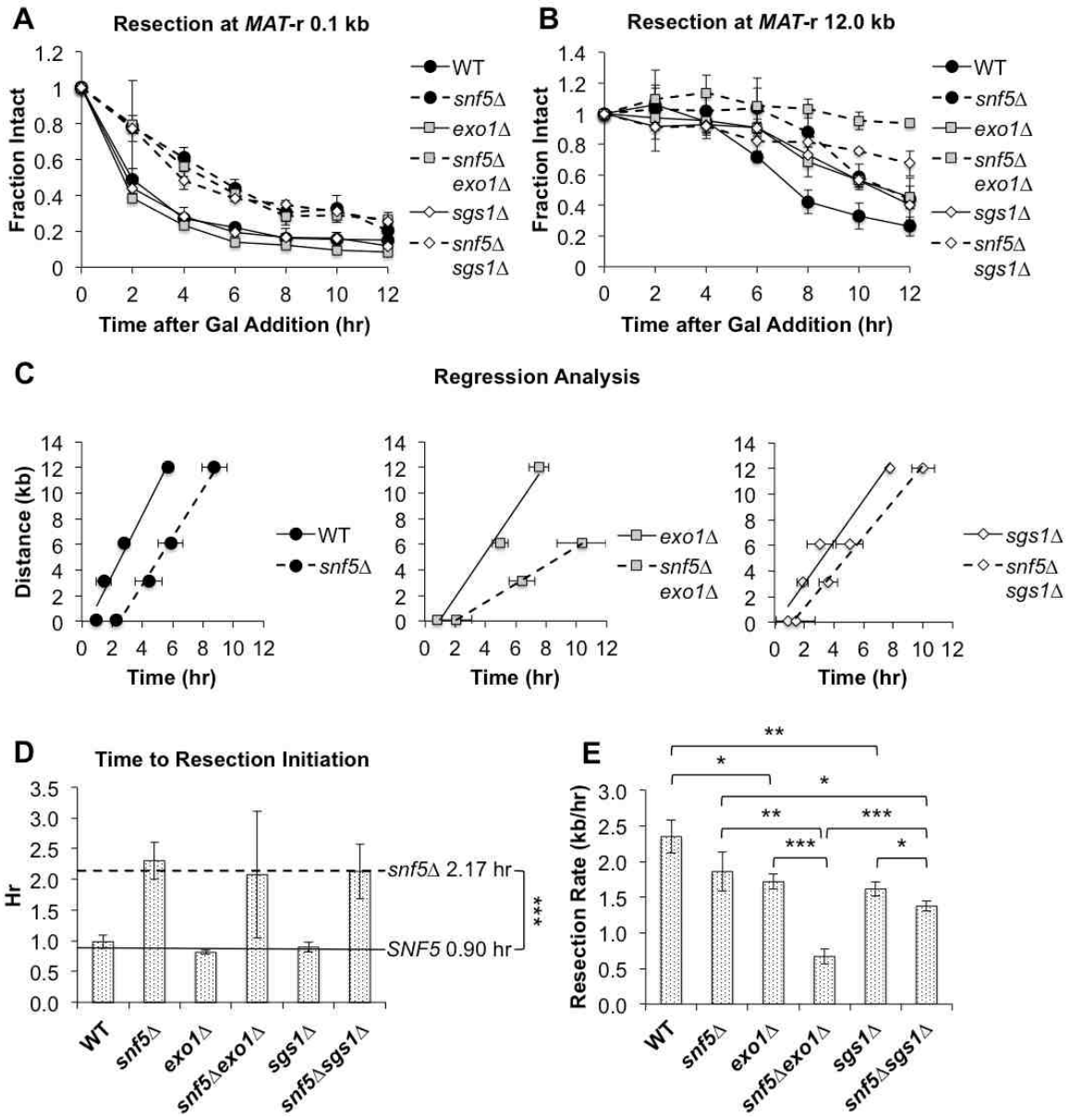

Figure 2.9. Long-range resection is delayed in *snf5*Δ cells and relies upon Exo1. Asynchronous WT, *snf5*Δ, *exo1*Δ, *snf5*Δ*exo1*Δ, *sgs1*Δ, and *snf5*Δ*sgs1*Δ cells (n=3) were harvested at 2 hr intervals after addition of galactose to induce a *MAT* DSB. Resection was monitored by qPCR with primers annealing either 0.1 kb (A) or 12.0 kb (B) to the right of the *MAT* DSB. (C) The time for 25% resection to occur (0.75 fraction intact) at positions to the right of the *MAT* DSB. (D) The time for 25% resection to occur immediately adjacent to the *MAT* was designated as the time to resection initiation, and (E) resection rates were calculated by determining the slopes of the graphs by linear regression analysis. Error bars denote one standard deviation. Statistical comparisons between strains were assessed by Student's *t*-Test. * = $p<0.05$. ** = $p<0.01$. *** = $p<0.001$.

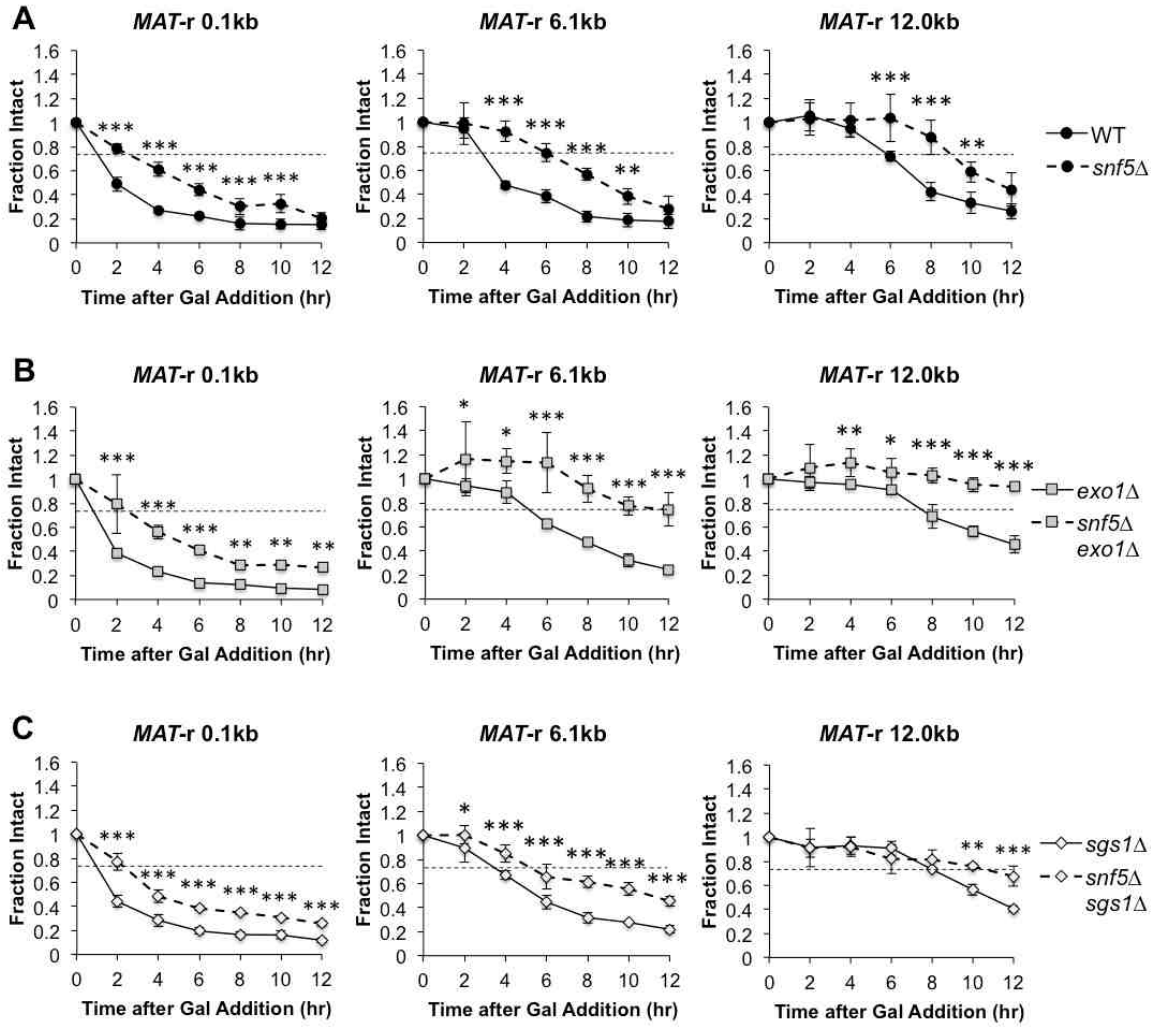

Figure 2.10. Long-range resection in WT, *snf5*Δ, *exo1*Δ, *snf5*Δ*exo1*Δ, *sgs1*Δ, and *snf5*Δ*exo1*Δ cells. Asynchronous WT and mutant cells were harvested after addition of galactose to induce a *MAT* DSB. Resection was monitored by qPCR with primers annealing 0.1 kb, 6.1 kb, and 12.0 kb to the right of the DSB. (A) WT (n=3) and *snf5*Δ (n=3); (B) *exo1*Δ (n=3) and *snf5*Δ*exo1*Δ (n=3); (C) *sgs1*Δ (n=3) and *snf5*Δ*sgs1*Δ (n=3). Error bars denote one standard deviation. Statistical differences between strains at time points were assessed by two-way ANOVA with Holm-Sidak post-hoc analysis. * = $p<0.05$ ** = $p<0.01$ *** = $p<0.001$. The dashed line represents the 0.75 fraction intact DNA signal used in the distance versus time plots in Figure 2.9.

only on SWI/SNF and not Exo1 or Dna2-STR (**Fig 2.9D**). Using linear regression analysis to obtain resection rates (Eapen et al., 2012) (**Chapter 2.3**), we found that there was no significant difference in the resection rate between WT and *snf5*Δ cells (**Fig 2.9E**). Thus, these data provide strong evidence that the resection phenotype of *snf5*Δ is characterized by a delay in initiation but does not involve a significant reduction in resection velocity. The deletion of either *EXO1* or *SGS1* only reduced the rate of resection by ~25%, demonstrating that either pathway can largely compensate for the loss of the other (**Fig 2.9E**). When combined with *snf5*Δ, the loss of *SGS1* again led to a ~25% decrease in resection rate compared to the *snf5*Δ single mutant, suggesting that Dna2-STR has a relatively minor role in long-range resection in the absence of SWI/SNF, and/or the Exo1 pathway can still compensate for the loss of Dna2-STR in the absence of *SNF5*. (**Fig 2.9E**). In contrast, the loss of *EXO1* in *snf5*Δ cells led to a ~65% decrease in resection rate compared to *snf5*Δ (**Fig 2.9E**). These observations suggested that SWI/SNF is critical for orchestrating the participation of Dna2-STR at the *MAT* DSB, as cells are disproportionately reliant upon Exo1 to accomplish long-range resection in the absence of functioning SWI/SNF.

To address the relationship between SWI/SNF and the Exo1 and Dna2-STR pathways, we examined the effect of *snf5*Δ on the recruitment of Exo1 and Dna2 to the *MAT* DSB (**Fig 2.11**), and found that the recruitment of both Exo1-Myc and Dna2-Myc was impaired in *snf5*Δ cells compared to WT (**Fig 2.11A-B**). However, while maximal Exo1-Myc recruitment was decreased by ~50%, maximal Dna2-Myc recruitment was decreased by ~90% in *snf5*Δ cells (**Fig 2.11C**). This suggested that Exo1 has a decreased reliance on SWI/SNF to load onto breaks compared to Dna2-STR (**Fig 2.11**). Together,

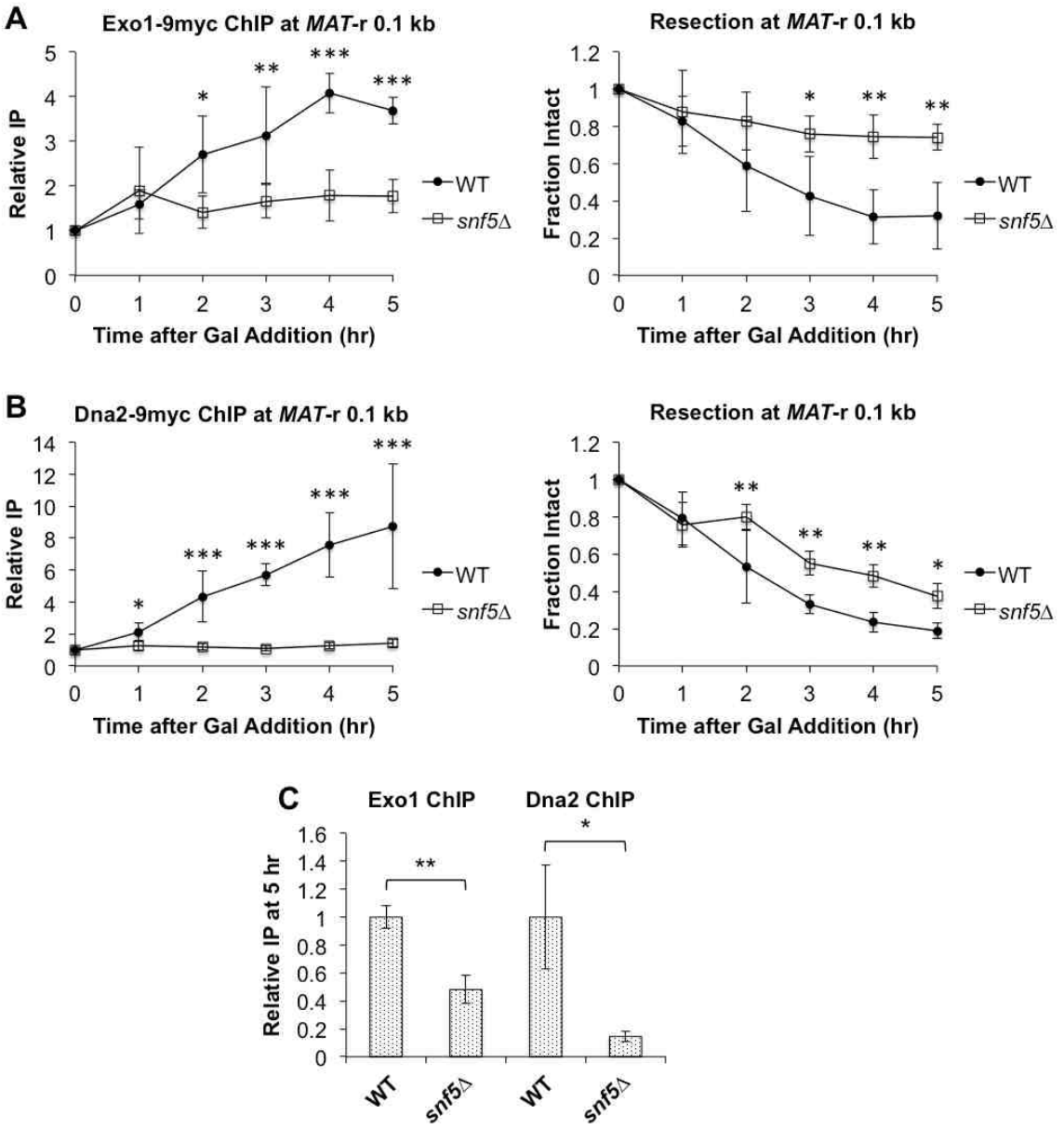

Figure 2.11. Recruitment of Exo1 and Dna2 to a *MAT* DSB is impaired in *snf5*Δ cells. Asynchronous WT (n=3) and *snf5*Δ (n=3) strains containing Exo1-Myc or Dna2-Myc were harvested at 1 hr intervals after addition of galactose to induce a *MAT* DSB. Recruitment of (A) Exo1-Myc or (B) Dna2-Myc 0.1 kb to the right of the *MAT* DSB was monitored by ChIP (left) and DNA end resection was simultaneously monitored (right). Error bars denote one standard deviation. Statistical differences between strains at time points were assessed by two-way ANOVA with Holm-Sidak post-hoc analysis. * = $p<0.05$ ** = $p<0.01$ *** = $p<0.001$. (C) Recruitment of Exo1-Myc and Dna2-Myc at 5 hr in *snf5*Δ relative to recruitment in WT, which was set as 1. Error bars denote one standard deviation. Statistical differences between recruitment at 5gr in WT and *snf5*Δ cells were assessed by Student's *t*-Test. * = $p<0.05$ ** = $p<0.01$.

these results demonstrated that SWI/SNF acts early in the long-range resection process to coordinate the timely initiation of resection and subsequent loading of long-range resection factors, and that in the absence of functional SWI/SNF, Exo1-mediated resection constitutes the primary pathway.

Nucleosome eviction is delayed in *snf5*Δ

After a DSB is formed at *MAT*, nucleosomes are rapidly evicted for many kilobases on both sides of the break, a process that facilitates the recruitment of the Rad51 recombinase and therefore later steps in HR (Tsukuda et al., 2005). As SWI/SNF has nucleosome eviction activity and is recruited to a *MAT* DSB (Bennett et al., 2013; Chai, 2005; Kwon et al., 1994), we examined whether nucleosome displacement was impaired at a *MAT* DSB in *snf5*Δ cells, thereby accounting for the reduced recruitment of MRX and the delay in end resection and Rad51 recruitment at the *MAT* DSB. We monitored nucleosome eviction by FLAG-H2B ChIP at several positions near the *MAT* locus after DSB induction in WT and *snf5*Δ cells, and compared nucleosome occupancy to end resection (**Fig 2.12A-C**). In WT cells, both FLAG-H2B eviction and DNA end resection initiated within one hr after formation of the *MAT* DSB and extended rapidly to more distal positions, whereas FLAG-H2B eviction and end resection were concurrently delayed in *snf5*Δ. The close relationship between nucleosome eviction and end resection in both WT and *snf5*Δ cells strongly suggested that the two processes are linked. Interestingly, nucleosome eviction appeared to slightly precede end resection in WT but not *snf5*Δ cells (**Fig 2.12A-C**), although the difference was trending and not significant (**Fig 2.13**). Taken together, our results argue that nucleosome eviction and DNA end

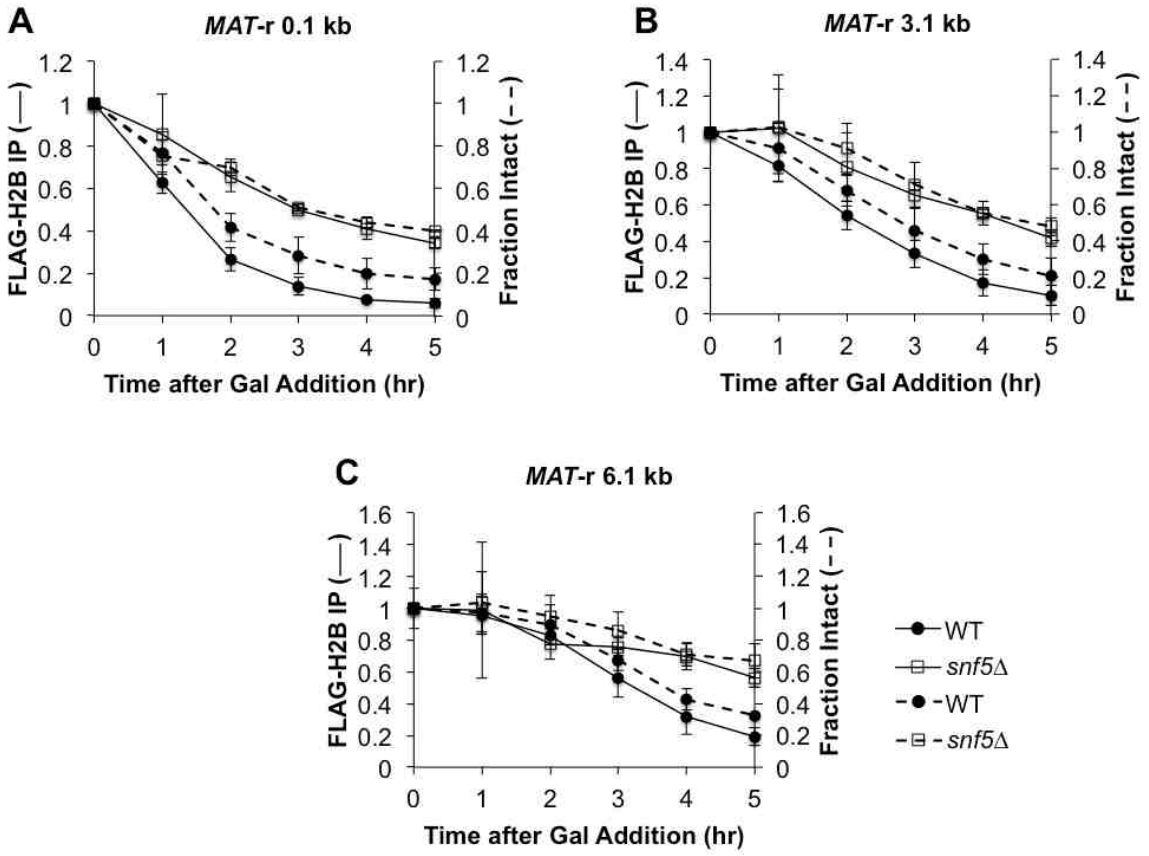

Figure 2.12. Nucleosome eviction at *MAT* is delayed in *snf5*Δ cells. Asynchronous WT (n=4) and *snf5*Δ (n=3) cells containing FLAG-H2B were harvested at 1 hr intervals after addition of galactose to induce a *MAT* DSB. H2B eviction was monitored by ChIP (solid lines) using qPCR with primers that anneal (A) 0.1 kb; (B) 3.1 kb; and (C) 6.1 kb to the right of the DSB, and resection was simultaneously monitored (dashed lines). Error bars denote one standard deviation.

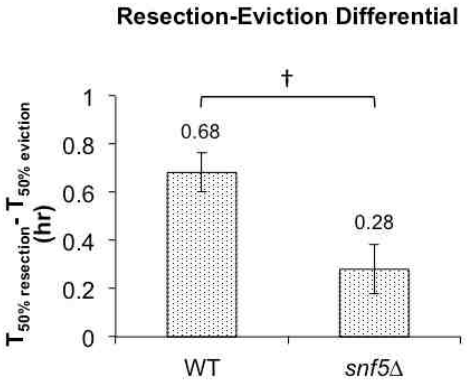

Figure 2.13. Temporal relationship between nucleosome eviction and DNA end resection in WT and *snf5*Δ cells. The difference in time between DNA end resection and FLAG-H2B eviction (resection-eviction differential) was calculated by interpolating the time for 50% resection and 50% FLAG-H2B eviction to occur at the same position and subtracting these values. Differentials were calculated for four different positions (*MAT*-r 0.1, 1.8, 3.1, and 6.1 kb) to the right of the *MAT* DSB and averaged. Statistical significance between WT and *snf5*Δ was assessed by Student's *t*-test. † = trend ($p<0.1$). Values represent WT (n=4) and *snf5*Δ (n=3) biological replicates.

resection during HR are tightly linked, and that SWI/SNF contributes a significant role to the timely initiation of both processes.

2.5 Discussion

In this study, we have identified a novel role for the SWI/SNF ATP-dependent nucleosome remodeler in facilitating early events during DNA DSB repair by HR in *S. cerevisiae*. Previous research demonstrated that SWI/SNF is recruited to a *MAT* DSB in yeast where it functions at or just preceding strand invasion during mating-type switching, a prototypical gene conversion event (Chai, 2005). In the absence of functional SWI/SNF, single-strand annealing (SSA), an HR subtype in which two homologous sequences are annealed after extensive end resection at a DSB (Bhargava et al., 2016), is also reduced (Chai, 2005). These phenotypes suggested a possible role for the remodeling complex in DNA end resection, a prerequisite for HR/SSA. The present study demonstrates that the initiation of DNA end resection is significantly delayed in a *snf5*Δ mutant, thereby identifying an early role for the SWI/SNF complex in HR. This role appears to be mediated through the recruitment and/or stabilization of a distinct pool of MRX to DSBs to promote HR, and is related to the function of SWI/SNF in nucleosome eviction, as outlined in the model in **Fig 2.14.**

In the absence of functional SWI/SNF, there was an approximately 75 min delay in the resection of DNA just proximal to a *MAT* DSB, but once initiated, long-range resection occurred with similar kinetics as in a WT cell. While SWI/SNF is recruited late to a *MAT* DSB and is detectable only ~0.75 hr after DSB induction (Chai, 2005), our results demonstrated that resection initiated at ~0.9 hr post-break induction in WT cells.

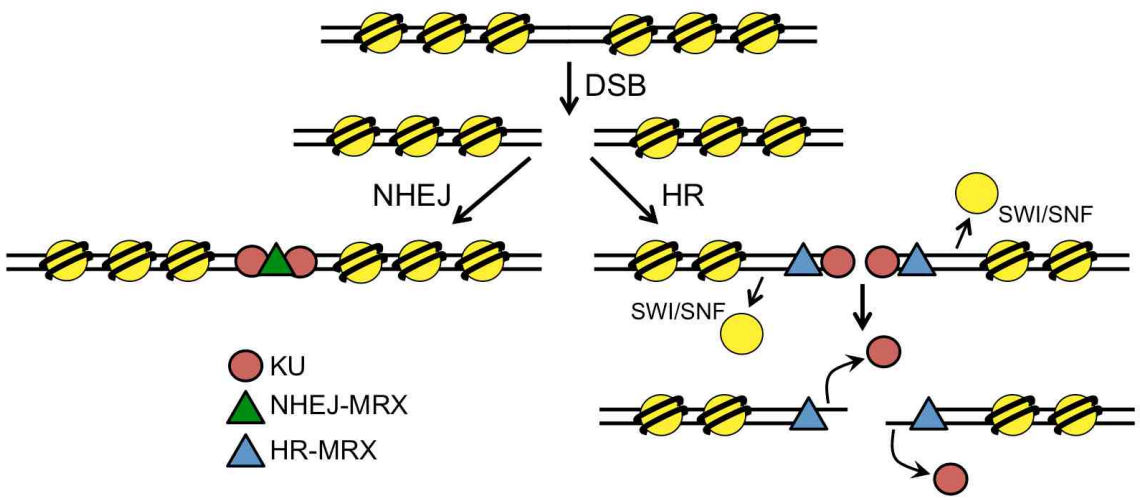

Figure 2.14. Model for the role of SWI/SNF in the initiation of HR repair. Only initial events in the repair of a DSB by NHEJ or HR are shown. After a DSB is formed, KU rapidly associates with broken ends and recruits Dnl4-Lif1, leading to the recruitment of a pool of NHEJ-MRX that tethers broken ends and stimulates end ligation that is essential for repair by NHEJ (left panel). Recruitment of SWI/SNF to a DSB promotes nucleosome eviction in the vicinity of the break, leading to the recruitment or stabilization of a distinct pool of HR-active MRX (right panel). The nuclease activity of MRX promotes the initiation of end resection, which leads to the displacement of KU. Long-range resection factors, Exo1 and Dna2-STR are then recruited, the ssDNA overhang is coated with RPA, and the DNA damage checkpoint is activated. RPA is replaced with the Rad51 recombinase and the nucleoprotein filament initiates homology search for HR repair.

Thus, DNA end resection begins shortly after detectable SWI/SNF recruitment. In contrast, the initiation of long-range resection in *snf5*Δ cells did not occur until more than two hours after DSB induction. This suggests that SWI/SNF acts rapidly upon its recruitment to orchestrate the successful initiation of end resection. In contrast, the Fun30 nucleosome remodeler is not required for efficient resection initiation but plays an important role in long-range resection by removing the inhibitory Rad9 checkpoint protein from nucleosomes (Chen et al., 2013b; Costelloe et al., 2013; Eapen et al., 2012).

An intricate choreography of events occurs at DSBs to determine the choice between the NHEJ and HR pathways, including a complex relationship between the pathway-regulating MRX/MRN and KU complexes. KU binds to dsDNA with high affinity (Blier et al., 1993) and recruits Dnl4-Lif1 to form a DNA-protein complex that recruits MRX (Zhang et al., 2007). The NHEJ-specific functions of MRX include tethering broken ends to maintain their intermolecular proximity, stimulating end ligation by Dnl4-Lif1, and providing a key interaction between Xrs2 and Lif1 that is essential for NHEJ (Chen et al., 2001; Oh et al., 2016). In contrast, during G2/M phase, the MRX complex is able to evict KU from DSB ends and initiate 5′ to 3′ end resection in conjunction with Sae2/CtIP, creating a ssDNA substrate that is not amenable to classical end joining and requires HR for repair (Garcia et al., 2012; Ira et al., 2004; Wu et al., 2008). Thus, MRX has both NHEJ-active and HR-active roles with non-overlapping and opposing activities, leading to the proposal that there are two different modes of MRX recruitment to DNA DSBs that lead to its distinct activities (Emerson and Bertuch, 2016; Wu et al., 2008; Zhang et al., 2007).

Our study demonstrated that SWI/SNF is required for the efficient recruitment of MRX to a *MAT* DSB. In contrast, the association of KU with the *MAT* DSB was not affected in the *snf5*Δ mutant, and the retention of KU over time was significantly increased. Previous research found that NHEJ, as measured by a plasmid-based end-joining assay, is intact in both *snf5*Δ and *snf2*Δ mutants, while HR/SSA is defective(Chai, 2005). We therefore suggest that SWI/SNF is specifically required for the recruitment or stabilization of a distinct pool of MRX that is active in HR. MRX has multiple roles in HR, including initiation of DNA end resection (Daley et al., 2015; Garcia et al., 2012), recruitment of long-range resection factors (Shim et al., 2010), and activation of the DNA damage response (Oh et al., 2016; Tsabar and Haber, 2013). In support of a role for SWI/SNF in regulating HR-active MRX functions, our data showed that in a *snf5*Δ mutant the initiation of DNA end resection was delayed, recruitment of long-range resection factors was reduced, and the DNA damage response was significantly impaired. Thus, all the known functions of HR-active MRX at a DSB are either lost or greatly diminished in the absence of SWI/SNF.

Another nucleosome remodeler, the RSC complex, has also been demonstrated to regulate the association of MRX with a *MAT* DSB. However, unlike SWI/SNF, RSC acts very early after break induction and facilitates the recruitment of both KU and MRX (Shim et al., 2007). RSC catalyzes the sliding of nucleosomes proximal to the break to create a stretch of nucleosome-free DNA that facilitates the recruitment of factors for both HR and NHEJ (Chambers et al., 2012; Kent et al., 2007; Shim et al., 2007). Also, unlike SWI/SNF mutants, RSC mutants have defects in both NHEJ and HR (Chai, 2005; Chambers et al., 2012; Shim et al., 2007; 2005). Moreover, there appears to be functional

differences between RSC isoforms, and contrasting results have been obtained with plasmid versus chromosomal end joining assays in RSC mutants (Chai, 2005; Chambers et al., 2012; Shim et al., 2007; 2005). A general picture that emerges from these combined studies supports a model in which RSC works rapidly after DSB induction to create a chromatin microenvironment that is generally conducive for DSB repair, while SWI/SNF acts more specifically to promote HR through recruiting or stabilizing an HR-active pool of MRX.

Although the absence of functional SWI/SNF does not affect long-range resection, a surprising finding was that *snf5*Δ cells depend on Exo1 rather than Dna2-STR for long-range resection. Previous *in vitro* studies demonstrated that Dna2-STR more readily processes nucleosomal templates than Exo1 because of the ability of Sgs1 to unwind DNA from nucleosomes (Adkins et al., 2013). In addition, Dna2-STR can also compensate for the loss of the nuclease activity of MRX in DSB repair (Budd and Campbell, 2009), thus making it a logical candidate to substitute for the loss of HR-active MRX in the *snf5*Δ strain. However, this phenotype may also be explained by the observation that Dna2 recruitment is almost completely abolished in *snf5*Δ cells, similar to the loss of Dna2 recruitment to a *MAT* DSB in *rad50*Δ and *mre11*Δ strains (Shim et al., 2010). It is likely, therefore, that Exo1 has a greater ability to load onto a DSB in the absence of MRX than Dna2-STR.

The increased binding of KU to DSB ends and the reliance on Exo1 for long-range resection in *snf5*Δ cells is paradoxical since KU binding is known to block Exo1 activity (Mimitou and Symington, 2010; Shim et al., 2010). Previous data have demonstrated that KU association with DSBs *in vivo* is dynamic (Zhang et al., 2007).

Together with the recent discovery that phosphorylation of KU reduces its affinity for DNA ends *in vivo* and increases accessibility of DSB ends to Exo1 *in vitro*, it appears that Exo1 could initiate processing of DSB ends when KU transiently dissociates (Lee et al., 2015). Alternatively, the successive cycles of end joining and HO cleavage at *MAT* may create the opportunity for Exo1 to occasionally process the breaks before KU can associate. Either way, once the minimum amount of resection has occurred to recruit RPA and nucleate a Rad51 nucleofilament, KU binding will be repelled (Krasner et al., 2015) and multiple chromatin remodelers will be recruited by Rad51 (Bennett et al., 2013) to assist in processing the chromatin landscape to allow Exo1 to proceed with resection.

Nucleosome eviction is a conserved activity during the repair of DSBs in both yeast and mammals (Berkovich et al., 2007; Li and Tyler, 2016; Tsukuda et al., 2005). An open question in the field is the identity of the factors that evict nucleosomes from DNA during HR *in vivo*. Previous research demonstrated that both MRX and the INO80 ATP-dependent nucleosome remodeler contribute to the removal of nucleosomes near a *MAT* DSB, although eviction eventually occurs after a delay (Tsukuda et al., 2005; 2009). Our data showed that nucleosome eviction was delayed in *snf5*Δ cells in a manner that temporally paralleled the delay in resection initiation in this mutant, suggesting that both events are coupled. In both WT and *snf5*Δ cells, FLAG-H2B eviction and DNA end resection occurred at approximately the same time. This supports the view that that SWI/SNF increases the efficiency of nucleosome eviction, and that eviction is a prerequisite for the efficient recruitment of HR dependent MRX and resection initiation. Thus, there may be redundant nucleosome eviction pathways during HR that are

mediated by different factors, including ATP-dependent nucleosome remodelers as well as helicases such as Sgs1, all of which co-operate to ensure the generation of nucleosome-free recombinogenic ssDNA that can be efficiently coated by Rad51.

In conclusion, we have demonstrated that SWI/SNF plays a role in the initiation of end resection at the *MAT* DSB in yeast and is critical for the robust recruitment of MRX to broken ends. The small pool of MRX that is recruited in *snf5*Δ cells lacks the well-known functions of MRX in HR, including resection initiation, recruitment of the long-range resection machinery, and activation of the DDR, suggesting that SWI/SNF orchestrates the recruitment and/or stabilization of an HR-active pool of MRX to DNA DSBs that has distinct activities compared to NHEJ-active MRX. Furthermore, we suggest that this role of SWI/SNF is mediated through its activity in nucleosome eviction at a DSB. SWI/SNF is an important tumor suppressor that is mutated in approximately 20 percent of human malignancies (Kadoch et al., 2013; Wilson and Roberts, 2011), and recent studies have shown that mammalian SWI/SNF is recruited to DSBs, where it contributes important roles in activating the DNA damage response and recruiting repair proteins to damaged DNA (Kwon et al., 2015; Park et al., 2006; Smith-Roe et al., 2015). Furthermore, a recent study showed that SWI/SNF contributes to end resection and HR in mammalian cells (Vélez-Cruz et al., 2016). Thus, we believe our study sheds light on important and conserved roles for the SWI/SNF complex in maintaining genomic and epigenomic stability during DNA double-strand break repair.

Chapter 3

Optimization of native and formaldehyde iPOND techniques for use in suspension cells

Wiest, NE and Tomkinson, AE. Optimization of native and formaldehyde iPOND techniques for use in suspension cells. Submitted to *Methods in Enzymology* on February 2, 2017. Accepted for publication.

3.1 Abstract

The isolation of proteins on nascent DNA (iPOND) technique developed by the Cortez laboratory allows a previously unparalleled ability to examine proteins associated with replicating and newly synthesized DNA in mammalian cells. Both the original, formaldehyde-based iPOND technique and a more recent derivative, accelerated native iPOND (aniPOND), have mostly been performed in adherent cell lines. Here, we describe modifications to both protocols for use with suspension cell lines. These include cell culture, pulse, and chase conditions that optimize sample recovery in both protocols using suspension cells and several key improvements to the published aniPOND technique that reduce sample loss, increase signal to noise, and maximize sample recovery. Additionally, we directly and quantitatively compare the iPOND and aniPOND protocols to test the strengths and limitations of both. Finally, we present a detailed protocol to perform the optimized aniPOND protocol in suspension cell lines.

3.2 Introduction

Techniques to examine the dynamics of protein association and dissociation at replication forks and with newly synthesized DNA in mammalian cells have until recently lagged behind their counterparts in lower eukaryotes. In *Saccharomyces* sp., for example, replication origins are generally predictable due to their dependence on defined and validated sequence elements (Hyrien, 2015; Nieduszynski, 2006), thereby allowing for the proteins associated with replicating DNA to be monitored by employing chromatin immunoprecipitation to capture proteins that are bound adjacent to recently fired origins (Kanemaki and Labib, 2006; Trujillo and Osley, 2012). In contrast, metazoan replication origins are less predictable and sequence independent (Hyrien, 2015), preventing the same approach from being applied to study replication of the mammalian genome and epigenome. While techniques such as BrdU co-immunofluorescence and singe-molecule fluorescence resonance energy transfer (FRET) imaging can provide valuable information about protein occupancy and relative positioning on replicating DNA (Duderstadt et al., 2014), techniques in mammalian cells to spatiotemporally monitor the dynamics of protein association and dissociation at replication forks and with newly replicated DNA as the fork moves away have been lacking. The development of the isolation of proteins on nascent DNA (iPOND) technique, first described in 2011 by the Cortez laboratory (Sirbu et al., 2011; 2012), has led to novel insights into the repertoire of proteins present at active and stalled replication forks and the temporal links between replicative DNA synthesis, nucleosome assembly, and chromatin maturation (**Fig 3.1A**).

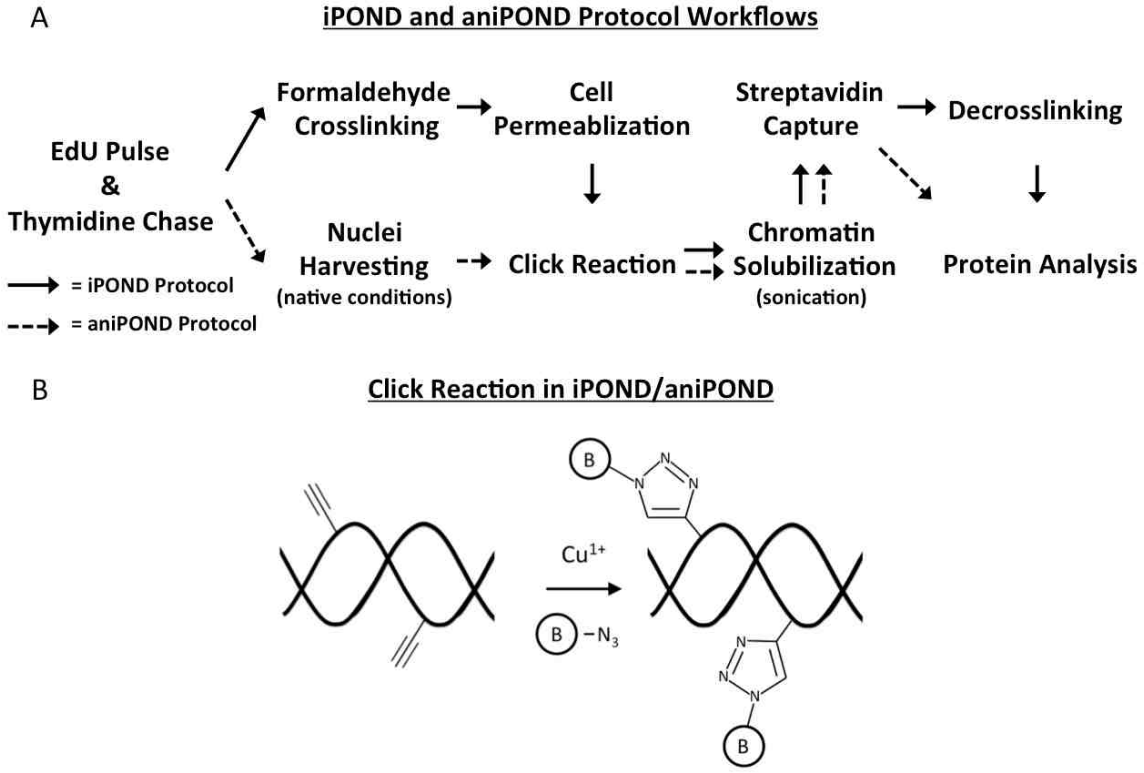

Figure 3.1. The iPOND and aniPOND protocol workflows and click reaction. (A) The major steps for both iPOND and aniPOND are illustrated. (B) An illustration of the iPOND/aniPOND click reaction, in which they alkyne moieties from the incorporated EdU are covalently linked to the azide moieties of biotin-azide in the presence of reduced copper.

The iPOND technique is based upon the altered chemical properties of 5-ethynyl-2′-deoxyuridine (EdU), a thymidine analog containing a reactive alkyne group that is readily incorporated into living cells both *in vitro* and *in vivo* (Chehrehasa et al., 2009). Addition of EdU to the media results in the incorporation of EdU into the newly synthesized DNA in place of thymidine. The extent of EdU incorporation is determined by the length of incubation in the EdU-containing media. Furthermore, incorporation can be effectively terminated by the replacement of the EdU-containing media with thymidine-containing media. By incubating with thymidine for different times following the EdU pulse, chromatin can be isolated at different stages post-replicative synthesis to monitor events such as histone deposition and chromatin maturation. After cross-linking with formaldehyde, EdU-containing genomic DNA is covalently conjugated to biotin via a copper-catalyzed azide-alkyne cycloaddition reaction (**Fig 3.1B**), known as a click chemistry reaction (Presolski et al., 2009). The click chemistry reaction in the iPOND protocol involves the conjugation of biotin-azide to EdU in the presence of Cu^{1+} that is generated by the reduction of copper sulfate in the presence of sodium ascorbate (Sirbu et al., 2012). A consequence of Cu^{1+} generated in the click reaction is the fragmentation of DNA (Meneghini, 1997), which in the iPOND and aniPOND protocols leads to DNA fragments with a mean distribution of ~150 bp.

After the click reaction, the biotin-labeled DNA with accompanying covalently-linked proteins is affinity purified using streptavidin beads. Proteins associated with the newly synthesized DNA are eluted from the streptavidin beads by thermal decrosslinking in the presence of SDS and then identified by either immunoblotting or mass spectrometry (see “Proteomic analyses of the eukaryotic replication machinery” in this

volume). To date, the iPOND protocol has been utilized to catalog the proteins present at replication forks (including the identification of the new replication protein Znf24) (Lopez-Contreras et al., 2013; Sirbu et al., 2013), probe the changes in replication fork protein composition under stress conditions including fork stalling, fork collapse, and hypoxia (Dungrawala et al., 2015; Min et al., 2013; Olcina et al., 2016; Sirbu et al., 2011; Wang et al., 2015), identify the epigenetic regulators present on replicating DNA in embryonic stem cells (Aranda et al., 2014), monitor the association of clinically relevant target proteins with replicating DNA (Wells et al., 2013), and examine the factors recruited to replicating viral genomes (Dembowski and DeLuca, 2015).

A limitation of the iPOND technique is the need for decrosslinking of the formaldehyde-fixed chromatin before proteins can be analyzed. Thermal decrosslinking, especially of large proteins and protein complexes, is an inefficient process that can limit the recovery of many proteins. To address this, a modified protocol named accelerated native iPOND (aniPOND) was reported in 2013 (Leung et al., 2013). While based on the same click reaction chemistry as iPOND, the chromatin fraction containing EdU-labeled DNA is isolated under native, non-denaturing conditions in the aniPOND protocol, thereby eliminating the need for decrosslinking (**Fig 3.1A**). The aniPOND technique was reported to have an increased overall protein yield compared to iPOND, a finding that was borne out in a study examining replication factors recruited to Herpes simplex virus 1 genomes (Dembowski and DeLuca, 2015), and to increase recovery of large chromatin remodeling complexes (Leung et al., 2013). Given the different approaches to capturing EdU-associated proteins, it is likely that iPOND and aniPOND are complementary

techniques that may provide information on different but overlapping sets of proteins associated with replicating DNA and newly deposited chromatin.

Among publications utilizing either the iPOND or aniPOND techniques, only two studies have utilized suspension cells (Sirbu et al., 2013; Wells et al., 2013). Suspension cell lines such as lymphocytes may present an attractive alternative to adherent cell lines for certain studies, such as when specialized genetic models are present in suspension cells or in the study of replication abnormalities in leukemia cell lines. Here, we describe optimizations for performing both iPOND and aniPOND experiments with suspension cells. In the following sections, we will detail: (i) growth and cell handling conditions for suspension cells to avoid sample loss during the pulse and chase steps of both iPOND and aniPOND, (ii) critical modifications to the published aniPOND protocol that reduce sample loss, increase chromatin recovery, and reduce non-specific background, (iii) a direct, quantitative comparison of the iPOND and optimized aniPOND protocols using suspension cells, and (iv) a detailed protocol for optimized aniPOND utilizing quantitative near-infrared fluorescence immunoblotting (**Appendix A**).

3.3 Suspension Cell Growth and Handling for iPOND and aniPOND

The aniPOND and iPOND techniques require from 60 to 100 million cells per standard sample, respectively (Leung et al., 2013; Sirbu et al., 2012). It is important that the cells cultured for these experiments are growing optimally to ensure maximum EdU incorporation and reproducibility between experiments. Below, we describe variables that are important for the growth of B-lymphocytes and strategies to obtain maximal growth that can be applied to other suspension cell lines. In addition, the considerations for cell

handling during the initial pulse and chase phases of iPOND/aniPOND are different for suspension cells compared with adherent cell lines. We describe how to avoid sample loss during these steps with suspension cells to ensure maximum downstream signal recovery.

Optimizing growth conditions to obtain iPOND/aniPOND cell numbers

The growth of both adherent and suspension cells is sensitive to multiple environmental variables including temperature, pH, O_2 and CO_2 content, nutrient and metabolite concentration, and the presence of growth factors from serum, nearby cells, and exogenous stimulating factors. Before attempting iPOND or aniPOND, it is critical to optimize growth conditions in order to reproducibly obtain large cultures of rapidly dividing cells. Utilizing poorly and inconsistently growing cell populations for iPOND and aniPOND may lead to problems with EdU incorporation and reproducibility between experiments. Below we describe key variables that impacted the growth of a mouse B cell line in suspension.

First, we found that the surface area for gas exchange was a critical factor in determining the cell density that can be reached before cell proliferation starts to plateau. While some laboratories grow suspension cells in flasks that are upright, simply laying flasks on their side to increase surface area for gas exchange significantly increased the proliferative capacity of mouse B-cells, especially at high cell densities (**Fig 3.2A**). Furthermore, in addition to increasing that maximum number of cells obtained, cells grown in flasks on their side doubled ~40% faster than those grown in flasks upright (**Fig 3.2A**). As an alternative, spinner flasks may be used to constantly mix media and increase

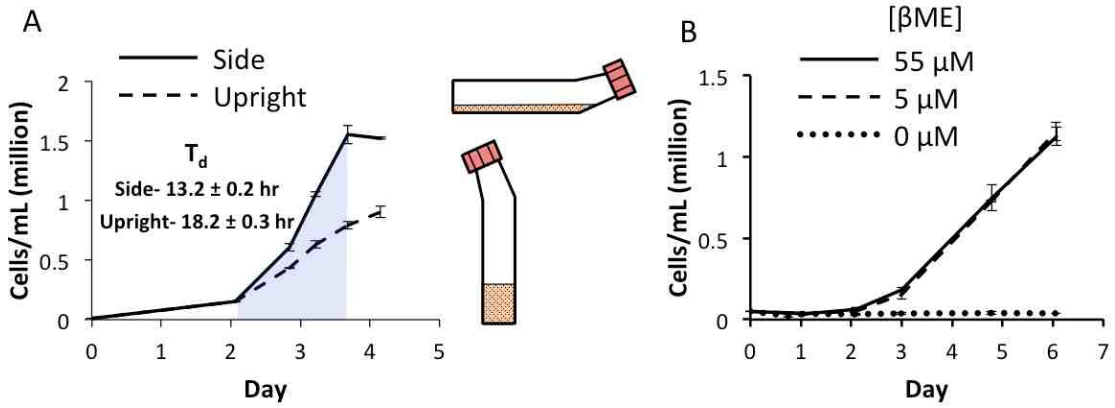

Figure 3.2. Important considerations for suspension cell growth. (A) Growth curves for CH12F3 mouse B-cell lymphoma cells incubated in 100 mL of media in T175 flasks either upright or on their sides to increase surface area for gas exchange. Doubling times (T_d) were calculated using the least squares fitting method over the exponential phase (shaded). (B) Growth curves for CH12F3 cells grown with the indicated concentrations of β-mercaptoethanol (βME). For all conditions, n=2 independent biological replicates. Error bars ± S.D.

aeration during growth. Second, certain suspension cell lines such as lymphocytes are dependent upon β-mercaptoethanol (βME) for proliferation and survival (Metcalf et al., 1975). For example, when the βME is omitted from the media, mouse B-cell growth stops completely (**Fig 3.2B**). Since βME is volatile and loses its reducing potential over time while in storage, it must be added freshly to media in flasks during cell dilution rather than to the stock media. Third, it is very important to avoid cell overgrowth. For many suspension cell lines, this occurs at approximately 1.5 x 10^6 cells/mL and should be determined experimentally under the optimized growth conditions (**Fig. 3.2A**). If EdU labeling is carried out in overgrown cell populations, a significant but variable fraction of the cells will not be replicating. Furthermore, overgrowth may result in the introduction of confounding factors such as epigenetic changes into the cell population. Thus, we recommend restarting the population from early passage frozen cells if overgrowth occurs to increase consistency between experiments.

Handling of suspension cells during pulse and chase

The EdU pulse-labeling and chase phases of the iPOND and aniPOND protocols are essentially identical (**Fig 3.1A**). Cells that have been grown to large numbers in a manner that maximizes proliferative capacity (see above) are labeled with EdU. After incubation in the EdU-containing media for a defined time, cells are either processed immediately, or resuspended in thymidine-containing medium and then incubated for different times prior to processing. A disadvantage of utilizing suspension cells in the iPOND and aniPOND protocols compared to adherent cells is the need for centrifugation to pellet cells in order to resuspend them in the chase medium. Our observations indicate

that mouse B-cells undergo morphological changes after centrifugation (**Fig 3.3A-C**) and became sticky, adhering to the surfaces of the tissue culture flasks even in flasks that are hydrophobically coated (not shown). As a result of this centrifugation-induced adherence with flask surfaces, approximately half of the downstream sample was lost when cells were resuspended in chase medium and incubated in flasks on their side (**Fig 3.3D**). By instead setting flasks upright during the chase step, the B-cells had much less surface area to adhere to and settled more slowly, leading to an almost complete elimination of the sample loss observed in chase samples (**Fig 3.3E**). Thus, while a greater surface area for gas exchange facilitates maximal growth to the cell numbers required for iPOND and aniPOND, this surface area becomes a liability when performing the chase step because centrifugation induces cellular stress and morphological changes that promote adherence to flask surfaces.

3.4 Optimizations to the aniPOND Protocol to Increase Functionality

While the native aniPOND protocol was reported to offer multiple advantages over the traditional formaldehyde-based iPOND technique, including faster processing time and greater sensitivity (Leung et al., 2013), we experienced technical difficulties when initially implementing the protocol in both SV40-immortalized human fibroblasts and mouse B-cells. Specifically, we observed a high degree of sample loss and non-specific binding to the streptavidin beads. Through systematically troubleshooting the steps of the original protocol, we have made multiple modifications to the original aniPOND protocol that reproducibly reduce sample loss, increase signal to noise, and maximize sample recovery in aniPOND experiments with mouse B cells that we present

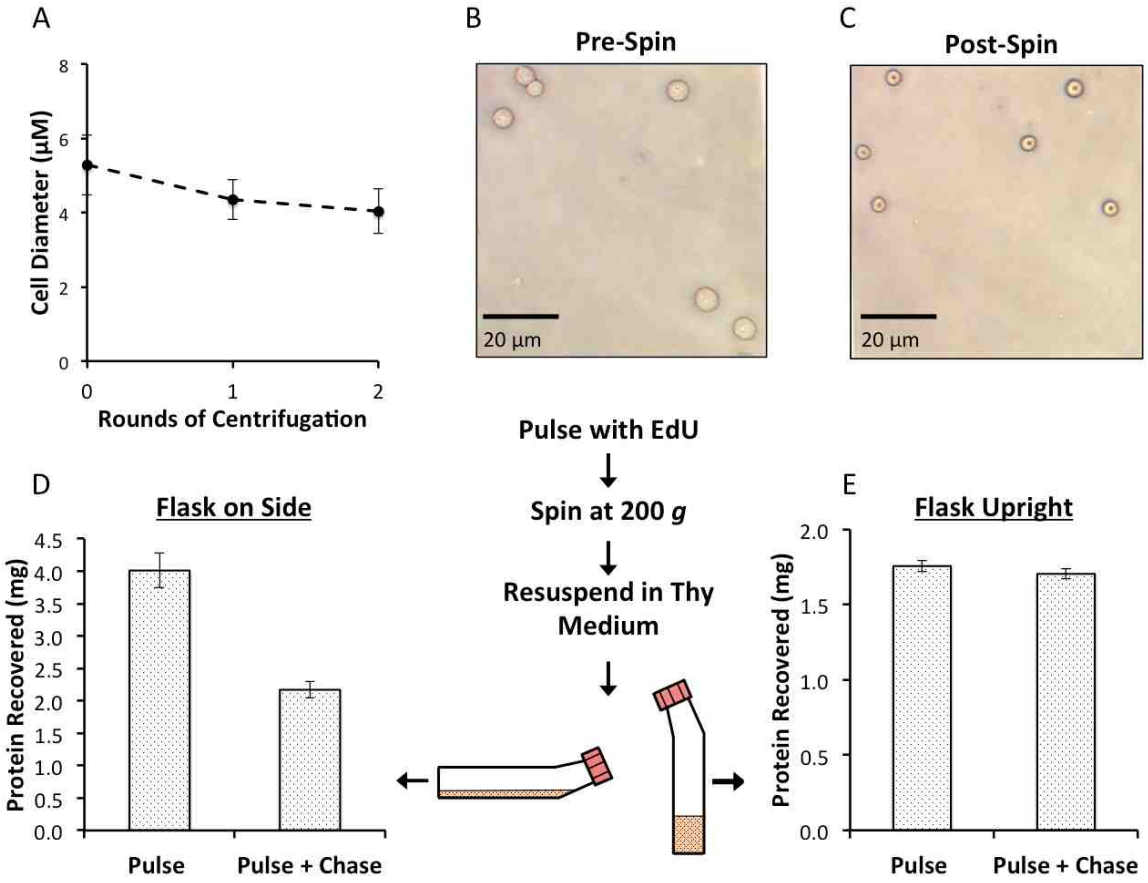

Figure 3.3. Centrifugation of mouse B-cells during the iPOND/aniPOND pulse and chase protocol leads to morphological changes and preventable sample loss. CH12F3 mouse B-cell lymphoma cells were subjected to rounds of standard cell centrifugation (200 *g* x 5 min). The diameters of cells (A) were measured by Image J software analysis of photos taken of cells both before (B) and after (C) centrifugation. A minimum of 15 cell diameters was measured per round, and error bars represent the S.D. of measurements from two independent samples. Note the biconcave morphology of post-spin cells. After resuspending cells in thymidine medium, the chase sample flasks were either incubated on the side or upright before proceeding. To test the downstream sample recovery, the protein content of sonicated chromatin was measured in cells that were either incubated in thymidine medium in flasks on their sides and then processed for iPOND (D), or cells that were incubated in thymidine medium in flasks that were positioned upright and then processed for aniPOND (E).

below. In describing the revised protocol below, we discuss the modifications in the context of chromatin biology to facilitate adaptation of the aniPOND technique to other cell lines.

Optimized sonication regimen

After isolating nuclei containing the EdU-labeled DNA as described in the published aniPOND protocol (Leung et al., 2013), the EdU-containing genomic DNA is conjugated to biotin-azide by the click reaction within the nuclei (**Fig 3.1B**). The next major step in both the iPOND and aniPOND protocols is to solubilize the chromatin by sonication to generate fragments of chromatin that are amenable to pulldown with streptavidin beads (**Fig 3.1A**). The original iPOND protocol (Sirbu et al., 2012) calls for sonicating on ice with 20-second pulses followed by 40 second rests between pulses using a microtip sonicator on 13-16W output, with the number of rounds depending on the sample volume. Successful solubilization is immediately observable by clarification of the lysate. The published aniPOND protocol (Leung et al., 2013) uses a more stringent sonication regimen that incorporates 12 x 10-second pulses on ice at output setting 3 to 4 (~ 10W of output) with 10 second rests in-between pulses. Additionally, the aniPOND protocol incorporates two prior wash steps (sonication washes), in which nuclei are resuspended in buffer, sonicated for 10 seconds, spun down, and then resuspended in buffer again (**Fig 3.4A**). In our initial attempts to perform that aniPOND protocol, we observed that the sonication washes appeared to solubilize significant portions of the nuclei since the nuclei pellets were much smaller after each of the sonication wash steps. Indeed, when we quantitated the amount of both protein and DNA (therefore chromatin)

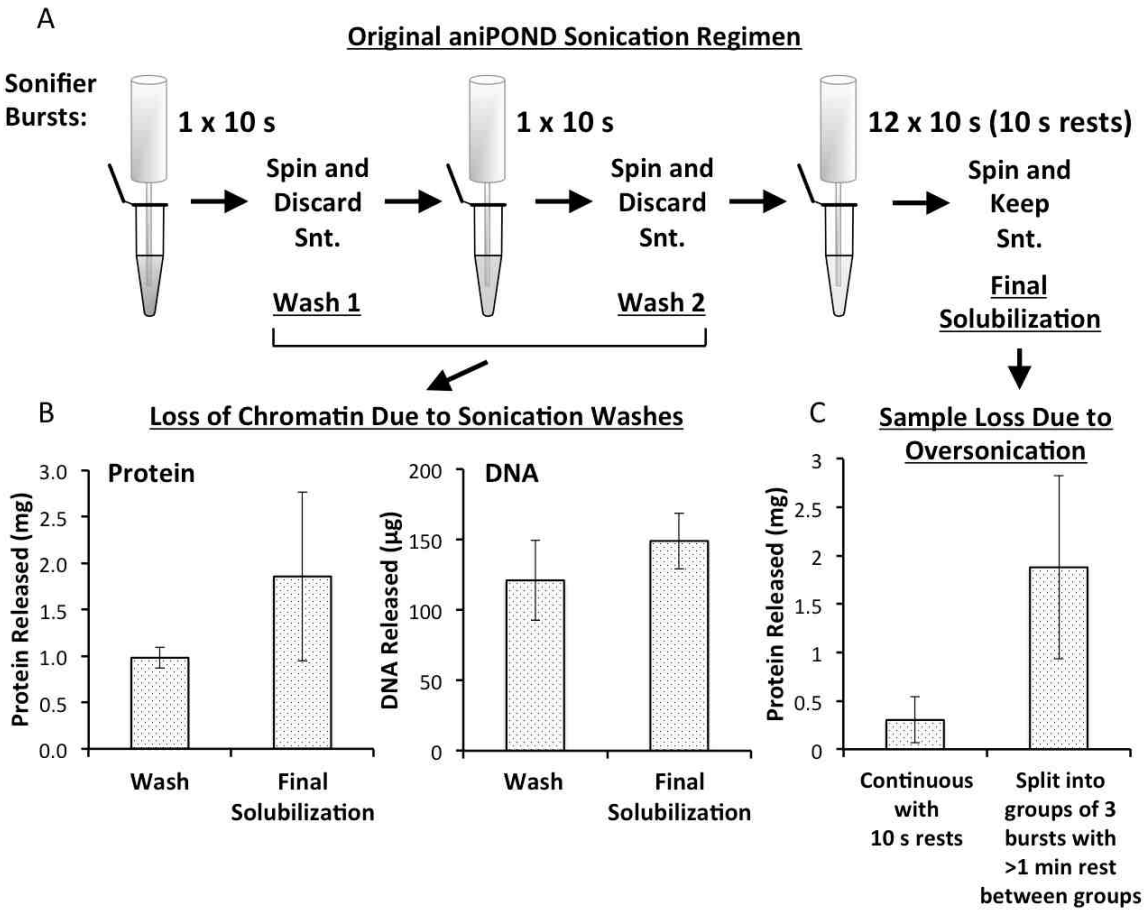

Figure 3.4. The original aniPOND sonication regimen leads to sample loss at two steps. (A) Schematic of the original aniPOND sonication regimen. (B) Supernatant was recovered after spinning down nuclei following the sonication wash steps ("Wash") and assayed for protein via Bradford assay and DNA by nanodrop spectrophotometer (Thermo Fisher Sci.) following column DNA purification. Results were juxtaposed to protein and DNA measurements obtained following the final solubilization of the nuclei ("Final Solubilization"). (C) The original final solubilization protocol of 12 rounds of 10" on, 10" off, on ice ("Continuous with 10 s rests") was compared to a modified protocol consisting of four groups of three rounds of 10" on, 10" off, on ice with at least one minute of rest between groups on ice ("Split into groups of 3 bursts with >1 min rest between groups"). For all samples, signal represents the mean of two independent biological replicates. Error bars ± S.D.

solubilized by the two wash steps, we found that these two initial wash sonications released nearly as much chromatin as the final solubilization step involving 12 sonication pulses (**Fig 3.4B**). Thus, as much as 50% of the chromatin is lost during the sonication wash steps. We also observed that that the final aniPOND chromatin solubilization protocol— 12 rounds of 10 seconds on, 10 seconds off, on ice— was leading to excessive foaming and splashing of sample in the later rounds, even on the lowest recommended setting (output 3). Since over-sonication can cause protein aggregation (Stathopulos et al., 2004), in addition to potentially damaging to proteins due to sample overheating, we tested if the giving the samples more rest on ice between sonication assisted in chromatin recovery. Indeed, we found that performing the bursts in rounds of three times 10 seconds on, 10 seconds, with at least a minute rest on ice before the next round of three, markedly increased sample recovery (**Fig 3.4C**), indicating that care needs to be taken in the final solubilization step to avoid overheating.

As solubilization of chromatin by sonication is critical for maximum recovery of biotin-labeled DNA, we investigated the factors that influence sonication efficiency. A previous study on chromatin compaction demonstrated that increasing levels of monovalent cations lead to greater degrees of chromatin compaction *in vitro*, with peak *in vitro* compaction occurring at greater than approximately 60 mM NaCl (Thoma et al., 1979). In addition, the same study demonstrated that relatively low concentrations of divalent cation, for example 0.5 mM Mg^{2+}, also cause maximum *in vitro* compaction. In the published aniPOND protocol (Leung et al., 2013), cells are first harvested in a nucleus extraction buffer containing 3 mM Mg^{2+}, followed by washing and the click reaction that occur in PBS-based buffers containing ~130mM NaCl. These buffers have

cation concentrations higher than that shown to maximally compact chromatin *in vitro.* Notably, collapsed chromatin morphology was observed by electron microscopy in nuclei prepared using the same nonionic detergent and concentration as the published the aniPOND protocol (Stuart et al., 1977). Thus, we expect that under these conditions the chromatin inside the isolated nuclei will be collapsed into more compacted structures that may be initially resistant to sonication. To create conditions in which compacted, potentially sonication-resistant chromatin relaxes and becomes vulnerable to sonication, we removed the two sonication wash steps in the original aniPOND sonication regimen (**Fig 3.4A**) and replaced them with two 30 minute rotations in the aniPOND protocol buffer B1, a low salt, non-ionic detergent sonication buffer containing EDTA to chelate diavlent cations (25 mM NaCl, 2 mM EDTA, 50 mM Tris-HCl pH 8.0, and 1% IGEPAL CA630). This alteration prior to sonication increased the fraction of chromatin solubilized from less than 50% to approximately 80% (**Fig 3.5A**), presumably by creating conditions that promote *in vitro* chromatin relaxation. Comparing the fractions of histone H4 solubilized by sonication to the remaining insoluble histone H4 after sonication (pellet) by immunoblotting revealed that, in line with the protein measurements, pre-incubation in buffer B1 resulted in the majority of the histone H4 being solubilized (**Fig 3.5B**). Based on these results, we designed the optimized sonication regimen displayed in **Figure 3.5C** that both reduces sample loss during sonication and increases the amount of chromatin solubilized.

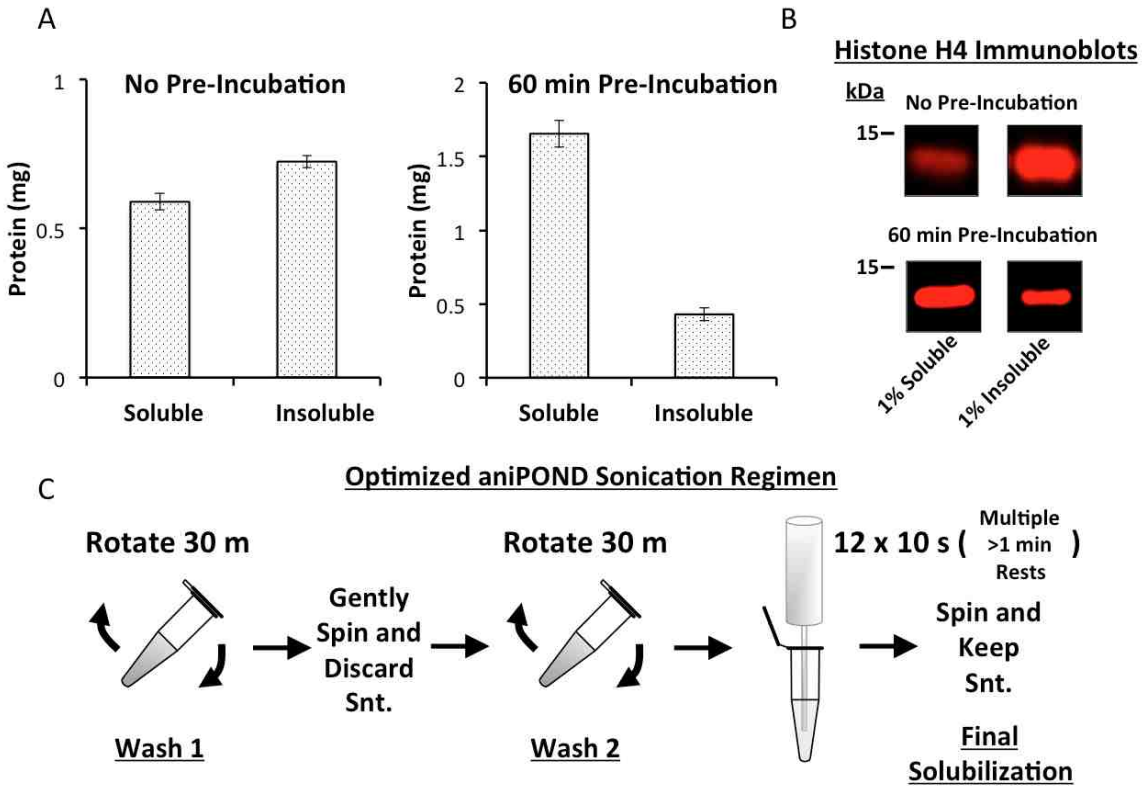

Figure 3.5. Pre-incubation of nuclei in low salt, EDTA-containing buffer B1 leads to more efficient solubilization of chromatin. (A) Comparisons of protein released by sonication to the remaining insoluble protein levels (pellet) in aniPOND samples either resuspended in B1 and sonicated immediately ("No Pre-Incubation") or in samples rotated twice for 30 min in B1 before sonication ("60 min Pre-Incubation"). Signal represents the mean of two independent biological replicates. Error bars ± S.D. (B) Representative immunoblots with histone H4 antibody (Abcam ab17036) comparing 1% of the sonication-solubilized protein fraction with 1% of the insoluble (pellet) fraction. 1% soluble and 1% insoluble bands for "No Pre-Incubation" and "60 min Pre-Incubation" blots were run on the same gels testing multiple conditions. The indicated bands were cropped from the image captures obtained by acquisition of near-infrared western blots using a Li-Cor Odyssey Fc instrument. Uncropped images are readily available upon request. (C) Schematic of the optimized aniPOND sonication regimen. Two gentle rotation washes in B1 buffer designed to encourage chromatin decompaction followed by a final solubilization step with 12 rounds of sonication and multiple rounds of >1 min rests (we recommend six groups of 2 x 10" on, 10" off, on ice with at least one minute of additional rest on ice between groups).

Preventing chromatin precipitation in sonicated chromatin

Following chromatin solubilization by sonication as discussed above, the next step in the published aniPOND protocol (Leung et al., 2013) is to dilute the chromatin solubilized in low salt buffer B1 equally with physiologic-salt buffer B2 (150 mM NaCl, 2 mM EDTA, 50 mM Tris-HCl pH 8.0, and 0.5% IGEPAL CA630) to bring the NaCl concentration closer to physiologic levels before incubation with streptavidin beads. Under these conditions, the solubilized chromatin isolated as described above turned opaque upon addition of buffer B2 (**Fig 3.6A**). This is consistent with early observations from the chromatin literature reporting that increasing the salt concentrations of native chromatin preparations towards physiologic salt concentrations led to decreased solubility of histones and precipitation of a fraction of the chromatin containing, in addition to other proteins, essentially all histone H1 (Tatchell, 1978). Notably, maximum nucleosome insolubility occurred in that study at about ~0.1 M NaCl, a concentration close to that obtained by diluting the chromatin solubilized in buffer B1 (25 mM NaCl) with buffer B2 (150 mM NaCl) in the published aniPOND protocol (Leung et al., 2013). Indeed, upon microscopic examination, we observed that diluting the low salt B1 buffer-sonicated chromatin with physiologic salt buffer B2 resulted in the formation of visible aggregates (**Fig 3.6B**). After centrifugation, we determined that these aggregates contained about half the total chromatin, whereas almost no chromatin was lost if it was maintained at a low salt concentration (**Fig 3.6C**). Thus aniPOND samples, which are essentially concentrated low-salt native chromatin preparations, are highly sensitive to increasing salt concentrations and so we recommend maintaining the solubilized chromatin in low salt B1 buffer.

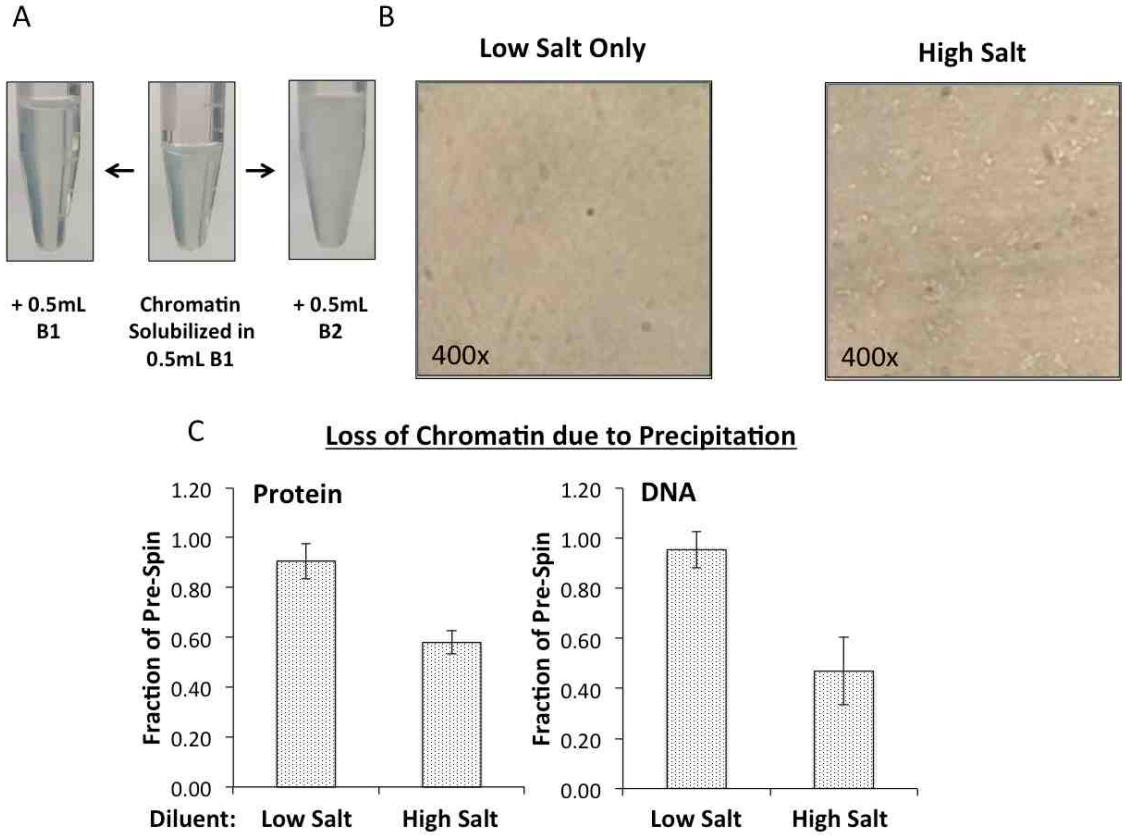

Figure 3.6. Dilution of chromatin solubilized by sonication in low salt buffer B1 with physiologic salt buffer B2 leads to chromatin aggregation and sample loss after clarification centrifugation. (A) Photographs of 1.5 mL tubes containing chromatin solubilized by sonication in 0.5 mL low salt buffer B1 before and after addition of 0.5 mL of physiologic salt buffer B2 or more buffer B1. (B) Photographs of preparations of chromatin solubilized by sonication in low salt buffer B1 that has been diluted either with more buffer B1 ("Low Salt Only") or with physiologic salt buffer B2 ("High Salt") at 400x magnification with a light microscope. Note the multitudinous small white aggregates in the high salt sample. (C) The contents of the aggregates formed upon adding either low salt buffer B1 ("Low Salt") or physiologic salt buffer B2 ("High Salt") to chromatin solubilized in buffer B1 were evaluated by measuring the protein and DNA content of the chromatin fraction before and after a clarification centrifugation spin. Signal represents the mean of two independent biological replicates. Error bars ± S.D.

Eliminating sources of background

After the biotin-labeled fraction of the solubilized chromatin has been pulled down using streptavidin beads, bound proteins are eluted by boiling in SDS-containing sample buffer. The eluted fraction contains proteins that were pulled down both by the streptavidin-biotin interaction, as well as any proteins that nonspecifically associated with the beads. Both the iPOND and aniPOND protocols utilize either a no-EdU or a no-click control (NCC) sample, in which either the DNA is not labeled with EdU or the click reaction does not contain biotin-azide (in both cases the newly-synthesized DNA is not conjugated to biotin), in order to account for the non-specific binding of proteins to the beads.

We observed on multiple occasions when using the published aniPOND protocol of diluting chromatin solubilized in low salt buffer B1 with physiologic salt buffer B2 that there was a high degree background binding in NCC samples that included both histone (histone H4) and non-histone (PCNA) chromatin proteins (**Fig 3.7A**). Since histones comprise approximately half of the protein content of chromatin, some level of histone background may be anticipated (van Holde, 1989) whereas PCNA is present at much lower levels than histone proteins. The problem of nonspecific PCNA binding in NCC samples was resolved by the changes in the chromatin preparation described above that reduced chromatin aggregation. In samples that were maintained in low salt buffer B1 after sonication, no PCNA was observed in the NCC pulldown lanes and PCNA unloading from newly replicated DNA was clearly observable (**Fig 3.7B**).

While the non-specific PCNA binding was caused by chromatin aggregation, the non-specific binding of histones was not reduced by preventing chromatin aggregation.

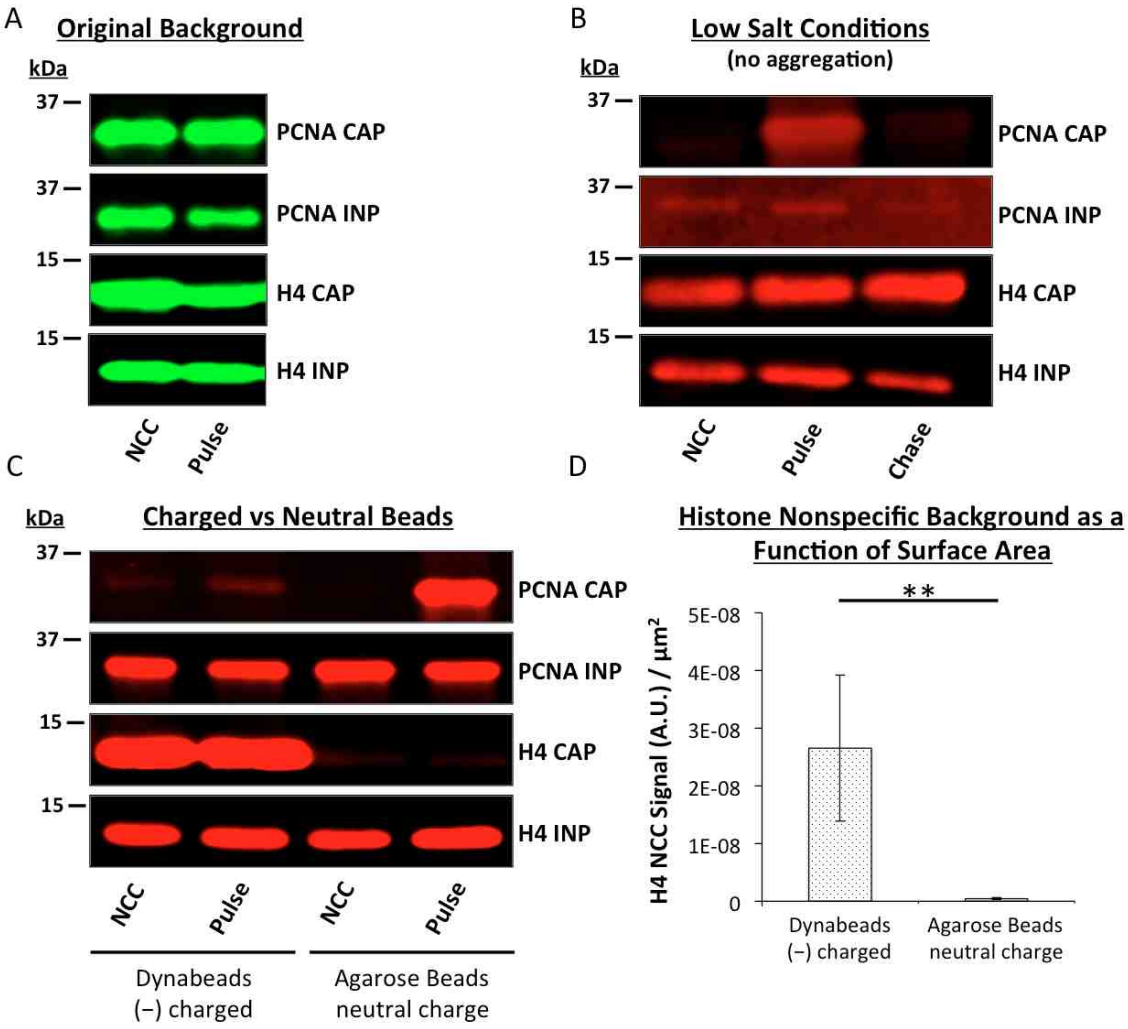

Figure 3.7. Sources of background in the aniPOND protocol. (A) CH12F3 mouse B-cells were processed for aniPOND using the published method of diluting chromatin solubilized in low salt buffer B1 with physiologic salt buffer B2 before pulldown with Dynabeads MyOne Streptavidin C1 beads (Thermo Fisher Sci.). NCC= no-click control. Pulse = 10 minute EdU pulse. CAP= 50% of proteins captured by beads. INP = 1% of pre-pulldown chromatin. (B) As in A, but diluting chromatin solubilized in low salt buffer B1 with additional low salt buffer B1 to prevent chromatin aggregation. Chase = 10 min EdU pulse followed by 60 min thymidine chase. (C) As in B, but comparing pulldown with either Dynabeads or Pierce High Capacity Streptavidin Agarose (Thermo Fisher Sci.) as indicated. (D) Histone H4 NCC signal from 4-5 independent experiments as quantified by Li-Cor near-infrared western blotting was normalized to the total surface area of the beads added for pulldown. Statistical significance between average H4 NCC signal per μm^2 was assessed by one-way ANOVA. ** = $p < 0.01$. Beads surface area was calculated using publically available product information.

This prompted us to consider the characteristics of the beads themselves. Based on recently published iPOND experiments (Dungrawala et al., 2015), we were using Dynabeads MyOne C1 Streptavidin beads (Thermo Fisher Sci.). These beads have a hydrophilic, negatively charged surface that can potentially form charge-based interactions with positively charged proteins. To determine if charge-based interactions may contribute to non-specific protein binding, we compared negatively charged Dynabeads with neutral streptavidin agarose beads (**Fig 3.7C**). In this experiment, both sets of beads yielded signal above noise for PCNA, with larger specific signal obtained with the streptavidin agarose. While similar high levels histone H4 were retained on the negatively charged Dynabeads in both the NCC and EdU pulse samples, very little H4 binding to the associated with the neutral streptavidin agarose beads was detected in either sample. We estimated that negatively charged Dynabeads had ~60x more non-specifically bound histone H4 background per μm^2 of surface area than streptavidin agarose (**Fig 3.7D)**. The absence of specific histone H4 binding in a 10 min EdU pulse sample is consistent with subsequent studies indicating that H4 deposition occurs rapidly after ~15 min. Thus, the neutrally charged streptavidin agarose beads accurately recapitulated the presence of PCNA at the replication fork while avoiding nonspecific histone binding.

Optimization limitations

A limitation to the optimizations that we have presented above is that we have only studied the aniPOND protocol in suspension cells with mouse B-lymphocytes. While we believe that many of our observations reflect fundamental properties of

chromatin biology and should thus be broadly applicable, it is nonetheless possible that other types of suspension cell lines will behave differently in both the growth conditions necessary to generate aniPOND cell numbers as well as the during the protocol itself.

3.5 Comparison of iPOND and Optimized aniPOND in Suspension Cells

Previous comparisons of the iPOND and aniPOND techniques have suggested that the protein yield is higher in aniPOND compared with iPOND, and that the two techniques may isolate different but overlapping sets of proteins (Dembowski and DeLuca, 2015; Leung et al., 2013). We reasoned that, while certain large proteins and protein complexes may decrosslink poorly in the iPOND protocol, proteins that interact transiently with replicating DNA may require crosslinking for detection. To quantitatively address the strengths and limitations of both protocols, we directly compared the iPOND and optimized aniPOND techniques using identical quantities of mouse B-cells over a 60-minute time course (**Fig 3.8A**), and calculated the beads capture signals as a percent of input using near-infrared immunoblotting. Consistent with the hypothesis the formaldehyde crosslinking assists in the capture of transient interactions, Lig1 was only detectable in both capture and input samples using iPOND (**Fig 3.8B**). In contrast, PCNA, which is topologically linked to DNA at the replication fork, was detected efficiently by both iPOND and aniPOND, with ~50% more efficient capture in the aniPOND protocol (**Fig 3.8C**). There was a large difference in the efficiency of histone H4 capture between the iPOND and aniPOND protocols, with ~5x more histone H4 captured by aniPOND (**Fig 3.8D**). Nonetheless, both techniques demonstrated the expected turnover of the H4K5ac mark (**Fig 3.8E**). A comparison of the pre-pulldown

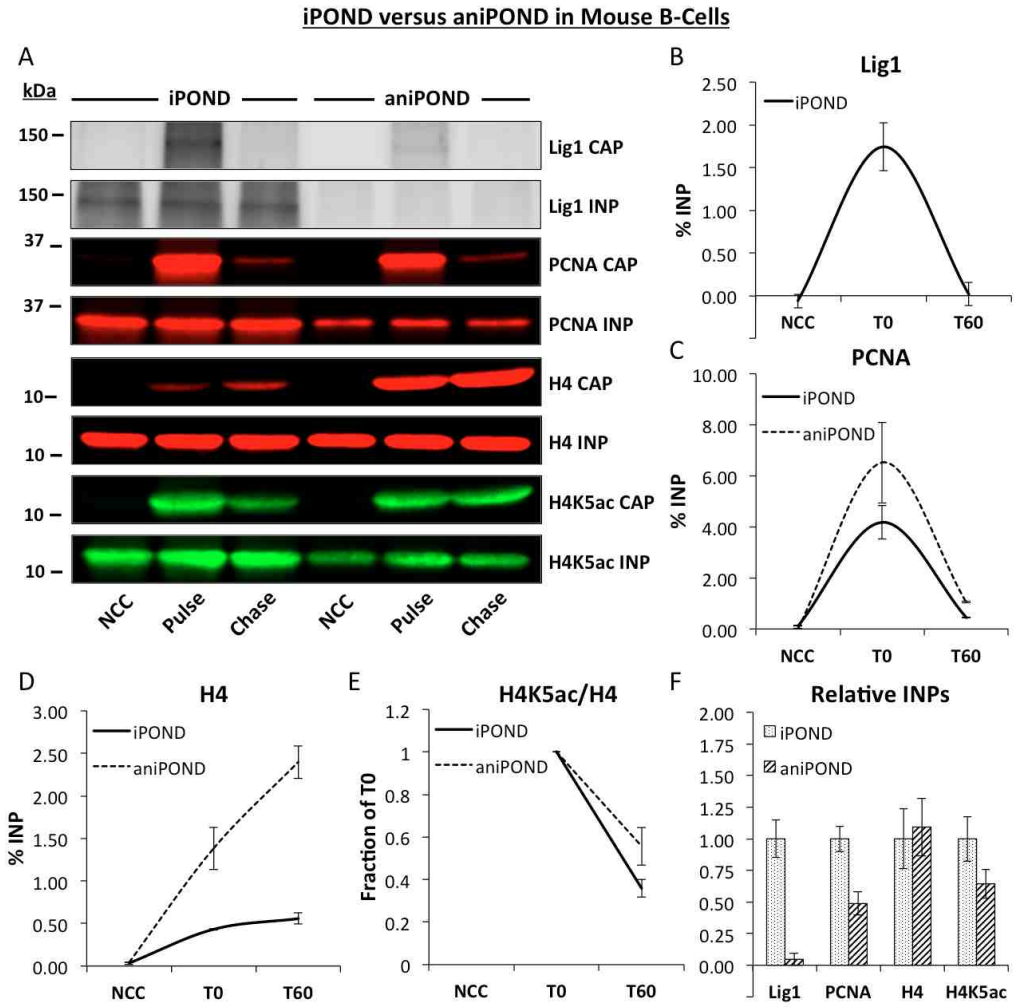

Figure 3.8. Direct comparison of the iPOND and optimized aniPOND techniques. (A) 90 million CH12F3 mouse B-cell lymphoma cells were processed for either iPOND according to the published protocol (Sirbu et al., 2012), or optimized aniPOND as described in this chapter. No-click control ("NCC"), 15 min EdU pulse ("Pulse"), and 15 min EdU pulse followed by 60 min thymidine chase ("Chase") samples were performed for each protocol simultaneously. 50% of proteins captured by streptavidin beads ("CAP") and 1% of pre-pulldown input ("INP") were analyzed on the same SDS-PAGE gels for the indicated proteins. Antibodies used were Rabbit anti-Lig1 (in house) 1:2,500, Mouse anti-PCNA (Santa Cruz sc-56) 1:200, Mouse anti-H4 (Abcam ab17036) 1:1,000, and Rabbit anti-H4K5ac (Abcam 51997) 1:10,000, followed by incubation with Goat anti-Rabbit 800nm 1:5,000 or Goat anti-Mouse 680nm 1:5,000 NIR fluorescent secondary antibodies and detection with an Odyssey NIR imaging system (Li-Cor Biosciences). The capture of Lig1 (B), PCNA (C), and H4 (D) was assessed as a percent of input, with the pulse samples indicated as T0 and the chase samples indicated as T60, and the removal of the H4K5ac mark was monitored (E). Pre-pulldown input signals for the indicated proteins were compared as a fraction of iPOND INP (F). For all quantitations, signal represents the mean of two independent biological replicates. Error bars ± S.D.

chromatin content (input) of the iPOND and aniPOND samples demonstrated that almost no Lig1 is present in aniPOND chromatin preparations (**Fig 3.8F**), while PCNA, H4, and H4K5ac are present. Thus, iPOND detects transiently interacting proteins that are lost from chromatin during aniPOND sample preparation whereas the aniPOND protocol very efficiently captures chromatin proteins that remain associated under native conditions.

One of the rationales for the development of the aniPOND protocol was to avoid thermal decrosslinking (Leung et al., 2013). To test the requirement for thermal decrosslinking, we boiled iPOND samples for different amounts of time and compared to aniPOND samples (**Fig 3.9**). We found that 25 min of boiling, as suggested in the iPOND protocol (Sirbu et al., 2012), was sufficient to decrosslink both Lig1 and histone H4 (**Fig 3.9**). However, in line with the hypothesis that large chromatin modifying enzymes inefficiently decrosslink, DNMT1 never resolved out of a high molecular weight smear into a clearly identifiable band, even after one hour of boiling (**Fig 3.9**). In contrast, DNMT1 was clearly detectable in the aniPOND sample. Based on these data, we recommend utilizing iPOND to test the association of transiently-interacting proteins with newly-synthesized DNA, and we recommend utilizing the optimized aniPOND protocol described in this chapter to examine histone proteins and large chromatin modifying complexes that inefficiently decrosslink. Together, these results provide evidence for the strengths and limitations of both iPOND and aniPOND, and highlight the complementary nature of these techniques.

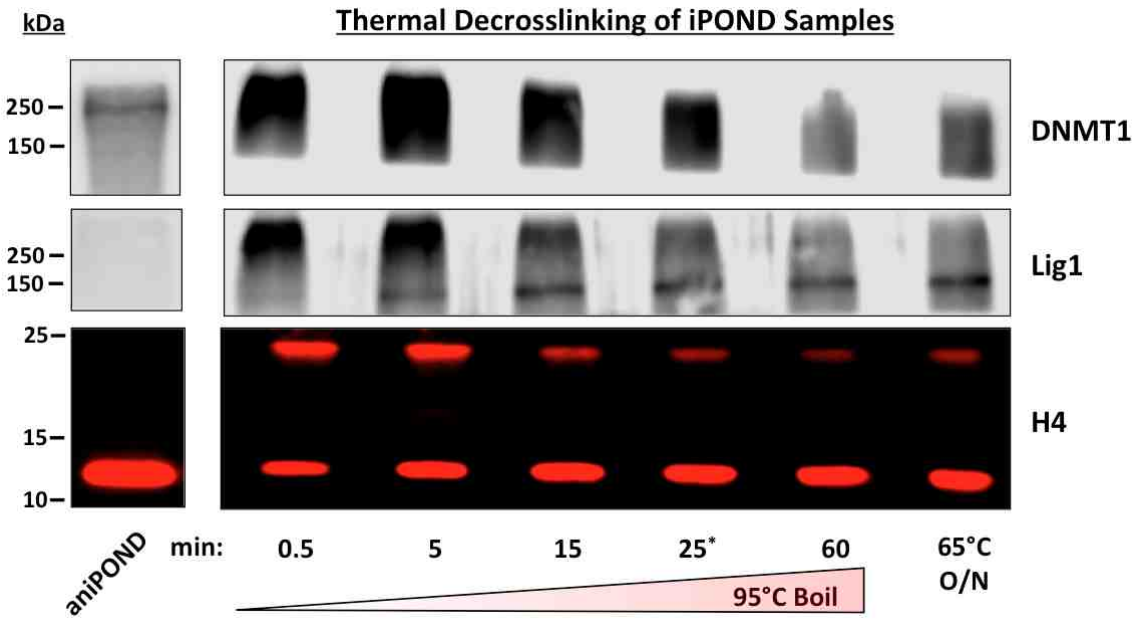

Figure 3.9. Assessing the efficiency of thermal decrosslinking of iPOND samples. CH12F3 mouse B-cell lymphoma cells were processed for either iPOND or aniPOND. iPOND input samples were boiled for varying amounts of time as indicated or placed at 65°C overnight. * indicates the recommended boiling time in the published protocol (Sirbu et al., 2012). 1% input samples were resolved on SDS-PAGE gels and probed for DNMT1 (Mouse anti-DNMT1 1:200, Santa Cruz sc-271729), Lig1 (Rabbit anti-Lig1 1:2,500, in house), and histone H4 (Mouse anti-H4 1:1,000, Abcam 17036), followed by detection of DNMT1 and Lig1 with HRP-conjugated secondary antibodies (Bio-Rad) or histone H4 with Goat anti-Mouse 680nm 1:5,000 NIR secondary antibody (Li-Cor Biosciences).

3.6 Protocol for Optimized aniPOND in Suspension Cells

The protocol for performing the optimized accelerated native isolation of proteins on nascent DNA (aniPOND) technique in suspension that incorporates the modifications described in this chapter is found in **Appendix A**.

Chapter 4

Role of DNA Ligase I in Chromatin Assembly and Maturation

4.1 Introduction

During the mammalian cell cycle, genomic DNA must be copied once and only once. In addition, patterns of histone modification and DNA methylation must be duplicated to ensure that epigenetic regulation is the same in both daughter cells (Probst et al., 2009). There is compelling evidence that DNA methylation, and chromatin assembly and maturation are tightly coupled with the DNA replication machinery (Chen and Dent, 2013). Since the homotrimeric ring protein proliferating cell nuclear antigen (PCNA) participates in DNA replication, chromatin assembly, and DNA methylation, it is likely that this protein plays a key role in coordinating these processes (Boehm et al., 2016). Other factors that contribute to epigenetic inheritance during DNA replication include a network of histone chaperones and histone PTM readers and writers (Burgess and Zhang, 2013; Hammond et al., 2017; Jasencakova and Groth, 2010), many of which are recruited by key interactions with replication proteins, including PCNA and RPA (Liu et al., 2017; Zhang et al., 2017).

At the replication fork, PCNA acts as a processivity factor for both leading and lagging strand DNA synthesis (Chilkova et al., 2007). The function of PCNA on the lagging strand is more complex as it acts as a molecular platform that coordinates the sequential action of the enzymes involved in Okazaki fragment synthesis, processing, and ligation (Dovrat et al., 2014; Sporbert, 2005). The assembly of nucleosomes is initiated by the PCNA-interacting chromatin assembly factor, CAF1, that deposits newly

synthesized histones H3 and H4 (Shibahara and Stillman, 1999), followed by deposition of H2A-H2B dimers by other chaperones such as FACT and Nap1 (Aguilar Gurrieri et al., 2016; Mao et al., 2016). The assembly of nucleosomes on the newly replicated DNA precedes the addition of histone modifications to duplicate the epigenetic marks that were present on the parental DNA and the removal of H4K5 and K12 acetyl marks on newly synthesized H4 (Almouzni and Cedar, 2016; Sirbu et al., 2011). Because the intact lagging strand is generated by the joining of thousands of Okazaki fragments, the unloading of PCNA from DNA is critical to recycle this key protein for subsequent cycles of Okazaki fragment synthesis, processing, and ligation. PCNA unloading occurs in the context of chromatin assembly, chromatin maturation, and DNA methylation as shown in **Fig 4.1**.

Under normal circumstances, mammalian Okazaki fragments are joined by DNA ligase I (Lig 1), which interacts with PCNA that is topologically linked to DNA (Montecucco et al., 1998; Song et al., 2007). In the absence of Lig1, mounting evidence suggests that DNA ligase III is able to substitute during DNA replication (Arakawa et al., 2012; Arakawa and Iliakis, 2015; Han et al., 2014). However, there are as yet uncharacterized differences in Okazaki fragment metabolism in the absence of Lig1, and both cellular and animal models of Lig1 deficiency demonstrate genome instability (Cremaschi et al., 2015; Harrison et al., 2002), suggesting that Lig1 contributes multiple roles towards the protection of genome stability.

Recently, the Elg1-replication factor C-like complex (Elg1-RLC) was demonstrated to contribute to replication-dependent PCNA unloading in budding yeast (Kubota et al., 2015; 2013), a function that is likely conserved in the human Elg1

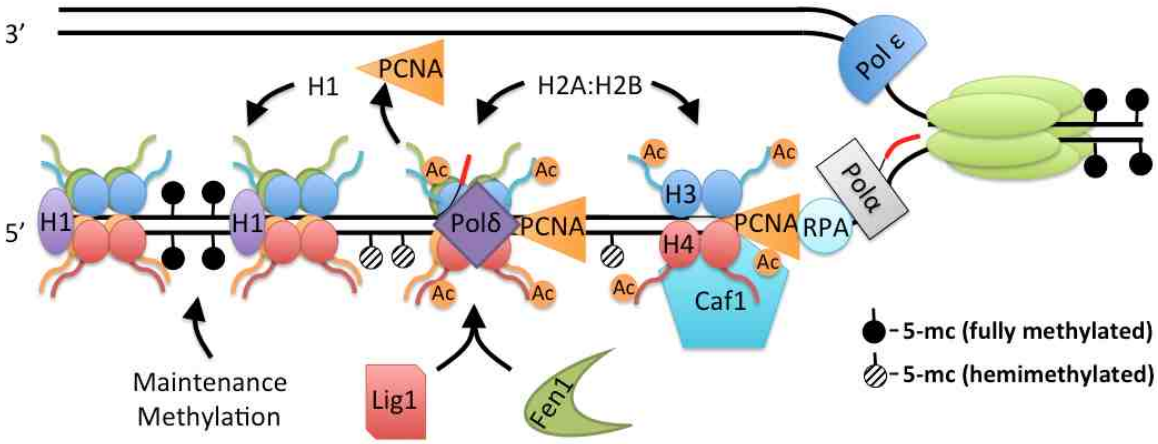

Figure 4.1. Events on the lagging strand during DNA replication. Polα/primase deposits a short RNA-DNA hybrid primer that Polδ extends in coordination with its processivity factor PCNA. Concurrent with Okazaki fragment synthesis, PCNA recruits Caf1 to begin nucleosome reassembly by the deposition of $(H3\text{-}H4)_2$. Polδ-PCNA synthesizes into the following nucleosome, which was completed by the addition of H2A-H2B. The hybrid primer is displaced by Polδ-PCNA and cleaved by PCNA-recruited Fen1, leaving a gap between adjacent Okazaki fragments. Nicks between Okazaki fragments are normally annealed by Lig1 that is targeted to the lagging strand by PCNA. Concurrent with these events, parental histone marks are restored, the H4K5 and K12 acetyl marks that label newly synthesized H4 are removed, linker histone H1 is deposited, and hemimethylated bases generated by the semiconservative replication of 5-methylcytosine (5-mc) are fully restored by maintenance methylation.

ortholog ATAD5 (Huang et al., 2016). Interestingly, the Elg1-RLC complex in budding yeast was shown to require DNA ligation for efficient PCNA unloading, as the induced degradation of the yeast replicative ligase Cdc9 led to the stabilization of PCNA on chromatin post-replication, though it was slowly unloaded over time (Kubota et al., 2015). In addition to potentially assisting in PCNA unloading, the sites of Okazaki fragment ligation in yeast also occur most frequently at the position of nucleosomes dyads, suggesting that ligation and nucleosome deposition are also linked processes (Smith and Whitehouse, 2013). However, many questions about the role of DNA ligase in chromatin assembly and maturation in both yeast and mammalian cells remain to be answered.

At the same time that chromatin maturation is taking place, DNA methylation occurs on newly replicated DNA to generate full methylated DNA that is wrapped around nucleosomes (Auclair and Weber, 2012; Meng et al., 2015). Both of these processes are also linked to PCNA. In the case of DNA methylation, interactions of the DNA maintenance methyltransferase, DNMT1, and UHRF1 with PCNA help target the DNA methylation machinery to newly-synthesized DNA (Liu et al., 2013). Additionally, association of the H3K9 methyltransferase G9A with DNMT1 has been demonstrated to facilitate DNA methylation and preserve methylation at critical regulatory elements such as imprinting control regions in stem cells (Esteve et al., 2006; Zhang et al., 2016). Notably, disruption of methylation by DNMT1 is an oncogenic event that causes genetic and epigenetic changes that are hallmarks of cancer cells (Pacaud et al., 2014). The interactions and process of maintenance DNA methylation on replicating DNA are illustrated in **Fig 4.2.**

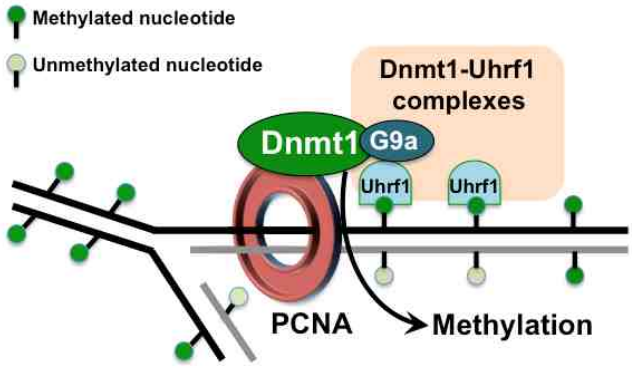

Figure 4.2. Process and coordination of maintenance methylation on replicating DNA. The replicative sliding clamp PCNA acts as a platform to recruit the maintenance methyltransferase DNMT1 to replicating DNA. Dnmt1 forms a complex with UHRF1 that is essential for its recruitment to hemimethylated DNA. Additionally, Dnmt1 interacts with the H3K9 methyltransferase G9a to promote DNA methylation at genomic regulatory sites such as imprinting control regions.

While *LIG1* knockout human cell lines have yet to be generated, a single case of human DNA ligase I deficiency has been described. This individual was immunodeficient and sun sensitive, exhibited growth and developmental delays, and was possibly predisposed to cancer (Teo and Arlett, 1982; Teo et al., 1983a). Genetic and biochemical studies using a cell line generated from donated epithelial cells from this patient, called 46BR cells, demonstrated that both copies of *LIG1* were mutated with one allele encoding an inactive protein due to an amino acid change close to the active site lysine (Q566K) and the other allele encoding a polypeptide (R771W) with only 5% remaining activity (Barnes et al., 1992). Notably, DNA ligase I-deficient mice generated by knock-in of the allele encoding the *LIG1* R771W variant exhibited an increased incidence of spontaneous epithelial-derived tumors (Harrison et al., 2002).

Since it is not known whether the genome instability and cancer predisposition conferred by DNA ligase I deficiency is a consequence of perturbations in Okazaki fragment processing or epigenetic changes, I have examined the role of reduced DNA ligase I in the early and late steps of chromatin assembly and maturation in mammalian cells. I have obtained preliminary data demonstrating that Lig1 deficiency in both human and mouse cells does not affect PCNA turnover or H4 deposition. However, chromatin maturation, as measured by the deposition of linker histone H1 onto newly synthesized DNA, is abnormal in *Lig1* Δ/Δ mouse B-cells. These results correlated with reduced occupancy of total H1 on bulk chromatin and altered H1 isoform composition in *Lig1* Δ/Δ mouse B-cells. In addition, I observed reduced levels of DNMT1 and associated proteins in subcellular fractions of *Lig1* Δ/Δ mouse B-cells and a possible kinetic impairment in the recruitment of UHRF1 to replicating DNA. Finally, I observed significantly increased

levels of γH2A.X in *Lig1* Δ/Δ mouse B-cells. Together, these data suggest novel roles for Lig1 in chromatin maturation and DNA methylation after replication that may have important implications in genome and epigenome stability.

4.2 Materials and Methods

iPOND and aniPOND

The investigation of proteins on nascent DNA (iPOND) technique was performed as published (Sirbu et al., 2012), and the accelerated native iPOND protocol was performed according to the optimized protocol described in **Chapter 3** and **Appendix A**.

Cell Lysates and Subcellular Fractionation

Whole cell lysates (WCL), soluble, and chromatin fractions of CH12F3 mouse B-cells were prepared as follows (**Fig 4.3**). For WCL generation, 2.5 x 10^7 exponentially growing cells were gently washed in PBS and resuspended in 250 µL ice-cold RIPA buffer supplemented with 1x protease inhibitor cocktail (Sigma-Aldrich P8340) and 1 mM PMSF. Samples were sonicated with a Branson 250 Sonifier on output 3 for two rounds of 10 seconds each, with 10 seconds on ice between sonication, followed by centrifugation for 10 min at 16,400 x *g* at 4°C. 200 µL of clarified WCL were removed and 200 µL of 2x Laemli buffer (4% SDS, 20% glycerol, 125 mM Tris-HCl pH 6.8, 0.01% bromophenol blue, supplemented with 5% v/v β-mercaptoethanol) were added, followed by boiling of samples for 5 min.

Subcellular fractionation of CH12F3 mouse B-cells was performed by modifying a previously described protocol (Méndez and Stillman, 2000) as follows: 5 x 10^7

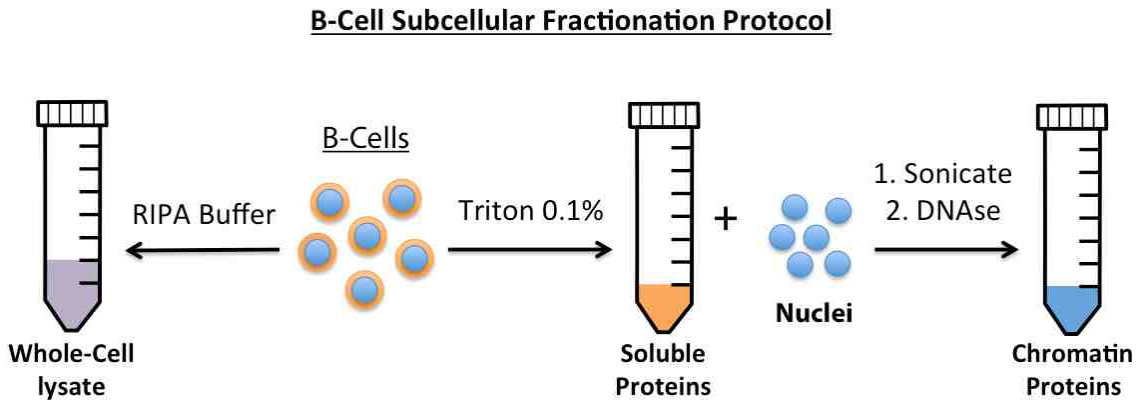

Figure 4.3. Schematic illustration of the protocol to obtain RIPA whole cell lysates, triton-extracted soluble proteins, and sonicated, DNAsed chromatin proteins.

exponentially growing cells were gently washed in PBS and resuspended in 0.5 mL non-denaturing lysis buffer (0.34 M sucrose, 10% glycerol, 10 mM HEPES pH 7.5, 10 mM KCl, 3 mM $MgCl_2$, 0.1% Triton X-100) supplemented with 1 mM DTT, 1x protease inhibitor cocktail, and 1 mM PMSF. Samples were incubated on ice for 5 min, followed by centrifugation for 4 min at 1,300 x *g* at 4C, yielding a pellet (nuclei) and supernatant (crude soluble fraction). 0.4 mL of supernatant were carefully removed and clarified by centrifugation for 10 min at 16,400 x *g* at 4°C. 0.3 mL of the clarified soluble fraction were carefully removed, 300 µL of 2x Laemli buffer supplemented with 5% β-mercaptoethanol were added, and the sample was boiled for 5 min. The nuclei pellet was washed three times with 1 mL of ice-cold non-denaturing lysis buffer supplemented with 1 mM DTT, 1x protease inhibitor cocktail, and 1 mM PMSF, and then resuspended in 250 µL of DNAse solution (1x RQ1 DNAse buffer, 20U RQ1 DNAse; Promega M6101). Nuclei were sonicated with a Branson 250 sonifier on output 3 for three rounds of 10 seconds, with 10 seconds on ice between sonications, followed by incubation at 37°C for 10 min to allow DNA digestion by the RQ1 DNAse enzyme. 250 µL of 2x Laemli buffer supplemented with 5% β-mercaptoethanol were added, samples were boiled for 5 min, and then clarified by centrifugation at 16,400 x *g* for 10 min at room temperature. Protein contents of WCL, soluble, and chromatin fractions were measured by a Bradford assay with BSA standards (Bradford, 1976). Western blots for subcellular fraction experiments are found in **Appendix B**.

Quantitative Near-Infrared (NIR) Fluorescence Immunoblotting

Quantitative NIR immunoblotting was performed essentially as described in **Appendix A**. For iPOND and aniPOND experiments, 1% of input (INP) and 50% of beads capture (CAP) sample were resolved on freshly prepared SDS-PAGE gels and probed with the following antibodies: Mouse anti-UHRF1 1:200 (Santa Cruz sc-373750), Mouse anti-PCNA 1:200 (Santa Cruz sc-56), Mouse anti-histone H4 1:1,000 (Abcam ab17036), and Rabbit anti-histone H4K5ac 1:10,000 (Abcam ab51997). For WCL and subcellular fraction experiments, 40 μg of protein was resolved on freshly prepared SDS-PAGE gels and probed with the following antibodies: Mouse anti-DNMT1 1:200 (Santa Cruz sc-271729), Rabbit anti-G9A 1:1,000 (Abcam ab185050), Rabbit anti-Lig1 1:2,500 (in house), Rabbit anti-Lig4 1:200 (Santa Cruz sc-28232), Mouse anti-Lig3 1:200 (Santa Cruz sc-135883), Mouse anti-PCNA 1:200 (Santa Cruz sc-56), Rabbit anti-GAPDH 1:1,000 (Cell Signaling Technology 2118S), Mouse anti-Histone H1 1:200 (Santa Cruz sc-8030), Mouse anti-Histone H1.0 1:500 (Abcam, ab11079), Rabbit anti-Histone H1.2 1:500 (Proteintech 15446-1-AP), Rabbit anti-Histone H1.4 1:500 (Abcam ab105522), Mouse anti-Histone H4 1:1,000 (Abcam ab17036), Rabbit anti-Histone H4K5ac 1:10,000 (Abcam ab51997), and Mouse anti-γH2A.X 1:1,000 (BioLegend 613402). Blots were either probed with horseradish peroxidase (HRP)-conjugated secondary antibody (Bio-Rad) and developed with SuperSignal West Femto Maximum Sensitivity Substrate (Thermo Fisher Sci.), or with 680nm or 800nm NIR fluorescent secondary antibodies and developed with an Odyssey Fc NIR imaging system (Li-Cor Biosciences). Band intensities were quantitated with Image Studio software (Li-Cor Biosciences), using 3-pixel local background subtraction.

4.3 Preliminary Results and Discussion

Early steps of chromatin assembly and maturation appear largely unaffected by reduction in Lig1 activity in human cells

To test the role of Lig1 in chromatin maturation in human cells, I utilized derivatives of the *lig1* mutant 46BR cell line. The 46BR.1G1 cell line was previously established by immortalization of 46BR cells, and subsequent studies generated a stable derivative expressing a WT FLAG-LIG1 complement (**Fig 4.4A**). I tested the role of human Lig1 in early events of chromatin deposition and maturation by performing aniPOND over a time course in which a 10 min EdU pulse was followed by either no chase (to capture proteins at the replication fork) or a 60 min thymidine chase (to capture proteins assembling on newly replicated chromatin). This protocol was applied in 46BR.1G1 derivatives containing an empty vector control (VC), WT FLAG-LIG1 complemented cells (WTC), or in previously complemented cells that had lost expression of the recombinant *LIG1* (**Fig 4.4B**). Quantitation of the beads capture samples as a percent of input revealed no difference in the occupancy of PCNA at the replication fork or in PCNA unloading after a 60 min chase between VC and WTC cells (**Fig 4.4C**, left panel). This suggests that PCNA unloading in human cells is not enhanced by the actions of the replicative DNA ligase, unlike in budding yeast (Kubota et al., 2015). Interestingly, even though Okazaki fragment ligation is impaired in extracts from 46BR.1G1 cells (Levin et al., 2000), I observed no difference in the efficiency of deposition of H4 between VC and WTC cells (**Fig 4.4C**, middle panel). However, there was a small increase in the fraction of H4 acetylated on Lysine 5 in the VC cells compared to the WTC (**Fig 4.4C**, right panel).

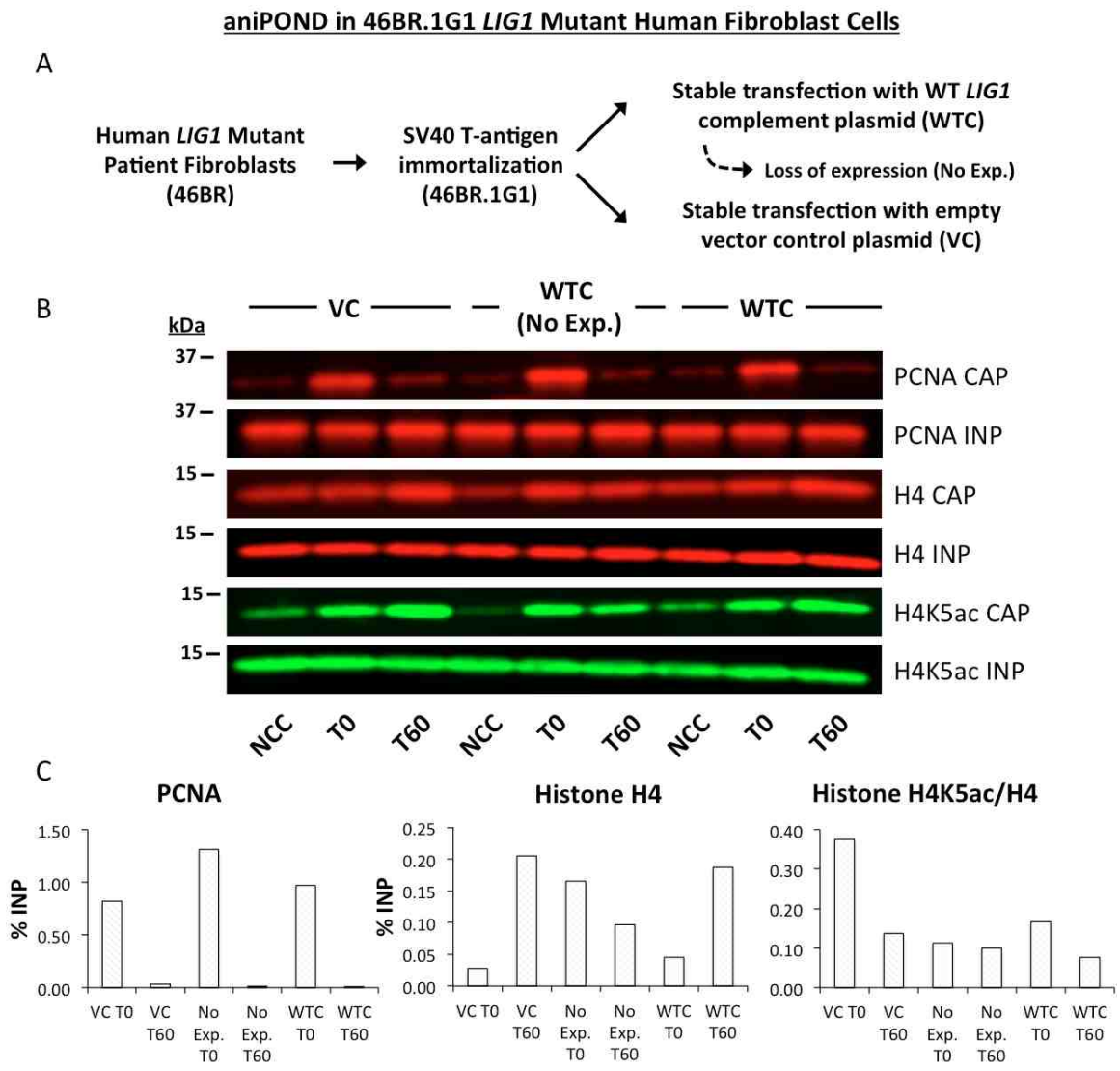

Figure 4.4. Role of Lig1 in PCNA unloading, H4 deposition, and H4K5ac turnover in human *LIG1* mutant fibroblasts. (A) Strategy utilized for development of the human *LIG1* mutant cell line 46BR.1G1 and its derivatives. Steps in the published literature (?) indicated by solid lines. A derivative of *Flag-LIG1*-complemented WTC that lost *LIG1* expression over cell passaging is indicated with dashed line. Cell line names are indicated in parentheses. (B) aniPOND results in 46BR.1G1 vector control (VC) and WT *LIG1* complemented (WTC) cells, and a WTC derivative that lost *LIG1* expression (No Exp.). CAP = 33 % beads capture. INP = 0.25% pre-pulldown input. NCC = No-click control. T0 = 10 min EdU pulse. T60 = 10 min EdU pulse followed by 60 min thymidine chase. (C) Quantitations of CAP signals as a % of input and the ratio of H4K5ac to H4. n=1 for all quantitations.

The preliminary aniPOND data in 46BR.1G1 cells were confounded by differences in protein expression and association with replication forks. As indicated in **Fig 4.4A**, the WTC cells lost expression of FLAG-LIG1 over time. In the aniPOND experiment, these non-expressing complemented cells had altered dynamics of PCNA, histone H4, and histone H4K5ac turnover compared to both VC and WTC cells (**Fig 4.4B-C**). When I tested the expression of the wild-type FLAG-LIG1 in 46BR.1G1 WTC cells from three different sources, I observed that all three had different steady state levels of FLAG-LIG1, leading to differences in the total Lig1 expression compared to control cells (**Fig 4.5A**). When PCNA association with the replication fork was tested by aniPOND between three different VC and WTC 46BR.1G1 derivatives from different sources, I observed different levels of PCNA occupancy between VC and WTC derivatives (**Fig 4.3B-C**). In addition to the expression variability of FLAG-LIG1, another confounding factor was the presence of the mutant Lig1 from the endogenous *LIG1*^{R771W} allele in 46BR.1G1 cells. While only containing 5% of the catalytic activity of WT Lig1 (Barnes et al., 1992), this mutant protein could potentially play a dominant negative role in interrupting the roles of Lig1 in Okazaki fragment processing and chromatin maturation.

It is worth noting that the 46BR.1G1 cell line might still be a valuable resource for studying the role of Lig1 in chromatin maturation. Although expression of *LIG1* varied among the three sources of VC and WTC cells (**Fig 4.5A**), there were derivatives

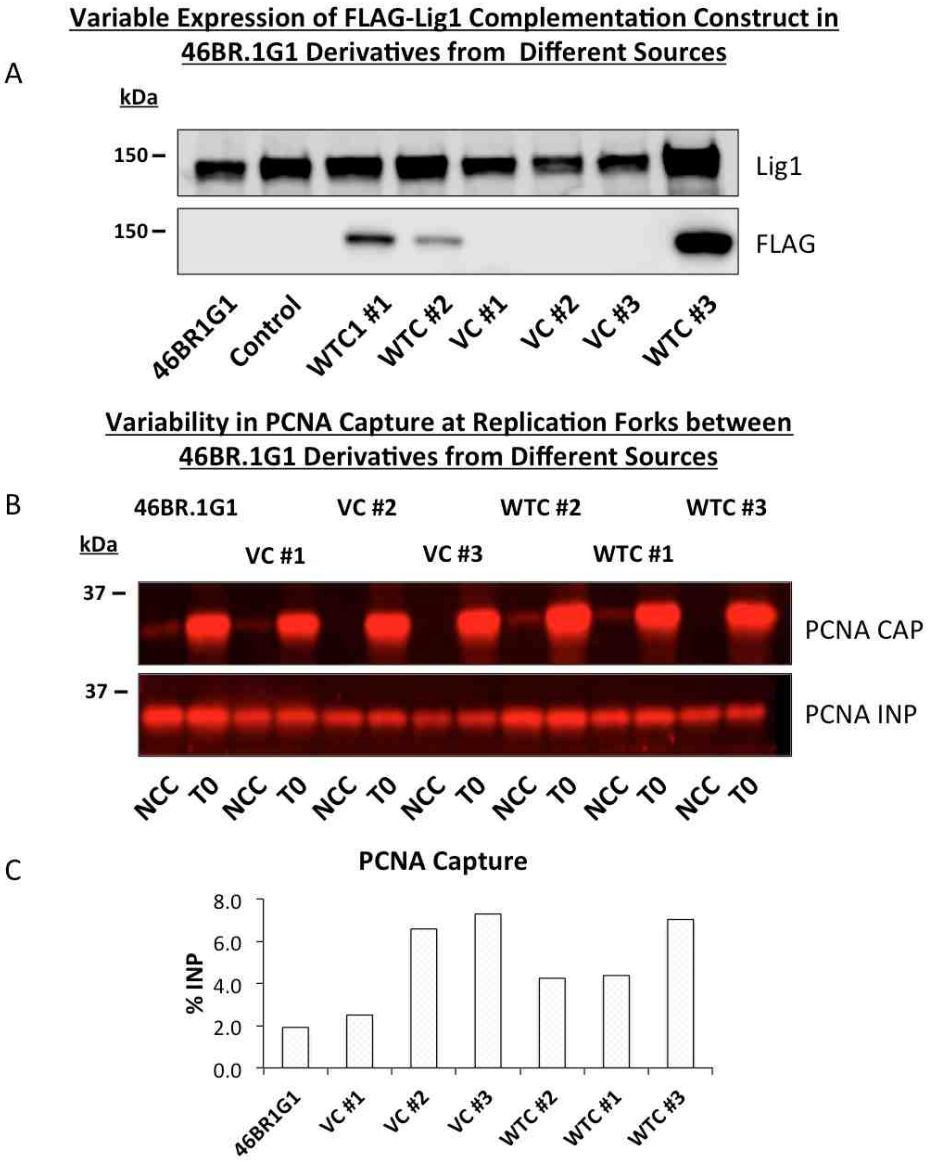

Figure 4.5. Unstable Lig1 expression in complemented 46BR.1G1 derivatives. (A) Basal protein levels of total Lig1 and FLAG-Lig1 from the stably integrated complementation vector in 46BR1G1 derivatives from different sources. WTC = wild-type stably complemented derivative. VC = empty vector stably complemented ctonrol derivative. "Control" = *LIG1* $^{+/+}$ human fibroblast control cell line (GM00847). (B) aniPOND in derivatives 46BR.1G1 VC and WTC cell lines from different sources probing for PCNA occupancy at replication forks. NCC = No-click control. T0 = 10 min EdU pulse . (C) Quantitations of PCNA CAP signals as a % of input between derivatives. n=1 for all quantitations.

in which Lig1 levels matched those in control cells. For example, WTC #1 had total Lig1 levels that approximate those in the control GM00847 *LIG1*$^{+/+}$ fibroblast control cell line, and VC #1 had reduced Lig1 levels similar to those in the parental 46BR.1G1 cell line (**Fig 4.5A**). With carefully controlled passaging and frequent monitoring of total Lig1 and FLAG-Lig1 levels relative to appropriate controls, the unstable expression problem could potentially be mitigated. Alternate approaches to study the roles of human Lig1 in chromatin assembly and maturation include the development and characterization of new cell lines from patients with different *LIG1* mutations (Mitra et al., 2014), complementation of 46BR.1G1 cells with more stably expressing vectors such as bicistronic internal ribosomal entry site (IRES) vectors (Gurtu, 1996), treatment of human cells with Lig1-specific chemical inhibitors (Zhong et al., 2008), or genome editing with CRISP/Cas9 technology (Ran et al., 2013).

Early events in chromatin assembly and maturation appear nearly identical between WT and* Lig1 Δ/Δ *mouse B-cells

To address the problems to data interpretation in the aniPOND experiments with derivatives of the 46BR.1G1 cell line described above, I obtained a recently developed *Lig1* knockout in the CH12F3 mouse-B cell lymphoma line that was generated by sequential gene targeting of *Lig1* Exons 18-19 (Han et al., 2014; Nakamura et al., 1996). Unlike 46BR.1G1 human fibroblast cells, the CH12F3 *Lig1* Δ/Δ mouse B-cells were not reported to have increased sensitivity to most DNA damaging agents, with the exception of a mild sensitivity to MMS (Han et al., 2014; Teo et al., 1983a). These differences may reflect interspecies variation in the reliance upon Lig1 and Lig3 for DNA replication and

repair. There were conflicting reports as to the effects of expressing wild-type Lig1 on the growth rates of 46BR.1G1 human fibroblasts, with one group reporting that they double ~ 33% faster after complementation with wild-type *LIG1* (Soza et al., 2009). I confirmed that, as reported (Han et al., 2014), the WT and *Lig1* Δ/Δ CH12F3 mouse B-cells double with identical rates and that Lig1 protein is not detectable in the *Lig1* Δ/Δ mouse B-cells by immunoblotting (**Fig 4.6**).

I assessed the role of Lig1 in chromatin maturation by measuring the levels of proteins and histone PTMs involved in the histone deposition and chromatin maturation process (**Fig 4.1**) by the iPOND and aniPOND techniques in CH12F3 WT and *Lig1* Δ/Δ cells. I investigated the unloading of PCNA in these cells by the aniPOND technique using a 15 min EdU pulse followed by either no chase or a 10-30 minute chase with thymidine (**Fig 4.7**). In accord with our results using the 46BR.1G1 human fibroblast cell lines, PCNA unloading was identical in WT and *Lig1* Δ/Δ cells (**Fig 4.7B**, left panel), arguing that either the mammalian replicative ligase does not enhance PCNA unloading during DNA replication or there are compensatory mechanisms. Also consistent with the results from the 46BR.1G1 human fibroblast cells was the observation that histone H4 deposition was almost identical between WT and *Lig1* Δ/Δ mouse B-cells (**Fig 4.7B**, middle panel) whereas the fraction of acetylated H4K5 on newly deposited chromatin was slightly higher in the *Lig1* Δ/Δ mouse B-cells (**Fig 4.7B**, right), suggesting a possible slight delay in H4K5ac turnover in the absence of Lig1. It should be noted that all of these results are still preliminary and must be confirmed with additional biological replicates.

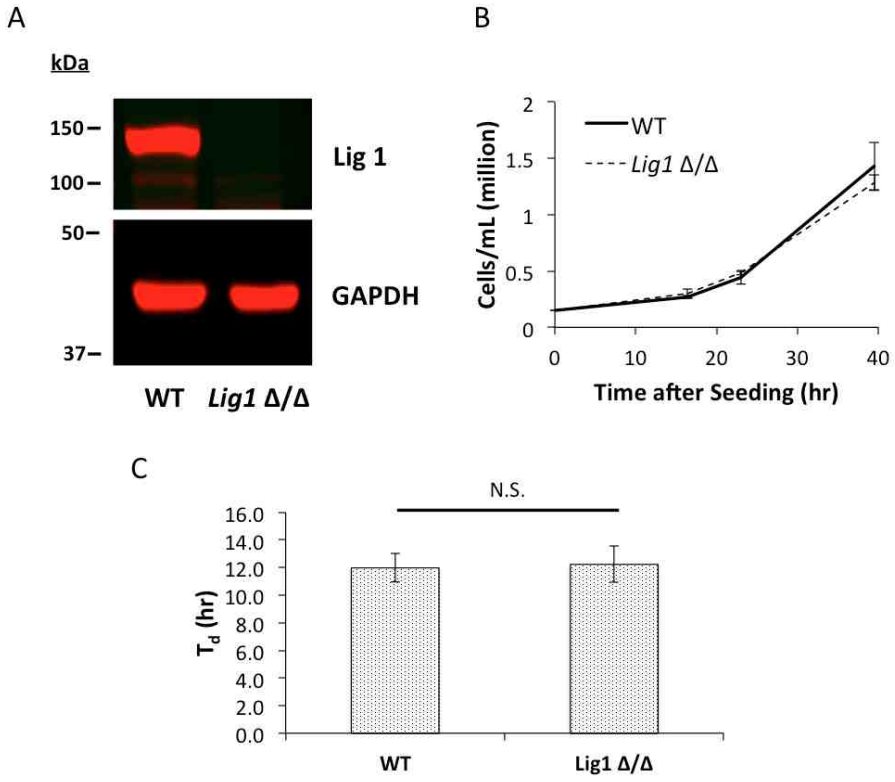

Figure 4.6. Characterization of Lig1 expression and growth in WT and *Lig1* Δ/Δ CH12F3 mouse B-cell lymphoma cells. (A) Expression of Lig1 and GAPDH in whole-cell lysates. (B) Growth of WT and *Lig1* Δ/Δ cells under aniPOND conditions. n= 2 independent biological replicates. Error bars ± S.D. (C) Doubling times for WT and *Lig1* Δ/Δ cells from 5 independent iPOND or aniPOND experiments. Error bars ± S.D. Statistical difference between mean WT and *Lig1* Δ/Δ doubling-time was assessed by Student's *t*-test. N.S. = not significant.

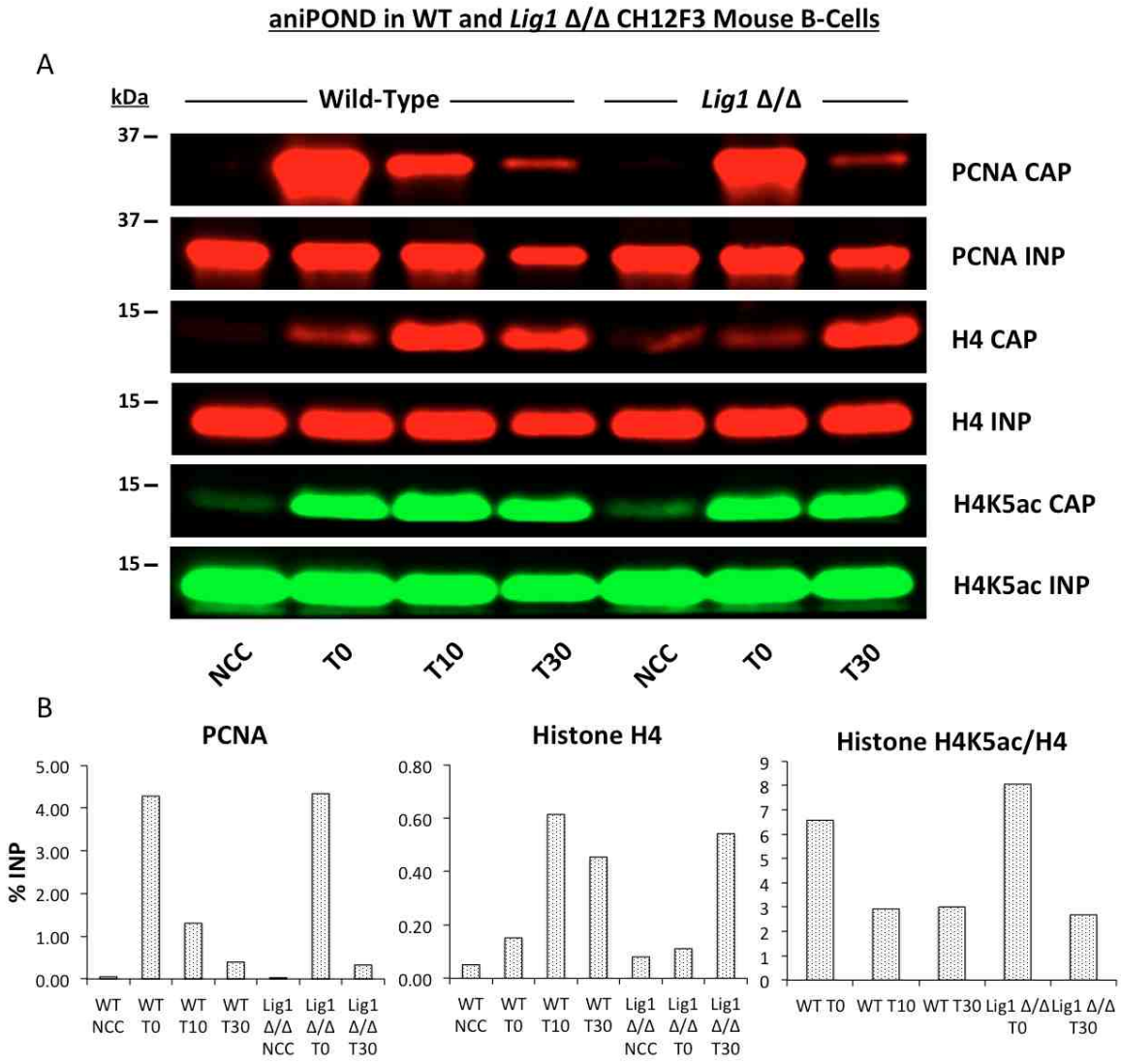

Figure 4.7 Role of Lig1 in PCNA unloading, H4 deposition, and H4K5ac turnover in mouse B-cells. (A) aniPOND in CH12F3 WT and *Lig1* Δ/Δ mouse B-cell lymphoma cells. CAP = 50% of beads capture proteins. INP = 1% of pre-pulldown proteins. NCC = No-click control. T0 = 15 min EdU pulse. T10 = 15 min EdU pulse followed by 10 min thymidine chase. T30 = 15 min EdU pulse followed by 30 min thymidine chase. Note that T10 in *Lig1* Δ/Δ was lost during experiment. (B) Quantitation of CAP signals as a % INP and the ratio of H4K5ac to H4. n=1 for all quantitations.

As the aniPOND and iPOND techniques may yield different but complementary sets of information (see **Chapter 3.5**), I also examined early events in chromatin assembly and maturation by the original formaldehyde-based iPOND technique in CH12F3 WT and *Lig1* Δ/Δ cells. As seen in **Fig 4.8**, the similarity in PCNA turnover in WT and *Lig1* Δ/Δ cells seen in aniPOND was recapitulated by the iPOND technique. The dynamics of H4 deposition and H4K5ac turnover were also similar, although the beads pulldown of histone proteins was much less efficient in the iPOND technique (also see **Fig 3.8)**. Interestingly, deposition of histone H1 was observed with wild-type mouse B-cells after a 30 minute thymidine chase, but not observed with *Lig1* Δ/Δ B-cells (**Fig 4.8**), suggesting a possible defect in H1 deposition in the Lig1 deficient B-cells. It should be noted that the band for H1 did not appear in the INP samples and was significantly larger than the reported size of ~30 kDa for histone H1, raising questions about the specificity of this antibody (Santa Cruz sc-10806), which interacted with multiple bands in separate WCL blots (not shown). To determine the significance of this result, I conducted a more thorough investigation of histone H1 isoforms and their deposition on newly synthesized genomic DNA in WT and *Lig1* Δ/Δ B-cells using different immunoreagents and experimental strategies, as described below.

Replication-coupled histone H1 deposition is impaired in* Lig1 Δ/Δ *mouse B-cells

I next sought to more thoroughly characterize the role of Lig1 in the deposition of histone H1 on newly replicated DNA. While histone H1 deposition is supposed to be a mark of late chromatin maturation, mass spectrometry databases for both iPOND and the related biotin-dUTP labeling technique have identified H1 isoforms associated with DNA

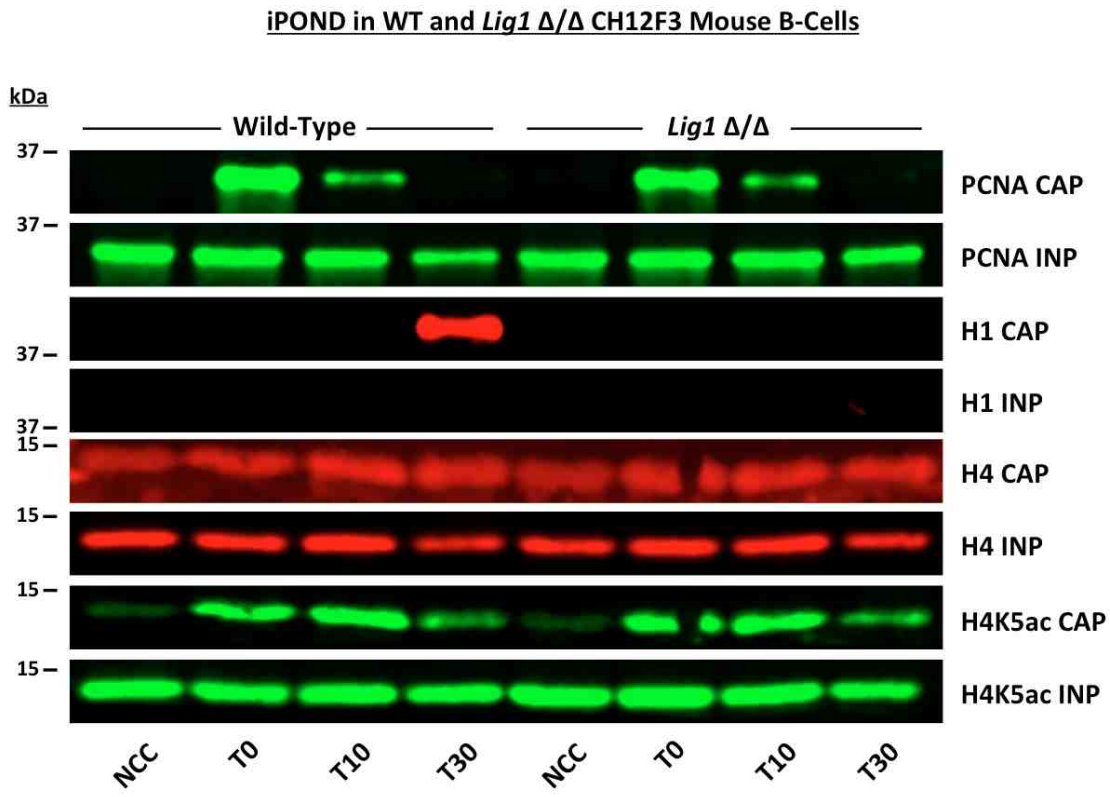

Figure 4.8. iPOND in WT and *Lig1* Δ/Δ CH12F3 mouse B-cells. CAP = 50% of beads capture proteins. INP = 1% of pre-pulldown proteins. NCC = No-click control. T0 = 15 min EdU pulse. T10 = 15 min EdU pulse followed by 10 min thymidine chase. T30 = 15 min EdU pulse followed by 30 min thymidine chase.

immediately after passage of the replication fork (Alabert et al., 2014; Dungrawala et al., 2015). Histone H1 is difficult to study due to the presence of 11 isoforms, many of which have very high sequence homology and are expressed in a cell cycle and tissue-specific manner (Happel et al., 2014; Harshman et al., 2013). Moreover, there are many open questions in the H1 field, including the identity of the H1 chaperone(s) and the mechanisms that regulate H1 deposition onto newly synthesized DNA (Harshman et al., 2013).

To test if Lig1 regulates H1 deposition, I performed aniPOND with WT and *Lig1* Δ/Δ CH12F3 mouse B-cells and probed for histone H1 using a widely utilized monoclonal antibody that recognizes multiple H1 isoforms (clone AE-4; **Fig 4.9A**). My results demonstrated that a strong band at 25 kDa was rapidly deposited in WT cells whereas only a very faint 25 kDa signal was observed in both beads capture and input samples in *Lig1* Δ/Δ cells (**Fig 4.9A-B**). While the 25 kDa histone H1 expressed as a percent of INP of *Lig1* Δ/Δ cells approached the same percentage as in WT cells after 30 min, there was significantly less 25 kDa histone H1 in the *Lig1* Δ/Δ aniPOND input (INP) samples (**Fig 4.9C**), suggesting that *Lig1* Δ/Δ cells have less total 25 kDa histone H1 on chromatin. I noted the presence of multiple faint H1 bands at ~33-35 kDa in the aniPOND INP samples probed with the pan-H1 antibody; these bands were present at equivalent levels in INPs from both WT and *Lig1* Δ/Δ cells (**Fig 4.9A**, see the INP blot). As certain isoforms of histone H1 are expressed in S-phase (H1.1, H1.2, H1.3, H1.4, and H1.5) while others are expressed in a replication-independent manner (H1.0, H1.10), it is possible that the aniPOND results could be indicative of a difference in isoform deposition between WT and *Lig1* Δ/Δ cells (Happel et al., 2014).

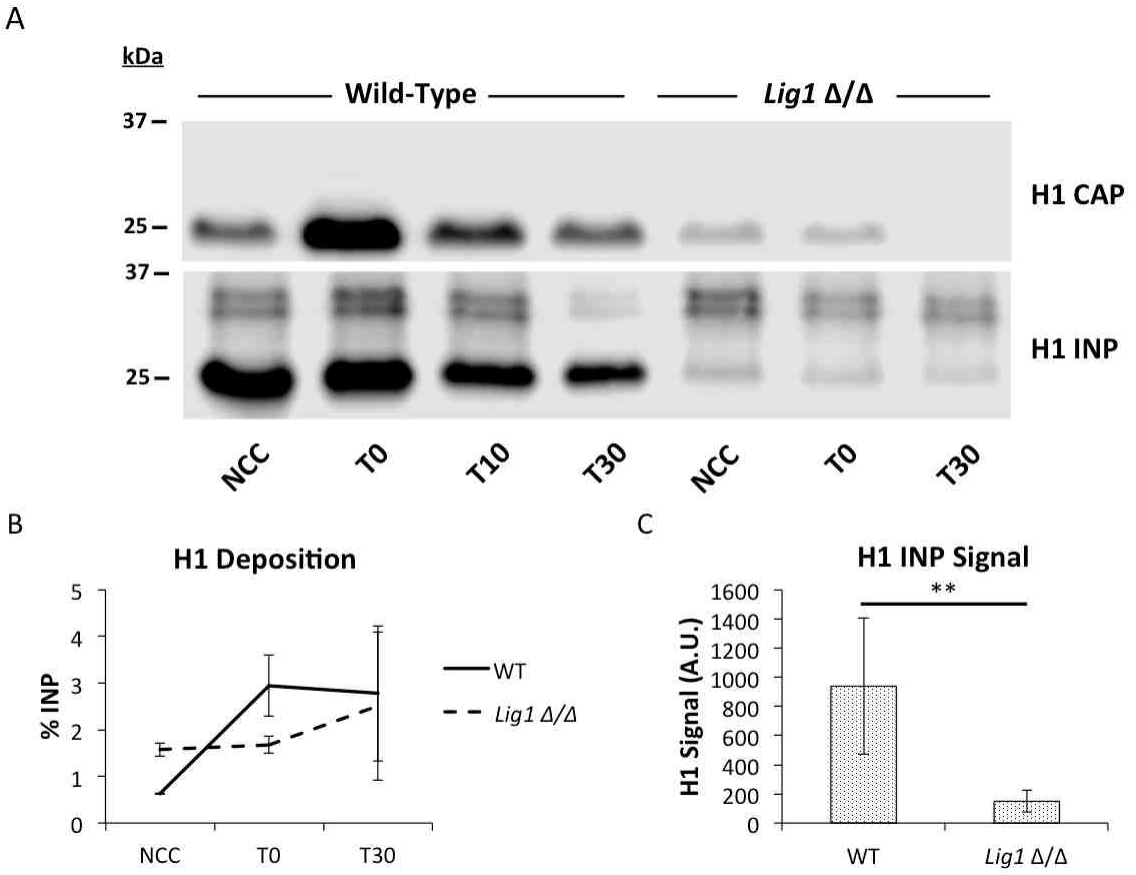

Figure 4.9. Dynamics of histone H1 recruitment in WT and *Lig1* Δ/Δ mouse B-cells. (A) aniPOND in CH12F3 WT and *Lig1* Δ/Δ mouse B-cell lymphoma cells. CAP = 50% of beads capture proteins. INP = 1% of pre-pulldown proteins. NCC = No-click control. T0 = 15 min EdU pulse. T10 = 15 min EdU pulse followed by 10 min thymidine chase. T30 = 15 min EdU pulse followed by 30 min thymidine chase. Note that T10 in *Lig1* Δ/Δ was lost during experiment. (B) Quantitation of CAP signals as a % INP. n=2 independent biological replicates. Error bars ± S.D. The 25 kDa H1 band was analyzed. (C) Raw H1 INP values for six different WT and *Lig1* Δ/Δ aniPOND samples from two independent aniPOND experiments. Samples were generated from similar numbers of cells, and the 25 kDa H1 band was analyzed as this was the dominant species observed being deposited on newly synthesized DNA. Higher molecular weight bands may represent alternate H1 isoforms or H1 modified by post-translational modification.

To further investigate the abnormality in histone H1 deposition in *Lig1* Δ/Δ cells observed by aniPOND, I performed subcellular fractionation to measure the levels of total H1 and replication-dependent and independent H1 isoforms in whole cell, soluble, and chromatin fractions of WT and *Lig1* Δ/Δ cells, to the extent allowable by the commercially available H1 immunoreagents (**Fig 4.10**). These results demonstrated that total H1 levels were decreased in all fractions in *Lig1* Δ/Δ cells compared to WT cells (**Fig 4.10A**). Interestingly, while the total H1 signal was lower in *Lig1*Δ/Δ cells whole-cell lysates, soluble, and chromatin fractions, the replication-independent isoform H1.0 was significantly increased in *Lig1* Δ/Δ whole-cell lysates and chromatin fraction compared to WT (**Fig 4.10B**). In contrast, no significant differences were observed between WT and *Lig1* Δ/Δ cell fractions for the replication-dependent isoform H1.4 (**Fig 4.8C**). There may also be differences in other (replication dependent) histone H1 isoforms between WT and *Lig1* Δ/Δ cells but our ability to measure the differences in other isoforms is limited due to the availability of commercial antibodies, as previously reported (Harshman et al., 2013). Therefore, alternate approaches will be necessary to further characterize alterations in the relative steady state levels of histone H1 isoforms and H1 deposition onto new chromatin in *Lig1* Δ/Δ cells. These approaches could include aniPOND-SILAC-mass spectrometry to quantitatively compare the ratio of histone H1 isoforms between WT and *Lig1* Δ/Δ cells at time points after replication as well as testing the replication-coupled deposition and cellular levels of H1 and H1 isoforms in other models of Lig1 deficiency such as *Lig1* null MEFs and 46BR.1G1 cells (Bentley et al., 1996; 2002). It may also be possible to perform genome editing with CRISPR/Cas9 to epitope tag H1 isoforms in order to facilitate their immunodetection.

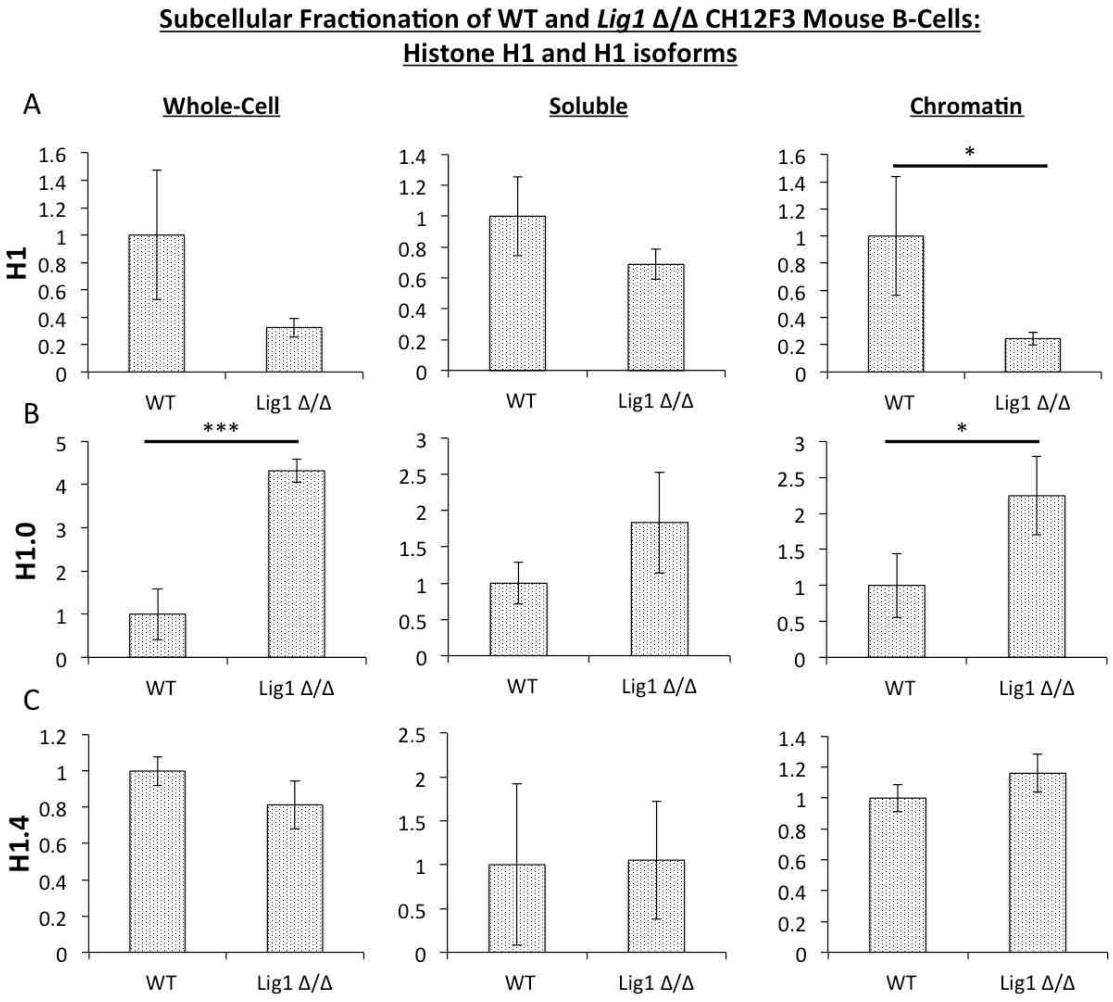

Figure 4.10. Analysis of total histone H1 and H1 isoform protein levels in subcellular fractions of WT and *Lig1* Δ/Δ mouse B-cells. Four independent exponentially growing WT and *Lig1* Δ/Δ cell populations were processed for whole-cell lysates (left panel), soluble (middle panel), and chromatin (right panel) fractions and assayed for pan-H1 (A), and the H1 isoforms H1.0 (B) and H1.4 (C). For total H1 the 25 kDa band was measured, for H1.0 the ~28 kDa bad was measured, and for H1.4 the ~30 kDa band was measured (see Appendix C). H1 band intensities in whole-cell lysates and soluble fractions were normalized to GAPDH, and H1 levels in chromatin fractions were normalized to H4. The signals were further normalized to set the signal for WT as 1. Error bars ± S.D. Statistical difference between WT and *Lig1* Δ/Δ was assessed by Student's *t*-test. * = $p<0.05$ ** = $p<0.01$ *** = $p<0.001$. See Appendix B for individual blots.

Other alterations in* Lig1 Δ/Δ *B-cells: DNA methylation machinery and steady state γH2A.X levels

The reduction in total histone H1 levels on chromatin in *Lig1* Δ/Δ B-cells is predicted to impact other cellular processes. Previous research has demonstrated that histone H1 physically interacts with DNMT1 and DNMT3B to promote DNA methylation and silencing of specific gene regions in ES cells (Yang et al., 2013). Moreover, in cells with reduced H1 content, global changes in nucleosome architecture occur that affect nucleosome spacing and transcription of specific subsets of genes (Fan et al., 2005). To address the possible effect of *Lig1* Δ/Δ on the DNA methylation machinery, I initially examined the levels of proteins involved in DNA methylation (**Fig 4.2**), including DNMT1, UHRF1, and G9A (Liu et al., 2013; Zhang et al., 2016), in cellular fractions (**Fig 4.11**). Interestingly, the levels of all three of these DNA methylation factors were significantly decreased in either whole-cell lysates or soluble fractions from *Lig1* Δ/Δ cells compared to WT cells, whereas their association with chromatin was not different between the two strains (**Fig 4.11A-C**). To address the possibility that methylation factors could have the same occupancy on total chromatin but a defect in recruitment to replicating DNA in *Lig1* Δ/Δ cells, I measured the recruitment of UHRF1 to replicating DNA by aniPOND (**Fig 4.12A**). The preliminary results revealed an effect of *Lig1* deletion of the kinetics of UHRF1 recruitment to chromatin: 50% less UHRF1 was recruited to the replication fork initially. In addition, UHRF1 occupancy on newly-synthesized DNA was prolonged in *Lig1* Δ/Δ cells relative to WT cells with 30 and 60 minutes chase (**Fig 4.12B**). Together, my results suggest a possible

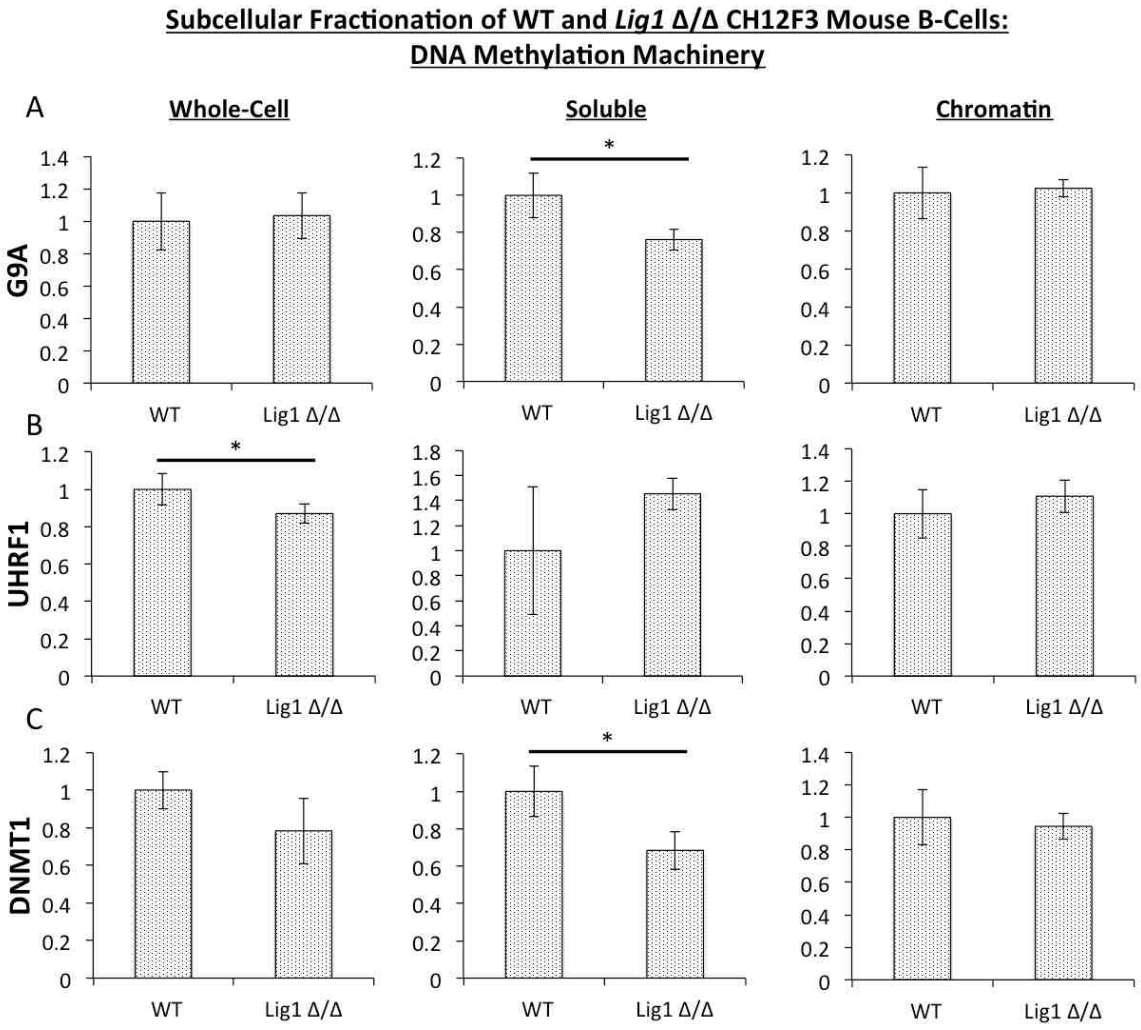

Figure 4.11. Analysis of DNA methylation factors in subcellular fractions of WT and *Lig1* Δ/Δ mouse B-cells. Four independent WT and *Lig1* Δ/Δ cell populations were processed for whole-cell lysates (left panel), soluble (middle panel), and chromatin (right panel) fractions and assayed for the levels of G9A (A), UHRF1 (B), and DNMT1 (C). Whole-cell lysates and soluble fractions were normalized to GAPDH, and chromatin fractions were normalized to H4. The signals were further normalized to the signals in WT cells, which were set as 1. Error bars ± S.D. Statistical difference between WT and *Lig1* Δ/Δ was assessed by Student's *t*-test. * = $p<0.05$ ** = $p<0.01$ *** = $p<0.001$. See Appendix B for individual blots.

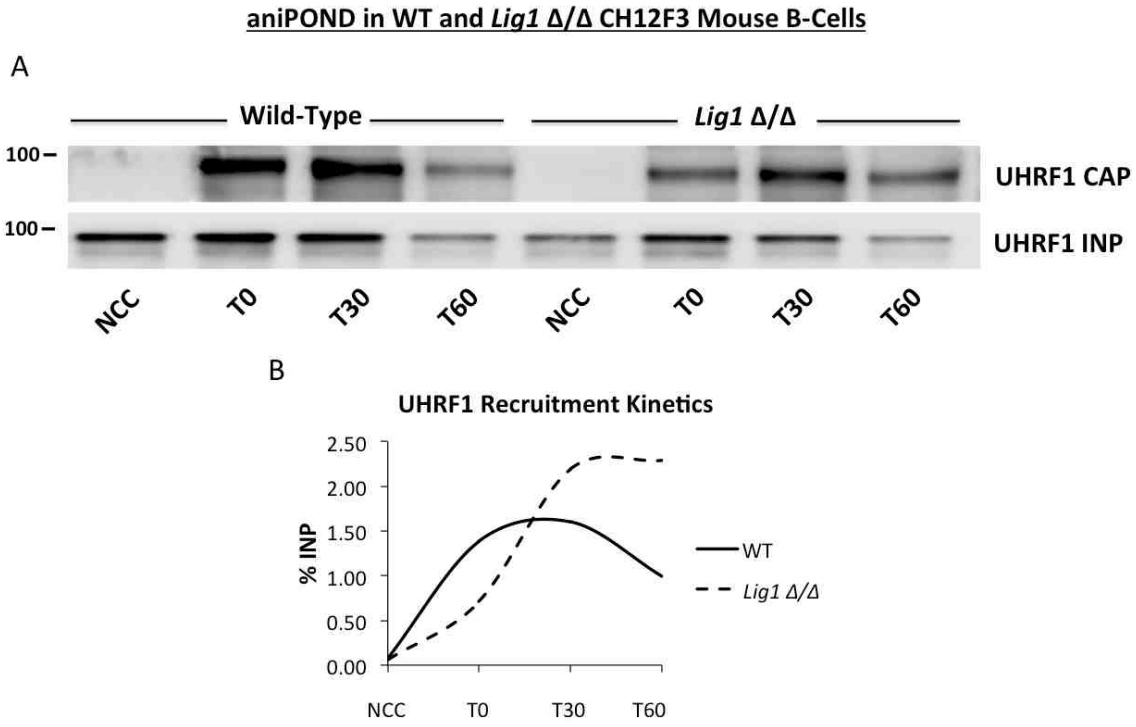

Figure 4.12. Role of Lig1 in UHRF1 recruitment to newly synthesized DNA in mouse B-cells. (A) aniPOND in CH12F3 WT and *Lig1* Δ/Δ mouse B-cell lymphoma cells. CAP = 50% of beads capture proteins. INP = 1% of pre-pulldown proteins. NCC = No-click control. T0 = 15 min EdU pulse. T30 = 15 min EdU pulse followed by 30 min thymidine chase. T60 = 15 min EdU pulse followed by 60 min thymidine chase. Experiment was performed by a rotation student, Ms. Seema Khattri Bhandari, under my supervision. (B) Quantitation of CAP signals as a % INP. n=1 experiment.

role for Lig1 in the recruitment and subsequent release the DNA methylation machinery. Future directions to investigate the potential link between Lig1 and DNA methylation may include monitoring the recruitment of DNMT1 and G9A to newly synthesized DNA by aniPOND and measuring the levels of both global DNA methylation and DNA methylation on newly synthesized DNA. Furthermore, interactions between both histone H1 and Lig1 and DNA methylation factors can be probed by both *in vivo* and *in vitro* co-immunoprecipitation assays to identify the key interactions that mediate the maintenance of DNA methylation and its link to Lig1.

The phenotypes observed in the preliminary data discussed in this chapter suggest novel roles for Lig1 in determining the steady state levels of the histone H1 isoforms and the deposition of the linker histone H1 onto newly replicated DNA as well as in mediating the timely recruitment of the DNA methylation machinery to replication forks. As both histone H1 and the DNA methylation machinery protect against genome stability, it might be expected that genomic stress would occur when these processes are perturbed. Indeed, I found that the levels of γH2A.X were significantly elevated in both whole-cell lysates and on chromatin of *Lig1* Δ/Δ cells compared to WT (**Fig 4.13**). The same result of elevation levels of γH2A.X was also observed in 46BR.1G1 *LIG1* mutant human fibroblasts (Soza et al., 2009). In summary, the data in this chapter provide the first evidence that the mammalian replicative DNA ligase may coordinate events in chromatin maturation and DNA methylation.

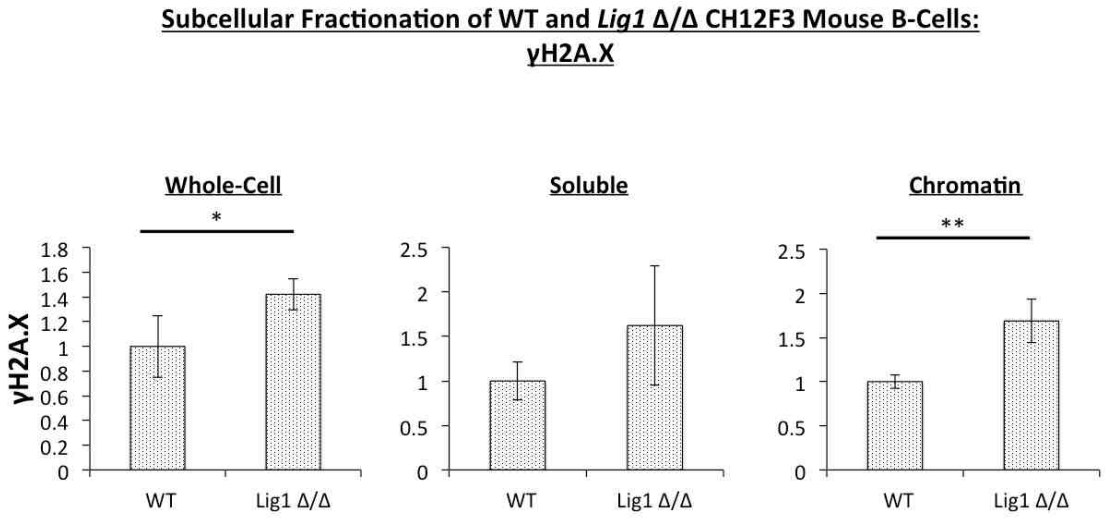

Figure 4.13. Analysis of γH2A.X levels in in subcellular fractions of WT and *Lig1* Δ/Δ mouse B-cells. Four independent WT and *Lig1* Δ/Δ cell populations were processed for whole-cell lysates (left panel), soluble (middle panel), and chromatin (right panel) fractions and assayed for γH2A.X levels by western blot analysis. Signals in whole-cell lysates and soluble fractions were normalized to GAPDH, and signals in chromatin fractions were normalized to H4. The signals were further normalized to the signals in WT cells, which was set as 1. Error bars ± S.D. Statistical difference between WT and *Lig1* Δ/Δ was assessed by Student's *t*-test. * = $p<0.05$ ** = $p<0.01$ *** = $p<0.001$. See Appendix B for individual blots.

Chapter 5

Summary, Conclusions, and Future Directions

5.1 Summary and Conclusions

Specific Aim 1

In Specific Aim 1 (**Chapter 2**), I addressed the hypothesis that the activity of the SWI/SNF ATP-dependent nucleosome remodeler at DNA DSBs promotes HR-repair by facilitating DNA end resection and repair factor recruitment. I built upon previous data demonstrating that SWI/SNF is essential for HR repair of DNA DSBs in budding yeast, where it plays a critical but previously undefined early role in the repair process (Chai, 2005). By performing quantitative PCR analysis of DNA content next to a defined, site-specific DSB at the yeast mating-type (*MAT*) locus, I characterized a novel role for SWI/SNF in promoting the initiation of DNA end resection during DSB repair. I demonstrated that *snf5*Δ mutants have a delay of approximately 1.3 hr in the initiation of DNA end resection after *MAT* DSB formation; however, once resection initiated in *snf5*Δ mutants, it proceeded with WT kinetics. This phenotype is opposite to the recently discovered role for the Fun30 ATP-dependent nucleosome remodeler in promoting long-range resection. In *fun30*Δ mutants, resection initiates in a timely manner but proceeds slowly due to a failure to evict the yeast 53BP1 ortholog Rad9 from chromatin (Chen et al., 2013b; Costelloe et al., 2013; Eapen et al., 2012). My characterization of the role of SWI/SNF in DNA end resection identifies at least one of the chromatin regulators that help the DNA end resection machinery initiate the processing of DNA that is tightly wrapped around nucleosomes.

To address the role of SWI/SNF in repair factor recruitment, I employed chromatin immunoprecipitation (ChIP) to quantitatively assess the recruitment of HR and NHEJ repair factors to the *MAT* DSB at time points after DSB induction. I found that approximately 4.5x less MRX was recruited to the *MAT* DSB in *snf5*Δ cells, whereas the association of KU with the *MAT* DSB was increased and stabilized over time. Intriguingly, previous data had demonstrated that NHEJ, as measured by a plasmid end-joining assay, was intact in *snf5*Δ and *snf2*Δ cells (Chai, 2005), even though MRX is a critical NHEJ factor in yeast (Iwasaki et al., 2016). This led to the model that the pool of MRX that is recruited to a DSB in *snf5*Δ cells may be active only in NHEJ.

To investigate the model that the pool of MRX recruited to the *MAT* DSB in *snf5*Δ cells does not participate in HR, I tested the published roles of MRX in DSB repair by HR, which include evicting KU from DSB ends (Wu et al., 2008), initiating DNA end resection (Garcia et al., 2012), activating the DNA damage response (DDR) (Oh et al., 2016), and recruiting long-range resection factors (Shim et al., 2010). First, I found by utilizing a ChIP assay that KU was stabilized on DNA ends in *snf5*Δ cells, indicating a lack of eviction. Second, as mentioned above, I found that the initiation of DNA end resection in *snf5*Δ cells was significantly delayed. Third, I observed that DDR activation after DSB induction, as measured by Western blot analysis of Rad53 phosphorylation, was severely impaired in *snf5*Δ cells. Fourth, I observed using ChIP that the recruitment of the long-range resection nucleases Exo1 and Dna2 to the *MAT* DSB was significantly decreased in *snf5*Δ cells. Together, these data demonstrated that all of the known roles of MRX in HR repair of DSBs are compromised in the absence of functioning SWI/SNF,

supporting a model in which SWI/SNF orchestrates the recruitment or stabilization of an HR-active pool of MRX to the *MAT* DSB.

To determine if the nucleosome eviction capability of SWI/SNF participates in its role at DNA DSBs, I measured the eviction of histone H2B adjacent to the *MAT* DSB over time by ChIP. In this assay, I found that nucleosome eviction was delayed in *snf5*Δ cells. Intriguingly, by comparing H2B eviction with experimentally matched resection values obtained by qPCR, I observed that nucleosome eviction appeared to briefly precede resection in WT cells, whereas it is essentially concurrent with resection in *snf5*Δ cells. These data suggested that SWI/SNF acts to increase the efficiency of nucleosome eviction at a *MAT* DSB, an action that may facilitate its role in promoting the recruitment or stabilization of an HR-active pool of MRX at DSBs.

From the above Specific Aim 1 data, I conclude that SWI/SNF orchestrates the recruitment of an HR-active pool of MRX to DNA DSBs in yeast. I propose that the activity of SWI/SNF at a DSB facilitates the timely removal of nucleosomes in the vicinity of the break and thereby promotes the efficient initiation of both initial and long-range DNA end resection. These findings are incorporated into a revised model of chromatin remodeling at a DNA DSB in yeast in **Fig 5.1.**

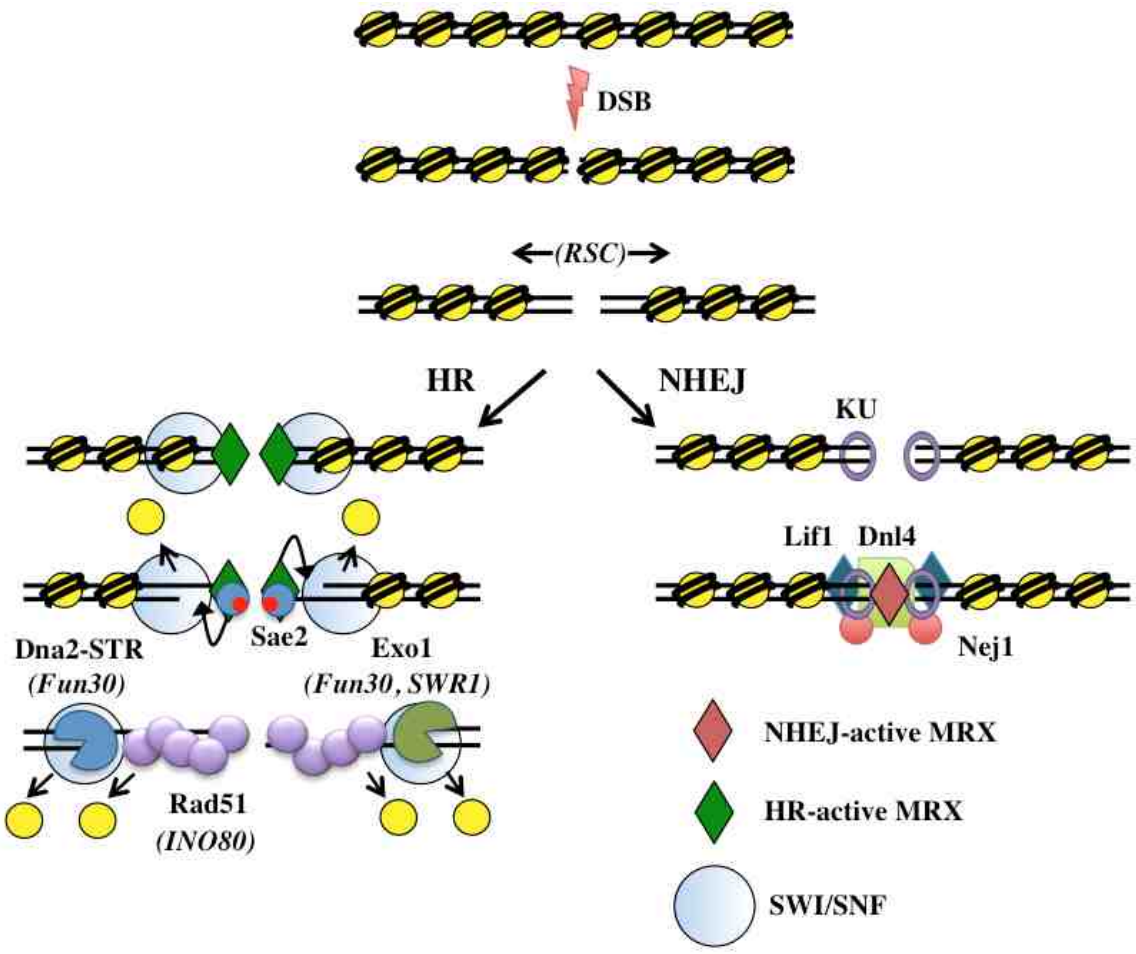

Figure 5.1. Revised model for chromatin remodeling during DNA double-strand break repair in yeast. Data from this dissertation suggest that the SWI/SNF complex orchestrates the recruitment or stabilization of an HR-active pool of MRX (green) at a DSB. The HR-active MRX is able to efficiently initiate the process of DNA end resection in conjunction with Sae2 and recruit Exo1 and Dna2-STR for long-range resection. The role of SWI/SNF in this process may be mediated by its activity in nucleosome eviction. In the absence of SWI/SNF, the end joining complex consisting of KU, Dnl4-Lif1, and Nej1 recruits an NHEJ-active pool (red) of MRX that bridges ends and facilitates intermolecular ligation. See Chapter 5.2 for a discussion of the roles of the various remodelers in DSB repair.

Specific Aim 2

In Specific Aim 2 (**Chapter 4**), I addressed the hypothesis that ligation of Okazaki fragments by DNA Ligase I represents a key regulatory step linking lagging-strand DNA synthesis and chromatin reassembly and maturation on nascent DNA in mammalian cells. I built upon previous data demonstrating that the sites of Okazaki fragment joining correspond to the dyad axis of nucleosomes in the yeast genome (Smith and Whitehouse, 2013), and that the ligation of Okazaki fragments contributes to PCNA unloading from yeast DNA during replication, a process important for genome stability (Kubota et al., 2015). Therefore, Okazaki fragment ligation in yeast appears to be a key step that regulates nucleosome positioning and PCNA recycling during replication. Alternatively, the assembly of nucleosomes on newly synthesized DNA may determine the site of Okazaki fragment joining.

To determine the roles of the mammalian replicative ligase DNA Ligase I in chromatin assembly and maturation, I employed the recently developed isolation of proteins on nascent DNA (iPOND) technique and its derivative, accelerated native iPOND (aniPOND) in both human and mouse cell models of Lig1 deficiency. As the aniPOND technique is reported to more efficiently capture proteins associated with nascent DNA (Leung et al., 2013), in particular large chromatin modifying complexes that may not be decrosslinked efficiently in the formaldehyde-based iPOND technique, I utilized aniPOND as the primary method of analysis in Aim 2.

I found that the published aniPOND technique suffered from poor protein recovery and low signal to noise. Therefore, I optimized aniPOND by sequentially

troubleshooting the steps of the published protocol, and identified multiple key optimizations that eliminated background and greatly increased the signal (**Chapter 3**). The optimized aniPOND protocol (**Appendix A**) efficiently captures histone proteins, and demonstrates improved capture of proteins associated with newly synthesized DNA relative to the iPOND technique, with one exception - formaldehyde-based iPOND is required to capture transient interactions (such as by Lig1) that are lost during processing in the native aniPOND protocol.

I first addressed the role of mammalian Lig1 in the unloading of PCNA and the assembly of new histones on newly synthesized DNA. I found using iPOND and aniPOND techniques in both human and mouse cell models of Lig1 deficiency that Lig1 does not coordinate the unloading of PCNA from replicating DNA. Additionally, I found that histone H4 is deposited with similar kinetics in both Lig1 proficient and deficient cells. These data indicated that Lig1 does not coordinate PCNA unloading and nucleosome deposition in mammalian cells or that there is a functionally redundant mechanism.

I next addressed the role of Lig1 in chromatin maturation. To this end, I monitored the removal of the H4K5ac mark that labels newly synthesized H4 incorporated into chromatin on daughter DNA strands, and found a potential impairment in removal of this histone modification in Lig1 deficient human and mouse cells. However, the effect of Lig1 deficiency on H4K5ac removal was modest and the result will need to be validated with biological replicates. In contrast, I observed a profound effect of Lig1 deficiency on the deposition of H1 onto newly synthesized DNA. In *Lig1* Δ/Δ mouse B-cells, no H1 signal above background was observed on newly synthesized

DNA by the aniPOND technique, whereas robust deposition H1 deposition was observed in WT mouse B-cells. These results suggested that replication-dependent H1 deposition might be impaired in the absence of Lig1.

I followed up these results by examining subcellular fractions of WT and *Lig1* Δ/Δ B-cells to assess for global alterations in proteins. My results demonstrated that there was a statistically significant decrease in total H1 on bulk chromatin in *Lig1* Δ/Δ cells. Interestingly, the occupancy of the replication-independent H1.0 isoform was increased on chromatin in *Lig1* Δ/Δ cells, suggesting that Lig1 may coordinate the deposition of replication-dependent H1 isoforms, and that, in the absence of Lig1 activity, the replication-independent H1.0 variant occupies the linker region between nucleosomes. As replication-dependent histone H1 isoforms H1.1-H1.5 (with the exception of H1.3) have been demonstrated to physically interact with both the maintenance and *de novo* DNA methyltransferases DNMT1 and DNMT3A/3B, respectively (Yang et al., 2013), I next assessed the occupancy of DNMT1 and its functional binding partners UHRF1 and G9A in fractions from WT and *Lig1* Δ/Δ B-cells (see **Fig 4.2**). All three of these factors showed reduced levels in different subcellular fractions of *Lig1* Δ/Δ B-cells, though their occupancy on chromatin was not altered. As UHRF1 coordinates the actions of DNMT1 with replicating DNA (Liu et al., 2013), I monitored the association of UHRF1 with newly synthesized DNA by aniPOND, and observed a kinetic delay in UHRF1 recruitment in *Lig1* Δ/Δ cells. While these results require replication and validation by alternate experimental approaches, they nonetheless provide the first evidence that mammalian Lig1 coordinates key events in chromatin maturation after replication, including the deposition of histone H1 and the recruitment of DNA methylation factors.

From the above Specific Aim 2 data, I conclude that mammalian Lig1 is not required for efficient deposition of nucleosomes or the removal of PCNA from replicating DNA. However, Lig1 may coordinate the replication-coupled deposition of histone H1 onto newly synthesized DNA, and facilitate the recruitment of DNA methylation machinery. These findings are incorporated into a revised model of chromatin deposition and maturation presented in **Fig 5.2.**

5.2 Future Directions

Chromatin remodeling during DNA DSB repair

The novel roles that I have identified for the SWI/SNF complex in this dissertation address multiple gaps in the literature. The role of SWI/SNF in facilitating timely DNA end resection may explain the previously observed reduction in single-strand annealing (SSA) in *snf5*Δ and *snf2*Δ cells (Chai, 2005), as SSA is a long-range resection based process (Bhargava et al., 2016). Secondly, it has been suggested that either there are two pools of MRX that function in different DSB repair pathways or two different modes of the recruitment MRX to DSBs lead to its distinct and contradictory roles in HR versus NHEJ (Emerson and Bertuch, 2016; Wu et al., 2008; Zhang et al., 2007). The data presented in this dissertation demonstrating that the roles of MRX in HR are compromised in *snf5*Δ cells supports the model that SWI/SNF orchestrates the recruitment or stabilization of an HR-active pool of MRX, especially since NHEJ is unaffected by the loss of SWI/SNF (Chai, 2005). However, while this study provides information on important gaps in the literature, it also raises more questions for future research to address.

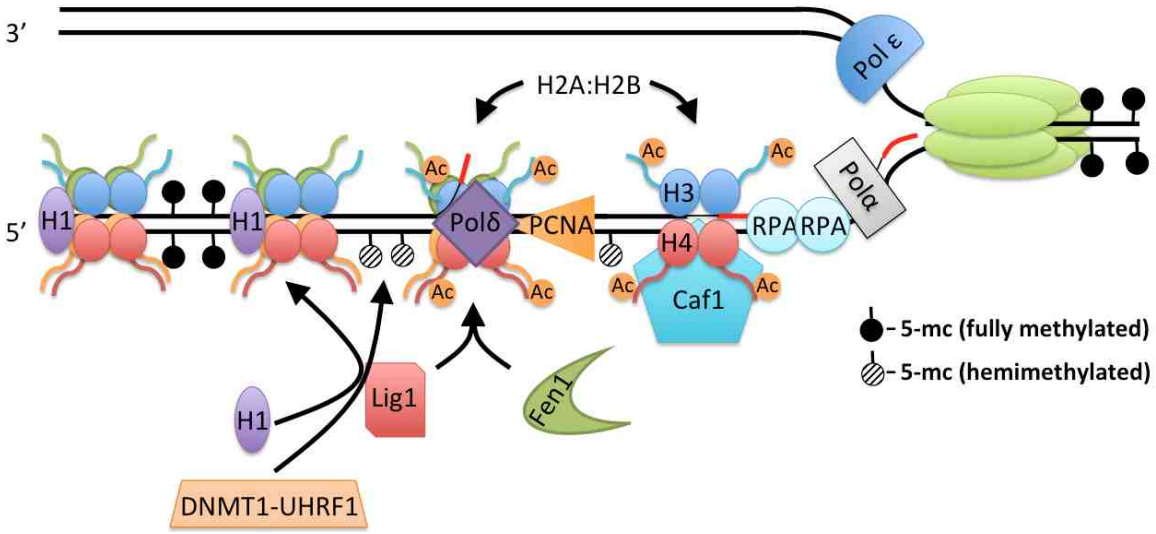

Figure 5.2. Revised model for chromatin assembly/maturation and DNA methylation on the lagging-strand. Data from this dissertation suggest that Lig1 coordinates the replication-coupled deposition of histone H1 on newly assembled chromatin. Additionally, preliminary data suggest that Lig1 coordinates the timely recruitment of DNMT1-UHRF1, which regulates maintenance methylation of hemimethylated CpG sites on daughter strands {Hermann:2004jb}. Notably, data from this dissertation strongly suggest that PCNA unloading and H4 deposition occur independently of Lig1 in mammalian cells.

The first question is the additional roles of SWI/SNF in HR. A delay in resection does not explain the complete absence of gene conversion observed in *snf5*Δ mutants (Chai, 2005). Interestingly, even though my data demonstrate that both RPA and Rad51 are efficiently recruited (after a delay) many kb away from the DSB, published data havedemonstrated a complete lack of strand invasion in *snf5*Δ and *snf2*Δ mutants (Chai, 2005). Thus, SWI/SNF must mediate an additional role in either homology search or strand invasion. One possibility is that SWI/SNF acts to remodel chromatin on the donor strand so that synapsis can be successfully achieved. To test this, nucleosome occupancy at the donor sequence could be monitored in WT, *snf5*Δ, and strains expressing an ATPase dead mutant of SWI/SNF after *MAT* DSB induction in a donor-containing strain. The ATPase dead SWI/SNF mutant would also help to separate the presence of the SWI/SNF complex from its enzymatic activity, as it is possible that SWI/SNF could act as a binding platform for other repair factors that facilitate strand invasion.

A second intriguing question is the identity of factors that evict nucleosomes from DSBs. My data demonstrated that nucleosome eviction is delayed in *snf5*Δ in a manner that parallels the delay in resection; however, nucleosome eviction efficiently occurs after the ~1.3hr delay. This question could be addressed by examining the phenotypes of mutants with defects in multiple chromatin remodelers. For example, a highly relevant strain to examine would be a *snf5*Δ*arp8*Δ double mutant in which both the SWI/SNF and INO80 chromatin remodelers are inactivated, as the INO80 complex was also demonstrated to contribute to nucleosome eviction at a *MAT* DSB (Tsukuda et al., 2005). It is important to mention that *in vitro* data suggest that the resection machinery is capable of independently evicting nucleosomes, especially the Sgs1-Dna2 helicase-

nuclease complex (Adkins et al., 2013). Therefore, both chromatin remodelers and resection factors may have redundant roles in nucleosome eviction. An experiment to separate the roles of the resection machinery and chromatin remodelers in the eviction of nucleosomes would be to block DNA end resection by placing an inverted Ty1 transposon repeat element to form a nuclease-resistant secondary structure near the *MAT* DSB (Zhu et al., 2008). Thus, if nucleosome eviction immediately stopped along with the resection machinery at the transposon repeat, then this would suggest that either the DNA end resection machinery evicts nucleosomes or the chromatin remodelers migrate with the resection machinery, as suggested for Fun30 (Chen et al., 2013b). Alternatively, if nucleosome eviction continued to spread along dsDNA after the resection machinery stalled, this would support the model that ATP-dependent nucleosome remodelers evict nucleosomes independently of end resection.

Another incompletely answered question is the teleology behind the recruitment of at least five different ATP-dependent chromatin-remodeling complexes to DSBs (see **Fig 5.1**). A potential explanation may be that certain complexes have specialized roles. The RSC complex is recruited very early after DSB formation and appears to create a chromatin microenvironment conducive to both HR and NHEJ by sliding nucleosomes at the break (Chambers et al., 2012; Kent et al., 2007; Shim et al., 2007). This appears to be a specialized role, as both HR and chromosomal NHEJ are compromised in RSC mutants (Chai, 2005; Shim et al., 2005), implying that the other remodelers cannot fully compensate for the loss of RSC. Additionally, during long-range resection Fun30 has a specialized role in evicting Rad9 from nucleosomes and SWR1 replaces H2A with H2A.Z to facilitate resection by Exo1 (Adkins et al., 2013; Chen et al., 2013b). In

contrast, the Ino80 and SWI/SNF complexes are now both demonstrated to influence nucleosome eviction around DSBs (Tsukuda et al., 2005); however, nucleosome eviction eventually occurs in mutants of both complexes (Tsukuda et al., 2005). These data suggest the possibility that SWI/SNF and INO80 have redundant roles in nucleosome eviction. The different phenotypes of SWI/SNF and INO80 mutants, such as the lack of a DNA resection defect in a *arp8*Δ mutant (Tsukuda et al., 2005), indicates that they also have unique roles. Future experiments to further define the contributions of the INO80 and SWI/SNF complexes to DSB repair will provide insights into the degree of their functional overlap in DSB repair and the specialized roles of each.

Roles of Lig1 and Lig3 in chromatin maturation and DNA methylation

Both PCNA unloading and H4 deposition on newly synthesized DNA were unaffected in human and mouse cell models of Lig1 deficiency as measured by iPOND and optimized aniPOND. This was somewhat surprising considering the connections between nucleosome positioning and PCNA unloading with Okazaki fragment ligation by the replicative ligase in yeast (Kubota et al., 2015; Smith and Whitehouse, 2013). Since Lig3 can compensate for the loss of Lig1 in both chicken DT40 cells and mouse embryonic fibroblasts, this discrepancy may be due to the backup role of Lig3 in DNA replication in higher eukaryotes (Arakawa et al., 2012; Arakawa and Iliakis, 2015; Bentley et al., 1996; 2002). Interestingly, even though chicken and mouse cells deficient for Lig1 are viable, DNA ligase I deficiency does result in impaired Okazaki fragment processing and ligation (Arakawa et al., 2012; Bentley et al., 2002; Levin et al., 2000), indicating that Lig3 does not fully compensate for Lig1.

Although PCNA unloading was not dependent on Lig1, an unanswered question is whether PCNA unloading is coupled to ligation itself in mammalian cells as it is in yeast. An experiment to test this question would be to briefly treat Lig1 deficient cells such as *Lig1* Δ/Δ MEFs or mouse B-cells with a chemical inhibitor of Lig3 and test whether PCNA unloading is affected using iPOND/optimized aniPOND approaches (Chen et al., 2008; Zhong et al., 2008). Since the accumulation of unligated Okazaki fragments could confound results by stopping DNA replication (as measured by DNA fiber analysis or BrdU incorporation), it may be necessary to pretrea the cells with checkpoint kinase (ATM/ATR) inhibitors to allow the replication fork to continue (Szyjka et al., 2008; Willis and Rhind, 2009). If PCNA accumulates and fails to turn over on newly synthesized DNA in *Lig1* Δ/Δ cells treated with a Lig3 inhibitor in the context of equal replication fork rates, then this would suggest that ligation itself is a conserved signal for PCNA unloading. Alternatively, higher eukaryotes may have additional regulatory mechanisms to ensure PCNA recycling at replication forks in the absence of Okazaki fragment ligation. Another approach would be to use a Lig1 inhibitor in cells deficient for either Xrcc1 or Lig3.

While the deposition of histone H4 appears unaffected by Lig1 deficiency in human and mouse cells, my data demonstrated that the deposition of linker histone H1 appears to depend upon Lig1, suggesting that chromatin maturation is coupled to Lig1 or ligation. My preliminary data in mouse *Lig1*Δ/Δ B-cells demonstrated a striking reduction in H1 deposition onto newly synthesized DNA that was corroborated by the reduction in H1 occupancy on bulk chromatin. These preliminary data lead to many questions.

The first and foremost question is the strength of these observations. The limited number of aniPOND experiments (n=2) demonstrating the H1 deposition defect and the utilization of a single Lig1 deficient cell line limit the scope and power of my observations. This potential significant link between Lig1 and H1 deposition could be strengthened in the following ways. First, enough independent biological replicates of the aniPOND experiment need to be performed to allow statistical comparisons between WT and Lig1 deficient cells to be made. Second, the optimized aniPOND and subcellular fractionation experiments exploring the defect in H1 deposition on newly synthesized DNA and bulk chromatin should be repeated in other models of Lig1 deficiency, including *Lig1* knockout MEFs (Bentley et al., 1996), 46BR.1G1 *LIG1* mutant human fibroblasts (Barnes et al., 1992), and mouse and human cells treated with chemical inhibitors of Lig1 (Chen et al., 2008; Zhong et al., 2008). A critical control for *Lig1* Δ/Δ mouse cell experiments will be wild type *Lig1*-complemented derivatives to eliminate off-target effects as a consequence of constructing the Lig1 deficient strain. An additional control will be the measurement of mRNA levels of the different H1 isoforms to rule out deposition defects due to changes in expression of H1 encoding genes.

If the defect in H1 deposition is recapitulated across different models of Lig1 deficiency, then subsequent experiments should aim to determine the mechanism underlying this phenotype. For example, complementation of *Lig1* Δ/Δ cell lines with mutant versions of *Lig1* will help to determine protein domains and specific amino acids necessary for this role. Mass spectrometry of Lig1 isolated from replicating cell chromatin may help to identify the histone chaperone involved in Lig1-mediated H1 deposition. The relevance of any detected interactions would need to be verified by either

Lig1 or H1 chaperone mutants that abolish the Lig1-chaperone interaction. Unbiased proteomic approaches such as SILAC iPOND/optimized aniPOND-mass spectrometry will also assist in the identification of H1 isoforms that are deposited in a Lig1-mediated manner, as the immuno-reagents available to identify specific H1 isoforms are limited (Harshman et al., 2013). If complementation of *Lig1* Δ/Δ cells with *LIG1* restores the WT distribution of histone H1 isoforms, then it needs to be determined whether *LIG1* influences either the transcription of the individual isoforms or their stability. Strategies to address this include next generation sequencing (NGS) of WT and *Lig1* Δ/Δ cells to compare H1 isoform gene expression (or WT and Lig1-inhibitor treated cells to observe the effect of acute Lig1 deficiency on transcription), and the monitoring of H1 isoform protein stability by using cyclohexamide treatment in WT and *Lig1*Δ/Δ cells, or Lig1-inhibitor treated cells.

My data also suggested a possible role for Lig1 in recruiting UHRF1, a critical component of the maintenance DNA methylation machinery (Bostick et al., 2007; Liu et al., 2013; Pacaud et al., 2014), to newly synthesized DNA as measured by aniPOND. Additionally, I observed significant reductions in the levels of DNA methylation factors (DNMT1, UHRF1, and G9A) in whole-cell and soluble (but not chromatin) fractions of *Lig1* Δ/Δ B-cells. Similar to the strategy for exploring the H1 deposition defect, multiple independent biological repeats would first need to be performed and different models of Lig1 deficiency explored to strengthen and validate these initial results connecting Lig1 to the recruitment of DNA methylation factors. If the preliminary results presented in this dissertation are validated, the global levels of 5-methylcytosine in Lig1 proficient versus deficient cells should then be assayed to determine if the interaction of Lig1 and

methylation machinery factors impacts global methylation (Kurdyukov and Bullock, 2016). Another strategy to monitor replication-coupled DNA methylation would be to purify the DNA from aniPOND samples and measure the 5-mc content at time points after replication. It is possible that maintenance methylation would be delayed on newly synthesized DNA in the absence of Lig1; however, global DNA methylation levels may ultimately be maintained post replication methylation because of the affinity of DNMT1 for hemimethylated DNA (Hermann et al., 2004). Alternatively, site-specific DNA methylation may be perturbed in the absence of Lig1, a possibility that could be addressed by bisulfite sequencing of Lig1 proficient and deficient cell genomes (Li and Tollefsbol, 2011).

Identifying novel links between genetic and epigenetic stability with iPOND and optimized aniPOND

The optimized aniPOND protocol presented in this dissertation (**Chapter 3** and **Appendix A**) holds great promise to help identify new links between genetic and epigenetic stability. While the original iPOND technique and a related method called nascent chromatin capture (NCC) are currently being utilized to probe repertoires of proteins and histone PTMs associated with newly synthesized DNA, both of these techniques have the same disadvantage of relying upon stringent formaldehyde fixation during sample preparation (Alabert et al., 2014; Dungrawala et al., 2015). As I demonstrated in **Fig 3.9**, thermal decrosslinking of formaldehyde fixed iPOND samples is an inefficient process that limits the recovery of large proteins such as DNMT1.

Therefore, optimized aniPOND-mass spectrometry experiments may help to elucidate the chromatin modifiers that cells rely upon during normal and stressed DNA replication.

The horizons of iPOND and aniPOND experiments need not be limited to S-phase DNA replication. iPOND/aniPOND-MS experiments in G1-blocked cells exposed to DNA damaging agents that generate lesions requiring nucleotide excision repair (NER) or long-patch base excision repair (BER) could potentially identify novel NER and BER factors and allow the study of chromatin regulation during these repair processes. Similarly, iPOND/aniPOND-MS could be adapted to capture proteins associated with DNA replication in other repair events such as HR. In theory, the iPOND technique could even be modified to capture RNAs associated with nascent DNA, thereby opening new avenues to study the role of regulatory RNAs in DNA replication and repair. The iPOND and optimized aniPOND techniques hold great promise for helping to unlock fundamental processes that link genome and epigenome stability under both physiological and disease states.

5.3 Narrative Summary

In this dissertation, I have addressed two hypotheses in two independent Specific Aims regarding key processes that maintain genetic and epigenetic stability during DNA DSB repair and DNA replication in eukaryotes. Broadly speaking, Specific Aim 1 examined the role of a conserved and clinically relevant ATP-dependent nucleosome remodeler in the disruption of nucleosomes at a DSB in budding yeast and further identified novel roles for this remodeler in facilitating the repair of these dangerous lesions by the high fidelity HR pathway. Specific Aim 2 examined novel mechanisms

that help to re-establish chromatin after its complete disruption during DNA replication, addressing a poorly understood but fundamental process that helps cells maintain their transcriptional programs, chromatin packaging, and identity. Finally, I optimized a powerful, recently developed technique that promises to herald new breakthroughs in both the discovery and understanding of processes that link genetic and epigenetic stability.

Appendix A

Protocol for Optimized aniPOND in Suspension Cells

Below is the optimized protocol for accelerated native isolation of proteins on nascent DNA (aniPOND) using suspension cells that is based upon the published aniPOND protocol (Leung et al., 2013) and incorporates the modifications described above. The protocol is designed for 8 x 10^7 suspension cells.

1. Suspension cell growth to aniPOND experimental numbers

1.1 Equipment

- Cell culture incubator
- Biological safety cabinet
- 250 mL canted neck suspension culture flasks with ventilation cap (USA Sci., cat. no. 5665-8190)
- T175 canted neck flasks with ventilation cap (Sarstedt, cat. no. 83.3912.002)
- T225 ventilation cap flasks (USA Sci., cat. no. CC7682-4822)
- Hemocytometer (Fisher Sci., cat. no. 02-671-10)

1.2 Buffers and Reagents

- Cell culture medium, e.g. RPMI 1640 (Thermo Fisher Sci., cat. no. 11875135) and additives including 10% fetal bovine serum (Sigma-Aldrich, cat. no. F2442) and 55mM (100x) β-mercaptoethanol for tissue culture (Thermo Fisher Sci., cat. no. 21985023).

1.3 Procedure

1. Rapidly thaw a vial of early passage suspension cells, such as CH12F3 mouse B-cell lymphoma cells, in a 37°C water bath and immediately dilute into the appropriate pre-warmed media supplemented with necessary additives such as 10% fetal bovine serum and 55 μM β-mercaptoethanol that are required for optimal growth.
2. Perform routine subculturing in 20 mL of appropriate media in a hydrophobic-coated ventilation cap flask laid flat to increase surface area for gas exchange in a cell culture incubator set to the appropriate temperature and CO_2 (standard settings are 37°C and 5% CO_2 content).
3. Establish a growth curve for your cell line(s), such as that in **Fig 3.2A**, by periodic counting with a hemocytometer. Calculate the doubling time (T_d) of the cells in exponential-phase growth and ensure that the calculated T_d matches the reported T_d in the literature.
4. Passage cells by diluting into fresh medium before overgrowth is reached, preferably in mid exponential phase. Keep careful track of the passage number of the cells and do not over passage. For many cell lines, this means using before ~20 passages after thawing.
5. Once optimal growth conditions are established, dilute cells for aniPOND using the T_d of the cell line(s) to estimate the number of cells necessary to obtain 8 x 10^7 cells in ~48 hr. For example, if the T_d = 12hr and the cells are desired to be ready in 48 hr, 5 x 10^6 cells would be diluted into 80 mL of warm media in a T175

canted neck flask. In this manner, 8 x 10^7 cells will be ready in 48 hr at a density of 1 x 10^6/mL, which is mid exponential phase for many cell lines.

6. Count the cells by hemocytometer during the growth phase up to the starting point of the aniPOND protocol to ensure that doubling time is optimal.
7. One day prior to starting the aniPOND protocol, place media for 5-ethynyl-2'-deoxyuridine (EdU) pulse and thymidine chase in the incubator to equilibrate temperature and CO_2 content. For the EdU pulse media, calculate 2 mL/ 80 mL culture (make up 25% extra to account for losses due to evaporation etc.). For the thymidine chase media, calculate 80 mL for each chase sample (make up 10% extra to account for losses due to evaporation etc.).

1.4 Notes

1. It is essential that the cells utilized have an established growth curve in your laboratory and are growing in an optimal manner. Frequent cell counting will allow determination of doubling-times to determine if proliferation is optimal.
2. While the addition of antibiotics to the media may help prevent bacterial contamination, this may also mask underlying contamination. We suggest performing routine subculturing without antibiotics and performing monthly PCR-based *Mycoplasma* testing.
3. Multiple routine passages may be performed in the same flask to reduce costs. This does, however, increase the risk of contamination over time. We suggest changing routine subculture flasks on a weekly basis.

2. EdU pulse, thymidine chase, and click reaction

2.1 Equipment

- Cell culture incubator
- Biological safety cabinet
- Swinging-bucket tabletop centrifuge for 15 and 50 mL tubes
- Rotating platform for 1.5 mL and 15 mL tubes at 4°C (in a cold room or refrigerator)

2.2 Buffers and Reagents

- Flasks with 8 x 10^7 suspension cells in mid exponential growth phase in 80 mL of media
- Flask with pre-equilibrated media for EdU pulse (2 mL/sample, plus some extra)
- Flask(s) with pre-equilibrated media for thymidine chase (80 mL/chase sample, plus some extra)
- Dimethyl sulfoxide (DMSO, EMDMillipore cat. no. MX1458-6)
- EdU (Sigma Aldrich, cat. no. T511285). Dissolve in DMSO to a final concentration of 10 mM. Aliquot and store at -20°C protected from light for up to one year. Thaw at 37°C immediately before use.
- Thymidine (Sigma-Aldrich, cat. no. T9250). Dissolve in PBS to a final concentration of 100 mM, filter sterilize, aliquot and store at -20°C for up to three years. Thaw at 37°C immediately before use.

- Biotin-PEG3-azide (Sigma-Aldrich, cat. no. 762024). Dissolve in DMSO to a final concentration of 50 mM. Aliquot and store at -20°C protected from light for up to one year. Thaw at 37°C immediately before use.
- NaCl. A 5 M stock in double-distilled, filter sterilized and stored at 4°C.
- HEPES. A 500 mM stock in double-distilled water, adjusted to pH 7.2 with KOH, filter sterilized, and stored at 4°C.
- $MgCl_2$. A 300 mM stock in double-distilled water, filter sterilized and stored at 4°C.
- Sucrose. A 1.2 M stock in double-distilled water, filter sterilized and stored at 4°C.
- IGEPAL CA630 (Sigma-Aldrich, cat. no. I8896). A 10% v/v stock in double-distilled water, filter sterilized and stored at 4°C for a few months.
- Pre-chilled nucleus extraction buffer (NEB; 20 mM HEPES-KOH pH 7.2, 50 mM NaCl, 3 mM $MgCl_2$, 300 mM sucrose, 0.5% IGEPAL CA630) freshly prepared.
- Pre-chilled phosphate-buffered saline (PBS; 137 mM NaCl, 2.68 mM KCl, 1.47 mM KH_2PO_4, 9.55 mM Na_2HPO_4, pH 7.45). A 10x autoclaved stock solution can be prepared and stored at room temperature (RT).
- Copper (II) sulfate pentahydrate (Sigma-Aldrich, cat. no. 203165). Dissolve to a final concentration of 100 mM in double-distilled H_2O and store at RT for up to three months.
- (+)-Sodium L-ascorbate (Sigma-Aldrich, cat. no. A4034). Dissolve to a final concentration of 100 mM in double-distilled H_2O and place on ice immediately before use in click reaction setup.

- Click/no-click control (NCC) reaction mixture. To prepare 10 mL for one sample, add *in order*: 8.8 mL ice-cold PBS, 5 µL of 50 mM biotin-PEG3-aizde (or 5 µL of DMSO for NCC), 1 mL of 100 mM (+)-sodium L-ascorbate, and 200 µL of 100 mM copper (II) sulfate. Scale up the quantity of reaction mixture for the number of samples, and always prepare fresh click reaction/NCC mixture.

2.3 Procedure

1. Prepare the overnight pre-equilibrated media for EdU pulse by adding EdU to a final concentration of 410 µM.
2. Prepare the overnight pre-equilibrated media for thymidine chase by adding thymidine to a final concentration of 10 µM.
3. To begin pulse, add 2 mL of the 410 µM EdU in media to the 80 mL of cells in the first flask (final concentration, 10 µM EdU), gently mix with 5-10 rotations, start a timer counting up for time of pulse, and set the flask in the 37°C incubator standing upright to reduce surface area for cells to stick. It is imperative that every sample be treated in the same manner (see *Notes* below).
4. After 7.5 min has expired on timer for pulse, remove pulse flask(s) from the incubator to the biological safety cabinet.
5. Pour cells from pulse flask(s) into 2 x 50 mL labeled tubes each and set in swinging-bucket tabletop centrifuge.
6. After 9 min has expired on timer for pulse, centrifuge at 200 x *g* for 4 min at RT.

For chase samples <u>only</u> during centrifugation:

- Pour ~35 mL of room temperature PBS into the flask(s). Rotate the PBS around and aspirate off to wash out EdU-containing pulse media.
- Add 55 mL of warm thymidine media to the flask(s).

7. After centrifugation has finished (~13 min on pulse timer), gently remove tubes to biological safety cabinet and aspirate pulse medium without disturbing pellets.
8. At exactly 15 min on the pulse timer, either completely resuspend the cell pellet in 25 mL of thymidine chase media and proceed to step 9 for chase samples, or resuspend in 10 mL of ice-cold nucleus extraction buffer (NEB) for pulse or no-click control (NCC) samples and proceed to step 15. Combine the two ½ pellets from the two 50 mL tubes for each sample in the same 25 mL of chase media or 10 mL NEB.
9. CHASE SAMPLES: Pipette the cells in 25 mL of thymidine media into the PBS-washed flasks already containing 55 mM of warm chase media for a final chase volume of 80 mL. Start a timer counting up for chase, and remove to 37°C incubator. Set the flasks standing upright in the incubator to reduce surface area for cells to adhere to.
10. 7.5 min before the desired chase time (for example, at minute 22.5 of a desired 30-minute chase sample), remove chase flask(s) from the incubator to the biological safety cabinet.
11. Pour cells from pulse flask(s) into 2 x 50 mL labeled tubes and set in swinging-bucket tabletop centrifuge.
12. 6 min before the desired chase time, centrifuge at 200 x *g* for 4 min at RT.

13. After spin has finished (~2 min before desired chase time), gently remove tubes to biological safety cabinet and aspirate chase medium without disturbing pellets.
14. When the desired chase time has arrived, immediately resuspend the pellet in 10 mL of ice-cold NEB. Combine the two ½ pellets from the two 50 mL tubes for each sample in the same 10 mL of ice-cold NEB.
15. ALL SAMPLES: Rotate in NEB at 4°C for 15 minutes to obtain nuclei.
16. Centrifuge the nuclei for 10 min at 500 x *g* at 4°C to pellet.
    - Optional: After centrifugation, remove 1 mL of solubilized proteins above the nuclei to a 1.5 mL tube for protein measurement later. The amount of soluble protein is proportional to the total starting amount of cells.
17. Aspirate the NEB and resuspend the nuclei in 10 mL ice-cold PBS with a serological pipette to wash.
18. Centrifuge the nuclei for 10 min at 500 x *g* at 4°C to pellet.
19. During the centrifugation, prepare the click reaction/NCC mixture as described in *Buffers and Reagents*.
20. Aspirate the PBS wash and completely resuspend nuclei in 10mL of click/NCC reaction mixture.
21. Rotate samples at 4°C for 60 minutes.
22. Centrifuge the nuclei for 10 min at 500 x *g* at 4°C to pellet.
23. Aspirate the click/NCC reaction mixture and resuspend the nuclei in 10 mL ice-cold PBS with a serological pipette to wash.
24. Centrifuge the nuclei for 10 min at 500 x *g* at 4°C to pellet.

25. Either proceed to **5.3** immediately, or freeze nuclei on dry ice and store at -80°C for up to 2 weeks before proceeding.

2.4 Notes

1. Consistency between aniPOND samples is critical. Large variations in the time of EdU pulse or thymidine chase between samples will confound results. We have established a set of conventions that we adhere to for every aniPOND sample:
    I. Pulses are designed so that the *total time* in EdU is 15 min. This includes time during spins and after pelleting before resuspension in thymidine chase media or NEB.
    II. Centrifugations are performed at 200 x *g* for 4 min at RT with moderate acceleration and deceleration.
    III. If performing two samples simultaneously (for example, a treated and untreated), leave exactly one minute between samples and maintain this separation and the order of sample processing until nuclei harvesting. This allows time for individual sample processing so that total time in EdU or thymidine media for each individual sample remains constant.
    IV. If staggering multiple time points (for example, a 30 minute chase with a 60 minute chase), allot one minute of extra time to pour samples into 50 mL tubes before starting centrifugation (step 10).
    V. Record the total time of each sample in EdU and thymidine media (for chase samples).

2. Nuclei should largely remain individual and not form clumps during the nucleus extraction, PBS washing, and click reaction steps. If macroscopically visible clumps of nuclei form, ensure that the $MgCl_2$ concentration of the NEB is correct, the PBS formulation contains at least 130 mM NaCl, and that nuclei spins are being performed at 500 x *g*.
3. The nuclei may change color slightly after click reaction (from white to slightly yellow/green). Occasionally, a small amount of Cu^{1+} will form a brown precipitate that spins down with the nuclei. This precipitate does not interfere with downstream processing.

3. Solubilization and pulldown of biotin-labeled chromatin

3.1 Equipment

- Rotating platform for 1.5 mL tubes at 4°C
- Refrigerated microcentrifuge for 1.5 mL tubes at 4°C
- Microtip sonicator such as a Branson 250 cell disruptor with double step microtip (Emerson, cat. no. 101-063-196 and VWR 33996-243)
- Spectrophotometer and cuvettes for protein measurements
- Nanodrop spectrophotometer (Thermo Fisher Sci.) for DNA measurements
- DNA purification columns (such as Qiagen, cat. no. 28104)
- Agarose gel electrophoresis system
- UV lamp gel imaging system (such as Bio-Rad, cat. no. 1708195)

3.2 Buffers and Reagents

- Same as in 2.2, plus:
- EDTA. A 500 mM stock in double-distilled water, adjusted to pH 8.0, filter sterilized, and stored at 4°C.
- Tris-HCl pH 6.8 and pH 8.0. A 1M stock in double-distilled water, adjusted to correct pH with HCl, autoclaved, and stored at RT.
- Sodium dodecyl sulfate (SDS). A 10% solution prepared in double-distilled water and stored at RT.
- $CaCl_2$. A 1M stock in double-distilled water prepared and stored at RT.
- Bromophenol blue.
- Bovine serum albumin (BSA).
- Agarose for DNA analysis (such as BioExpress, cat. no. E-3120)
- Ethidium bromide.
- RNAse A (such as Thermo Fisher Sci., cat. no. 12091021).
- Pronase (such as Sigma, cat. no. P6911). A 20 mg/mL stock in double-distilled water prepared and stored at -20°C.
- Buffer B1 (25 mM NaCl, 2 mM EDTA, 50 mM Tris-HCl pH 8.0, 1% IGEPAL CA630). Prepare fresh before use, and add protease inhibitors (such as Sigma-Aldrich, cat. no. P8340).
- High capacity streptavidin agarose (Pierce, cat. no. 20359).
- 2x Laemli buffer (4% SDS, 20% glycerol, 125 mM Tris-HCl pH 6.8, 0.01% bromophenol blue). Before use, add 50 µl of concentrated (14.3 M) β-

mercaptoethanol to 950 µl 2x Laemli buffer (final concentration, 5% v/v β-mercaptoethanol).

- TE buffer (10 mM Tris-HCl pH 8, 1 mM EDTA).
- Protein assay dye reagent (Bio-Rad, cat. no. 500-0006).

3.3 Procedure

1. Resuspend nuclei in 0.5 mL of ice-cold buffer B1 supplemented with protease inhibitors and transfer to a 1.5 mL tube.
2. Rotate at 4°C for 30 minutes.
3. Centrifuge nuclei for 10 min at 500 x *g* at 4°C to pellet.
4. Aspirate supernatant.
5. Resuspend nuclei in 0.5 mL of ice-cold buffer B1 supplemented with protease inhibitors.
6. Rotate at 4°C for 30 minutes.
7. Solubilize chromatin with a microtip sonicator. Keep tubes on ice at all times, and perform 6 rounds of 2 x 10 seconds on, 10 seconds off on output 3 to 4 (~10W output) for a total of 12 10-second bursts. Between rounds, rest tubes on ice for at least one minute.
8. Centrifuge samples for 10 min at 16.1k x *g* at 4°C.
9. Carefully remove the clarified, sonicated chromatin fraction to a new 1.5 mL tube.
10. Measure the volume of sonicated chromatin and bring the volume to 1 mL by adding ice-cold buffer B1 supplemented with protease inhibitors.

11. Gently mix the sonicated chromatin samples and remove 20 µL (2%) to a new 1.5 mL tube as input (INP). Add 20 µL 2x Laemli buffer (with β-mercaptoethanol) to the input sample and store at -20°C until the next day.
12. OPTIONAL: Remove 10 µL (1%) to a new 1.5 mL tube for DNA analysis.

    DNA Analysis Steps:

    I. Add 79 µL of TE buffer and 1 µL of 10-20 mg/mL RNAse A and incubate at 37°C for 30 min to degrade RNA.

    II. Add 10 µL of 20 mg/mL pronase and 1 µL of 1M $CaCl_2$ and incubate at 42°C for 2 hr to digest proteins.

    III. Column purify DNA using a commercial kit.

    IV. Measure DNA quantity with a nanodrop spectrophotometer.

    V. Visualize DNA fragment size distribution by running >500 ng on a 1.3% Agarose/TAE gel, staining with 0.2 µg/mL ethidium bromide, and visualizing with a UV lamp gel imaging system. Compare fragments to an appropriate DNA ladder.
13. Measure the protein content of sonicated chromatin and the optional soluble fraction from **2.3** step 16 by Bradford assay with BSA standards.
14. Prepare streptavidin beads to be added to chromatin samples for pulldown. Each sample requires 100 µL of bead slurry (50% slurry). Remove enough volume of well-mixed beads (plus enough for two extra samples) to a 1.5 mL tube.
15. Mark the level of the beads slurry on the side of the tube.
16. Centrifuge the beads slurry for 2 min at 500 x *g* at 4°C.
17. Let the slurry sit on ice for 2 min to completely settle.

18. Gently remove the supernatant and add at least the same volume as the original beads slurry volume of ice cold buffer B1 to wash (no protease inhibitors necessary). For example, if 600 µL of beads slurry was removed, at least 600 µL of buffer B1 would be added to wash the beads.
19. Repeat steps 16-18 two more times for a total of three beads washes.
20. After the third wash, bring the volume of buffer B1 to the level of the original bead slurry volume as marked.
21. Pipette 100 µL of buffer B1-washed beads (50% slurry) into the sonicated chromatin samples, using cut-tip P200 tips, and mixing the beads well between additions to ensure equal addition to the different samples.
22. Rotate samples with beads overnight at 4°C.

3.4 Notes

1. Sonicator microtips can corrode and pit over time, leading to reduced output. Periodic polishing with metal sandpaper (such as 3M, cat. no. 11694) when corrosion is observed prolongs the life of the microtip before replacement is required.
2. It is recommended to check both protein and DNA recovery in each sample as a control in order to provide a measure of the efficiency of sonication.
3. Solubilized chromatin released by sonication should have a mean distribution of ~150 bp upon DNA analysis. Most of the DNA fragmentation occurs during the click reaction by the actions of Cu^{1+}.

4. Protein elution and quantitative Western analysis

4.1 Equipment

- Same as in 3.1, plus:
- 200 µL tapered gel loading tips (such as USA Sci., cat. no. 1252-0600)
- Low fluorescence background PVDF membrane (such as Bio-Rad, cat. no. 1620261) or nitrocellulose
- Blocking solution for near infrared (NIR) Western blotting (such as Li-Cor, cat. no. 927-50000)
- Odyssey Near-Infrared Imaging System (Li-Cor Biosciences)

4.2 Buffers and Reagents

- Same as in 3.2, plus:
- Tris buffered saline (TBS; 150 mM NaCl, 50 mM Tris-HCl, pH 7.5)
- TBST (TBS supplemented with 0.1% Tween-20)

4.3 Procedure

1. Centrifuge the bead capture samples for 2 min at 500 x *g* at 4°C.
2. Incubate on ice for 2 min to completely settle.
3. Gently aspirate the supernatant to ~ 100 µL above the beads and add 1 mL of buffer B1 (no protease inhibitors necessary).
4. Rotate samples for 5 min at 4°C to wash.
5. Repeat steps 1-4 three more times for a total of four washes.
6. After the final wash, centrifuge the beads capture samples for 2 min at 500 x *g* at 4°C.
7. Incubate on ice for 2 min to completely settle.

8. Gently aspirate the supernatant to ~ 100 µL above the beads, then pull the remainder of the wash from below the beads using 200 µL tapered gel loading tips. Press the tip against the bottom of the tube before pulling up to avoid taking up any beads.
9. Resuspend the washed beads from the capture samples in 100 µL of 2x Laemli buffer (with β-mercaptoethanol) with a cut-tip P200 tip.
10. Thaw INPs on ice.
11. Boil the beads capture (CAP) and INP samples for 15 min. Place safety caps on the tubes to prevent the caps from popping open during boiling.
12. Vortex CAP samples for 3 sec, and set both CAP and INP samples on ice for ~ 1 min to cool to RT.
13. Centrifuge the CAP and INP samples for at least 1 min at 1,500 x *g* at RT.
14. Remove the eluted CAP samples in Laemli buffer from below the beads using 200 µL tapered gel loading tips and transfer to new 1.5 mL tubes.
15. The CAP and INP samples can now either be stored at -20°C or processed for quantitative Western blot analysis immediately. If stored before use, thaw on ice and then briefly boil (2 min), cool on ice, centrifuge, and then proceed.
16. For quantitative Western analysis of the control proteins PCNA and histone H4, freshly prepare a 12% SDS-PAGE gel and perform standard gel electrophoresis. For near-infrared (NIR) detection of proteins, which we have found to be less sensitive than HRP detection, it is useful to load 20 µL of INP sample (1%) and 50 µL of CAP sample (50%).

17. Transfer proteins onto either nitrocellulose or low infrared-background PVDF membrane. Standard PVDF is unsuitable due to variable and potentially high fluorescent background.
18. Block membranes in NIR blocking solution. It is useful to dilute NIR blocking solution 1:3 in TBS, as full strength NIR blocking solutions can reduce antibody binding. Traditional milk-blocking solutions should be avoided as they may increase fluorescent background.
19. After blocking, cut the membrane at the 20 kDa marker. Incubate the >20 kDa membrane segment in Mouse anti-PCNA (Santa Cruz, cat. no. sc-56) diluted 1:200 in TBST and the <20 kDa segment in Mouse anti-H4 (Abcam, cat. no. ab17036) diluted 1:1,000 in TBST. Incubate in primary antibody for 4 hr at RT or overnight at 4°C.
20. Wash the membranes 4 times for 5 min with TBST at RT.
21. Incubate in secondary antibody for 1 hr at RT protected from light. For both primary antibodies, use Goat anti-mouse 680nm (Li-Cor Biosciences, cat. no. 925-68070) diluted 1:5,000 in TBS.
22. Wash the membranes 4 times for 5 min with TBST at RT.
23. Wash the membranes 1 time for 5 min with TBS.
24. Image blots with an Odyssey NIR imaging system using the 680nm channel. Expected Results (see **Fig 8**): PCNA should be present on DNA with a 15 min EdU pulse but should offload after thymidine chase. Histone H4 may be begin to be present with a 15 min EdU pulse, and will increase in signal with thymidine

chase as more histone is deposited post-replication. No-click control (NCC) CAP samples should have little to no signal.

4.4 Notes

1. For NIR Western blotting, great care must be taken when loading molecular weight marker ladders, as the dyes that stain marker proteins can strongly fluoresce in the NIR channels. A useful ladder is all blue pre-stained ladder (Bio-Rad, cat. no. 1610373), which fluoresces strongly in the 680nm channel. Load no more than 2.5 µL.

5. Troubleshooting

Problem	Reason(s) and Solution
Cells are growing poorly (T_d does not match published values)	Suboptimal proliferation may indicate the absence of a required growth factor, incorrect media conditions, suboptimal oxygenation, epigenetic changes from cell mistreatment, or *Mycoplasmsa* or other contamination. Ensure that the correct media and supplements are being used. Thaw a fresh stock from a vial of early passage cells. Grow cells in flasks on their side to increase surface area for gas exchange, and test for *Mycoplasma* contamination. Culturing cells without antibiotics will allow any low-level contamination to become evident.

Inefficient pulldown of control proteins (PCNA, H4) in click reaction samples	Failure at various steps can lead to low signal in click reaction samples. We recommend the following steps to resolve this issue: 1. Failure of click reaction. Any of the components of the click reaction may go off. We suggest ordering new EdU, biotin-PEG3-azide, and sodium ascorbate. To test if Cu^{1+} is being generated in the click reaction, a mock click reaction with purified genomic DNA (use a kit such as Thermo Fisher Sci., cat. no. K1820-01) can be performed and DNA fragmentation can be assessed by agarose gel electrophoresis with ethidium bromide staining. Intact fragmentation excludes the (+)-Sodium L-ascorbate and $CuSO_4$ as the source of the problem. 2. Antibody or Western blotting issues. A robust INP signal should be present for PCNA and H4. A weak INP signal suggests that either the antibody is expired or a step in the Western blotting process has failed, such as the transfer. 3. Failure of chromatin solubilization. To test if chromatin is being solubilized by sonication, compare the PCNA and H4 content of the insoluble pellet to the solubilized chromatin post-centrifugation (see **Fig 3.5B**). If a

	majority of chromatin is being retained in the pellet, consider maintenance of the sonicator by polishing/replacing the microtip. Additionally, ensure that buffer B1 has the proper composition. 4. Failure of beads pulldown or elution. Order new high capacity streptavidin beads and ensure that the SDS elution buffer (Laemli buffer) has correct composition and is supplemented with β-mercaptoethanol before use. 5. Reagent supplier. We have experienced multiple bad batches of click reagents from a single supplier. Consider switching suppliers if pulldown is not restored after performing solution steps 1-4 above.
Weak signal for protein of interest	If performing quantitative NIR fluorescence Western blotting, reduce the stringency of the wash steps and increase the concentration of NIR 2° antibody. Some proteins may require visualization with HRP-conjugated 2° antibody. High sensitivity chemiluminescence substrate (such as Thermo Fisher Sci., cat. no. 34095) development of blots probed with HRP-conjugated 2° antibody will allow detection of low abundance proteins that fall below the threshold of NIR detection. If signal is still not observed, increase the amount of starting material and verify that published iPOND or aniPOND mass spectrometry experiments detect your protein of interest on replicating DNA.

Appendix B

Near-Infrared Western blots of Subcellular Fractions of CH12F3 WT and *Lig1* Δ/Δ Mouse B-Cells

The NIR Western blots presented in this appendix were prepared according to the protocol in **Chapter 4.2** as illustrated in **Fig 4.3**. The Western blots contain samples from four independent passages of WT and *Lig1* Δ/Δ Mouse B-cells that were collected at the same time, treated in the same way, and run on the same freshly poured gels. For comparisons between the whole cell lysate (WCL), soluble, and chromatin fractions, the PVDF membranes that samples were transferred onto were identically blocked, incubated in the same aliquot of antibody, and analyzed at the same time on an Odyssey NIR imaging system (Li-Cor Biosciences). For the images presented here, identical settings on the Image Studio software (Li-Cor Biosciences) were applied to prevent false interpretations due to variations in brightness and contrast. The quantitations of the bands in these images are utilized in in **Fig 4.10**, **Fig 4.11**, and **Fig 4.13**.

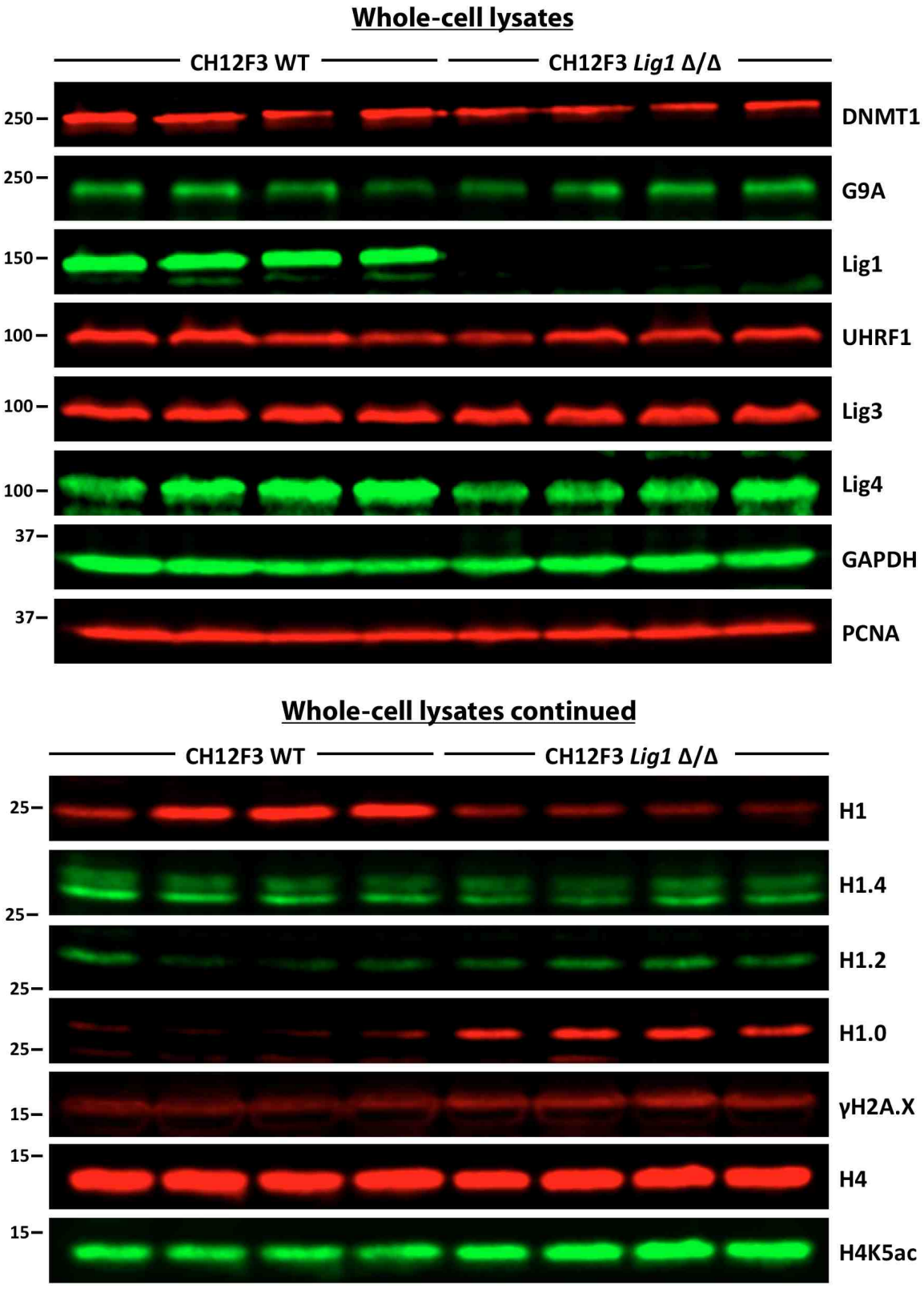
Whole-cell lysates
CH12F3 WT
CH12F3 Lig1 Δ/Δ
250
DNMT1
250
G9A
150
Lig1
100
UHRF1
100
Lig3
100
Lig4
37
GAPDH
37
PCNA
Whole-cell lysates continued
CH12F3 WT
CH12F3 Lig1 Δ/Δ
25
H1
25
H1.4
25
H1.2
25
H1.0
15
γH2A.X
15
H4
15
H4K5ac

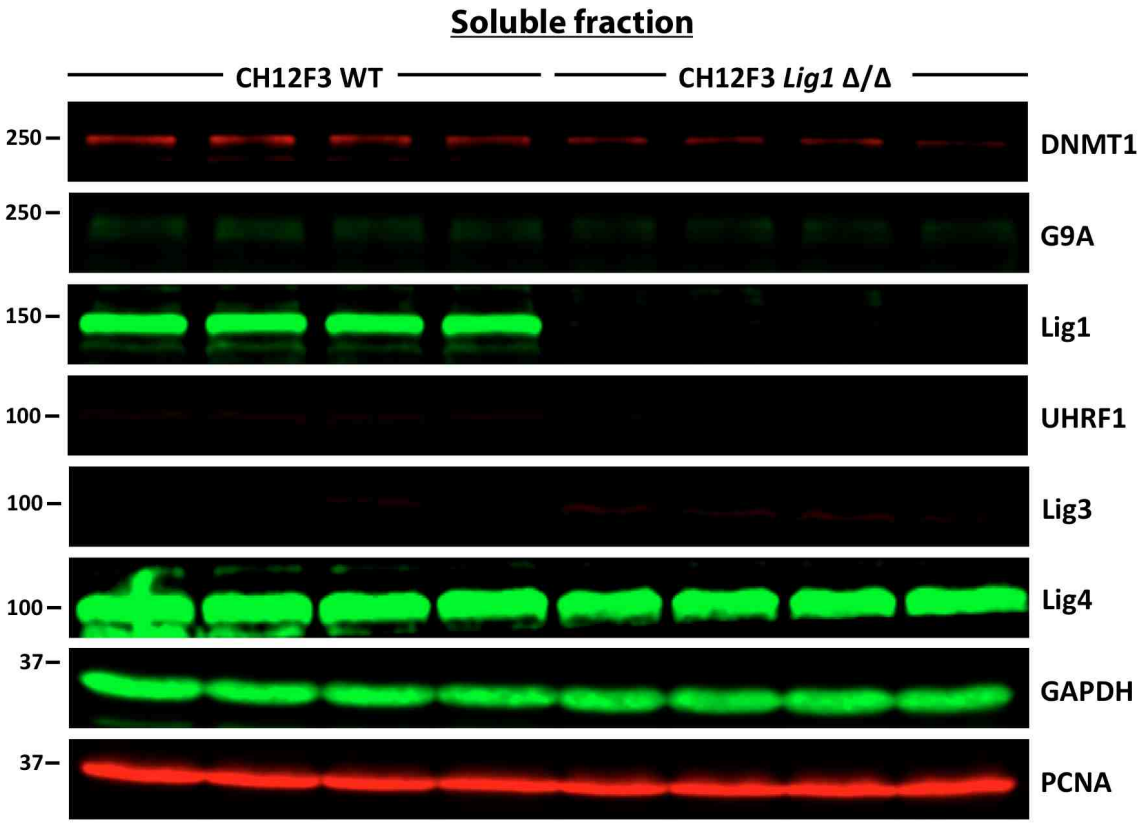
Soluble fraction
CH12F3 WT
CH12F3 Lig1 Δ/Δ
250
DNMT1
250
G9A
150
Lig1
100
UHRF1
100
Lig3
100
Lig4
37
GAPDH
37
PCNA

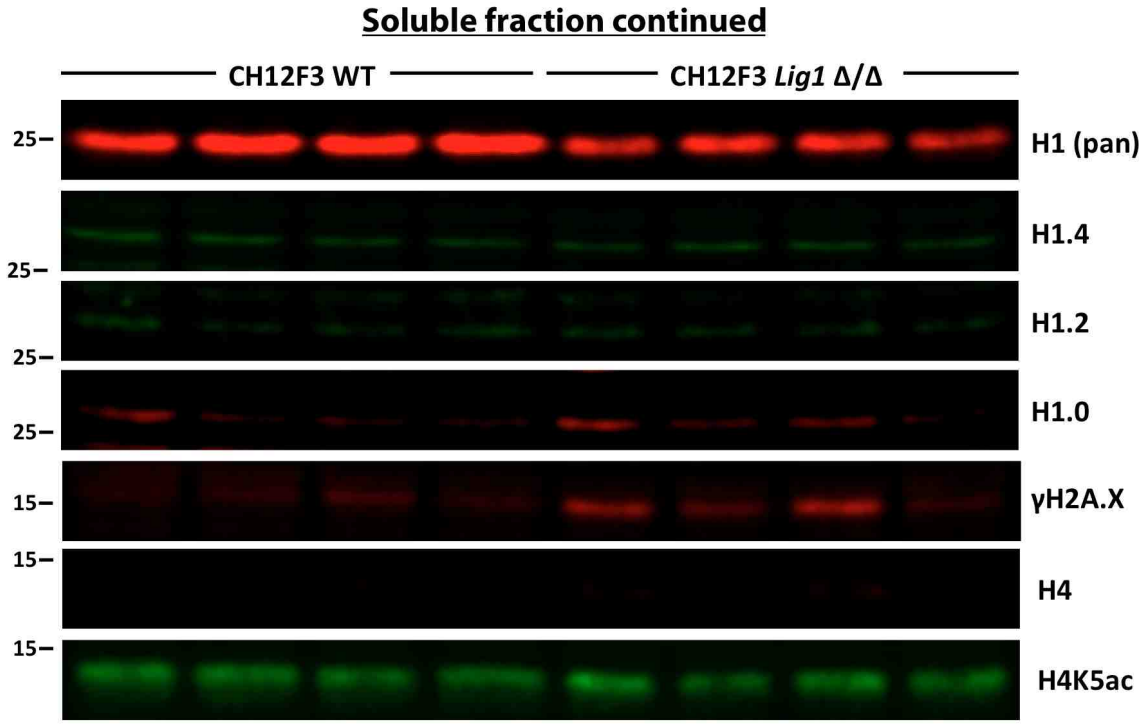
Soluble fraction continued
CH12F3 WT
CH12F3 Lig1 Δ/Δ
25
H1 (pan)
H1.4
25
H1.2
25
H1.0
25
γH2A.X
15
H4
15
H4K5ac
15

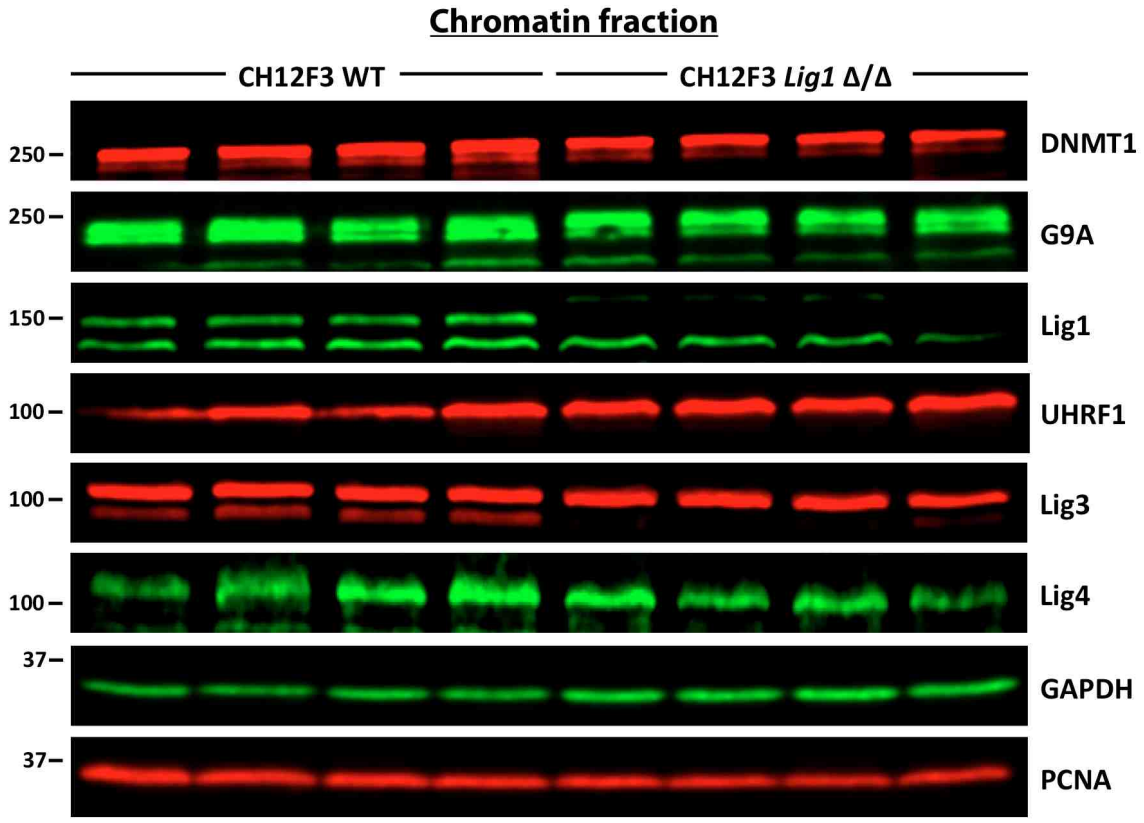
Chromatin fraction
CH12F3 WT
CH12F3 Lig1 Δ/Δ
250
250
150
100
100
100
37
37
DNMT1
G9A
Lig1
UHRF1
Lig3
Lig4
GAPDH
PCNA

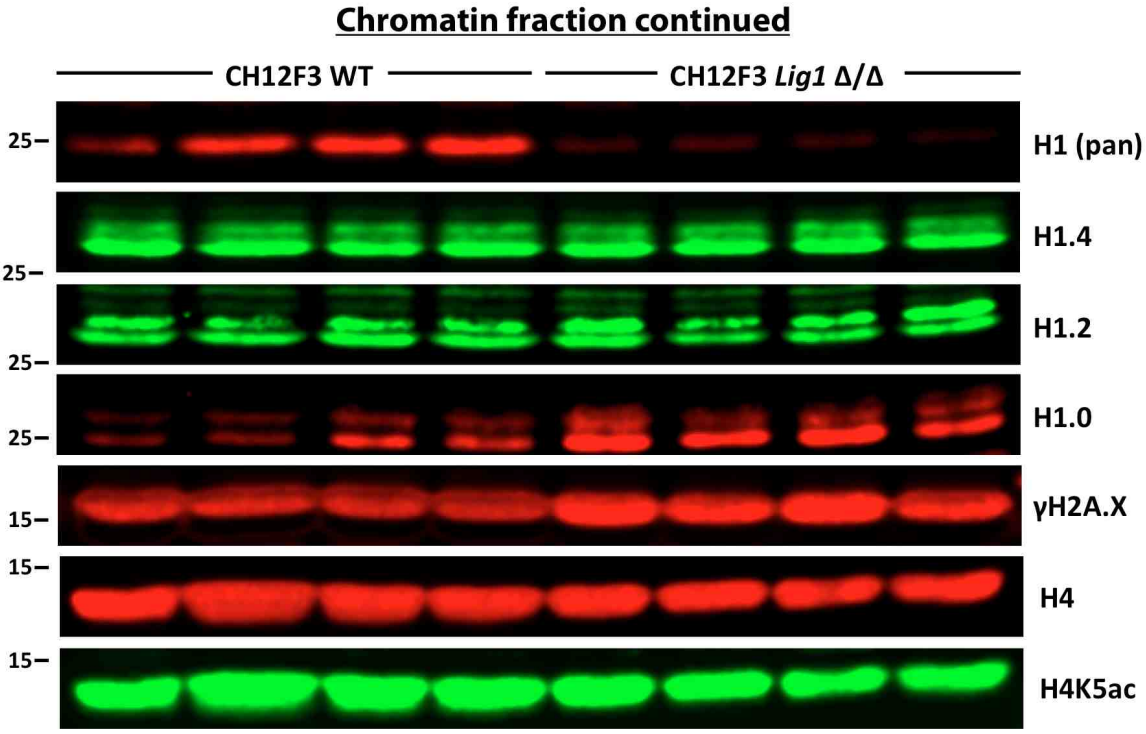
Chromatin fraction continued
CH12F3 WT
CH12F3 Lig1 Δ/Δ
25
25
25
25
15
15
15
H1 (pan)
H1.4
H1.2
H1.0
γH2A.X
H4
H4K5ac

Refrences

Aagaard, L., Laible, G., Selenko, P., Schmid, M., Dorn, R., Schotta, G., Kuhfittig, S., Wolf, A., Lebersorger, A., Singh, P.B., et al. (1999). Functional mammalian homologues of the Drosophila PEV-modifier Su(var)3-9 encode centromere-associated proteins which complex with the heterochromatin component M31. The EMBO Journal *18*, 1923–1938.

Aboussekhra, A., Biggerstaff, M., Shivji, M.K., Vilpo, J.A., Moncollin, V., Podust, V.N., Protić, M., Hübscher, U., Egly, J.M., and Wood, R.D. (1995). Mammalian DNA nucleotide excision repair reconstituted with purified protein components. Cell *80*, 859–868.

Adkins, N.L., Niu, H., Sung, P., and Peterson, C.L. (2013). Nucleosome dynamics regulates DNA processing. Nat Struct Mol Biol *20*, 836–842.

Aguilar Gurrieri, C., Larabi, A., Vinayachandran, V., Patel, N.A., Yen, K., Reja, R., Ebong, I.O., Schoehn, G., Robinson, C.V., Pugh, B.F., et al. (2016). Structural evidence for Nap1-dependent H2A–H2B deposition and nucleosome assembly. The EMBO Journal *35*, 1465–1482.

Akhtar, A., and Becker, P.B. (2000). Activation of transcription through histone H4 acetylation by MOF, an acetyltransferase essential for dosage compensation in Drosophila. Molecular Cell *5*, 367–375.

Alabert, C., Barth, T.K., Reverón-Gómez, N., Sidoli, S., Schmidt, A., Jensen, O.N., Imhof, A., and Groth, A. (2015). Two distinct modes for propagation of histone PTMs across the cell cycle. Genes & Development *29*, 585–590.

Alabert, C., Bukowski-Wills, J.-C., Lee, S.-B., Kustatscher, G., Nakamura, K., de Lima Alves, F., Menard, P., Mejlvang, J., Rappsilber, J., and Groth, A. (2014). Nascent chromatin capture proteomics determines chromatin dynamics during DNA replication and identifies unknown fork components. Nature Cell Biology *16*, 281–293.

Allfrey, V.G., Faulkner, R., and Mirsky, A.E. (1964). Acetylation and methylation of histones and their possible role in the regulation of RNA synthesis. Proc. Natl. Acad. Sci. U.S.a. *51*, 786–794.

Almouzni, G., and Cedar, H. (2016). Maintenance of Epigenetic Information. Cold Spring Harbor Perspectives in Biology *8*, a019372.

Amé, J.C., Rolli, V., Schreiber, V., Niedergang, C., Apiou, F., Decker, P., Muller, S., Höger, T., Menissier-de Murcia, J., and de Murcia, G. (1999). PARP-2, A novel mammalian DNA damage-dependent poly(ADP-ribose) polymerase. J. Biol. Chem. *274*, 17860–

17868.

Anand, R.P., Lovett, S.T., and Haber, J.E. (2013). Break-Induced DNA Replication. Cold Spring Harbor Perspectives in Biology *5*, a010397–a010397.

Arakawa, H., Bednar, T., Wang, M., Paul, K., Mladenov, E., Bencsik-Theilen, A.A., and Iliakis, G. (2012). Functional redundancy between DNA ligases I and III in DNA replication in vertebrate cells. Nucleic Acids Research *40*, 2599–2610.

Arakawa, H., and Iliakis, G. (2015). Alternative Okazaki Fragment Ligation Pathway by DNA Ligase III. Genes *6*, 385–398.

Aranda, S., Rutishauser, D., and Ernfors, P. (2014). Identification of a large protein network involved in epigenetic transmission in replicating DNA of embryonic stem cells. Nucleic Acids Research *42*, 6972–6986.

Araújo, S.J., Tirode, F., Coin, F., Pospiech, H., Syväoja, J.E., Stucki, M., Hübscher, U., Egly, J.M., and Wood, R.D. (2000). Nucleotide excision repair of DNA with recombinant human proteins: definition of the minimal set of factors, active forms of TFIIH, and modulation by CAK. Genes & Development *14*, 349–359.

Arney, K.L. (2004). Epigenetic aspects of differentiation. J. Cell. Sci. *117*, 4355–4363.

Arya, G., and Schlick, T. (2006). Role of histone tails in chromatin folding revealed by a mesoscopic oligonucleosome model. Proc. Natl. Acad. Sci. U.S.a. *103*, 16236–16241.

Arya, G., and Schlick, T. (2009). A Tale of Tails: How Histone Tails Mediate Chromatin Compaction in Different Salt and Linker Histone Environments †. J. Phys. Chem. A *113*, 4045–4059.

Auclair, G., and Weber, M. (2012). Mechanisms of DNA methylation and demethylation in mammals. Biochi *94*, 2202–2211.

Bannister, A.J., and Kouzarides, T. (2011). Regulation of chromatin by histone modifications. Nature Publishing Group *21*, 381–395.

Barnes, D.E., Stamp, G., Rosewell, I., Denzel, A., and Lindahl, T. (1998). Targeted disruption of the gene encoding DNA ligase IV leads to lethality in embryonic mice. Curr. Biol. *8*, 1395–1398.

Barnes, D.E., Tomkinson, A.E., Lehmann, A.R., Webster, A.D., and Lindahl, T. (1992). Mutations in the DNA ligase I gene of an individual with immunodeficiencies and cellular hypersensitivity to DNA-damaging agents. Cell *69*, 495–503.

Bell, S.P., and Labib, K. (2016). Chromosome Duplication in Saccharomyces cerevisiae. Genetics *203*, 1027–1067.

Bennardo, N., Cheng, A., Huang, N., and Stark, J.M. (2008). Alternative-NHEJ Is a

Mechanistically Distinct Pathway of Mammalian Chromosome Break Repair. PLoS Genet. *4*, e1000110.

Bennett, G., Papamichos-Chronakis, M., and Peterson, C.L. (2013). DNA repair choice defines a common pathway for recruitment of chromatin regulators. Nature Communications *4*, 2084.

Bentley, D., Selfridge, J., Millar, J.K., Samuel, K., Hole, N., Ansell, J.D., and Melton, D.W. (1996). DNA ligase I is required for fetal liver erythropoiesis but is not essential for mammalian cell viability. Nat. Genet. *13*, 489–491.

Bentley, D.J., Harrison, C., Ketchen, A.-M., Redhead, N.J., Samuel, K., Waterfall, M., Ansell, J.D., and Melton, D.W. (2002). DNA ligase I null mouse cells show normal DNA repair activity but altered DNA replication and reduced genome stability. J. Cell. Sci. *115*, 1551–1561.

Benyajati, C., and Worcel, A. (1976). Isolation, characterization, and structure of the folded interphase genome of Drosophila melanogaster. Cell *9*, 393–407.

Berkovich, E., Monnat, R.J., and Kastan, M.B. (2007). Roles of ATM and NBS1 in chromatin structure modulation and DNA double-strand break repair. Nature Cell Biology *9*, 683–690.

Bermudez, V.P., Farina, A., Raghavan, V., Tappin, I., and Hurwitz, J. (2011). Studies on Human DNA Polymerase and GINS Complex and Their Role in DNA Replication. Journal of Biological Chemistry *286*, 28963–28977.

Bétermier, M., Bertrand, P., and Lopez, B.S. (2014). Is Non-Homologous End-Joining Really an Inherently Error-Prone Process? PLoS Genet. *10*, e1004086.

Bhargava, R., Onyango, D.O., and Stark, J.M. (2016). Regulation of Single-StrandAnnealing and its Role inGenome Maintenance. Trends Genet. *32*, 566–575.

Bird, A. (2002). DNA methylation patterns and epigenetic memory. Genes & Development *16*, 6–21.

Blier, P.R., Griffith, A.J., Craft, J., and Hardin, J.A. (1993). Binding of Ku protein to DNA. Measurement of affinity for ends and demonstration of binding to nicks. J. Biol. Chem. *268*, 7594–7601.

Boboila, C., Oksenych, V., Gostissa, M., Wang, J.H., Zha, S., Zhang, Y., Chai, H., Lee, C.-S., Jankovic, M., Saez, L.-M.A., et al. (2012). Robust chromosomal DNA repair via alternative end-joining in the absence of X-ray repair cross-complementing protein 1 (XRCC1). Proc. Natl. Acad. Sci. U.S.a. *109*, 2473–2478.

Bochman, M.L., and Schwacha, A. (2009). The Mcm Complex: Unwinding the Mechanism of a Replicative Helicase. Microbiol. Mol. Biol. Rev. *73*, 652–683.

Boehm, E.M., Gildenberg, M.S., and Washington, M.T. (2016). The Many Roles of PCNA in Eukaryotic DNA Replication. In The Enzymes, (Elsevier), pp. 231–254.

Bonner, W.M., Redon, C.E., Dickey, J.S., Nakamura, A.J., Sedelnikova, O.A., Solier, S., and Pommier, Y. (2008). GammaH2AX and cancer. Nat Rev Cancer *8*, 957–967.

Bostick, M., Kim, J.K., Estève, P.-O., Clark, A., Pradhan, S., and Jacobsen, S.E. (2007). UHRF1 plays a role in maintaining DNA methylation in mammalian cells. Science *317*, 1760–1764.

Bottomley, M.J. (2004). Structures of protein domains that create or recognize histone modifications. EMBO Rep *5*, 464–469.

Bowman, G.D., and Poirier, M.G. (2015). Post-Translational Modifications of Histones That Influence Nucleosome Dynamics. Chem. Rev. *115*, 2274–2295.

Bradford, M.M. (1976). A rapid and sensitive method for the quantitation of microgram quantities of protein utilizing the principle of protein-dye binding. Anal. Biochem. *72*, 248–254.

Broomfield, S., Hryciw, T., and Xiao, W. (2001). DNA postreplication repair and mutagenesis in Saccharomyces cerevisiae. Mutat. Res. *486*, 167–184.

Brown, J.S., Lukashchuk, N., Sczaniecka-Clift, M., Britton, S., le Sage, C., Calsou, P., Beli, P., Galanty, Y., and Jackson, S.P. (2015). Neddylation Promotes Ubiquitylation and Release of Ku from DNA-Damage Sites. CellReports *11*, 704–714.

Bryant, H.E., Schultz, N., Thomas, H.D., Parker, K.M., Flower, D., Lopez, E., Kyle, S., Meuth, M., Curtin, N.J., and Helleday, T. (2005). Specific killing of BRCA2-deficient tumours with inhibitors of poly(ADP-ribose) polymerase. Nature *434*, 913–917.

Budd, M.E., and Campbell, J.L. (2009). Interplay of Mre11 Nuclease with Dna2 plus Sgs1 in Rad51-Dependent Recombinational Repair. PLoS ONE *4*, e4267.

Bunting, S.F., Callén, E., Wong, N., Chen, H.-T., Polato, F., Gunn, A., Bothmer, A., Feldhahn, N., Fernandez-Capetillo, O., Cao, L., et al. (2010). 53BP1 Inhibits Homologous Recombination in Brca1-Deficient Cells by Blocking Resection of DNA Breaks. Cell *141*, 243–254.

Burgess, R.J., and Zhang, Z. (2013). Histone chaperones in nucleosome assembly and human disease. Nature Publishing Group *20*, 14–22.

Butler, J.S., Koutelou, E., Schibler, A.C., and Dent, S.Y. (2012). Histone-modifying enzymes: regulators of developmental decisions and drivers of human disease. Epigenomics *4*, 163–177.

Caldecott, K.W., McKeown, C.K., Tucker, J.D., Ljungquist, S., and Thompson, L.H.

(1994). An interaction between the mammalian DNA repair protein XRCC1 and DNA ligase III. Molecular and Cellular Biology *14*, 68–76.

Caldecott, K.W., Tucker, J.D., Stanker, L.H., and Thompson, L.H. (1995). Characterization of the XRCC1-DNA ligase III complex in vitro and its absence from mutant hamster cells. Nucleic Acids Research *23*, 4836–4843.

Caldecott, K.W. (2008). Single-strand break repair and genetic disease. Nat Rev Genet *9*, 619–631.

Cannavo, E., and Cejka, P. (2014). Sae2 promotes dsDNA endonuclease activity within Mre11–Rad50–Xrs2 to resect DNA breaks. Nature *514*, 122–125.

Ceccaldi, R., Rondinelli, B., and D'Andrea, A.D. (2016). Repair Pathway Choices and Consequences at the Double-Strand Break. Trends in Cell Biology *26*, 52–64.

Cedar, H., and Bergman, Y. (2009). Linking DNA methylation and histone modification: patterns and paradigms. Nat Rev Genet *10*, 295–304.

Cejka, P. (2015). DNA End Resection: Nucleases Team Up with the Right Partners to Initiate Homologous Recombination. Journal of Biological Chemistry *290*, 22931–22938.

Celeste, A., Petersen, S., Romanienko, P.J., Fernandez-Capetillo, O., Chen, H.-T., Sedelnikova, O.A., Reina-San-Martin, B., Coppola, V., Meffre, E., Difilippantonio, M.J., et al. (2002). Genomic instability in mice lacking histone H2AX. Science *296*, 922–927.

Chai, B. (2005). Distinct roles for the RSC and Swi/Snf ATP-dependent chromatin remodelers in DNA double-strand break repair. Genes & Development *19*, 1656–1661.

Chambers, A.L., Brownlee, P.M., Durley, S.C., Beacham, T., Kent, N.A., and Downs, J.A. (2012). The Two Different Isoforms of the RSC Chromatin Remodeling Complex Play Distinct Roles in DNA Damage Responses. PLoS ONE *7*, e32016.

Chapman, J.R., Taylor, M.R.G., and Boulton, S.J. (2012). Playing the end game: DNA double-strand break repair pathway choice. Molecular Cell *47*, 497–510.

Chehrehasa, F., Meedeniya, A.C.B., Dwyer, P., Abrahamsen, G., and Mackay-Sim, A. (2009). EdU, a new thymidine analogue for labelling proliferating cells in the nervous system. Journal of Neuroscience Methods *177*, 122–130.

Chen, C.-C., and Tyler, J. (2008). Chromatin reassembly signals the end of DNA repair. Cc *7*, 3792–3797.

Chen, H., Lisby, M., and Symington, L.S. (2013a). RPA Coordinates DNA End

Resection and Prevents Formation of DNA Hairpins. Molecular Cell *50*, 589–600.

Chen, L., Trujillo, K., Ramos, W., Sung, P., and Tomkinson, A.E. (2001). Promotion of Dnl4-catalyzed DNA end-joining by the Rad50/Mre11/Xrs2 and Hdf1/Hdf2 complexes. Molecular Cell *8*, 1105–1115.

Chen, T., and Dent, S.Y.R. (2013). Chromatin modifiers and remodellers: regulators of cellular differentiation. Nat Rev Genet *15*, 93–106.

Chen, X., and Tomkinson, A.E. (2011). Yeast Nej1 Is a Key Participant in the Initial End Binding and Final Ligation Steps of Nonhomologous End Joining. Journal of Biological Chemistry *286*, 4931–4940.

Chen, X., Zhong, S., Zhu, X., Dziegielewska, B., Ellenberger, T., Wilson, G.M., MacKerell, A.D., and Tomkinson, A.E. (2008). Rational Design of Human DNA Ligase Inhibitors that Target Cellular DNA Replication and Repair. Cancer Res. *68*, 3169–3177.

Chen, X., Cui, D., Papusha, A., Zhang, X., Chu, C.-D., Tang, J., Chen, K., Pan, X., and Ira, G. (2013b). The Fun30 nucleosome remodeller promotes resection of DNA double-strand break ends. Nature *489*, 576–580.

Chen, X., Niu, H., Yu, Y., Wang, J., Zhu, S., Zhou, J., Papusha, A., Cui, D., Pan, X., Kwon, Y., et al. (2016). Enrichment of Cdk1-cyclins at DNA double-strand breaks stimulates Fun30 phosphorylation and DNA end resection. Nucleic Acids Research gkv1544.

Chilkova, O., Stenlund, P., Isoz, I., Stith, C.M., Grabowski, P., Lundstrom, E.B., Burgers, P.M., and Johansson, E. (2007). The eukaryotic leading and lagging strand DNA polymerases are loaded onto primer-ends via separate mechanisms but have comparable processivity in the presence of PCNA. Nucleic Acids Research *35*, 6588–6597.

Clapier, C.R., and Cairns, B.R. (2014). Chromatin remodeling complexes. Fundamentals of Chromatin.

Clark, D.J. (2010). Nucleosome positioning, nucleosome spacing and the nucleosome code. J. Biomol. Struct. Dyn. *27*, 781–793.

Clerici, M., Mantiero, D., Lucchini, G., and Longhese, M.P. (2005). The Saccharomyces cerevisiae Sae2 protein promotes resection and bridging of double strand break ends. J. Biol. Chem. *280*, 38631–38638.

Collart, M.A., and Oliviero, S. (2001). Preparation of yeast RNA. In Ausbel, F.M., Brent, R., Kingston, R.E., Moore, D.D., Seidman, J.G., Smith, J.A., and Struhl, K. (eds). Current Procotols in Molecular Biology (John Wiley & Sons). Section IV, Unit 13.12.

Conaway, R.C., and Conaway, J.W. (2009). The INO80 chromatin remodeling complex in transcription, replication and repair. Trends Biochem. Sci. *34*, 71–77.

Corneo, B., Wendland, R.L., Deriano, L., Cui, X., Klein, I.A., Wong, S.-Y., Arnal, S., Holub, A.J., Weller, G.R., Pancake, B.A., et al. (2007). Rag mutations reveal robust alternative end joining. Nature *449*, 483–486.

Costelloe, T., Louge, R., Tomimatsu, N., Mukherjee, B., Martini, E., Khadaroo, B., Dubois, K., Wiegant, W.W., Thierry, A., Burma, S., et al. (2013). The yeast Fun30 and human SMARCAD1 chromatin remodellers promote DNA end resection. Nature *489*, 581–584.

Cotner-Gohara, E., Kim, I.-K., Tomkinson, A.E., and Ellenberger, T. (2008). Two DNA-binding and nick recognition modules in human DNA ligase III. J. Biol. Chem. *283*, 10764–10772.

Cremaschi, P., Oliverio, M., Leva, V., Bione, S., Carriero, R., Mazzucco, G., Palamidessi, A., Scita, G., Biamonti, G., and Montecucco, A. (2015). Chronic Replication Problems Impact Cell Morphology and Adhesion of DNA Ligase I Defective Cells. PLoS ONE *10*, e0130561.

Crow, Y.J., Leitch, A., Hayward, B.E., Garner, A., Parmar, R., Griffith, E., Ali, M., Semple, C., Aicardi, J., Babul-Hirji, R., et al. (2006). Mutations in genes encoding ribonuclease H2 subunits cause Aicardi-Goutières syndrome and mimic congenital viral brain infection. Nat. Genet. *38*, 910–916.

Cuneo, M.J., Gabel, S.A., Krahn, J.M., Ricker, M.A., and London, R.E. (2011). The structural basis for partitioning of the XRCC1/DNA ligase III- BRCT-mediated dimer complexes. Nucleic Acids Research *39*, 7816–7827.

Daigaku, Y., Davies, A.A., and Ulrich, H.D. (2010). Ubiquitin-dependent DNA damage bypass is separable from genome replication. Nature *465*, 951–955.

Daley, J.M., Chiba, T., Xue, X., Niu, H., and Sung, P. (2014). Multifaceted role of the Topo III -RMI1-RMI2 complex and DNA2 in the BLM-dependent pathway of DNA break end resection. Nucleic Acids Research *42*, 11083–11091.

Daley, J.M., Niu, H., Miller, A.S., and Sung, P. (2015). Biochemical mechanism of DSB end resection and its regulation. DNA Repair *32*, 66–74.

Dalgaard, J.Z. (2012). Causes and consequences of ribonucleotide incorporation into nuclear DNA. Trends in Genetics *28*, 592–597.

Dang, W., and Bartholomew, B. (2007). Domain Architecture of the Catalytic Subunit in the ISW2-Nucleosome Complex. Molecular and Cellular Biology *27*, 8306–8317.

Das, C., Lucia, M.S., Hansen, K.C., and Tyler, J.K. (2009). nature07861. Nature *459*, 113–117.

Davis, A.J., and Chen, D.J. (2013). DNA double strand break repair via non-

homologous end-joining. Transl Cancer Res *2*, 130–143.

Dawson, M.A., and Kouzarides, T. (2012). Cancer Epigenetics: From Mechanism to Therapy. Cell *150*, 12–27.

De Ioannes, P., Malu, S., Cortes, P., and Aggarwal, A.K. (2012). Structural Basis of DNA Ligase IV-Artemis Interaction in Nonhomologous End-Joining. CellReports *2*, 1505–1512.

DeFazio, L.G., Stansel, R.M., Griffith, J.D., and Chu, G. (2002). Synapsis of DNA ends by DNA-dependent protein kinase. The EMBO Journal *21*, 3192–3200.

Dembowski, J.A., and DeLuca, N.A. (2015). Selective Recruitment of Nuclear Factors to Productively Replicating Herpes Simplex Virus Genomes. PLoS Pathog *11*, e1004939.

Devbhandari, S., Jiang, J., Kumar, C., Whitehouse, I., and Remus, D. (2017). Chromatin Constrains the Initiation and Elongation of DNA Replication. Molecular Cell *65*, 131–141.

Dhaenens, M., Glibert, P., Meert, P., Vossaert, L., and Deforce, D. (2014). Histone proteolysis: A proposal for categorization into 'clipping' and 'degradation'. Bioessays *37*, 70–79.

Doré, A.S., Furnham, N., Davies, O.R., Sibanda, B.L., Chirgadze, D.Y., Jackson, S.P., Pellegrini, L., and Blundell, T.L. (2006). Structure of an Xrcc4–DNA ligase IV yeast ortholog complex reveals a novel BRCT interaction mode. DNA Repair *5*, 362–368.

Dovrat, D., Stodola, J.L., Burgers, P.M.J., and Aharoni, A. (2014). Sequential switching of binding partners on PCNA during in vitro Okazaki fragment maturation. Proc Natl Acad Sci USA *111*, 14118–14123.

Dua, R., Levy, D.L., and Campbell, J.L. (1999). Analysis of the essential functions of the C-terminal protein/protein interaction domain of Saccharomyces cerevisiae pol epsilon and its unexpected ability to support growth in the absence of the DNA polymerase domain. J. Biol. Chem. *274*, 22283–22288.

Duderstadt, K.E., Reyes-Lamothe, R., van Oijen, A.M., and Sherratt, D.J. (2014). Replication-Fork Dynamics. Cold Spring Harbor Perspectives in Biology *6*, a010157–a010157.

Dulic, A., Bates, P.A., Zhang, X., Martin, S.R., Freemont, P.S., Lindahl, T., and Barnes, D.E. (2001). BRCT Domain Interactions in the Heterodimeric DNA Repair Protein XRCC1–DNA Ligase III †. Biochemistry *40*, 5906–5913.

Duncan, E.M., Muratore-Schroeder, T.L., Cook, R.G., Garcia, B.A., Shabanowitz, J., Hunt, D.F., and Allis, C.D. (2008). Cathepsin L Proteolytically Processes Histone H3

During Mouse Embryonic Stem Cell Differentiation. Cell *135*, 284–294.

Dungrawala, H., Rose, K.L., Bhat, K.P., Mohni, K.N., Glick, G.G., Couch, F.B., and Cortez, D. (2015). The Replication Checkpoint Prevents Two Types of Fork Collapse without Regulating Replisome Stability. Molecular Cell *59*, 998–1010.

Eapen, V.V., Sugawara, N., Tsabar, M., Wu, W.H., and Haber, J.E. (2012). The Saccharomyces cerevisiae Chromatin Remodeler Fun30 Regulates DNA End Resection and Checkpoint Deactivation. Molecular and Cellular Biology *32*, 4727–4740.

Ellenberger, T., and Tomkinson, A.E. (2008). Eukaryotic DNA Ligases: Structural and Functional Insights. Annu. Rev. Biochem. *77*, 313–338.

Emerson, C.H., and Bertuch, A.A. (2016). Consider the workhorse: Nonhomologous end-joining in budding yeast 1. Biochem. Cell Biol. *94*, 396–406.

Enright, H.U., Miller, W.J., and Hebbel, R.P. (1992). Nucleosomal histone protein protects DNA from iron-mediated damage. Nucleic Acids Research *20*, 3341–3346.

Esteve, P.O., Chin, H.G., Smallwood, A., Feehery, G.R., Gangisetty, O., Karpf, A.R., Carey, M.F., and Pradhan, S. (2006). Direct interaction between DNMT1 and G9a coordinates DNA and histone methylation during replication. Genes & Development *20*, 3089–3103.

Fan, Y., Nikitina, T., Zhao, J., Fleury, T.J., Bhattacharyya, R., Bouhassira, E.E., Stein, A., Woodcock, C.L., and Skoultchi, A.I. (2005). Histone H1 Depletion in Mammals Alters Global Chromatin Structure but Causes Specific Changes in Gene Regulation. Cell *123*, 1199–1212.

Fattah, F., Lee, E.H., Weisensel, N., Wang, Y., Lichter, N., and Hendrickson, E.A. (2010). Ku Regulates the Non-Homologous End Joining Pathway Choice of DNA Double-Strand Break Repair in Human Somatic Cells. PLoS Genet. *6*, e1000855.

Ferrari, M., Dibitetto, D., De Gregorio, G., Eapen, V.V., Rawal, C.C., Lazzaro, F., Tsabar, M., Marini, F., Haber, J.E., and Pellicioli, A. (2015). Functional Interplay between the 53BP1-Ortholog Rad9 and the Mre11 Complex Regulates Resection, End-Tethering and Repair of a Double-Strand Break. PLoS Genet. *11*, e1004928.

Ferretti, L.P., Lafranchi, L., and Sartori, A.A. (2013). Controlling DNA-end resection: a new task for CDKs. Front Genet *4*, 99.

Finan, J.D., Chalut, K.J., Wax, A., and Guilak, F. (2008). Nonlinear Osmotic Properties of the Cell Nucleus. Ann Biomed Eng *37*, 477–491.

Finch, J.T., and Klug, A. (1976). Solenoidal model for superstructure in chromatin. Proc. Natl. Acad. Sci. U.S.a. *73*, 1897–1901.

Flaus, A., and Owen-Hughes, T. (2011). Mechanisms for ATP-dependent chromatin remodelling: the means to the end. FEBS Journal *278*, 3579–3595.

Foster, E.R., and Downs, J.A. (2005). Histone H2A phosphorylation in DNA double-strand break repair. FEBS Journal *272*, 3231–3240.

Foster, S.S., Balestrini, A., and Petrini, J.H.J. (2011). Functional interplay of the Mre11 nuclease and Ku in the response to replication-associated DNA damage. Molecular and Cellular Biology *31*, 4379–4389.

Frank, K.M., Sekiguchi, J.M., Seidl, K.J., Swat, W., Rathbun, G.A., Cheng, H.L., Davidson, L., Kangaloo, L., and Alt, F.W. (1998). Late embryonic lethality and impaired V(D)J recombination in mice lacking DNA ligase IV. Nature *396*, 173–177.

Freudenreich, C.H. (2014). Chromatin modifications and DNA repair: beyond double-strand breaks. 1–18.

Friedberg, E.C., Walker, G.C., Siede, W., and Wood, R.D. (2005). DNA Repair and Mutagenesis (American Society for Microbiology Press).

Frosina, G., Fortini, P., Rossi, O., Carrozzino, F., Raspaglio, G., Cox, L.S., Lane, D.P., Abbondandolo, A., and Dogliotti, E. (1996). Two pathways for base excision repair in mammalian cells. J. Biol. Chem. *271*, 9573–9578.

Fu, Y.V., Yardimci, H., Long, D.T., Guainazzi, A., Bermudez, V.P., Hurwitz, J., van Oijen, A., Schärer, O.D., and Walter, J.C. (2011). Selective Bypass of a Lagging Strand Roadblock by the Eukaryotic Replicative DNA Helicase. Cell *146*, 931–941.

Fussner, E., Ching, R.W., and Bazett-Jones, D.P. (2011). Living without 30 nm chromatin fibers. Trends Biochem. Sci. *36*, 1–6.

Gaillard, P.H., Martini, E.M., Kaufman, P.D., Stillman, B., Moustacchi, E., and Almouzni, G. (1996). Chromatin assembly coupled to DNA repair: a new role for chromatin assembly factor I. Cell *86*, 887–896.

Gao, Y., Katyal, S., Lee, Y., Zhao, J., Rehg, J.E., Russell, H.R., and McKinnon, P.J. (2012). DNA ligase III is critical for mtDNA integrity but not Xrcc1-mediated nuclear DNA repair. Nature *471*, 240–244.

Garcia, V., Phelps, S.E.L., Gray, S., and Neale, M.J. (2012). Bidirectional resection of DNA double-strand breaks by Mre11 and Exo1. Nature *479*, 241–244.

Georgescu, R.E., Langston, L., Yao, N.Y., Yurieva, O., Zhang, D., Finkelstein, J., Agarwal, T., and O'Donnell, M.E. (2014). Mechanism of asymmetric polymerase assembly at the eukaryotic replication fork. Nat Struct Mol Biol *21*, 664–670.

Gerhold, C.-B., Hauer, M.H., and Gasser, S.M. (2015). INO80-C and SWR-C: Guardians

of the Genome. J. Mol. Biol. *427*, 637–651.

Girard, P.-M., Kysela, B., Härer, C.J., Doherty, A.J., and Jeggo, P.A. (2004). Analysis of DNA ligase IV mutations found in LIG4 syndrome patients: the impact of two linked polymorphisms. Hum. Mol. Genet. *13*, 2369–2376.

Gobbini, E., Cesena, D., Galbiati, A., Lockhart, A., and Longhese, M.P. (2013). Interplays between ATM/Tel1 and ATR/Mec1 in sensing and signaling DNA double-strand breaks. DNA Repair *12*, 791–799.

Grawunder, U., Wilm, M., Wu, X., Kulesza, P., Wilson, T.E., Mann, M., and Lieber, M.R. (1997). Activity of DNA ligase IV stimulated by complex formation with XRCC4 protein in mammalian cells. Nature *388*, 492–495.

Grawunder, U., Zimmer, D., Fugmann, S., Schwarz, K., and Lieber, M.R. (1998a). DNA ligase IV is essential for V(D)J recombination and DNA double-strand break repair in human precursor lymphocytes. Molecular Cell *2*, 477–484.

Grawunder, U., Zimmer, D., Kulesza, P., and Lieber, M.R. (1998b). Requirement for an interaction of XRCC4 with DNA ligase IV for wild-type V(D)J recombination and DNA double-strand break repair in vivo. J. Biol. Chem. *273*, 24708–24714.

Greeley, D., Crapo, J.D., and Vollmer, R.T. (1978). Estimation of the mean caliper diameter of cell nuclei. I. Serial section reconstriction method and endothelial nuclei from human lung. J Microsc *114*, 31–39.

Groth, A., Rocha, W., Verreault, A., and Almouzni, G. (2007). Chromatin Challenges during DNA Replication and Repair. Cell *128*, 721–733.

Gurtu, V.E.A., Yan, G., and Zhang, G. (1996). IRES Bicistronic Expression Vectors for Efficient Creation of Stable Mammalian Cell Lines. Biochemical and Biophysical Research Communications *229*, 295-298.

Haber, J.E. (2012). Mating-Type Genes and MAT Switching in Saccharomyces cerevisiae. Genetics *191*, 33–64.

Hackett, J.A., and Surani, M.A. (2012). DNA methylation dynamics during the mammalian life cycle. Philosophical Transactions of the Royal Society B: Biological Sciences *368*, 20110328–20110328.

Hammond, C.M., Strømme, C.B., Huang, H., Patel, D.J., and Groth, A. (2017). Histone chaperone networks shaping chromatin function. Nature Reviews Molecular Cell Biology 1–19.

Han, L., Masani, S., Hsieh, C.-L., and Yu, K. (2014). DNA Ligase I Is Not Essential for Mammalian Cell Viability. CellReports *7*, 316–320.

Hanahan, D., and Weinberg, R.A. (2011). Hallmarks of Cancer: The Next Generation. Cell *144*, 646–674.

Hansen, K.H., Bracken, A.P., Pasini, D., Dietrich, N., Gehani, S.S., Monrad, A., Rappsilber, J., Lerdrup, M., and Helin, K. (2008). A model for transmission of the H3K27me3 epigenetic mark. Nature Cell Biology *10*, 1291–1300.

Happel, N., Warneboldt, J., Hänecke, K., Haller, F., and Doenecke, D. (2014). H1 subtype expression during cell proliferation and growth arrest. Cc *8*, 2226–2232.

Hargreaves, D.C., and Crabtree, G.R. (2011). ATP-dependent chromatin remodeling: genetics, genomics and mechanisms. Nature Publishing Group 1–25.

Harrison, C., Ketchen, A.-M., Redhead, N.J., O'Sullivan, M.J., and Melton, D.W. (2002). Replication failure, genome instability, and increased cancer susceptibility in mice with a point mutation in the DNA ligase I gene. Cancer Res. *62*, 4065–4074.

Harshman, S.W., Young, N.L., Parthun, M.R., and Freitas, M.A. (2013). H1 histones: current perspectives and challenges. Nucleic Acids Research *41*, 9593–9609.

Hashimoto, Y., Puddu, F., and Costanzo, V. (2011). RAD51- and MRE11-dependent reassembly of uncoupled CMG helicase complex at collapsed replication forks. Nat Struct Mol Biol *19*, 17–24.

Helleday, T. (2011). The underlying mechanism for the PARP and BRCA synthetic lethality: Clearing up the misunderstandings. Molecular Oncology *5*, 387–393.

Helleday, T., Petermann, E., Lundin, C., Hodgson, B., and Sharma, R.A. (2008). DNA repair pathways as targets for cancer therapy. Nat Rev Cancer *8*, 193–204.

Henderson, L.M., Arlett, C.F., Harcourt, S.A., Lehmann, A.R., and Broughton, B.C. (1985). Cells from an immunodeficient patient (46BR) with a defect in DNA ligation are hypomutable but hypersensitive to the induction of sister chromatid exchanges. Proc. Natl. Acad. Sci. U.S.a. *82*, 2044–2048.

Hermann, A., Goyal, R., and Jeltsch, A. (2004). The Dnmt1 DNA-(cytosine-C5)-methyltransferase Methylates DNA Processively with High Preference for Hemimethylated Target Sites. Journal of Biological Chemistry *279*, 48350–48359.

Hewish, D.R., and Burgoyne, L.A. (1973). Chromatin sub-structure. The digestion of chromatin DNA at regularly spaced sites by a nuclear deoxyribonuclease. Biochem. Biophys. Res. Commun. *52*, 504–510.

Hoeijmakers, J.H. (2001). Genome maintenance mechanisms for preventing cancer. Nature *411*, 366–374.

Howes, T.R.L., and Tomkinson, A.E. (2012). DNA Ligase I, the Replicative DNA Ligase.

In Subcellular Biochemistry, (Dordrecht: Springer Netherlands), pp. 327–341.

Huang, F., Saraf, A., Florens, L., Kusch, T., Swanson, S.K., Szerszen, L.T., Li, G., Dutta, A., Washburn, M.P., Abmayr, S.M., et al. (2016). The Enok acetyltransferase complex interacts with Elg1 and negatively regulates PCNA unloading to promote the G1/S transition. Genes & Development.

Huertas, P., Cortés-Ledesma, F., Sartori, A.A., Aguilera, A., and Jackson, S.P. (2008). CDK targets Sae2 to control DNA-end resection and homologous recombination. Nature *455*, 689–692.

Hunt, C.R., Ramnarain, D., Horikoshi, N., Iyengar, P., Pandita, R.K., Shay, J.W., and Pandita, T.K. (2013). Histone Modifications and DNA Double-Strand Break Repair after Exposure to Ionizing Radiations. Radiation Research *179*, 383–392.

Hustedt, N., and Durocher, D. (2017). The control of DNA repair by the cell cycle. Nature Cell Biology *19*, 1–9.

Hyrien, O. (2015). Peaks cloaked in the mist: The landscape of mammalian replication origins. J. Cell Biol. *208*, 147–160.

Iftode, C., Daniely, Y., and Borowiec, J.A. (1999). Replication protein A (RPA): the eukaryotic SSB. Critical Reviews in Biochemistry and Molecular Biology *34*, 141–180.

Iida, T., Suetake, I., Tajima, S., Morioka, H., Ohta, S., Obuse, C., and Tsurimoto, T. (2002). PCNA clamp facilitates action of DNA cytosine methyltransferase 1 on hemimethylated DNA. Genes Cells *7*, 997–1007.

Illingworth, R.S., and Bird, A.P. (2009). CpG islands – "A rough guide." FEBS Letters *583*, 1713–1720.

Ira, G., Pellicioli, A., Balijja, A., Wang, X., Fiorani, S., Carotenuto, W., Liberi, G., Bressan, D., Wan, L., Hollingsworth, N.M., et al. (2004). DNA end resection, homologous recombination and DNA damage checkpoint activation require CDK1. Nature *431*, 1011–1017.

Irianto, J., Swift, J., Martins, R.P., McPhail, G.D., Knight, M.M., Discher, D.E., and Lee, D.A. (2013). Osmotic Challenge Drives Rapid and Reversible Chromatin Condensationin Chondrocytes. Biophysj *104*, 759–769.

Ismail, I.H., and Hendzel, M.J. (2008). The γ-H2A.X: Is it just a surrogate marker of double-strand breaks or much more? Environ. Mol. Mutagen. *49*, 73–82.

Iwasaki, D., Hayashihara, K., Shima, H., Higashide, M., Terasawa, M., Gasser, S.M., and Shinohara, M. (2016). The MRX Complex Ensures NHEJ Fidelity through Multiple Pathways Including Xrs2-FHA–Dependent Tel1 Activation. PLoS Genet. *12*,

e1005942.

Jaenisch, R., and Bird, A. (2003). Epigenetic regulation of gene expression: how the genome integrates intrinsic and environmental signals. Nat. Genet. *33*, 245–254.

Janke, C., Magiera, M.M., Rathfelder, N., Taxis, C., Reber, S., Maekawa, H., Moreno-Borchart, A., Doenges, G., Schwob, E., Schiebel, E., et al. (2004). A versatile toolbox for PCR-based tagging of yeast genes: new fluorescent proteins, more markers and promoter substitution cassettes. Yeast *21*, 947–962.

Jasencakova, Z., and Groth, A. (2010). Seminars in Cell & Developmental Biology. Semin. Cell Dev. Biol. *21*, 231–237.

Jasin, M., and Rothstein, R. (2013). Repair of Strand Breaks by Homologous Recombination. Cold Spring Harbor Perspectives in Biology *5*, a012740–a012740.

Jäckle, T., Hasel, C., Melzner, I., Brüderlein, S., Jehle, P.M., and Möller, P. (2001). Sustained hyposmotic stress induces cell death: apoptosis by defeat. Am. J. Physiol., Cell Physiol. *281*, C1716–C1726.

Jensen, R.E., and Herskowitz, I. (1984). Directionality and regulation of cassette substitution in yeast. Cold Spring Harb. Symp. Quant. Biol. *49*, 97–104.

Johnson, R.E., Klassen, R., Prakash, L., and Prakash, S. (2015). A Major Role of DNA Polymerase d in Replication of Both the Leading and Lagging DNA Strands. Molecular Cell *59*, 163–175.

Kadoch, C., and Crabtree, G.R. (2013). Reversible Disruption of mSWI/SNF (BAF) Complexes by the SS18-SSX Oncogenic Fusion in Synovial Sarcoma. Cell *153*, 71–85.

Kadoch, C., Hargreaves, D.C., Hodges, C., Elias, L., Ho, L., Ranish, J., and Crabtree, G.R. (2013). ng.2628 (1). Nature Publishing Group *45*, 592–601.

Kanemaki, M., and Labib, K. (2006). Distinct roles for Sld3 and GINS during establishment and progression of eukaryotic DNA replication forks. The EMBO Journal *25*, 1753–1763.

Kang, Y.-H., Galal, W.C., Farina, A., Tappin, I., and Hurwitz, J. (2012). Properties of the human Cdc45/Mcm2-7/GINS helicase complex and its action with DNA polymerase epsilon in rolling circle DNA synthesis. Proc. Natl. Acad. Sci. U.S.a. *109*, 6042–6047.

Kapoor, P., Bao, Y., Xiao, J., Luo, J., Shen, J., Persinger, J., Peng, G., Ranish, J., Bartholomew, B., and Shen, X. (2015). Regulation of Mec1 kinase activity by the SWI/SNF chromatin remodeling complex. Genes & Development *29*, 591–602.

Karras, G.I., and Jentsch, S. (2010). The RAD6 DNA Damage Tolerance Pathway Operates Uncoupled from the Replication Fork and Is Functional Beyond S Phase.

Cell *141*, 255–267.

Kass, S.U., Pruss, D., and Wolffe, A.P. (1997). How does DNA methylation repress transcription? Trends Genet. *13*, 444–449.

Katyal, S., and McKinnon, P.J. (2011). Disconnecting XRCC1 and DNA ligase III. Cc *10*, 2269–2275.

Kelley, M.R., Logsdon, D., and Fishel, M.L. (2014). Targeting DNA repair pathways for cancer treatment: what's new? Future Oncology *10*, 1215–1237.

Kennedy, B.P., and Davies, P.L. (1982). Chromatin reorganization during spermatogenesis in the winter flounder. J. Biol. Chem. *257*, 11160–11165.

Kent, N.A., Chambers, A.L., and Downs, J.A. (2007). Dual Chromatin Remodeling Roles for RSC during DNA Double Strand Break Induction and Repair at the Yeast MAT Locus. Journal of Biological Chemistry *282*, 27693–27701.

Kesti, T., Flick, K., Keränen, S., Syväoja, J.E., and Wittenberg, C. (1999). DNA polymerase epsilon catalytic domains are dispensable for DNA replication, DNA repair, and cell viability. Molecular Cell *3*, 679–685.

Korzhnev, D.M., and Hadden, M.K. (2016). Targeting the Translesion Synthesis Pathway for the Development of Anti-Cancer Chemotherapeutics. J. Med. Chem. *59*, 9321–9336.

Kramer, K.M., Brock, J.A., Bloom, K., Moore, J.K., and Haber, J.E. (1994). Two different types of double-strand breaks in Saccharomyces cerevisiae are repaired by similar RAD52-independent, nonhomologous recombination events. Molecular and Cellular Biology *14*, 1293–1301.

Krasner, D.S., Daley, J.M., Sung, P., and Niu, H. (2015). Interplay between Ku and Replication Protein A in the Restriction of Exo1-mediated DNA Break End Resection. Journal of Biological Chemistry *290*, 18806–18816.

Krejci, L., Altmannova, V., Spirek, M., and Zhao, X. (2012). Homologous recombination and its regulation. Nucleic Acids Research *40*, 5795–5818.

Kubota, T., Katou, Y., Nakato, R., Shirahige, K., and Donaldson, A.D. (2015). Replication-Coupled PCNA Unloading by the Elg1 Complex Occurs Genome-wide and Requires Okazaki Fragment Ligation. CellReports *12*, 774–787.

Kubota, T., Nishimura, K., Kanemaki, M.T., and Donaldson, A.D. (2013). Short Article. Molecular Cell *50*, 273–280.

Kubota, Y., Nash, R.A., Klungland, A., Schär, P., Barnes, D.E., and Lindahl, T. (1996). Reconstitution of DNA base excision-repair with purified human proteins:

interaction between DNA polymerase beta and the XRCC1 protein. The EMBO Journal *15*, 6662–6670.

Kunkel, T.A. (2004). DNA Replication Fidelity. Journal of Biological Chemistry *279*, 16895–16898.

Kunkel, T.A., and Burgers, P.M. (2014). news and views. Nat Struct Mol Biol *21*, 649–651.

Kurat, C.F., Yeeles, J.T.P., Patel, H., Early, A., and Diffley, J.F.X. (2017). Chromatin Controls DNA Replication Origin Selection, Lagging-Strand Synthesis, and Replication Fork Rates. Molecular Cell *65*, 117–130.

Kurdyukov, S., and Bullock, M. (2016). DNA Methylation Analysis: Choosing the Right Method. Biology *5*, 3.

Kwon, H., Imbalzano, A.N., Khavari, P.A., Kingston, R.E., and Green, M.R. (1994). Nucleosome disruption and enhancement of activator binding by a human SW1/SNF complex. Nature *370*, 477–481.

Kwon, S.-J., Lee, S.-K., Na, J., Lee, S.-A., Lee, H.-S., Park, J.-H., Chung, J.-K., Youn, H., and Kwon, J. (2015). Targeting BRG1 chromatin remodeler via its bromodomain for enhanced tumor cell radiosensitivity in vitro and in vivo. Molecular Cancer Therapeutics *14*, 597–607.

Lakshmipathy, U., and Campbell, C. (1999). The human DNA ligase III gene encodes nuclear and mitochondrial proteins. Molecular and Cellular Biology *19*, 3869–3876.

Lakshmipathy, U., and Campbell, C. (2000). Mitochondrial DNA ligase III function is independent of Xrcc1. Nucleic Acids Research *28*, 3880–3886.

Lakshmipathy, U., and Campbell, C. (2001). Antisense-mediated decrease in DNA ligase III expression results in reduced mitochondrial DNA integrity. Nucleic Acids Research *29*, 668–676.

Langston, L.D., and O'Donnell, M. (2008). DNA polymerase delta is highly processive with proliferating cell nuclear antigen and undergoes collision release upon completing DNA. J. Biol. Chem. *283*, 29522–29531.

Lazzaro, F., Novarina, D., Amara, F., Watt, D.L., Stone, J.E., Costanzo, V., Burgers, P.M., Kunkel, T.A., Plevani, P., and Muzi-Falconi, M. (2012). RNase H and Postreplication Repair Protect Cells from Ribonucleotides Incorporated in DNA. Molecular Cell *45*, 99–110.

Le Chalony, C., Hoffschir, F., Gauthier, L.R., Gross, J., Biard, D.S., Boussin, F.D., and Pennaneach, V. (2012). Partial complementation of a DNA ligase I deficiency by DNA ligase III and its impact on cell survival and telomere stability in mammalian cells.

Cell. Mol. Life Sci. *69*, 2933–2949.

Lee, H.-S., Park, J.-H., Kim, S.-J., Kwon, S.-J., and Kwon, J. (2010). A cooperative activation loop among SWI/SNF, γ-H2AX and H3 acetylation for DNA double-strand break repair. The EMBO Journal 1–12.

Lee, K.-J., Saha, J., Sun, J., Fattah, K.R., Wang, S.-C., Jakob, B., Chi, L., Wang, S.-Y., Taucher-Scholz, G., Davis, A.J., et al. (2015). Phosphorylation of Ku dictates DNA double-strand break (DSB) repair pathway choice in S phase. Nucleic Acids Research.

Lee, R.S., Stewart, C., Carter, S.L., Ambrogio, L., Cibulskis, K., Sougnez, C., Lawrence, M.S., Auclair, D., Mora, J., Golub, T.R., et al. (2012). A remarkably simple genome underlies highly malignant pediatric rhabdoid cancers. J. Clin. Invest. *122*, 2983–2988.

Lee, S.E., Moore, J.K., Holmes, A., Umezu, K., Kolodner, R.D., and Haber, J.E. (1998). Saccharomyces Ku70, mre11/rad50 and RPA proteins regulate adaptation to G2/M arrest after DNA damage. Multiple Values Selected *94*, 399–409.

Leung, K.H.T., Abou El Hassan, M., and Bremner, R. (2013). A rapid and efficient method to purify proteins at replication forks under native conditions. BioTechniques *55*, 204–206.

Levin, D.S., Bai, W., Yao, N., O'Donnell, M., and Tomkinson, A.E. (1997). An interaction between DNA ligase I and proliferating cell nuclear antigen: implications for Okazaki fragment synthesis and joining. Proc. Natl. Acad. Sci. U.S.a. *94*, 12863–12868.

Levin, D.S., McKenna, A.E., Motycka, T.A., Matsumoto, Y., and Tomkinson, A.E. (2000). Interaction between PCNA and DNA ligase I is critical for joining of Okazaki fragments and long-patch base-excision repair. Curr. Biol. *10*, 919–922.

Li, Q., Zhou, H., Wurtele, H., Davies, B., Horazdovsky, B., Verreault, A., and Zhang, Z. (2008). Acetylation of Histone H3 Lysine 56 Regulates Replication-Coupled Nucleosome Assembly. Cell *134*, 244–255.

Li, X., and Tyler, J.K. (2016). Nucleosome disassembly during human non-homologous end joining followed by concerted HIRA- and CAF-1-dependent reassembly. Elife *5*.

Li, Y., and Tollefsbol, T.O. (2011). DNA Methylation Detection: Bisulfite Genomic Sequencing Analysis. In Methods in Molecular Biology, (Totowa, NJ: Humana Press), pp. 11–21.

Lia, G., Praly, E., Ferreira, H., Stockdale, C., Tse-Dinh, Y.C., Dunlap, D., Croquette, V., Bensimon, D., and Owen-Hughes, T. (2006). Direct Observation of DNA Distortion by the RSC Complex. Molecular Cell *21*, 417–425.

Lieber, M.R. (2010a). The Mechanism of Double-Strand DNA Break Repair by the Nonhomologous DNA End-Joining Pathway. Annu. Rev. Biochem. *79*, 181–211.

Lieber, M.R. (2010b). NHEJ and its backup pathways in chromosomal translocations. Nat Struct Mol Biol *17*, 393–395.

Lindahl, T. (1993). Instability and decay of the primary structure of DNA. Nature *362*, 709–715.

Liu, S., Xu, Z., Leng, H., Zheng, P., Yang, J., Chen, K., Feng, J., and Li, Q. (2017). RPA binds histone H3-H4 and functions in DNA replication-coupled nucleosome assembly. Science *355*, 415–420.

Liu, W.H., Roemer, S.C., Port, A.M., and Churchill, M.E.A. (2012). CAF-1-induced oligomerization of histones H3/H4 and mutually exclusive interactions with Asf1 guide H3/H4 transitions among histone chaperones and DNA. Nucleic Acids Research *40*, 11229–11239.

Liu, X., Gao, Q., Li, P., Zhao, Q., Zhang, J., Li, J., Koseki, H., and Wong, J. (2013). UHRF1 targets DNMT1 for DNA methylation through cooperative binding of hemi-methylated DNA and methylated H3K9. Nature Communications *4*, 1563.

Llorente, B., and Symington, L.S. (2004). The Mre11 Nuclease Is Not Required for 5" to 3" Resection at Multiple HO-Induced Double-Strand Breaks. Molecular and Cellular Biology *24*, 9682–9694.

Lopez-Contreras, A.J., Ruppen, I., Nieto-Soler, M., Murga, M., Rodriguez-Acebes, S., Remeseiro, S., Rodrigo-Perez, S., Rojas, A.M., Mendez, J., Muñoz, J., et al. (2013). A Proteomic Characterization of Factors Enriched at Nascent DNA Molecules. CellReports *3*, 1105–1116.

Lorch, Y., Maier-Davis, B., and Kornberg, R.D. (2006). Chromatin remodeling by nucleosome disassembly in vitro. Proc. Natl. Acad. Sci. U.S.a. *103*, 3090–3093.

Lord, C.J., and Ashworth, A. (2008). Targeted therapy for cancer using PARP inhibitors. Current Opinion in Pharmacology *8*, 363–369.

Lou, Z., Minter-Dykhouse, K., Franco, S., Gostissa, M., Rivera, M.A., Celeste, A., Manis, J.P., van Deursen, J., Nussenzweig, A., Paull, T.T., et al. (2006). MDC1 Maintains Genomic Stability by Participating in the Amplification of ATM-Dependent DNA Damage Signals. Molecular Cell *21*, 187–200.

Lu, X., Tan, C.K., Zhou, J.Q., You, M., Carastro, L.M., Downey, K.M., and So, A.G. (2002). Direct Interaction of Proliferating Cell Nuclear Antigen with the Small Subunit of DNA Polymerase. Journal of Biological Chemistry *277*, 24340–24345.

Luger, K., and Richmond, T.J. (1998). The histone tails of the nucleosome. Curr. Opin.

Genet. Dev. *8*, 140–146.

Luger, K., Mäder, A.W., Richmond, R.K., Sargent, D.F., and Richmond, T.J. (1997). Crystal structure of the nucleosome core particle at 2.8 A resolution. Nature *389*, 251–260.

Luger, K., Dechassa, M.L., and Tremethick, D.J. (2012). New insights into nucleosome andchromatin structure: an ordered stateor a disordered affair? Nature Reviews Molecular Cell Biology *13*, 436–447.

Lukas, C., Melander, F., Stucki, M., Falck, J., Bekker-Jensen, S., Goldberg, M., Lerenthal, Y., Jackson, S.P., Bartek, J., and Lukas, J. (2004). Mdc1 couples DNA double-strand break recognition by Nbs1 with its H2AX-dependent chromatin retention. The EMBO Journal *23*, 2674–2683.

Lydeard, J.R., Lipkin-Moore, Z., Sheu, Y.-J., Stillman, B., Burgers, P.M., and Haber, J.E. (2010). Break-induced replication requires all essential DNA replication factors except those specific for pre-RC assembly. Genes & Development *24*, 1133–1144.

MacAlpine, D.M., and Almouzni, G. (2013). Chromatin and DNA Replication. Cold Spring Harbor Perspectives in Biology *5*, a010207–a010207.

Mackey, Z.B., Niedergang, C., Murcia, J.M., Leppard, J., Au, K., Chen, J., de Murcia, G., and Tomkinson, A.E. (1999). DNA ligase III is recruited to DNA strand breaks by a zinc finger motif homologous to that of poly(ADP-ribose) polymerase. Identification of two functionally distinct DNA binding regions within DNA ligase III. J. Biol. Chem. *274*, 21679–21687.

Mackey, Z.B., Ramos, W., Levin, D.S., Walter, C.A., McCarrey, J.R., and Tomkinson, A.E. (1997). An alternative splicing event which occurs in mouse pachytene spermatocytes generates a form of DNA ligase III with distinct biochemical properties that may function in meiotic recombination. Molecular and Cellular Biology *17*, 989–998.

Makridakis, N.M. (2012). Translesion DNA polymerases and cancer. 1–8.

Mao, P., Kyriss, M.N.M., Hodges, A.J., Duan, M., Morris, R.T., Lavine, M.D., Topping, T.B., Gloss, L.M., and Wyrick, J.J. (2016). A basic domain in the histone H2B N-terminal tail is important for nucleosome assembly by FACT. Nucleic Acids Research gkw588.

Margueron, R., and Reinberg, D. (2010). Chromatin structure and theinheritance of epigenetic information. Nat Rev Genet *11*, 285–296.

Marushige, Y., and Marushige, K. (1978). Chapter 5 Methods for Isolation of Nuclei from Spermatozoa. In Methods in Cell Biology, (Elsevier), pp. 59–73.

Matsumoto, Y., Kim, K., Hurwitz, J., Gary, R., Levin, D.S., Tomkinson, A.E., and Park, M.S. (1999). Reconstitution of proliferating cell nuclear antigen-dependent repair of apurinic/apyrimidinic sites with purified human proteins. J. Biol. Chem. *274*, 33703–33708.

Mayes, K., Qiu, Z., Alhazmi, A., and Landry, J.W. (2014). ATP-Dependent Chromatin Remodeling Complexes as Novel Targets for Cancer Therapy. In Advances in Cancer Research, (Elsevier), pp. 183–233.

McKenna, E.S., Sansam, C.G., Cho, Y.J., Greulich, H., Evans, J.A., Thom, C.S., Moreau, L.A., Biegel, J.A., Pomeroy, S.L., and Roberts, C.W.M. (2008). Loss of the Epigenetic Tumor Suppressor SNF5 Leads to Cancer without Genomic Instability. Molecular and Cellular Biology *28*, 6223–6233.

McKinnon, P.J., and Caldecott, K.W. (2007). DNA Strand Break Repair and Human Genetic Disease. Annu. Rev. Genom. Human Genet. *8*, 37–55.

Mehta, A., and Haber, J.E. (2014). Sources of DNA double-strand breaks and models of recombinational DNA repair. Cold Spring Harbor Perspectives in Biology *6*, a016428.

Mello, J.A., Silljé, H.H.W., Roche, D.M.J., Kirschner, D.B., Nigg, E.A., and Almouzni, G. (2002). Human Asf1 and CAF-1 interact and synergize in a repair-coupled nucleosome assembly pathway. EMBO Rep *3*, 329–334.

Meneghini, R. (1997). Iron homeostasis, oxidative stress, and DNA damage. Free Radical Biology and Medicine *23*, 783–792.

Meng, H., Cao, Y., Qin, J., Song, X., Zhang, Q., Shi, Y., and Cao, L. (2015). DNA methylation, its mediators and genome integrity. Int. J. Biol. Sci. *11*, 604–617.

Metcalf, D., Nossal, G.J., Warner, N.L., Miller, J.F., Mandel, T.E., Layton, J.E., and Gutman, G.A. (1975). Growth of B-lymphocyte colonies in vitro. J. Exp. Med. *142*, 1534–1549.

Méndez, J., and Stillman, B. (2000). Chromatin association of human origin recognition complex, cdc6, and minichromosome maintenance proteins during the cell cycle: assembly of prereplication complexes in late mitosis. Molecular and Cellular Biology *20*, 8602–8612.

Ménissier de Murcia, J., Ricoul, M., Tartier, L., Niedergang, C., Huber, A., Dantzer, F., Schreiber, V., Amé, J.-C., Dierich, A., LeMeur, M., et al. (2003). Functional interaction between PARP-1 and PARP-2 in chromosome stability and embryonic development in mouse. The EMBO Journal *22*, 2255–2263.

Mimitou, E.P., and Symington, L.S. (2008). Sae2, Exo1 and Sgs1 collaborate in DNA double-strand break processing. Nature *455*, 770–774.

Mimitou, E.P., and Symington, L.S. (2010). Ku prevents Exo1 and Sgs1-dependent resection of DNA ends in the absence of a functional MRX complex or Sae2. The EMBO Journal *29*, 3358–3369.

Min, W., Bruhn, C., Grigaravicius, P., Zhou, Z.-W., Li, F., Krüger, A., Siddeek, B., Greulich, K.-O., Popp, O., Meisezahl, C., et al. (2013). Poly(ADP-ribose) binding to Chk1 at stalled replication forks is required for S-phase checkpoint activation. Nature Communications *4*, 2993.

Mitra, A.K., Singh, A., Indian Genome Variation Consortium, and Rath, S.K. (2014). LIG1 polymorphisms: the Indian scenario. J. Genet. *93*, 459–469.

Mladenov, E., Magin, S., Soni, A., and Iliakis, G. (2016). Seminars in Cancer Biology. Semin. Cancer Biol. *37-38*, 51–64.

Modrich, P. (2006). Mechanisms in eukaryotic mismatch repair. J. Biol. Chem. *281*, 30305–30309.

Montecucco, A., Rossi, R., Levin, D.S., Gary, R., Park, M.S., Motycka, T.A., Ciarrocchi, G., Villa, A., Biamonti, G., and Tomkinson, A.E. (1998). DNA ligase I is recruited to sites of DNA replication by an interaction with proliferating cell nuclear antigen: identification of a common targeting mechanism for the assembly of replication factories. The EMBO Journal *17*, 3786–3795.

Montecucco, A., Savini, E., Weighardt, F., Rossi, R., Ciarrocchi, G., Villa, A., and Biamonti, G. (1995). The N-terminal domain of human DNA ligase I contains the nuclear localization signal and directs the enzyme to sites of DNA replication. The EMBO Journal *14*, 5379–5386.

Moser, J., Kool, H., Giakzidis, I., Caldecott, K., Mullenders, L.H.F., and Fousteri, M.I. (2007). Sealing of Chromosomal DNA Nicks during Nucleotide Excision Repair Requires XRCC1 and DNA Ligase IIIα in a Cell-Cycle-Specific Manner. Molecular Cell *27*, 311–323.

Moynahan, M.E., and Jasin, M. (1997). Loss of heterozygosity induced by a chromosomal double-strand break. Proc. Natl. Acad. Sci. U.S.a. *94*, 8988–8993.

Mueller-Planitz, F., Klinker, H., and Becker, P.B. (2013). Nucleosome sliding mechanisms: new twists in a looped history. Nat Struct Mol Biol *20*, 1026–1032.

Musselman, C.A., Lalonde, M.-E., Côté, J., and Kutateladze, T.G. (2012). Perceiving the epigenetic landscape through histone readers. Nature Publishing Group *19*, 1218–1227.

Muzi-Falconi, M., Giannattasio, M., Foiani, M., and Plevani, P. (2003). The DNA Polymerase _-Primase Complex: Multiple Functions and Interactions. The Scientific World JOURNAL *3*, 21–33.

Nakamura, M., Kondo, S., Sugai, M., Nazarea, M., Imamura, S., and Honjo, T. (1996). High frequency class switching of an IgM+ B lymphoma clone CH12F3 to IgA+ cells. Int. Immunol. *8*, 193–201.

Nash, R.A., Caldecott, K.W., Barnes, D.E., and Lindahl, T. (1997). XRCC1 protein interacts with one of two distinct forms of DNA ligase III. Biochemistry *36*, 5207–5211.

Newman, E.A., Lu, F., Bashllari, D., Wang, L., Opipari, A.W., and Castle, V.P. (2015). Alternative NHEJ Pathway Components Are Therapeutic Targets in High-Risk Neuroblastoma. Molecular Cancer Research *13*, 470–482.

Ng, H.-H., Robert, F., Young, R.A., and Struhl, K. (2002). Genome-wide location and regulated recruitment of the RSC nucleosome-remodeling complex. Genes & Development *16*, 806–819.

Nieduszynski, C.A. (2006). Genome-wide identification of replication origins in yeast by comparative genomics. Genes & Development *20*, 1874–1879.

Noda, A., Hirai, Y., Hamasaki, K., Mitani, H., Nakamura, N., and Kodama, Y. (2013). Unrepairable DNA double-strand breaks that are generated by ionising radiation determine the fate of normal human cells. J. Cell. Sci. *125*, 5280–5287.

Nussenzweig, A., and Nussenzweig, M.C. (2007). A Backup DNA Repair Pathway Moves to the Forefront. Cell *131*, 223–225.

Oakley, G.G., and Patrick, S.M. (2010). Replication protein A: directing traffic at the intersection of replication and repair. Front Biosci (Landmark Ed) *15*, 883–900.

Ogawa, T., and Okazaki, T. (1980). Discontinuous DNA replication. Annu. Rev. Biochem. *49*, 421–457.

Oh, J., Al-Zain, A., Cannavo, E., Cejka, P., and Symington, L.S. (2016). Xrs2 Dependent and Independent Functions of the Mre11-Rad50 Complex. Molecular Cell 1–22.

Okano, S., Lan, L., Caldecott, K.W., Mori, T., and Yasui, A. (2003). Spatial and Temporal Cellular Responses to Single-Strand Breaks in Human Cells. Molecular and Cellular Biology *23*, 3974–3981.

Okano, S., Lan, L., Tomkinson, A.E., and Yasui, A. (2005). Translocation of XRCC1 and DNA ligase IIIalpha from centrosomes to chromosomes in response to DNA damage in mitotic human cells. Nucleic Acids Research *33*, 422–429.

Olcina, M.M., Giaccia, A.J., and Hammond, E.M. (2016). Isolation of Proteins on Nascent DNA in Hypoxia and Reoxygenation Conditions. In Advances in Experimental Medicine and Biology, (Cham: Springer International Publishing), pp. 27–40.

Osley, M.A., Tsukuda, T., and Nickoloff, J.A. (2007). ATP-dependent chromatin remodeling factors and DNA damage repair. Mutation Research/Fundamental and Molecular Mechanisms of Mutagenesis *618*, 65–80.

Oum, J.H., Seong, C., Kwon, Y., Ji, J.H., Sid, A., Ramakrishnan, S., Ira, G., Malkova, A., Sung, P., Lee, S.E., et al. (2011). RSC Facilitates Rad59-Dependent Homologous Recombination between Sister Chromatids by Promoting Cohesin Loading at DNA Double-Strand Breaks. Molecular and Cellular Biology *31*, 3924–3937.

O'Driscoll, M., Cerosaletti, K.M., Girard, P.M., Dai, Y., Stumm, M., Kysela, B., Hirsch, B., Gennery, A., Palmer, S.E., Seidel, J., et al. (2001). DNA ligase IV mutations identified in patients exhibiting developmental delay and immunodeficiency. Molecular Cell *8*, 1175–1185.

Pacaud, R., Brocard, E., Lalier, L., Hervouet, E., Vallette, F.M., and Cartron, P.-F. (2014). The DNMT1/PCNA/UHRF1 disruption induces tumorigenesis characterized by similar genetic and epigenetic signatures. Sci. Rep. *4*.

Paedon, J.F., and Wilkins, M.H.F. (1972). A super-coil model for nucleohistone. J. Mol. Biol. *68*, 115–124.

Panier, S., and Boulton, S.J. (2013). Double-strand break repair:53BP1 comes into focus. Nature Reviews Molecular Cell Biology *15*, 7–18.

Panier, S., and Durocher, D. (2013). Push back to respond better: regulatory inhibition of the DNA double-strand break response. Nature Reviews Molecular Cell Biology *14*, 661–672.

Park, J.-H., Park, E.-J., Lee, H.-S., Kim, S.-J., Hur, S.-K., Imbalzano, A.N., and Kwon, J. (2006). Mammalian SWI/SNF complexes facilitate DNA double-strand break repair by promoting gamma-H2AX induction. The EMBO Journal *25*, 3986–3997.

Pascal, J.M., O'Brien, P.J., Tomkinson, A.E., and Ellenberger, T. (2004). Human DNA ligase I completely encircles and partially unwinds nicked DNA. Nature *432*, 473–478.

Perera, R.L., Torella, R., Klinge, S., Kilkenny, M.L., Maman, J.D., and Pellegrini, L. (2013). Mechanism for priming DNA synthesis by yeast DNA polymerase α. Elife *2*, e00482.

Peterson, C.L., and Herskowitz, I. (1992). Characterization of the yeast SWI1, SWI2, and SWI3 genes, which encode a global activator of transcription. Cell *68*, 573–583.

Peterson, C.L., Dingwall, A., and Scott, M.P. (1994). Five SWI/SNF gene products are components of a large multisubunit complex required for transcriptional enhancement. Proc. Natl. Acad. Sci. U.S.a. *91*, 2905–2908.

Postow, L., Ghenoiu, C., Woo, E.M., Krutchinsky, A.N., Chait, B.T., and Funabiki, H. (2008). Ku80 removal from DNA through double strand break–induced ubiquitylation. J. Cell Biol. *182*, 467–479.

Presolski, S.I., Hong, V.P., and Finn, M.G. (2009). Copper-Catalyzed Azide-Alkyne Click Chemistry for Bioconjugation (Hoboken, NJ, USA: John Wiley & Sons, Inc.).

Price, B.D., and D'Andrea, A.D. (2013). Chromatin Remodeling at DNA Double-Strand Breaks. Cell *152*, 1344–1354.

Probst, A.V., Dunleavy, E., and Almouzni, G. (2009). Epigenetic inheritance during the cell cycle. Nature Reviews Molecular Cell Biology *10*, 192–206.

Puebla-Osorio, N., Lacey, D.B., Alt, F.W., and Zhu, C. (2006). Early Embryonic Lethality Due to Targeted Inactivation of DNA Ligase III. Molecular and Cellular Biology *26*, 3935–3941.

Racki, L.R., Yang, J.G., Naber, N., Partensky, P.D., Acevedo, A., Purcell, T.J., Cooke, R., Cheng, Y., and Narlikar, G.J. (2009). The chromatin remodeller ACF acts as a dimeric motor to space nucleosomes. Nature *462*, 1016–1021.

Ran, F.A., Hsu, P.D., Wright, J., Agarwala, V., Scott, D.A., and Zhang, F. (2013). Genome engineering using the CRISPR-Cas9 system. Nature Protocols *8*, 2281–2308.

Rassool, F.V., and Tomkinson, A.E. (2010). Targeting abnormal DNA double strand break repair in cancer. Cell. Mol. Life Sci. *67*, 3699–3710.

Rathke, C., Baarends, W.M., Awe, S., and Renkawitz-Pohl, R. (2014). Biochimica et Biophysica Acta. BBA - Gene Regulatory Mechanisms *1839*, 155–168.

Rathmell, W.K., and Chu, G. (1994). A DNA end-binding factor involved in double-strand break repair and V(D)J recombination. Molecular and Cellular Biology *14*, 4741–4748.

Rayner, E., van Gool, I.C., Palles, C., Kearsey, S.E., Bosse, T., Tomlinson, I., and Church, D.N. (2016). A panoply of errors: polymeraseproofreading domain mutationsin cancer. Nat Rev Cancer *16*, 71–81.

Reijns, M.A.M., Rabe, B., Rigby, R.E., Mill, P., Astell, K.R., Lettice, L.A., Boyle, S., Leitch, A., Keighren, M., Kilanowski, F., et al. (2012). Enzymatic Removal of Ribonucleotides from DNA Is Essential for Mammalian Genome Integrity and Development. Cell *149*, 1008–1022.

Riballo, E., Critchlow, S.E., Teo, S.H., Doherty, A.J., Priestley, A., Broughton, B., Kysela, B., Beamish, H., Plowman, N., Arlett, C.F., et al. (1999). Identification of a defect in DNA ligase IV in a radiosensitive leukaemia patient. Curr. Biol. *9*, 699–702.

Rodier, F., Munoz, D.P., Teachenor, R., Chu, V., Le, O., Bhaumik, D., Coppe, J.P., Campeau, E., Beausejour, C.M., Kim, S.H., et al. (2010). DNA-SCARS: distinct nuclear structures that sustain damage-induced senescence growth arrest and inflammatory cytokine secretion. J. Cell. Sci. *124*, 68–81.

Rogakou, E.P., Pilch, D.R., Orr, A.H., Ivanova, V.S., and Bonner, W.M. (1998). DNA double-stranded breaks induce histone H2AX phosphorylation on serine 139. J. Biol. Chem. *273*, 5858–5868.

Roos, W.P., and Kaina, B. (2013). Cancer Letters. Cancer Letters *332*, 237–248.

Rossetto, D., Truman, A.W., Kron, S.J., and Côté, J. (2010). Epigenetic Modifications in Double-Strand Break DNA Damage Signaling and Repair. Clinical Cancer Research *16*, 4543–4552.

Routh, A., Sandin, S., and Rhodes, D. (2008). Nucleosome repeat length and linker histone stoichiometry determine chromatin fiber structure. Proc. Natl. Acad. Sci. U.S.a. *105*, 8872–8877.

Roy, R., Chun, J., and Powell, S.N. (2012). BRCA1and BRCA2: different roles in a common pathway of genome protection. 1–11.

Saha, A., Wittmeyer, J., and Cairns, B.R. (2005). Chromatin remodeling through directional DNA translocation from an internal nucleosomal site. Nat Struct Mol Biol *12*, 747–755.

Saleh-Gohari, N., Bryant, H.E., Schultz, N., Parker, K.M., Cassel, T.N., and Helleday, T. (2005). Spontaneous homologous recombination is induced by collapsed replication forks that are caused by endogenous DNA single-strand breaks. Molecular and Cellular Biology *25*, 7158–7169.

San Filippo, J., Sung, P., and Klein, H. (2008). Mechanism of Eukaryotic Homologous Recombination. Annu. Rev. Biochem. *77*, 229–257.

Schnitzler, G.R., Cheung, C.L., Hafner, J.H., Saurin, A.J., Kingston, R.E., and Lieber, C.M. (2001). Direct Imaging of Human SWI/SNF-Remodeled Mono- and Polynucleosomes by Atomic Force Microscopy Employing Carbon Nanotube Tips. Molecular and Cellular Biology *21*, 8504–8511.

Schulz, L.L. (2006). The histone chaperone ASF1 localizes to active DNA replication forks to mediate efficient DNA replication. The FASEB Journal.

Schwabish, M.A., and Struhl, K. (2007). The Swi/Snf Complex Is Important for Histone Eviction during Transcriptional Activation and RNA Polymerase II Elongation In Vivo. Molecular and Cellular Biology *27*, 6987–6995.

Sfeir, A., and Symington, L.S. (2015). Microhomology-Mediated End Joining: A Back-

up Survival Mechanism or DedicatedPathway? Trends Biochem. Sci. *40*, 701–714.

Shao, Z., Davis, A.J., Fattah, K.R., So, S., Sun, J., Lee, K.-J., Harrison, L., Yang, J., and Chen, D.J. (2012). Persistently bound Ku at DNA ends attenuates DNA end resection and homologous recombination. DNA Repair *11*, 310–316.

Shen, X., Mizuguchi, G., Hamiche, A., and Wu, C. (2000). A chromatin remodelling complex involved in transcription and DNA processing. Nature *406*, 541–544.

Shibahara, K., and Stillman, B. (1999). Replication-dependent marking of DNA by PCNA facilitates CAF-1-coupled inheritance of chromatin. Cell *96*, 575–585.

Shim, E.Y., Hong, S.J., Oum, J.H., Yanez, Y., Zhang, Y., and Lee, S.E. (2007). RSC Mobilizes Nucleosomes To Improve Accessibility of Repair Machinery to the Damaged Chromatin. Molecular and Cellular Biology *27*, 1602–1613.

Shim, E.Y., Chung, W.-H., Nicolette, M.L., Zhang, Y., Davis, M., Zhu, Z., Paull, T.T., Ira, G., and Lee, S.E. (2010). Saccharomyces cerevisiae Mre11/Rad50/Xrs2 and Ku proteins regulate association of Exo1 and Dna2 with DNA breaks. The EMBO Journal *29*, 3370–3380.

Shim, E.Y., Ma, J.-L., Oum, J.-H., Yanez, Y., and Lee, S.E. (2005). The yeast chromatin remodeler RSC complex facilitates end joining repair of DNA double-strand breaks. Molecular and Cellular Biology *25*, 3934–3944.

Shogren-Knaak, M., Ishii, H., Sun, J.-M., Pazin, M.J., Davie, J.R., and Peterson, C.L. (2006). Histone H4-K16 acetylation controls chromatin structure and protein interactions. Science *311*, 844–847.

Sibanda, B.L., Critchlow, S.E., Begun, J., Pei, X.Y., Jackson, S.P., Blundell, T.L., and Pellegrini, L. (2001). Crystal structure of an Xrcc4-DNA ligase IV complex. Nat. Struct. Biol. *8*, 1015–1019.

Simsek, D., and Jasin, M. (2010). Alternative end-joining is suppressed by the canonical NHEJ component Xrcc4–ligase IV during chromosomal translocation formation. Nat Struct Mol Biol *17*, 410–416.

Simsek, D., Brunet, E., Wong, S.Y.-W., Katyal, S., Gao, Y., McKinnon, P.J., Lou, J., Zhang, L., Li, J., Rebar, E.J., et al. (2011). DNA Ligase III Promotes Alternative Nonhomologous End-Joining during Chromosomal Translocation Formation. PLoS Genet. *7*, e1002080.

Simsek, D., Furda, A., Gao, Y., Artus, J., Brunet, E., Hadjantonakis, A.-K., Van Houten, B., Shuman, S., McKinnon, P.J., and Jasin, M. (2012). Crucial role for DNA ligase III in mitochondria but not in Xrcc1-dependent repair. Nature *471*, 245–248.

Sinha, K.K., Gross, J.D., and Narlikar, G.J. (2017). Distortion of histone octamer core

promotes nucleosome mobilization by a chromatin remodeler. Science *355*, eaaa3761.

Sirbu, B.M., Couch, F.B., Feigerle, J.T., Bhaskara, S., Hiebert, S.W., and Cortez, D. (2011). Analysis of protein dynamics at active, stalled, and collapsed replication forks. Genes & Development *25*, 1320–1327.

Sirbu, B.M., McDonald, W.H., Dungrawala, H., Badu-Nkansah, A., Kavanaugh, G.M., Chen, Y., Tabb, D.L., and Cortez, D. (2013). Identification of Proteins at Active, Stalled, and Collapsed Replication Forks Using Isolation of Proteins on Nascent DNA (iPOND) Coupled with Mass Spectrometry. Journal of Biological Chemistry *288*, 31458–31467.

Sirbu, B.M., Couch, F.B., and Cortez, D. (2012). Monitoring the spatiotemporal dynamics of proteins at replication forks and in assembled chromatin using isolation of proteins on nascent DNA. Nature Protocols *7*, 594–605.

Skulte, K.A., Phan, L., Clark, S.J., and Taberlay, P.C. (2014). Chromatin remodeler mutations in human cancers: epigenetic implications. Epigenomics *6*, 397–414.

Smith, D.J., and Whitehouse, I. (2013). Intrinsic coupling of lagging-strand synthesis to chromatin assembly. Nature *483*, 434–438.

Smith, Z.D., and Meissner, A. (2013). DNA methylation: roles inmammalian development. Nat Rev Genet *14*, 204–220.

Smith-Roe, S.L., Nakamura, J., Holley, D., Chastain, P.D., Rosson, G.B., Simpson, D.A., Ridpath, J.R., Kaufman, D.G., Kaufmann, W.K., and Bultman, S.J. (2015). SWI/SNF complexes are required for full activation of the DNA-damage response. Oncotarget *6*, 732–745.

Sobel, R.E., Cook, R.G., Perry, C.A., Annunziato, A.T., and Allis, C.D. (1995). Conservation of deposition-related acetylation sites in newly synthesized histones H3 and H4. Proc. Natl. Acad. Sci. U.S.a. *92*, 1237–1241.

Song, W., Levin, D.S., Varkey, J., Post, S., Bermudez, V.P., Hurwitz, J., and Tomkinson, A.E. (2007). A Conserved Physical and Functional Interaction between the Cell Cycle Checkpoint Clamp Loader and DNA Ligase I of Eukaryotes. Journal of Biological Chemistry *282*, 22721–22730.

Sonoda, E., Sasaki, M.S., Buerstedde, J.M., Bezzubova, O., Shinohara, A., Ogawa, H., Takata, M., Yamaguchi-Iwai, Y., and Takeda, S. (1998). Rad51-deficient vertebrate cells accumulate chromosomal breaks prior to cell death. The EMBO Journal *17*, 598–608.

Soza, S., Leva, V., Vago, R., Ferrari, G., Mazzini, G., Biamonti, G., and Montecucco, A. (2009). DNA Ligase I Deficiency Leads to Replication-Dependent DNA Damage and

Impacts Cell Morphology without Blocking Cell Cycle Progression. Molecular and Cellular Biology *29*, 2032–2041.

Sporbert, A. (2005). PCNA acts as a stationary loading platform for transiently interacting Okazaki fragment maturation proteins. Nucleic Acids Research *33*, 3521–3528.

Stathopulos, P.B., Scholz, G.A., Hwang, Y.-M., Rumfeldt, J.A.O., Lepock, J.R., and Meiering, E.M. (2004). Sonication of proteins causes formation of aggregates that resemble amyloid. Protein Sci. *13*, 3017–3027.

Stern, M., Jensen, R., and Herskowitz, I. (1984). Five SWI genes are required for expression of the HO gene in yeast. J. Mol. Biol. *178*, 853–868.

Stewart, G.S., Wang, B., Bignell, C.R., Taylor, A.M.R., and Elledge, S.J. (2003). MDC1 is a mediator of the mammalian DNA damage checkpoint. Nature *421*, 961–966.

Strahl, B.D., and Allis, C.D. (2000). The language of covalent histone modifications. Nature *403*, 41–45.

Stuart, S.E., Clawson, G.A., Rottman, F.M., and Patterson, R.J. (1977). RNA transport in isolated myeloma nuclei. Transport from membrane-denuded nuclei. J. Cell Biol. *72*, 57–66.

Stunnenberg, H.G., and Vermeulen, M. (2011). Towards cracking the epigenetic code using a combination of high-throughput epigenomics and quantitative mass spectrometry-based proteomics. Bioessays *33*, 547–551.

Sudarsanam, P., and Winston, F. (2000). The Swi/Snf family nucleosome-remodeling complexes and transcriptional control. Trends Genet. *16*, 345–351.

Sudarsanam, P., Iyer, V.R., Brown, P.O., and Winston, F. (2000). Whole-genome expression analysis of snf/swi mutants of Saccharomyces cerevisiae. Proc. Natl. Acad. Sci. U.S.a. *97*, 3364–3369.

Sung, P., and Klein, H. (2006). Mechanism of homologous recombination: mediators and helicases take on regulatory functions. Nature Reviews Molecular Cell Biology *7*, 739–750.

Symington, L.S. (2016). Mechanism and regulation of DNA end resection in eukaryotes. Critical Reviews in Biochemistry and Molecular Biology *51*, 195–212.

Symington, L.S., and Gautier, J. (2011). Double-strand break end resection and repair pathway choice. Annu. Rev. Genet. *45*, 247–271.

Szerlong, H.J., and Hansen, J.C. (2011). Nucleosome distribution and linker DNA: connecting nuclear function to dynamic chromatin structureThis paper is one of a

selection of papers published in a Special Issue entitled 31st Annual International Asilomar Chromatin and Chromosomes Conference, and has undergone the Journal's usual peer review process. Biochem. Cell Biol. *89*, 24–34.

Szyjka, S.J., Aparicio, J.G., Viggiani, C.J., Knott, S., Xu, W., Tavare, S., and Aparicio, O.M. (2008). Rad53 regulates replication fork restart after DNA damage in Saccharomyces cerevisiae. Genes & Development *22*, 1906–1920.

Taddei, A., Roche, D., Sibarita, J.B., Turner, B.M., and Almouzni, G. (1999). Duplication and maintenance of heterochromatin domains. J. Cell Biol. *147*, 1153–1166.

Tan, B.C.-M., Chien, C.-T., Hirose, S., and Lee, S.-C. (2006). Functional cooperation between FACT and MCM helicase facilitates initiation of chromatin DNA replication. The EMBO Journal *25*, 3975–3985.

Tan, M., Luo, H., Lee, S., Jin, F., Yang, J.S., Montellier, E., Buchou, T., Cheng, Z., Rousseaux, S., Rajagopal, N., et al. (2011). Identification of 67 Histone Marks and Histone Lysine Crotonylation as a New Type of Histone Modification. Cell *146*, 1016–1028.

Tatchell, G.K. (1978). Physical structure and reconstitution of chromatin core particels. Phd Thesis (van Holde, K., supervisor). Oregon State University.

Taylor, R.M., Whitehouse, J., Cappelli, E., Frosina, G., and Caldecott, K.W. (1998). Role of the DNA ligase III zinc finger in polynucleotide binding and ligation. Nucleic Acids Research *26*, 4804–4810.

Tebbs, R.S., Flannery, M.L., Meneses, J.J., Hartmann, A., Tucker, J.D., Thompson, L.H., Cleaver, J.E., and Pedersen, R.A. (1999). Requirement for the Xrcc1 DNA base excision repair gene during early mouse development. Dev. Biol. *208*, 513–529.

Teo, I.A., and Arlett, C.F. (1982). The response of a variety of human fibroblast cell strains to the lethal effects of alkylating agents. Carcinogenesis *3*, 33–37.

Teo, I.A., Arlett, C.F., Harcourt, S.A., Priestley, A., and Broughton, B.C. (1983a). Multiple hypersensitivity to mutagens in a cell strain (46BR) derived from a patient with immuno-deficiencies. Mutat. Res. *107*, 371–386.

Teo, I.A., Broughton, B.C., Day, R.S., James, M.R., Karran, P., Mayne, L.V., and Lehmann, A.R. (1983b). A biochemical defect in the repair of alkylated DNA in cells from an immunodeficient patient (46BR). Carcinogenesis *4*, 559–564.

Thoma, F., Koller, T., and Klug, A. (1979). Involvement of histone H1 in the organization of the nucleosome and of the salt-dependent superstructures of chromatin. J. Cell Biol. *83*, 403–427.

Thomas, J.O. (1999). Histone H1: location and role. Curr. Opin. Cell Biol. *11*, 312–317.

Tomimatsu, N., Mukherjee, B., Hardebeck, M.C., Ilcheva, M., Camacho, C.V., Harris, J.L., Porteus, M., Llorente, B., Khanna, K.K., and Burma, S. (2013). Phosphorylation of EXO1 by CDKs 1 and 2 regulates DNA end resection and repair pathway choice. Nature Communications *5*, 1–10.

Tomkinson, A.E., Lasko, D.D., Daly, G., and Lindahl, T. (1990). Mammalian DNA ligases. Catalytic domain and size of DNA ligase I. J. Biol. Chem. *265*, 12611–12617.

Tomkinson, A.E., Howes, T.R.L., and Wiest, N.E. (2013). DNA ligases as therapeutic targets. Transl Cancer Res *2*.

Tremethick, D.J. (2007). Higher-Order Structures of Chromatin: The Elusive 30 nm Fiber. Cell *128*, 651–654.

Trujillo, K.M., and Osley, M.A. (2012). A Role for H2B Ubiquitylation in DNA Replication. Molecular Cell *48*, 734–746.

Trujillo, K.M., Tyler, R.K., Ye, C., Berger, S.L., and Osley, M.A. (2011). A genetic and molecular toolbox for analyzing histone ubiquitylation and sumoylation in yeast. Methods *54*, 296–303.

Tsabar, M., and Haber, J.E. (2013). Chromatin modifications and chromatin remodeling during DNA repair in budding yeast. Curr. Opin. Genet. Dev. *23*, 166–173.

Tsukuda, T., Fleming, A.B., Nickoloff, J.A., and Osley, M.A. (2005). Chromatin remodelling at a DNA double-strand break site in Saccharomyces cerevisiae. Nature *438*, 379–383.

Tsukuda, T., Trujillo, K.M., Martini, E., and Osley, M.A. (2009). Analysis of chromatin remodeling during formation of a DNA double-strand break at the yeast mating type locus. Methods *48*, 40–45.

Turinetto, V., and Giachino, C. (2015). Multiple facets of histone variant H2AX: a DNA double-strand-break marker with several biological functions. Nucleic Acids Research *43*, 2489–2498.

Turinetto, V., Orlando, L., Sanchez-Ripoll, Y., Kumpfmueller, B., Storm, M.P., Porcedda, P., Minieri, V., Saviozzi, S., Accomasso, L., Cibrario Rocchietti, E., et al. (2012). High Basal γH2AX Levels Sustain Self-Renewal of Mouse Embryonic and Induced Pluripotent Stem Cells. Stem Cells *30*, 1414–1423.

Ulrich, H.D., and Takahashi, T. (2013). Readers of PCNA modifications. Chromosoma *122*, 259–274.

Unal, E., Arbel-Eden, A., Sattler, U., Shroff, R., Lichten, M., Haber, J.E., and Koshland, D. (2004). DNA damage response pathway uses histone modification to assemble a

double-strand break-specific cohesin domain. Molecular Cell *16*, 991–1002.

van Holde, K.E. (1989). Springer series in molecular biology: Chromatin (Springer-Verlag New York Inc.).

Varga-Weisz, P.D., and Becker, P.B. (2006). Regulation of higher-order chromatin structures by nucleosome-remodelling factors. Curr. Opin. Genet. Dev. *16*, 151–156.

Venter, J.C., Adams, M.D., Myers, E.W., Li, P.W., Mural, R.J., Sutton, G.G., Smith, H.O., Yandell, M., Evans, C.A., Holt, R.A., et al. (2001). The sequence of the human genome. Science *291*, 1304–1351.

Vélez-Cruz, R., Manickavinayaham, S., Biswas, A.K., Clary, R.W., Premkumar, T., Cole, F., and Johnson, D.G. (2016). RB localizes to DNA double-strand breaks and promotes DNA end resection and homologous recombination through the recruitment of BRG1. Genes & Development *30*, 2500–2512.

Vijayakumar, S., Dziegielewska, B., Levin, D.S., Song, W., Yin, J., Yang, A., Matsumoto, Y., Bermudez, V.P., Hurwitz, J., and Tomkinson, A.E. (2009). Phosphorylation of Human DNA Ligase I Regulates Its Interaction with Replication Factor C and Its Participation in DNA Replication and DNA Repair. Molecular and Cellular Biology *29*, 2042–2052.

Wang, G., Li, Y., Wang, P., Liang, H., Cui, M., Zhu, M., Guo, L., Su, Q., Sun, Y., McNutt, M.A., et al. (2015). PTEN regulates RPA1 and protects DNA replication forks. Nature Publishing Group *25*, 1189–1204.

Wang, H., Rosidi, B., Perrault, R., Wang, M., Zhang, L., Windhofer, F., and Iliakis, G. (2005). DNA ligase III as a candidate component of backup pathways of nonhomologous end joining. Cancer Res. *65*, 4020–4030.

Wang, T., Xu, C., Liu, Y., Fan, K., Li, Z., Sun, X., Ouyang, H., Zhang, X., Zhang, J., Li, Y., et al. (2012). Crystal Structure of the Human SUV39H1 Chromodomain and Its Recognition of Histone H3K9me2/3. PLoS ONE *7*, e52977.

Wang, X., and Haber, J.E. (2004). Role of Saccharomyces Single-Stranded DNA-Binding Protein RPA in the Strand Invasion Step of Double-Strand Break Repair. PLoS Biol *2*, e21.

Waters, L.S., Minesinger, B.K., Wiltrout, M.E., D'Souza, S., Woodruff, R.V., and Walker, G.C. (2009). Eukaryotic Translesion Polymerases and Their Roles and Regulation in DNA Damage Tolerance. Microbiol. Mol. Biol. Rev. *73*, 134–154.

Watson, J.D., and Crick, F.H. (1953). Molecular structure of nucleic acids; a structure for deoxyribose nucleic acid. Nature *171*, 737–738.

Watson, J.D., and Baker, T.A. (2008). Molecular Biology of the Gene (Addison-

Wesley).

Weier, H.U., Wang, M., Mullikin, J.C., Zhu, Y., Cheng, J.F., Greulich, K.M., Bensimon, A., and Gray, J.W. (1995). Quantitative DNA fiber mapping. Hum. Mol. Genet. *4*, 1903–1910.

Wells, C.E., Bhaskara, S., Stengel, K.R., Zhao, Y., Sirbu, B., Chagot, B., Cortez, D., Khabele, D., Chazin, W.J., Cooper, A., et al. (2013). Inhibition of Histone Deacetylase 3 Causes Replication Stress in Cutaneous T Cell Lymphoma. PLoS ONE *8*, e68915.

White, C.I., and Haber, J.E. (1990). Intermediates of recombination during mating type switching in Saccharomyces cerevisiae. The EMBO Journal *9*, 663–673.

Widom, J. (1992). A relationship between the helical twist of DNA and the ordered positioning of nucleosomes in all eukaryotic cells. Proc. Natl. Acad. Sci. U.S.a. *89*, 1095–1099.

Williams, J.S., Lujan, S.A., and Kunkel, T.A. (2016). Processing ribonucleotides incorporated during eukaryotic DNA replication. Nature Reviews Molecular Cell Biology *17*, 350–363.

Willis, N., and Rhind, N. (2009). Regulation of DNA replication by the S-phase DNA damage checkpoint. Cell Div *4*, 13.

Wilson, B.G., and Roberts, C.W.M. (2011). SWI/SNF nucleosome remodellers and cancer. Nat Rev Cancer *11*, 481–492.

Woodcock, C.L., Frado, L.L., and Rattner, J.B. (1984). The higher-order structure of chromatin: evidence for a helical ribbon arrangement. J. Cell Biol. *99*, 42–52.

Wu, D., Topper, L.M., and Wilson, T.E. (2008). Recruitment and Dissociation of Nonhomologous End Joining Proteins at a DNA Double-Strand Break in Saccharomyces cerevisiae. Genetics *178*, 1237–1249.

Wu, P.Y., Frit, P., Meesala, S., Dauvillier, S., Modesti, M., Andres, S.N., Huang, Y., Sekiguchi, J., Calsou, P., Salles, B., et al. (2009). Structural and Functional Interaction between the Human DNA Repair Proteins DNA Ligase IV and XRCC4. Molecular and Cellular Biology *29*, 3163–3172.

Wyatt, H.D.M., and West, S.C. (2014). Holliday Junction Resolvases. Cold Spring Harbor Perspectives in Biology *6*, a023192–a023192.

Yadav, T., and Whitehouse, I. (2016). Replication-Coupled Nucleosome Assembly and Positioning by ATP-Dependent Chromatin- Remodeling Enzymes. CellReports *15*, 715–723.

Yan, C.T., Boboila, C., Souza, E.K., Franco, S., Hickernell, T.R., Murphy, M., Gumaste, S.,

Geyer, M., Zarrin, A.A., Manis, J.P., et al. (2007). IgH class switching and translocations use a robust non-classical end-joining pathway. Nature *449*, 478–482.

Yang, S.-M., Kim, B.J., Norwood Toro, L., and Skoultchi, A.I. (2013). H1 linker histone promotes epigenetic silencing by regulating both DNA methylation and histone H3 methylation. Proc. Natl. Acad. Sci. U.S.a. *110*, 1708–1713.

Yeeles, J.T.P., Poli, J., Marians, K.J., and Pasero, P. (2013). Rescuing Stalled or Damaged Replication Forks. Cold Spring Harbor Perspectives in Biology *5*, a012815–a012815.

Yeeles, J.T.P., Janska, A., Early, A., and Diffley, J.F.X. (2017). How the Eukaryotic Replisome Achieves Rapid and Efficient DNA Replication. Molecular Cell *65*, 105–116.

Zellweger, R., Dalcher, D., Mutreja, K., Berti, M., Schmid, J.A., Herrador, R., Vindigni, A., and Lopes, M. (2015). Rad51-mediated replication fork reversal is a global response to genotoxic treatments in human cells. J. Cell Biol. *208*, 563–579.

Zhang, H., Gan, H., Wang, Z., Lee, J.-H., Zhou, H., Ordog, T., Wold, M.S., Ljungman, M., and Zhang, Z. (2017). RPA Interacts with HIRA and Regulates H3.3 Deposition at Gene Regulatory Elements in Mammalian Cells. Molecular Cell *65*, 272–284.

Zhang, T., Termanis, A., Özkan, B., Bao, X.X., Culley, J., de Lima Alves, F., Rappsilber, J., Ramsahoye, B., and Stancheva, I. (2016). G9a/GLP Complex Maintains Imprinted DNA Methylation in Embryonic Stem Cells. CellReports *15*, 77–85.

Zhang, Y., Hefferin, M.L., Chen, L., Shim, E.Y., Tseng, H.-M., Kwon, Y., Sung, P., Lee, S.E., and Tomkinson, A.E. (2007). Role of Dnl4–Lif1 in nonhomologous end-joining repair complex assembly and suppression of homologous recombination. Nat Struct Mol Biol *14*, 639–646.

Zhang, Z., Shibahara, K., and Stillman, B. (2000). PCNA connects DNA replication to epigenetic inheritance in yeast. Nature *408*, 221–225.

Zhong, S., Chen, X., Zhu, X., Dziegielewska, B., Bachman, K.E., Ellenberger, T., Ballin, J.D., Wilson, G.M., Tomkinson, A.E., and MacKerell, A.D. (2008). Identification and Validation of Human DNA Ligase Inhibitors Using Computer-Aided Drug Design. J. Med. Chem. *51*, 4553–4562.

Zhou, C.Y., Johnson, S.L., Gamarra, N.I., and Narlikar, G.J. (2016). Mechanisms of ATP-Dependent Chromatin Remodeling Motors. Annu. Rev. Biophys. *45*, 153–181.

Zhou, Y., and Wang, T.S.F. (2004). A Coordinated Temporal Interplay of Nucleosome Reorganization Factor, Sister Chromatin Cohesion Factor, and DNA Polymerase Facilitates DNA Replication. Molecular and Cellular Biology *24*, 9568–9579.

Zhu, Z., Chung, W.-H., Shim, E.Y., Lee, S.E., and Ira, G. (2008). Sgs1 Helicase and Two Nucleases Dna2 and Exo1 Resect DNA Double-Strand Break Ends. Cell *134*, 981–994.

Zippo, A., Serafini, R., Rocchigiani, M., Pennacchini, S., Krepelova, A., and Oliviero, S. (2009). Histone Crosstalk between H3S10ph and H4K16ac Generates a Histone Code that Mediates Transcription Elongation. Cell *138*, 1122–1136.

Zofall, M., Persinger, J., Kassabov, S.R., and Bartholomew, B. (2006). Chromatin remodeling by ISW2 and SWI/SNF requires DNA translocation inside the nucleosome. Nat Struct Mol Biol *13*, 339–346.

Zou, Y., Liu, Y., Wu, X., and Shell, S.M. (2006). Functions of human replication protein A (RPA): From DNA replication to DNA damage and stress responses. J. Cell. Physiol. *208*, 267–273.